Eruption and emplacement of the 1.3-Ma Ongatiti Ignimbrite, New Zealand: Regional pathways, particle processes, and pumice evolution associated with a large-volume pyroclastic flow deposit

A thesis

submitted in fulfilment

of the requirements for the degree

of

Doctor of Philosophy in Earth Science

at

The University of Waikato

by

ELHAM YOUSEF ZADEH

THE UNIVERSITY OF
WAIKATO
Te Whare Wānanga o Waikato

2020

Abstract

Pyroclastic flows are the most devastating phenomena of explosive volcanic eruptions. These hazardous density currents are able to travel several tens of kilometers radially away from their source as fast, hot density currents. Due to the enveloping ash cloud, it is still impossible to directly study pyroclastic flows, however, their deposits (i.e. ignimbrites) provide useful insight into their internal processes. .

The Ongatiti Ignimbrite was sourced from Mangakino caldera (1600-950 ka), the oldest volcanic center in the Taupo Volcanic Zone, North Island, New Zealand. The crystal- and pumice-rich ignimbrite offers a unique opportunity to understand an ancient and large-volume pyroclastic flow as well as more details about particles processes and pumice evolution. The minimum deposit volume for the Ongatiti Ignimbrite has been revised to approximately 720 km^3, or 512 km^3 dense rock equivalent. Previous studies proposed ages from 1.21 to 1.28 Ma by dating methods, such as $^{40}Ar/^{39}Ar$, K/Ar and zircon fission track. This research used the (U-Th)/He method to determine an age of 1.3 Ma.

This study has combined field facies analysis and GIS methods to characterize the Ongatiti Ignimbrite. The topographic controls on the spatial distribution of the ignimbrite has been determined to understand pyroclastic flow pathways through valleys and over hills. The Ongatiti Ignimbrite was a landscape-modifying event that covered at least the western North Island and as far away as Auckland and Wellington. It is a welded to non-welded, columnar-jointed, cliff-forming deposit, that has been divided into nine facies based on the variation in pumice and lithic clast abundance, and welding rank.

This study also focuses on the texture and components of the ignimbrite matrix to better understand the magma fragmentation process, the transportational and depositional dynamics of the gas-ash fluid, and the post-emplacement processes. The microtextures of ignimbrite matrix were described and quantified by using optical microscopy, scanning electron microscopy, synchrotron x-ray microtomography, electron probe microanalysis and X-ray powder diffraction (XRD).

The matrix is poorly sorted and varies in the size and texture of ash-sized pumice fragments,

glass shards, crystals and lithic clasts. Glass shards range in shape between dominantly platy, Y-shaped, and complex shapes, and in size from a few microns to about 900 microns. The matrix is crystal-rich and comprises primary subhedral to anhedral volcanic crystals (plagioclase, quartz, pyroxene, hornblende, and Ti-Fe oxides and range between 100 to a few 1000 microns in size. The degree of welding in the matrix is defined by crystal-crystal contacts and deformation of glass shards around particles, and the highest degree of welding is shown by moderately deformed shards.

The physical characteristics and chemical composition of pumice clasts were determined, and the main pumice textures were recognised as vesicular, fibrous, microvesicular and dense type. Tomographic imaging shows different vesicularities and local crystal arrangement within pumice and ignimbrite. Glass chemical analysis shows two different groups, higher-silica (~80-81 wt%), and high-silica (76-78 wt%).

The Ongatiti Ignimbrite was emplaced by a super-eruption with a volcanic explosivity index (VEI) of 7, and eruptions of similar size could catastrophically bury a vast area of the North Island. The matrix of the Ongatiti Ignimbrite suggests complex particle interactions within the ash-gas fluid of pyroclastic flows. Microtomographic imaging of ignimbrite components offers new insights into understanding these complex processes.

Acknowledgments

The years of PhD thesis research were an intense journey but full of many personal and professional experiences, which have improved my abilities and knowledge.

The opportunity to study physical volcanology in New Zealand could never have been provided to me without group support. For this reason, I would like to express my gratitude to my supervisor, Dr. Adrian Pittari who gave me the opportunity of these experiences. I am under debt of Adrian's guidance, patience and many hours spent editing of my thesis. Special thanks to Prof. David. J. Lowe who supported me with a great deal of advice and many invaluable discussions. I thank Dr. Beth Fox and Dr. Shaun Barker for their guidance during my project.

Technical assistance from Annette Rodgers, Kirsty Vincent, Renat Radosinsky, Christopher Morcom and Noel Bates is greatly appreciated; they helped me during the project with my needs in the laboratory and field. Thanks to Dr. Ian Schipper for his assistance on the electron microprobe at Victoria University of Wellington for his precious guidance. Thanks to Martin Danišík at the John de Laeter Centre, Curtin University, Perth, for (U-Th)/He age dating. I would like to thank the administrative staff in the School of Science office, Gloria, Vicky and Fiona, who helped and guided me in different situations. Additionally, thank you to Cheryl, who kindly help me with my thesis editing and formatting. I sincerely thank you for all that you did for me.

I would like to thank the Australian Synchrotron and the New Zealand Synchrotron Group for accepting and financially supporting our beam time proposal; also the staff at the Australian Synchrotron, in particular the Imaging and Medical Beam Line and IMBL scientist Anton Maksimento who helped me with the facilities and acquiring images for my project. Ian Schipper (Victoria University of Wellington) also provided independent advice on synchrotron imaging. Thanks for the financial support that was provided by the Waikato Doctoral Scholarship, Broad Memorial Fund, Faculty of Science and Engineering Student Trust Research Grant, and Study Award from the University of Waikato; also a travel grant from the Cities on Volcanoes conference (COV), and a Young Researcher Travel Grant from the Geological Society of New Zealand.

I am not probably able to name all of the people who helped and supported me, but I have

tried my best to remember most. As a part of this amazing endeavor, I have visited many places and people. There were many kind people at the Hinuera Quarry, Castle Rock Adventures, and also several farmers, whose names I cannot list, but they allowed me to collect samples on their properties.

My biggest thanks go to my family and friends, Tati, Mehran, Farnaz, Nazgol, Jafar, Keivan, Mohammad, Amy, Bérengère, Shamma, Naghmeh, Kourosh, Saling and Mario who were always present in supporting me to pass all the difficulties during these years. You all are special gifts in my life and I never forget your kindness.

Finally, my greatest thanks to the angel of my life whom I call her "mom" and my brother, Shahab, with his golden heart. Certainly, I could not finish this journey without their love even though they were thousands of kilometers away from me. Thank you very much for your encouragement, support and your faith in me.

To my dad in heaven

To my kindhearted mom

To my lovely brother

Table of contents

List of figures

List of tables

Chapter One

Introduction

1.1 Introduction

Hot, heterogeneous mixtures of volcanic fragments and gas, which flow across the ground due to their relatively higher density with respect to their surrounding environment, are known as pyroclastic density currents (PDC) (Branney & Kokelaar, 2002). Ignimbrites represent a type of pyroclastic density current deposit that is significantly rich in pumice and ash, is poorly sorted, and shows a large range of thicknesses, as well as relative proportions, sizes and types of pumice, crystals, ash and lithic clasts (e.g., Smith, 1979; Fisher & Schmincke, 1984; Wilson, 1986; Cas & Wright, 1987; Freundt *et al.*, 2000; Branney & Kokelaar, 2002). Ignimbrites are the most hazardous and devastating phenomena of explosive volcanic eruptions due to their volume, temperature, emplacement speed and long runout distance and lateral distribution from the source (Wilson *et al.*, 1995c; Freundt *et al.*, 2000).

Determining the interaction of pyroclastic flows with the topography is difficult, particularly the role of the paleotopography on prehistoric pyroclastic flows (Cas and Wright, 1987, Valentine *et al.*, 1992, Cook *et al.*,2016, Baez, et al., 2020). Detailed studies on the internal deposit stratigraphy and lithofacies can lead to the determination of depositional dynamics. Furthermore, previous work on ignimbrite lithofacies have paid little attention on the physical characteristics of the matrix, which could be responsible for controlling the fine-scale flow and emplacement processes in pyroclastic flows. Finally, studies of the juvenile clast textures in ignimbrites are considered to be an important source of data for understanding gas bubble development, magma dynamics and fragmentation processes.

The large-volume Ongatiti Ignimbrite was emplaced during a super-eruption that occurred sometime between 1.2 and 1.3 Ma from the Mangakino Volcanic Centre (MVC) during activity of the early Taupo Volcanic Zone. The Ongatiti Ignimbrite provides an ideal opportunity to document the deposit distribution and textural complexity of an ancient, large-volume, pyroclastic flow that has covered a vast area around its source caldera.

1.2 Aims and objectives

This aim of this study is to determine the eruption, emplacement and post-emplacement processes of the Ongatiti Ignimbrite.

To achieve this, aim this study addresses the following three objectives:

1. To determine the distribution of the ignimbrite in relation to the paleotopography, its facies variation vertically, radially, and proximal to distal from the MVC, and to constrain its age.
2. Understanding fine-scale eruption and post emplacement processes based on physical characteristics of the ignimbrite micro-texture and components.
3. Determination of the eruption history and dynamics due to physical and chemical characteristics of juvenile clasts and particularly volcanic glass.

1.3 Methodology

A range of field, desktop and laboratory methods have been used in this study. The stratigraphy and facies characteristics of the Ongatiti Ignimbrite were assessed in the field and were synthesized with data derived using geographical information systems (GIS) to generate a three-dimensional map of the ignimbrite distribution. The geological observations and generated maps were created to understand the effect of paleotopography on the pyroclastic flow path. To obtain a new independent age determination of the Ongatiti Ignimbrite, the (U-Th)/He method was used as this is a valuable method for tephrochronology and allows eruption dating within a time period between 50 ka to 1.5 Ma (Farley et al., 2002 and Danisik et al., 2017) . It means the (U-Th)/He method is extremely useful for geochronology of quaternary pyroclastics. Additionally, dating Ongatiti Ignimbrite by this method has been done for the first time, therefore it would be a valuable way for comparing obtained data with other geochronology methods.

To characterize the microtexture of the ignimbrite matrix and pumice clasts, a range of traditional and cutting-edge methods were used, including optical petrography, X-ray diffraction (XRD) analysis, scanning electron microscopy (SEM), backscattered electron image analysis (BSE), synchrotron X-ray computed microtomography (μ-CT). An ash-cooling experiment was conducted to assist with the interpretation of observed welding textures.

Geochemical data were acquired by energy dispersive spectrometry (EDS), X-ray fluorescence (XRF) spectrometry, electron probe microanalysis (EPMA) and laser ablation inductively coupled plasma mass spectrometry (LA-ICP-MS).

1.4 Study locations

All studied sites are located on the North Island and they were strategically selected to cover a regional distribution around the source caldera of the MVC. The proximal-medial outcrops include Hinuera Quarry, Tauranga, Peacockes (Waikato River), Castle Rock, Waipari Gorge east, Waipari Gorge west, Te Kuiti and Benneydale (Figure 1.1). Additionally, some distal deposits were studied at Harbour Road, Oparau Creek and Bryant Home (Figure 1.1).

The Hinuera Quarry, an active 'stone' quarry that has operated commercially since 1954, occurs amidst bluffs of the Ongatiti Ignimbrite along the western side of the Hinuera valley (Lowe & Pittari, 2019), located between Hamilton and Tauranga cities (384201.00 E, 5802482.00 S). At Tauranga, the Ongatiti Ignimbrite is exposed as bluffs on roadside outcrops (417219.00 E, 5821442.00 S) (Figure 1.1).

In the Waipari Gorge (Figure 1.1) on both east and west sides of the valley (west: 373588.00 E, 5768146.00 S and east: 373563.00 E, 5767471.00 S**)**, the Ongatiti Ignimbrite forms cliffs with wide individual jointing along the Waipari Gorge. The Ongatiti Ignimbrite at Castle Rock (370326.00 E, 5778629.00 S) is located in a valley near Wharepapa South and occurs as high cliffs with altered pumice. The altered pumice fragments have fallen out of the exposed ignimbrite surface creating holes that are notably suitable for rock climbing.

At Te Kuiti, the Ongatiti Ignimbrite was studied at a high bluff within Ongatiti Valley (351577.00 E, 5748692.00 S). The ignimbrite in the Peacockes section (Waikato River) occurs close to the Waikato River near Hamilton (352598.16 E, 5813043.55 S). The deposit in Benneydale section is situated near the Mangakino Caldera and is manifested as relative thin deposits at the top of the hills (362934.11 E, 5737924.32 S)

The distal tephra deposits in the Harbour Rd., Oparau Creek and Bryant Home, occur in the lowland areas of the western Waikato near the west coast of North Island (Figure 1.1).

1.5 Summary of chapters

The remainder of this chapter reviews the Taupo Volcanic Zone (TVZ), its eruption history and volcanic centres; the Mangakino Volcanic Centre (MVC) and previous work on the

Ongatiti Ignimbrite. **Chapter 2** describes the methods that have been used during the research.

Chapter 3 defines the mobility and emplacement of the Ongatiti Ignimbrite and the effect of the topography on a giant pyroclastic flow (>500 km^3 DRE). Different lithofacies within the ignimbrite are considered in relation to the paleotopography. In addition, the chronology of the ignimbrite is presented in Chapter 3.

Chapter 4 focuses on the microtexture and microscopic components of the ignimbrite matrix, including both primary particles and secondary alteration to understand the fine-scale eruption and flow processes, and hot post-emplacement modification process of the ignimbrite.

Chapter 5 gives specific attention to the physical and chemical characteristics of pumice fragments and volcanic glass shards within the ignimbrite and addresses questions about the processes of magma fragmentation and magmatic history of the Ongatiti eruption.

Chapter 6 reviews the key findings, and wider scientific implications from this research and some future directions.

Each chapter is structured as stand-alone scientific manuscripts and consequently there is some repetition between chapters particularly in the introductory sections of chapters 3, 4 and 5.

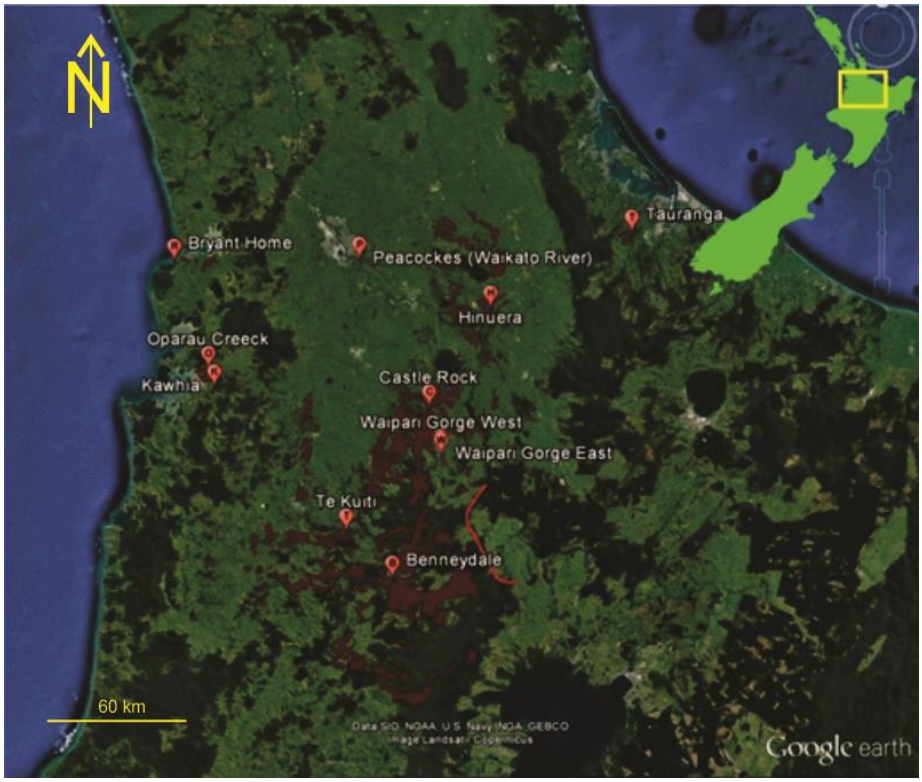

Figure 1.1**:** Map of the field locations and sampling areas (red pins) for studying the Ongatiti Ignimbrite (base map from Google Earth).The red solid line illustrates the border of the Mangakino Caldera and the red polygons show the distribution of Ongatiti Ignimbrite.

1.6 Super-eruptions

A super-eruption is described as generating an ejected magma mass larger than $1x10^{15}$ kg and for rhyolitic eruptions is estimated to be equivalent to a dense rock equivalent (DRE) volume of at least 450 km^3 (Sparks *et al.*, 2005; Self, 2006; Miller & Wark, 2008). The size and distribution of super-eruptions are greater than for those of other volcanoes, and therefore their power of destruction is significantly higher too (Wilson, 2008 and Miller and Wark, 2008). A caldera is a common landform mostly resulting from super-eruptions and is usually identified by sub circular and negative topographic features (Miller and Wark, 2008). During a super-eruption, a huge volume of material will be evacuated from the magma chamber, hence causing the collapse of the ground to form a caldera. The size of the caldera is directly related to the magnitude of the eruption and sometimes reaches a diameter of nearly 150 km such as Yellowston caldera, Toba caldera and Apolaki caldera. (Smith, 1979; Miller & Wark, 2008; Wilson, 2008). Previous volume reported for the Ongatiti Ignimbrite (Briggs *et al.*, 1993; Houghton *et al.*, 1995; McCormack *et al.*, 2009) are not clear about whether the Ongatiti eruption should be classified as a super-eruption. This question is addressed in this study with new volume estimates by estimation of the ignimbrite distribution and average thickness of deposition (Chapter 3).

1.7 Taupo Volcanic Zone

The NNE-SSW trending Taupo Volcanic Zone (TVZ) is approximately 300 km long and 60 km wide and is located in the central part of the North Island (Figure 1.3). It has been mostly a locus of explosive volcanism since ~2 Ma and is known for its varied eruptive deposits and frequency of eruptions (Wilson, 2008). This volcano-tectonic zone has produced at least 34 caldera-forming ignimbrite eruptions and a wide range of minor eruptions from at least eight rhyolitic calderas (Healy, 1964; Houghton *et al*., 1995; Wilson *et al.*, 1995; Allan *et al*., 2008; Leonard *et al*., 2010; Shane, 2017, Milicich *et al*., 2020).

The term "Taupo Zone" was originally used by Hochstetter (1859) to describe the area containing "rhyolitic and trachytic lava", with Quaternary eruptions and geothermal systems extending from Ruapehu to White Island. He also noted that the eruptive deposits consisted of several types of siliceous rocks dominated by rhyolitic rocks with pumice and obsidian. However, current studies show more rock complexity and wider areas than his estimation.

1.8 Tectonic setting

New Zealand sits obliquely along the convergent boundary between the Australian and Pacific plates. The Pacific plate is subducting beneath the Australian Plate along the Tonga-Kermadec and Hikurangi trenches (Figure 1.2). It seems subduction dates from early Miocene (Lamb, 2011). The major surface features, middle to upper crustal structures and active tectonics play a significant role in understanding the controls of the deep structures in the modern TVZ, especially on rifting processes and the nature and position of the major faults, which probably have formed obstacles to or pathways for fluids flowing at depth (Rowland & Sibson, 2004; Wilson *et al.*, 2009; Lamb, 2011).

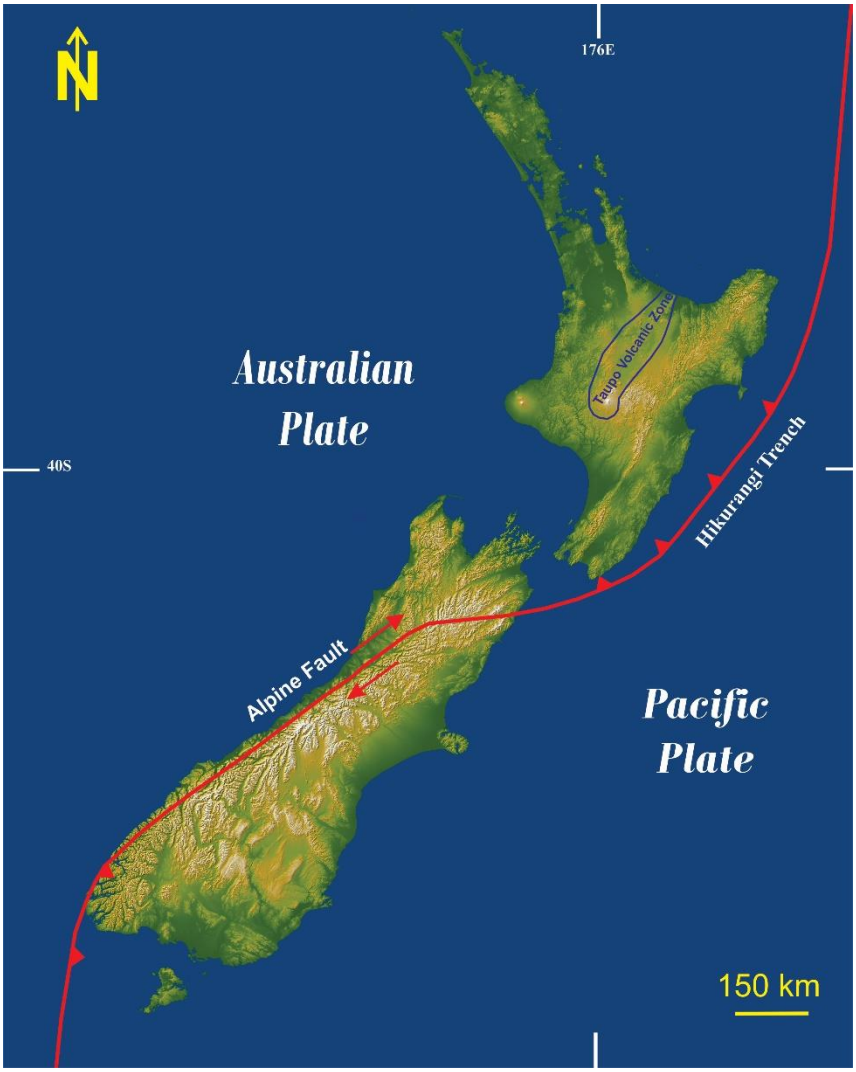

Figure 1.2**:** A simplified map of New Zealand (without scale) showing the plate boundary and location of the Taupo Volcanic Zone (base map from http:// earthobservatory.nasa.gov)

The subduction of the oceanic Pacific crust beneath continental Australian crust in the east of the North Island (Figure 1.2) has influenced the volcanism during the Quaternary (Cole, 1981). The central TVZ has produced nearly 15,000 km^3 of silicic deposits (Briggs *et al.*, 1993; Price *et al.*, 2005; Allan *et al.*, 2008), that make up Quaternary volcanic deposits in New Zealand (Ewart *et al.*, 1977; Wilson *et al.*, 1995c).

Three geographic segments have been identified in the TVZ (Figure 1.3) based on eruption style, volume, rate, and frequency of eruptions (Wilson *et al.*, 2009). The **Northern TVZ**, northeast of the Okataina Volcanic Centre. Comprises mostly andesitic-dacitic cones. The **Central TVZ** includes the region from the northern side of the Okataina Volcanic Centre (Figure 1.3) to the southern end of Lake Taupo and is characterised by silicic volcanism. Around 95 percent of the felsic volcanic products and geothermal systems are concentrated in the central part of the TVZ. The **Southern TVZ** segment includes the Pihanga-Kakaramea

chain of composite cones and extends to the isolated vents in southwest (North of Ruapehu) and is characterized by andesite-dacite composition (Figure 1.3), with some basalt, but no rhyolite. The eruption volume in this region is approximately one fifth that of Central TVZ. There are currently two active areas in White Island and Ruapehu-Tongariro, located in the northeast and southwest segments respectively (Cole, 1979; Graham *et al.*, 1995; Sutton *et al.*, 1995; Wilson *et al.*, 1995c; Wilson *et al.*, 2009; Wilson & Rowland, 2016).

The rhyolitic eruption history of the TVZ is comparable in size and structural complexity to the Yellowstone Volcanic Field (Wilson *et al.*, 1995c). However, it is likely that due to the thinner crust and active extension in the central North Island, rhyolitic eruptions in the TVZ have been less voluminous and more frequent since 1.68Ma (Wilson *et al.*, 1984; Wilson *et al.*, 1995c; Wilson & Rowland, 2016).

1.9 TVZ Volcanic Centres

During the active lifetime of the TVZ over the last 1.6 Ma, voluminous rhyolitic eruptions have shaped at least eight volcanic centres or calderas (Wilson *et al.*, 2009). Several calderas have been completely blanketed by newer deposits and are not exposed; however, they were identified by stratigraphic studies, faulting and geophysical anomalies. The collapse structures of calderas that are exposed, including the Taupo and Rotorua calderas, have been reported (Healy, 1964; Cole, 1979; Wilson, 1986; Nairn *et al.*, 1994). The locations and ages of the calderas are presented in Figure 1.3.

The earliest rhyolitic caldera, situated on the western border of the Central TVZ, is the main feature of the Mangakino Volcanic Centre (MVC). MVC was initially characterised as a volcanic centre by Blank (1965) and this recognition was subsequently confirmed as a caldera by Rogan (1982) based on a gravity anomaly. Rogan (1982) also identified the Kapenga Caldera which covers 250 km^2 and is composed of at least two different collapse segments of different ages (890 and 240 ka), one a basin in the northeast which is ~2.5 km deep and another, larger, basin in the south which is ~3 km deep (Wilson *et al.*, 1984; Wilson *et al.*, 2009).

Three others volcanic centres in the TVZ, Rotorua, Ohakuri, and Reporoa, have each shown just one caldera-forming eruption (Wilson *et al.*, 1984, 2009). The Rotorua caldera has a 20 km diameter and its collapse structure was recognised by a negative gravity anomaly (Rogan,1982). This caldera now includes Lake Rotorua. The Reporoa Volcanic Centre is a 15 x 10 km caldera and was initially identified by Modriniak and Studt (1959). The

topography, lithic components, as well as structural and geophysical arguments, have verified the presence, shape and the relationship of the Kaingaroa Ignimbrite to the caldera (Nairn *et al.*, 1994; Beresford & Cole, 2000).

Wilson *et al*. (1986) originally identified and explained the Whakamaru Caldera based on the presence of Whakamaru-group ignimbrite. Wilson *et al.* (2009) later described the caldera as originating from two eruptions but younger deposits have now buried it.

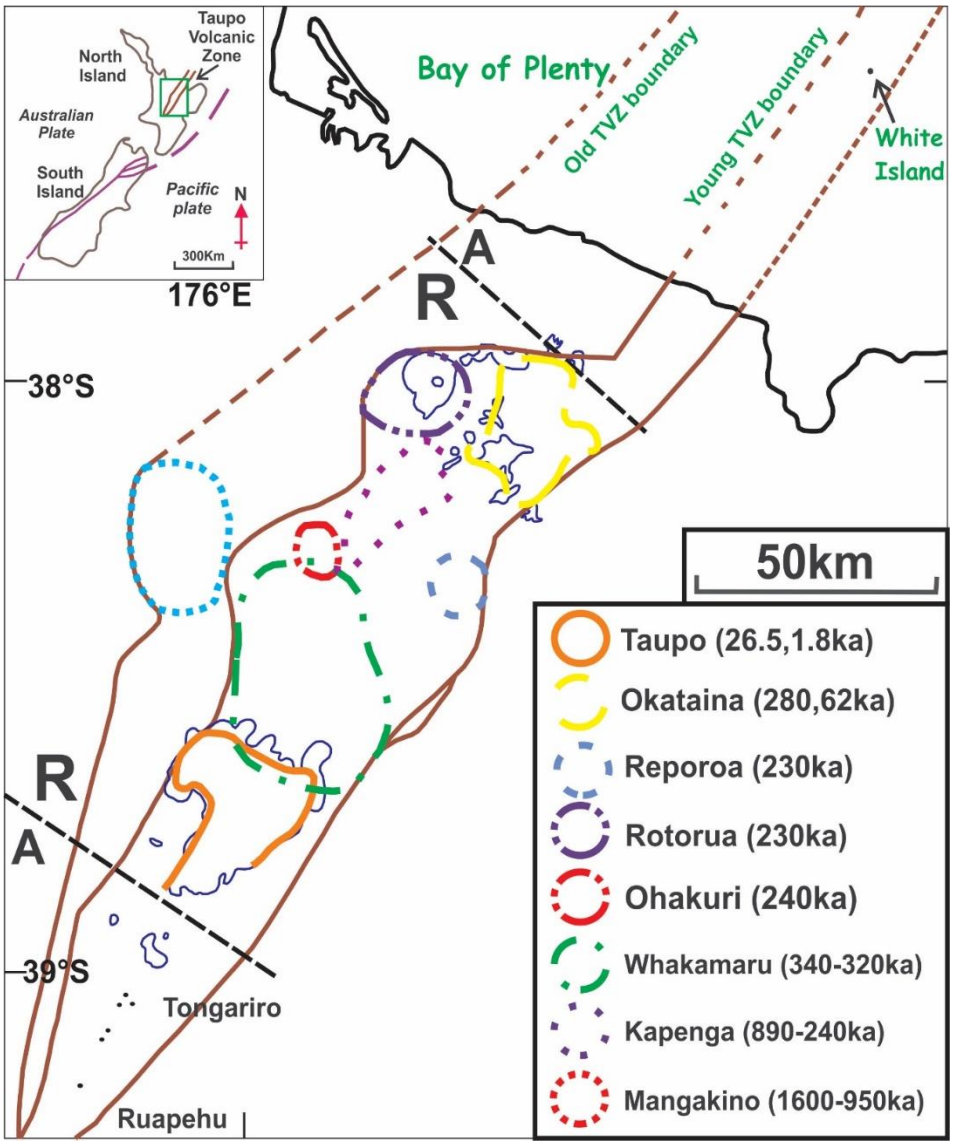

Figure 1.3**:** A summary of the TVZ and its calderas (modified from Wilson et al. 2009).The calderas illustrated based on their ages. The solid lines show clear boundaries and dashed lines illustrate uncertain boundaries (A=andesite dominated and R=rhyolite dominated).

The Okataina and Taupo Volcanic centres have the most recently active calderas and it is estimated that in the last ~50,000 years these calderas have produced 99 percent of the total volcanic mass in the centre of the TVZ (Wilson *et al*., 2009).

1.10 History of eruptions

Wilson *et al.* (1995, 2016) divided the TVZ into three periods based on temporal evolutions. The oldest period is denoted the **old TVZ** (2.0 Ma to 350 ka). Volcanic products in this segment have been poorly preserved (except for the products of the MVC) between geological events due to erosion and burial by younger deposits. Eruptive records from 350 ka to approximately ~50 ka define the next segment, namely **young TVZ** (note the younger age used here is based on dates reported for the Rototiti Tephra Formation by Danišík *et al*., 2012, and Flude & Storey, 2016. This 350–50 ka age range is associated with the major structural features of the TVZ (Leonard *et al*., 2010). The third segment, known as the **modern TVZ**, is characterised by volcanic activity between ~50 ka to the present time, and the deposits from this period have been extensively studied.

The beginning of the old TVZ was dominantly andesitic but within several hundred thousand years the silicic (rhyolitic) volcanism was established (Beresford & Cole, 2000; Price *et al.*, 2005; Wilson, 2008; Wilson & Rowland, 2016). The reason for this transition was explained by Wilson et al. (1995): the increase in rhyolitic production was due to increased heat flow which had an effect on crustal melting.

1.11 Mangakino volcanic centre

1.11.1 Overview

The earliest rhyolitic volcanic centre in the TVZ is located on the western boundary and is known as the Mangakino Volcanic Centre (MVC) (Figure 1.3). It was identified by geophysical and geological field studies (Blank, 1965; Stern, 1979; Rogan, 1982; Wilson *et al.*, 1984; Wilson *et al.*, 1995c).

It is estimated that the MVC, which comprises a caldera, has produced voluminous deposits measuring >1000 km^3 (DRE); however, due to erosion, faulting processes and burial by new sequences (dominantly lacustrine and fluvial sediments and the Whakamaru Ignimbrite) the caldera is poorly expressed (Briggs, 1976; Stern, 1979; Rogan, 1982; Wilson *et al.*, 2009).

Data obtained through $^{40}Ar/^{39}Ar$ age dating from Mangakino deposits display two distinct eruptive phases that formed the caldera: the first period occurred from 1.6 to 1.5 Ma, and the second phase from 1.21 to 0.95 Ma (Houghton *et al.*, 1995). MVC eruptions produced at least six major welded ignimbrites and two large-scale phreatomagmatic units (Wilson, 1984, 1986). Two lava domes and another ignimbrite (Marshall Ignimbrite) have been

mapped by Briggs *et al*. (1993). A summary of MVC eruptions is presented in Figure 1.4 and a summary of ages and eruption volumes in Table 1.1. The preserved deposits of MVC eruptions range in age from 1.68 to 0.95 Ma and comprise the Pakaumanu Group ignimbrites, including the Ngaroma Ignimbrite, Ongatiti Ignimbrite, Unit D, Ahuroa Ignimbrite and Rocky Hill Ignimbrite (Leonard *et al*., 2010).

1.11.2 History of previous works on the MVC

Hochstetter (1859) mapped fragmental rhyolites in Te Kuiti as the `Trachytic Lava and Tuff` Formation: the first study on ignimbrite sheets in the west of TVZ. Marshall (1934) described the acid rocks of the Taupo and Rotorua regions and showed them to form a distinct volcanic area. Further ignimbrite outcrops in the western TVZ were described by Marwick *et al.* (1946). The ignimbrites were first-grouped into the Pakaumanu Ignimbrites and Rocky Hill Ignimbrite, in the 'Geology of New Zealand' 1:250,000 map series by Kear (1960).

Martin (1961) revised and divided the Pakaumanu Ignimbrites into distinct units based on stratigraphic position, lithology, outcrop characteristics, and crystal fragment compositions. The units from oldest to newest were Ranginui Ignimbrite, Ngaroma Ignimbrite, Ongatiti Ignimbrite, Ahuroa Ignimbrite, Manunui Ignimbrite, and Rocky Hill Ignimbrite. A source vent for Ongatiti Ignimbrite close to Pureora, which is located near the present Mangakino Caldera, was proposed.

The lithic fragments were described for the first time by Blank (1965). In addition, he revised the units of Martin (1961) and the location of the current Mangakino Caldera was proposed as a source of most of the ignimbrites from the Pakaumanu Group. Geophysical studies were undertaken by Stern (1979) and, although a volcanic centre was not initially recognized, Rogan (1982) later identified a caldera structure. Wilson *et al.* (1984), based on previous geophysical and geological research, defined the boundaries of the MVC; Wilson (1986) modified the ignimbrite distribution and the Mangakino stratigraphy. The stratigraphy of volcanic deposits were described in detail in the Tokoroa-Kinleith area by Houghton *et al.* (1987a), in the Tokoroa-Kinleith area by Gifford (1988), and in the Waipa Valley by Moyle (1989).

Soengkono *et al.* (1992) determined the first reliable age for Ongatiti Ignimbrite based on a K/Ar age. Hastuti (1992) studied the erupted ignimbrites from MVC in the western boundary of the Taupo Volcanic Zone. Briggs *et al*. (1993), described the MVC geochemistry and

petrogenesis from whole rock pumice samples. The ages of the many ignimbrite deposits were determined using Ar/Ar methods by Houghton *et al.* (1995) and isothermal plateau fission track (ITPFT) methods by Black et al. (1996).

The stratigraphy, mineralogy, petrography, and geochemistry of ignimbrites in the western Tokoroa Plateau were described by Bennett (1997). Based on geophysical studies, petrology and geochemistry of the lithic clasts, a detailed and revised model was suggested by Krippner *et al.* (1998) for the MVC (Figure 1.5). They divided the MVC into two separate parts, the volcanic pile and the sub-volcanic crust, and they also introduced several other components of the MVC. Also, based on the lithic fragments description of MVC ignimbrites and rhyolitic lava lithics, they proposed that the explosive eruptions which produces rhyolitic lava were more voluminous than previously thought.

McGrath (2004) studied the Ahuroa Ignimbrite in Wharepapa South. Wilson *et al*. (2008) focused on the MVC as a geothermal field and continued previous work on geothermal studies. Altered rock units of the MVC in the subsurface were studied and zircon U-Pb ages were acquired. McCormack *et al*. (2009) worked on four Mangakino units (Rocky Hill, Ahuroa, Ongatiti, and Ngaroma) and determined ages based on xenocrystic zircons. In addition, they presented proof of the changing situation of assimilation.

The ignimbrites and their emplacement processes in the Ongatiti Valley were studied by Brink (2012). The composition and chronology of evolution of the MVC according to zircon trace element data were investigated by Cooper (2014). Proof for super-eruptions (Kidnappers, Rocky Hill and Ongatiti) in the MVC, a new magmatic system for the MVC and time spans between the Ongatiti, Ahuroa and Kidnappers eruptions (around 180 kyr) were presented by Cooper *et al*. (2016, 2017).

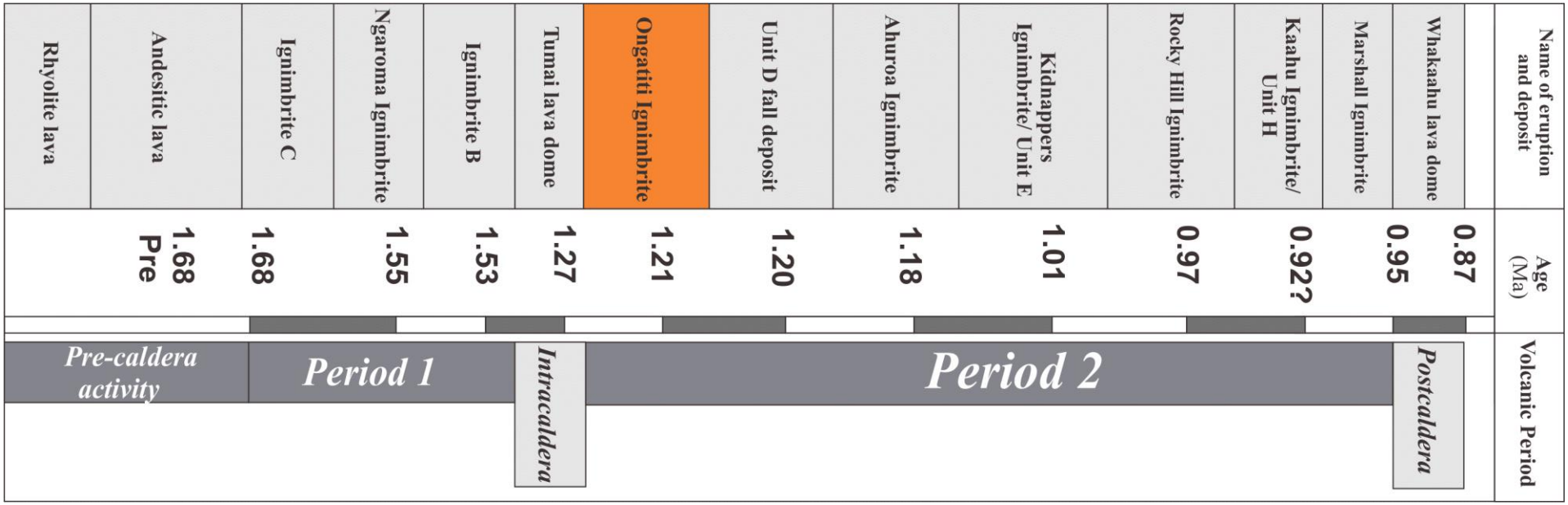

Figure 1.4**:** A summary of the eruption units, their ages and volcanic periods of the MVC units and their deposits (Wilson, 1986; Briggs *et al.*, 1993; Wilson *et al.*, 1995c; Krippner *et al.*, 1998; Stratford & Stern, 2008)

13

Table 1.1:A summary of the ages, volume and other characteristics of volcanic eruptions of the MVC units (Wilson *et al*., 1986b; Briggs *et al*., 1993; Wilson *et al*., 1995; Houghton *et al*., 1995; McCormack, 2009)

	Age (Ma)				Volume DRE (km^3)			Description	
	1 (Ar/Ar)	**2 ($^{40}Ar/^{39}Ar$)**	**3 Feldspar ($^{40}Ar/^{39}Ar$)**	**4 (K/Ar)**	**1**	**2**	**3**	**Exposures**	**Type of eruption**
Whakaahu lava dome	0.87±0.08				<1			Mapped	Effusive eruption
Marshall Ignimbrite	0.91±0.02	0.95±0.03			>50			Exposed outcrop	Explosive; pyroclastic flow
Kaahu Ignimbrite/Unit H	0.92±0.07				<0.5			Poorly exposed outcrop	Explosive; pyroclastic flow
Rocky Hill Ignimbrite	0.97±0.02	1.00±0.05	1.00±0.05	1.06±0.09	>300	300-1000	300-1000	Exposed outcrop	Caldera collapse formed via most voluminous eruptions
Kidnappers/Unit E Fall deposit	1.01±0.06	0.97±0.04			>300	100-300		Poorly exposed outcrop	Phreatoplinian eruption
Ahuroa Ignimbrite	1.19±0.03	1.18±0.02	1.18±0.02		>50	100-300	100-300	Exposed outcrop	Explosive and energetic pyroclastic flow
Unit D fall deposite	1.18±0.02	1.20±0.04			>10	100-300		Exposed outcrop	Phreatoplinian eruption
Ongatiti Ignimbrite	**1.23±0.02**	**1.21±0.04**	**1.21±0.04**	**1.25±0.09**	**>300**	**300-1000**	**300-1000**	**Exposed outcrop**	**Caldera collapse formed via most voluminous eruptions**
Tumai lava dome	1.27±0.05				<0.1			Mapped	Effusive eruption
Ignimbrite B	1.51±0.02	1.53±0.04				30-100		Very poorly exposed outcrop	Explosive; pyroclastic flow
Ngaroma Ignimbrite	1.60±0.03		1.60±0.04		>50	100-300	>50	Poorly exposed outcrop	Explosive; pyroclastic flow
Ignimbrite C	1.62±0.11	1.68±0.07			>10	30-100		Very poorly exposed outcrop	Explosive andesitic eruption
Andesitic lava								Abundant lithic clasts	Andesitic activity
Rhyolite lava domes								Lithic clasts	Effusive eruption

1-Briggs *et al* (1993), 2-Houghton *et al*(1995), 3-McCormack *et al.* (2009), 4-Soengkono et al(1992)

14

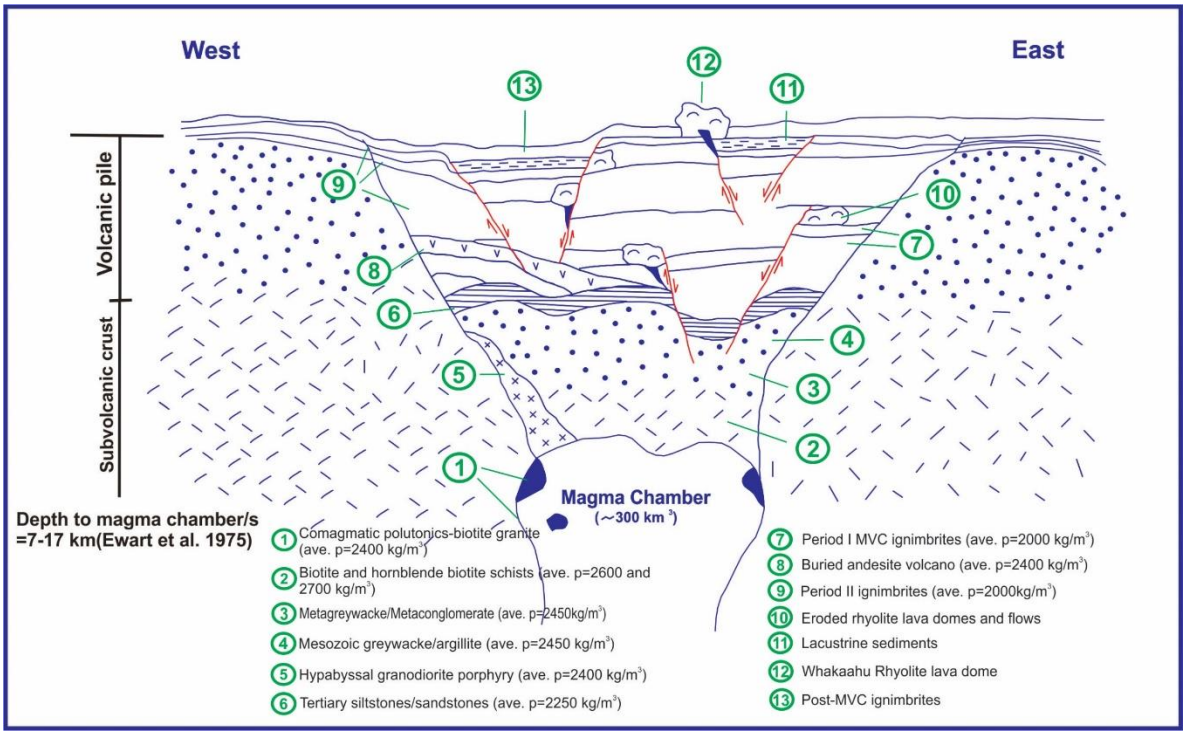

Figure 1.5: Schematic diagram of the Mangakino Volcanic Centre and its infilling stratigraphic components (modified after Krippner *et al*., 1998)

1.12 Ongatiti Ignimbrite

1.12.1 Introduction

The Ongatiti Ignimbrite has generally been described as a widespread, non-welded to partially welded, crystal-rich, rhyodacitic to rhyolitic ignimbrite which is exposed mostly in western areas of the central North Island. A super-eruption 1.21± 0.04 Ma (Wilson *et al.*, 1995c; McCormack *et al.*, 2009; Cooper & Wilson, 2014) deposited this extensive ignimbrite with a currently published volume between 300 to 1000 km^3 DRE (Cooper & Wilson, 2014). The distribution of surface outcrops of the Ongatiti Ignimbrite was shown by Briggs *et al*. (1993); however, based on surface and subsurface studies, the distribution extends farther to the north and east of the MVC as shown in the Figures 1.6a, b (Cooper & Wilson, 2014).

Briggs *et al*. (1996) identified the ignimbrite near Tauranga and due to texture and composition correlation with the rest of the Ongatiti Ignimbrite elsewhere they extended the ignimbrite boundary to Tauranga (Figure 1.6a). Later age dating (1.34 – 1.32 Ma) of the

studied deposits near Tauranga also show a good relationship with the Ongatiti Ignimbrite (Briggs *et al.* 2005). However, Cooper and Wilson (2014) disagreed with this deposit relationship so they didn't extend the area to Tauranga on their created map. They extend their proposed map close to Auckland based on association with distal correlatives of Alloway et al. (2004). Cooper and Wilson (2014) also extended the deposit to the east based on drill holes beneath the Waiotapu geothermal field (Wilson et al. 2010). In current research a map for distribution of the Ongatiti Ignimbrite has been proposed mostly based on the proximal and medial and distal deposits in chapter three.

The Ongatiti Ignimbrite was first described by Martin (1961) as a light yellow ignimbrite with abundant feldspar, minor quartz and also mafic crystals. Many authors have determined the ages of the Ongatiti Ignimbrite (Table 1.2). Briggs *et al*. (1993) reported that the Ongatiti Ignimbrite is composed of multiple flow units erupted in a series of directional lobes, and Wilson (1986) divided the deposit into two facies. The lower parts of Ongatiti Ignimbrite resulted from a highly energetic, violent and partly cooler flow that generated pumice-poor facies. The eruption then continued with a less energetic and hotter flow, which resulted in the upper, coarse-grained pumice-rich ignimbrite facies (Wilson, 1986; Briggs *et al*., 1993). The boundary between flow units is gradational, and there are sharp changes in the percentages and sizes of lithics and pumice.

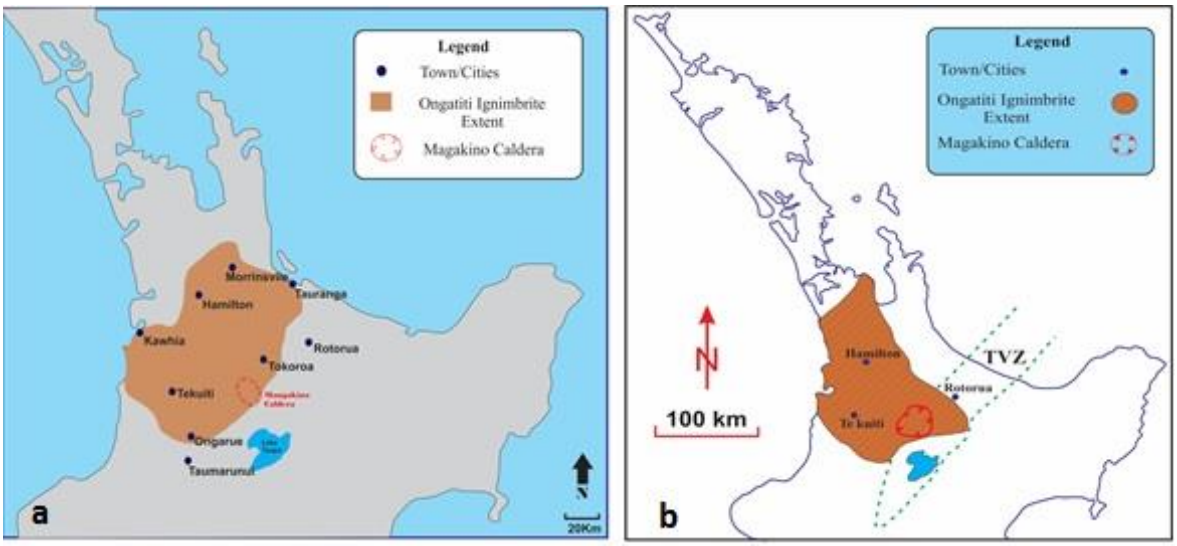

Figure 1.6: The Ongatiti Ignimbrite distribution based on (a) Briggs *et al.* (1993) and (b) Cooper *et al.* (2014).

The lower part of the ignimbrite is characterized by an abundance of crystals but is lithic-poor and pumice-poor (Wilson, 1986). The upper part is densely or partially welded and rich in lithics, pumice and crystals (Briggs *et al.*, 1993; McGrath, 2004), and includes large clasts of pumice, reported to have a fibrous texture, and which can attain diameters of up to 100 cm. Several lithic types were defined including andesite, rhyolite, greywacke, densely welded ignimbrite, and amphibolite and hornblende microdiorite (Briggs *et al*., 1993).

In some areas, a third unit was reported between the lower and upper parts. According to Briggs *et al*. (1993), who described the Ongatiti Ignimbrite in the Hinuera Quarry, a middle densely welded flow unit, which is moderately pumice-rich with abundant crystals, was recognised. Also, in the Ongatiti Valley, Brink (2012) introduced a transitional unit with an abrupt increase and abundance of pumice, and with dense welding at the base that becomes gradually weaker. The abundance and distribution of lithic fragments are low, with different clasts of greywacke, argillite, spherulitic and vitrophyric rhyolite lava and fine-grained, grey microdiorite fragments. Overall, the Ongatiti Ignimbrite is crystal-rich with different types and sizes of pumices. An upward coarsening of both pumice and lithic clasts is evident through the Ongatiti Ignimbrite (Wilson, 1986; Brink, 2012).

Different ages have been proposed for the Ongatiti Ignimbrite by several authors in the varied areas of the TVZ (Table 1.2).

Table 1.2: A summary of published age data for the Ongatiti Ignimbrite suggested by different authors

Author	**Age (Ma)**		**Method**
Soengkono *et al.* (1992)	1.25±0.09		K/Ar on hornblende
Pringle *et al.* (1992)	1.251 ± 0.060		$^{40}Ar/^{39}Ar$ on feldspar
Briggs et al. (1993)	1.23±0.02		Ar/Ar on feldspar
Houghton et al. (1995)	1.21±0.04		$^{40}Ar/^{39}Ar$ on feldspar
Black *et al.* (1996)	1.25±0.12		ITPFT[1]
Lowe et al. (2001)	1.28 ± 0.11		Zircon fission track
McCormack et al. (2009)	1.21±0.04		$^{40}Ar/^{39}Ar$
Briggs *et al.* (2005a)	Plateau age	1.32±0.01	$^{40}Ar/^{39}Ar$ on feldspar
	Isochron age	1.34±0.02	$^{40}Ar/^{39}Ar$ on feldspar

[1] ITPFT=Isothermal plateau fission track age on glass

Briggs *et al.* (2005b) identified two small outcrops of the welded portion of the sequence in the Tauranga Basin (west of the Wairoa River). He used Ar/Ar dating to determine 1.32±0.01 Ma (plateau age) or 1.34±0.02 Ma (isochron age) for the ignimbrite. In this study, using a different dating method, (U-Th)/He, new data from three locations of the Ongatiti Ignimbrite, are presented in Chapter 3.

Chapter Two

Methods

2.1 Computer mapping and field facies analysis

Fieldwork was carried out during 2015 to 2016. Field work initially involved selecting key outcrop exposures of the Ongatiti Ignimbrite distributed spatially around the MVC; and also, beyond map-forming units, to known exposures of the correlative unit known as Oparau Tephra (Lowe et al., 2001).

Stratigraphic logs were constructed at eight sites (Figure1.1) located on the northern and western side of the Mangakino Caldera and at varying distances from the caldera margin. Observations of facies included the outcrop appearance and contact relationships, degree of welding, geometry of bedforms and grain size grading, grain textural characteristics (size, sorting and roundness), lithic and pumice fragment sizes, types and their abundance, and free crystal types and their abundance, defined macroscopically in the field.

The maximum visible thickness at each site was measured, and textural characteristics were made typically at every one-metre interval or where texture changed. The maximum pumice and lithic clasts sizes were measured by taking the length of the maximum axes, and the aspect ratio of five largest clasts at the same stratigraphic height. The percentage abundances of the pumice and lithics were estimated visually using a comparison chart.

GIS mapping involved the application of available digital datasets to generate two and three-dimensional GIS-based maps of the distribution of the Ongatiti Ignimbrite. A DEM with a pixel size of 80 m was generated (source data from https://koordinates.com) for the study region and a digital geological map (scale 1:250,000) in the format of a vector-shape file was acquired from GNS Science QMap Geological map series (Heron, 2014) and modified for use in this study. Additional sources of data, including digital geomorphologic, drainage and boundary maps, obtained from Land Information New Zealand (LINZ) (http://data.linz.govt.nz), Landcare Research, Statistics New Zealand and Ollivier and Company (http://www.ollivier.co.nz), have been used in this study. Digital datasets were processed using Esri® ArcMap 10.3, and distances and areas were calculated to help explain

the role of paleotopography in the distribution of the ignimbrite.

2.2 Two dimensional microtexture

In total, 241 thin section were prepared from samples of bulk ignimbrite (169 samples), pumice clasts (61 samples) and lithics (12 samples). The thin-sections were analysed under microscope in both plane and cross-polarized light. Fifty thin-sections were polished, and these were used for SEM, BSE, EPMA and LA-ICP-MS methods.

2.2.1 Componentry and microscopic petrography

Systematic petrographic observations and point counting were undertaken on selected samples of bulk ignimbrite and pumice based on field location and stratigraphic position, and over the range of different types of pumice. The ignimbrite components comprise pumice fragments, crystals, lithics and matrix (glass shards). Components of pumice include phenocrysts, glass, vesicles and lithic fragments.

The components of ignimbrite <2 mm in size were quantified by point counting with a minimum 300 counts per thin section. Detailed studies on bulk ignimbrite documented crystal abundance, shape and size; lithic type, abundance and size; pumice abundance, size and types; and glass shard percentage and shape. Within pumice fragments, the phenocryst abundance, shape and type; as well as glass and vesicle percentage, and rare lithic clasts were documented.

2.2.2 Grain size analysis of ash layer

The grain size distributions of two thin ash layers found within the Ongatiti Ignimbrite at the Hinuera Quarry locality were determined by a Malvern Mastersizer at the University of Waikato.

2.2.3 Scanning Electron Microscopy (SEM)

SEM imaging using both secondary electrons and backscattered electrons (BSE) was used to observe the morphologies and micro-textures of the pumice fragments and components within the bulk ignimbrite matrix. Energy dispersive spectrometry (EDS) was used for obtaining elemental data of different components.

Two different types of samples were analysed by SEM. Polished thin sections of matrix and pumice were selected for BSE images and EDS analyses.

For visualizing the texture and morphology of matrix particles and pumice using secondary electron images, small size specimens (~1×1×1 cm) were extracted from fresh surfaces of selected samples.

Both sample types were mounted onto sample stubs using double-sided tape then coated in platinum using a Hitachi E1030 ion sputter coater.

SEM was carried out using the Hitachi S-4700 field emission SEM at the University of Waikato. For image acquisition, accelerating voltages were set at 5, 15 and 20 kV in secondary electron mode and for BSE it was set at 15 kV at different magnifications.

2.3 Three dimensional microtexture

2.3.1 Synchrotron X-ray microtomography

Synchrotron X-ray computed microtomography (μ-CT) in synchrotron X-ray μ-CT on the IMBL beam line at the Australian Synchrotron (Figure 2.1) was used for the first time to image the microtexture of ignimbrite matrix using the Ongatiti Ignimbrite as a case study. To resolve the bulk microtexture of ignimbrite at different grain size scales, from different locations, and to resolve the morphology of some key ignimbrite components were used. Various pumice types from the Ongatiti Ignimbrite were also examined.

Synchrotron X-ray source radiation enables sharper images of a large number of samples of varying textures, compared to other X-ray sources. There are two main advantages of using synchrotron X-ray sources for this study. Firstly, modern synchrotron X-ray sources were able to scan and obtain three-dimensional images in a shorter time, while maintaining high resolution, which means a larger number of samples could be analysed. Secondly, ignimbrites are texturally complex with varying particle sizes and shapes, and complex particle-particle contacts. A high intensity, monochromatic synchrotron X-ray beam could produce a sharper, better-contrasted image of the ignimbrite components, over conventional laboratory μ-CT sources (Voltolini *et al*., 2011; Baker *et al*., 2012).

Conventional methods of characterising ignimbrite microtexture have been limited to two-

dimensional optical and scanning secondary electron and back-scattered electron microscopy (SEM, BSE) on rock thin-sections. The three-dimensional microtexture of other volcanic materials (e.g. pumice, scoria, volcanic bombs) has been characterised using computed microtomography from various beam sources including synchrotron X-rays (Song *et al*., 2001; Shina *et al*., 2005; Polacci, *et al*., 2006; Shea *et al*., 2010; Giachetti *et al*., 2011; Voltolini *et al*., 2011; Baker *et al*., 2012; Schipper *et al*., 2013; Cronin and Torres-Orozco, 2013; Pardo *et al*., 2014). The ash matrix of ignimbrite, which has not yet been studied by microtomographic methods, has a complex and variable framework of glass shards, pumice fragments, crystals, rock fragments and interstitial pore space.

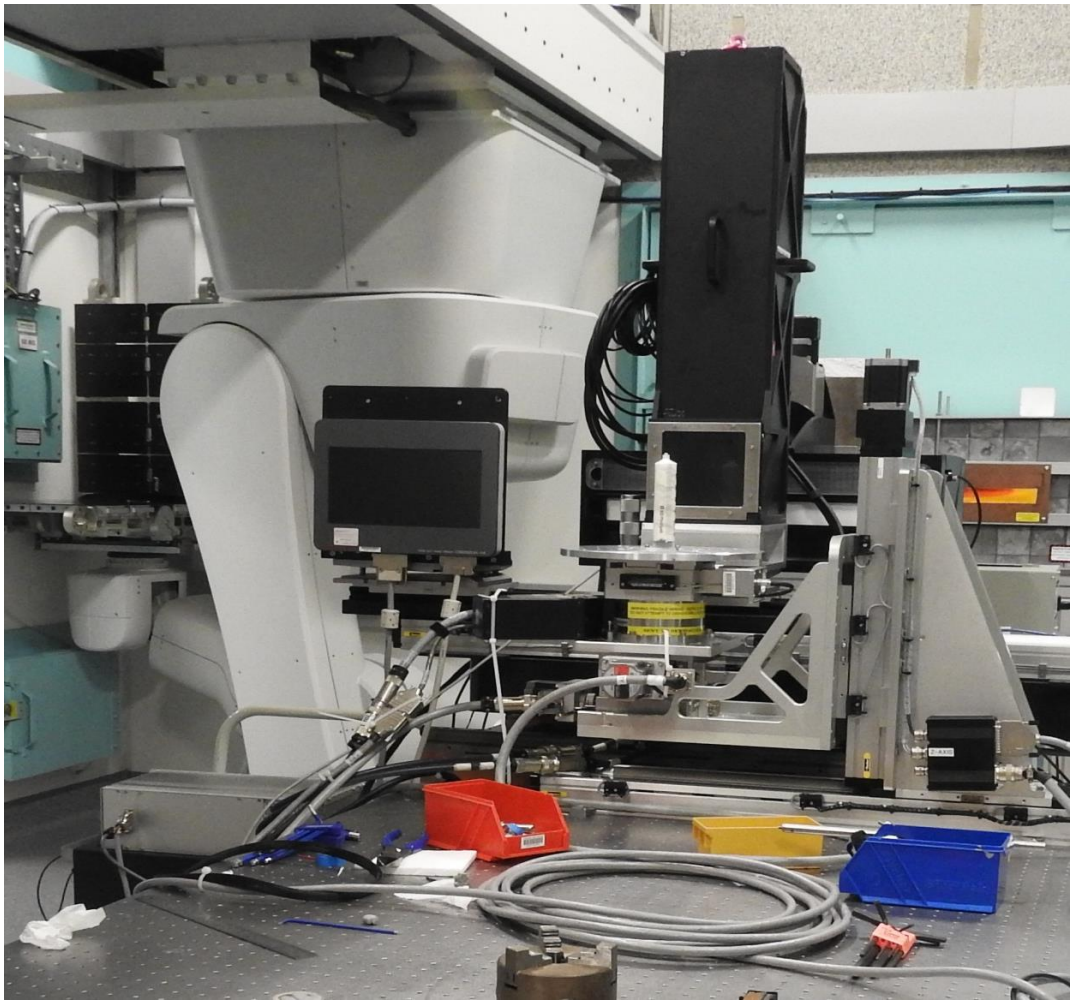

Figure 2.1**:** A view of the sample stage and detector in the 3B hutch (Ruby detector) of the IMBL facility of Australian Synchrotron

Nine pumice, 20 ignimbrite matrix, and two distal tephra samples were scanned (Table 2.1). At the beginning of the session, all of the samples to be scanned were laid out and sorted into three size categories: small (<24 mm diameter), medium (<54 mm diameter) and large (<117 mm diameter).

The beam used was the mode 3B beam in the nMono spectrum. The detector used was Ruby with 150 mm lens and 12-μm scintillator, and the object-to-detector distance was set at 30 cm. During each acquisition the following sequence occurred: (1) 40 dark scans (beam shut) and 40 flat scans (beam open, sample removed) were acquired; (2) the sample was rotated 180˚ and 1800 projections were acquired, and (3) 40 dark scans and 40 flat scans were acquired again. For samples that were longer (vertically) than the field of view, step 2 was repeated in a series of overlapping steps.

Table 2.1: List of samples, their locations, types (BR, bulk rock; Pum, pumice; Tep, tephra) and dimensions that were scanned at the Australian Synchrotron.

Name	**Location**	**Type**	**size (cm)**
C2	Castle Rock	BR+Pum	5×3×1.5
C16	Castle Rock	BR	2×1.5×1.5
C18	Castle Rock	BR	2×1.5×2
C25	Castle Rock	BR	3×3×1
T1	Tauranga	BR	1.3×1×1.5
T5	Tauranga	BR	2×2×1.5
TK13	TeKuiti	BR	2.5×1.5×1.5
TK28	TeKuiti	BR	2×2×1.5
TK27	TeKuiti	Pum	6.5×2.5×2
Tk31	TeKuiti	Pum	2×4×1
H1	Hinuera Quarry	Pum	1.5×1×1
H3	Hinuera Quarry	Pum	2.5×3×2
H1-2	Hinuera Quarry	BR	2×2×1
H1-7	Hinuera Quarry	BR	4×4×5
H1-16	Hinuera Quarry	BR	10.5×4×11.5
H2-6	Hinuera Quarry	BR	2×2×1
H1-17	Hinuera Quarry	BR	1×1×2.8
N12	Waipari Gorge east	BR	2×2×1
N15	Waipari Gorge east	BR	1.5×3×1.5
N14	Waipari Gorge east	Pum	17×12×11
W2	Waipari Gorge west	Pum	5.5×2×2
W6	Waipari Gorge west	Pum	2.5×2×3
W11	Waipari Gorge west	BR	3×2×1.5

w12	Waipari Gorge west	BR	2×2.5×0.5
W14	Waipari Gorge west	BR	1.5×2.5×2
W38	Waipari Gorge west	BR	2×2×1.5
Opa	Oparau	Tep	2×3.5×4
K2	Kawhia	Tep	4×4.5×2
P3	Waikato River	BR	3.5×2.5×2
P1	Waikato River	Pum	5.5×5.5×2.5
P2	Waikato River	Pum	4.5×4.5×3

Large and medium-sized samples were scanned individually; they were contained in a suitable-sized plastic container and supported with bubble wrap and tissue paper (Table 2.2). Small-sized samples were stacked vertically in a ~2.5 mm-diameter tube (2 to 4 samples in the tube), wrapped individually in tissue paper and separated by bubble wrap; the tube was scanned completely in serial steps.

Projections were processed by incorporating the dark and flat scans, and serial step images were stitched. All samples were processed to this stage. Vertical projections were then reconstructed into horizontal slices (32-bit) using XLICT Workflow software. Some problems were encountered with the reconstructions (e.g. ring artefacts), but parameters to minimise these effects were considered for selected samples. Slice images for each sample were visualised collectively, enhanced (e.g. brightness, contrast) in FIJI, and saved as 8-bit files. Then the image data were imported into Drishti for visualization of 3D models of the samples.

Table 2.2: Beam and acquisition parameters for each sample size

	Large samples	Medium samples	Small samples
No. of samples	4	5	28 (8 stacked tubes)
Beam	80 keV	50 keV	30 keV
Pixel size	50.5 μm	21 μm	9.43 μm
Projection image size	2320×701 pixels	2560×1650 pixels	2560×1650 pixels
Serial step interval	20 mm	20 mm	15 mm
No. of serial steps	3 to 8 steps	2 to 4 steps	7 to 8 (one 4) steps
Acquisition speed	0.5625 deg/s	0.5625 deg/s	0.3 deg/s

2.4 Geochemical methods

Several chemical analytical methods were carried out on the ignimbrite and pumice samples including electron probe microanalysis (EPMA), X-ray fluorescence (XRF) spectrometry and laser ablation inductively coupled mass spectrometry (LA-ICP-MS).

2.4.1 X-ray fluorescence spectrometry (XRF)

XRF spectrometry was undertaken on different types of pumice, and across different locations and stratigraphic sections. Major and trace element geochemical analysis were analysed using the Bruker Tiger S8 instrument at the School of Science, University of Waikato. Thirteen pumice samples were dried overnight at 100°C and then ground to fine powder using a tungsten carbide ring mill. The powdered samples were made into fused disks by combining 0.8 g of pumice powder with 8 g of LM100 flux. Fused disks were used to measure the major element concentrations.

To measure loss on ignition (LOI), ~ 1-2 g of sample placed in a crucible was heated to 1100 °C for 1 hour and the weight difference was measured before and after heating.

Trace element concentrations were measured using pressed pellets that were made by mixing ~7-8 g of sample powder with 20-25 drops (~0.85 g) of PVA binder and then pressing into an aluminum cup by a hydraulic press. Then to remove the binder the prepared pellets were heated to 70°C for at least two hours.

2.4.2 Electron Probe Microanalysis (EPMA)

The major-element composition of volcanic glass within 14 polished thin-sections was analyzed by using the JEOL JXA-8230 SuperProbe Electron Probe Microanalyser at the School of Geography, Environment and Earth Sciences, Victoria University of Wellington, together with in-house and international standards. Glass shards within the ignimbrite matrix and glass from pumice were analysed (Table 2.3).

Polished thin-sections were coated in carbon for conductivity. For glass analyses an electron gun voltage of 8 kV, a probe diameter of 3 μm for glass particles <10 μm in size, and a 1000 pA beam current were set.

Table 2.3: Sample names and, for each sample, the number of glass shards and points on pumice glass that were analysed by EPMA (H: Hinuera section, T: Tauranga section, P: Peacocks section or Waikato River, N: Waipari Gorge East, W: Waipari Gorge West, and Tk shows samples from Te Kuiti sections)

Sample	No. of shards analysed	No. of glass points on pumice analysed
H1-2	8	3
H2-6	5	5
H1-17	4	6
H7	0	6
H1	0	5
T1	7	3
T5	5	5
P3	4	1
P4	0	4
N5	5	5
W19	0	4
W20	7	4
Tk4	5	5
Tk8	0	6

2.4.3 Laser Ablation Inductively Coupled Plasma Mass Spectrometry (LA-ICP-MS)

The same thin sections that were analysed by EPMA were also analysed by LA-ICP-MS for determination of trace and rare earth element concentrations of volcanic glass. However, the individual points (glass shards and pumice spots) that were probed by LA-ICP-MS were different from the individual points analysed by EMPA.

A Resolution SE series Excimer 193 nm laser and an Agilent 8900 Triple Quadrupole inductively coupled plasma mass spectrometer in the School of Science, the University of Waikato, was used. The NIST612 and NIST610 glass standards were used for calibration. Glass standards were analysed at the start and end of each analysis session, and after approximately every 10 unknowns. The acquired data were processed using Iolite V 3.32.

2.5 Chronology

2.5.1 Zircon dating

To determine an independent age for the Ongatiti eruption at different sites, the (U-Th)/He radiometric dating method on zircons was applied. The different stages of sample preparation and zircon separation undertaken in the School of Science at the University of Waikato are listed below.

1. At 50°C, 2.5 kg of fresh bulk rock was dried in an oven.
2. Dried samples were crushed by rock-jaw crusher and Bico mill, and ground to approximately 0.5 mm diameter particles.
3. The sand size particles were washed, and four distinct fractions were separated based on different density using a Gemini Table (sample tray at 55 Hz, table at 22 Hz).
4. After overnight drying, fractions were divided into magnetic and non-magnetic particles using a Franz isodynamic vertical magnetic separator (at 1.0 A).
5. By applying a heavy liquid (sodium polytungstate-SPT-powder mixed with distilled water) with a specific gravity between 2.85 to 3.01 $g.cm^{-3}$, the light and heavy non-magnetic minerals were divided.
6. For further magnetic separation of the remaining heavy minerals, a Frantz inclined magnetic separator (15° front-to-back, 10° side-to-side, 0.5 A) were used as the final stage of separation.
7. For the last step, zircon crystals were picked under the microscope and the best and ideal zircon crystals (inclusion free, unbroken and wider than 60 μm) were picked under the microscope.

Zircons were sent to Dr Martin Danišík at Curtin University (Western Australia) and their individual ages were determined by the (U-Th)/He method according to Danišík *et al*. (2012, 2017).

2.6 X-ray powder diffraction (XRD)

For further determination of primary and secondary minerals within the Ongatiti Ignimbrite, XRD analysis was undertaken on 13 whole rock ignimbrite samples based on stratigraphic

position and across different locations. Samples (approximately 10 g each) were dried in an oven at 50°C overnight, and then by using the tungsten-carbide ring mill they were crushed into a fine powder. The dried powder samples were processed within the PANalytical Empyrean XRD machine in the School of Science and School of Engineering, University of Waikato. They were run using a copper K_α source for 2-80° (2Θ), at 50 seconds per step and the results then processed using Highscore Plus software.

2.7 Pumice vesicularity

Pumice fragments from different sites and lithofacies were selected for determining pumice vesicularity. Bulk pumice vesicularity was measured using the water immersion method of Houghton and Wilson (1989). Connected and isolated vesicularity on the sample clasts were measured by using a Quantachrome Ultrapycnometer in University of Waikato, Science school. The solid density was measured on the pycnometer using powdered samples.

To provide comparative data on the vesicularity, some polished thin sections were imaged using BSE and SEM for quantitative image analysis.

2.7.1 Clast bulk vesicularity

The bulk density of pumice clasts was determined by calculating the difference between the sample weight in air and in water (Houghton & Wilson, 1989). Then vesicularity was estimated by applying the dense rock equivalent (DRE) density and bulk density. The selected pumice clasts were dried for one night at 100°C and weighed in air as dry weight. They were then wrapped in one or more parafilm wax sheets.

After wrapping, the samples were weighed in water. Most pumice samples required lead ballast/s for floating prevention.

The specific gravity, S_g (or bulk density), and bulk vesicularity, V, of the samples were calculated by using the formula:

$$Sg = \frac{\mathrm{Wac}}{\mathrm{Wac} + \mathrm{Wws} - (\mathrm{Wcsb} - \mathrm{Wwb})}$$

and

$$V = \frac{100(\text{DRE density} - Sg)}{\text{DRE density}}$$

where weight of clast in air is W_{ac}, weight of the sheet in water is, W_{ws}, weight of the clasts, sheet and ballast in water is W_{csb}, and weight of the ballast in water is W_{wb}; and DRE density is the dense rock equivalent density (or solid density) See section 2.7.3 for method of determining solid density.

2.7.2 Connected vesicularity

Pumice clasts, being porous materials, are penetrated by gas provided by a gas-pycnometer, which calculates the volume accessed by the flowing gas. The gas accessibility of the connected pores in pumice is called the connected vesicularity and obtained density is named "solid density". The isolated vesicularity is the percentage of vesicles not accessed by gas. Nitrogen was used for gas-pycnometry.

Before each session on the gas-pycnometer, calibration of the sample cell volume, V_C, and added volume V_A, was carried out in ambient temperature. Maximum accuracy was achieved by frequent successive calibration runs.

After calibration, each sample was weighed. The pycnometer then measured the sample volume and its density was determined using the entered mass.

2.7.3 Solid density

To obtain the solid density, the dried pumice samples were crushed and run through the pynometery analysis of the powder. The solid density is considered as the dense rock equivalent (DRE) density.

The DRE density of our rhyolitic pumice was measured as 2.7 g/cm^3 in Waipari Gorge East and Waipari Gorge West and 2.6 g/cm^3 for other locations.

2.8 Cooling experiment

An experiment on two different grain size fractions of a volcanic ash deposit obtained from the TVZ was examined to test a hypothesis suggesting a relationship between grain size and degree of welding. Ash materials were separated on the basis of the grain size into two

groups, one group made up of coarse ash particles with a median size of 1.5–1.75 φ and the other was fine ash with a median size of 4.25–4.5 φ (grain sizes based on Fisher, 1961). Both size fractions had a volume of 80 cm^3 and they were heated to 200°C in an oven over night. A temperature probe was put inside the sample containers, and temperatures were measured repeatedly outside the oven during a total cooling period of 150 minutes. The temperature was measured every one minute for the first 60 minutes during a fast cooling rate. However, after 60 minutes, the time between recordings increased gradually until 150 minutes, when the temperature was stable.

Chapter Three

Mobility and emplacement of an ancient, large-volume pyroclastic flow, Ongatiti Ignimbrite, North Island, New Zealand

3.1 Introduction

Pyroclastic flows are hazardous phenomena that bury topography around volcanic centers. They originate from explosive volcanic eruptions and can travel more than 100 km from the source (Cas & Wright, 1987). Some ancient and giant pyroclastic flows, however, have been generated by a super-eruption. A super-eruption is described as having an ejected magma mass larger than $1x10^{15}$ kg and for rhyolitic eruptions is estimated to have produced a dense rock equivalent (DRE) erupted magma volume of more than 450 km^3 (Sparks *et al.*, 2005; Self, 2006; Miller & Wark, 2008; Heron, 2014). The volume and distribution of materials from super-eruptions, and hence their power of destruction, are significantly higher than other volcanoes (Miller & Wark, 2008; Wilson, 2008).

The Ongatiti Ignimbrite is one of the more voluminous rhyolitic ignimbrites in the North Island of New Zealand and was deposited during a super-eruption (e.g. Martin, 1961; Wilson, 1986; Briggs *et al*., 1993; Houghton *et al.*, 1995; Wilson et al., 2009). It is has generally recognized as a welded to non-welded, columnar-jointed and cliff-forming deposit exposed in the western North Island around and beyond the Mangakino Volcanic Centre (MVC), its source caldera.

This study investigates the proximal, medial, and distal emplacement processes, topographical controls and distribution of welding of the Ongatiti Ignimbrite. Field-based stratigraphic and facies characteristics are described and assessed with GIS data and a digital elevation model (DEM) of the deposit, and a new volume is estimated. A new (U-Th/He) age is also presented and discussed with respect to existing ages.

Analysis of mineralogical and geochemical characteristics, matrix/glass shard microtextures and physical characteristics of pumice fragments are reported later.

3.2 Geological Setting

3.2.1 Mangakino Volcanic Center (MVC)

The NNE-SSW trending Taupo Volcanic Zone (TVZ) is approximately 300 km long and 60 km wide and is located in the central part of the North Island. This volcano-tectonic area has been active for around two million years and has produced at least 34 caldera-forming ignimbrite eruptions and a wide range of minor eruptions from at least eight rhyolitic centres (Healy, 1964; Houghton *et al.*, 1995; Allan *et al.*, 2008).

The earliest rhyolitic caldera, situated on the western border of the TVZ, is the Mangakino Volcanic Centre (MVC) (Wilson *et al.*, 1984; Houghton *et al.*, 1995). The MVC (Figure3.1) was initially characterized as a volcanic centre by Blank (1965) and this was subsequently confirmed as a caldera by Rogan(1982) based on a gravity anomaly. The caldera has produced voluminous deposits measuring >1000km^3 (DRE); however, due to erosion and burial by new deposits, dominantly lacustrine and fluvial sediments and younger ignimbrites and tephras, the surface morphology of the caldera is poorly defined (Briggs, 1976; Stern, 1979; Rogan, 1982; Briggs *et al.*, 1993; Wilson *et al.*, 2009; Wilson & Rowland, 2016).A digital elevation model for the MVC is illustrated in Figure3.2.

Widespread, densely welded to welded ignimbrites, fall deposits, and minor lava domes comprise the succession of eruptive units that have been produced by the MVC (Wilson, 1986; Briggs *et al.*, 1993; Houghton *et al.*, 1995). Data obtained through $^{40}Ar/^{39}Ar$ age dating from MVC deposits display two distinct eruptive phases: the first period from1.6 to 1.5 Ma and the second between 1.21 to 0.95 Ma.

Figure 3.1: Photograph taken across the plateau that lie geographically above the Mangakino Caldera towards the southwestern caldera rim in the horizon. Titiraupenga and Pureora volcanic peaks can be seen in the centre. The flat land in the foreground, and on the horizon to the left of Titiraupenga, are underlain by the Whakamaru Ignimbrite, and younger pyroclastics, which now bury the Mangakino Caldera. Outflow ignimbrites, including those from the Mangakino and Whakamaru calderas, form the raised plateau on the horizon to the right of Titiraupenga. To the far right are raised Jurassic basement ranges.

The Ongatiti Ignimbrite is one the major ignimbrites that was emplaced during the second eruptive phase of MVC (Houghton *et al*., 1995).

3.2.2 Ongatiti Ignimbrite and its age

Martin (1961) first described the Ongatiti Ignimbrite as a welded, massive, crystal-rich ignimbrite consisting of abundant feldspar, quartz, and opaque minerals. He presented the type section above the Ongatiti Stream where the Ahuroa Road descends the southern slope of Rocky Hill, Pakaumanu Survey District (N83/282474, the old NZMS 1 grid reference map at scale 1:63,360).

Later studies on the Ongatiti Ignimbrite (e.g. Briggs *et al*., 1993; Houghton *et al*., 1995;(McCormack *et al.*, 2009); Leonard *et al.*, 2010; Cooper & Wilson, 2014),described it as a widespread, compound non-welded to partially welded, vitrophyric pumice- and crystal-rich, rhyodacitic to rhyolitic ignimbrite with moderate lithic clast content exposed mostly in western areas of the central North Island (Edbrooke, 2005; Leonard *et al.*, 2010) although it also occurs in eastern North Island (Briggs *et al*., 2005). The commonly accepted age for this extensive ignimbrite is 1.21±0.04 Ma (derived using Ar/Ar single-crystal laser fusion dating on a feldspar separate by Houghton *et al.*, 1995). Such an age is generally supported by age data summarised by Lowe et al. (2001) that include radiometric ages based on zircon fission track analysis (1.28 ± 0.11 Ma), isothermal-plateau fission track analyses on glass (1.25 ± 0.12, 1.23 ± 0.09 Ma), a K-Ar age on a hornblende separate (1.25 ± 0.09 Ma), and three ages based on Ar/Ar single-crystal laser fusion on feldspar separates (1.251 ± 0.060, 1.23 ± 0.02, and 1.24 ± 0.07 Ma).The error-weighted mean age for these samples, together with that of Houghton *et al*. (1995), is 1.231 ± 0.016 Ma (n = 8) (Lowe et al., 2001).Most recently, Briggs

et al. (2005) dated it to 1.32 ± 0.01 Ma and1.34 ± 0.02Ma using Ar/Ar analyses of feldspar separates. In addition, the deposit is magnetically reversed, lying in the Matuyam Chron >0.783 Ma(Black *et al.*, 1996; Lowe *et al*., 2001; Mark *et al*., 2017).Its volume (as deposited material) has been recorded as>300-1000 km^3(Wilson, 1986; Briggs *et al*., 1993; Houghton *et al.*, 1995). New data on both age and volume are presented here.

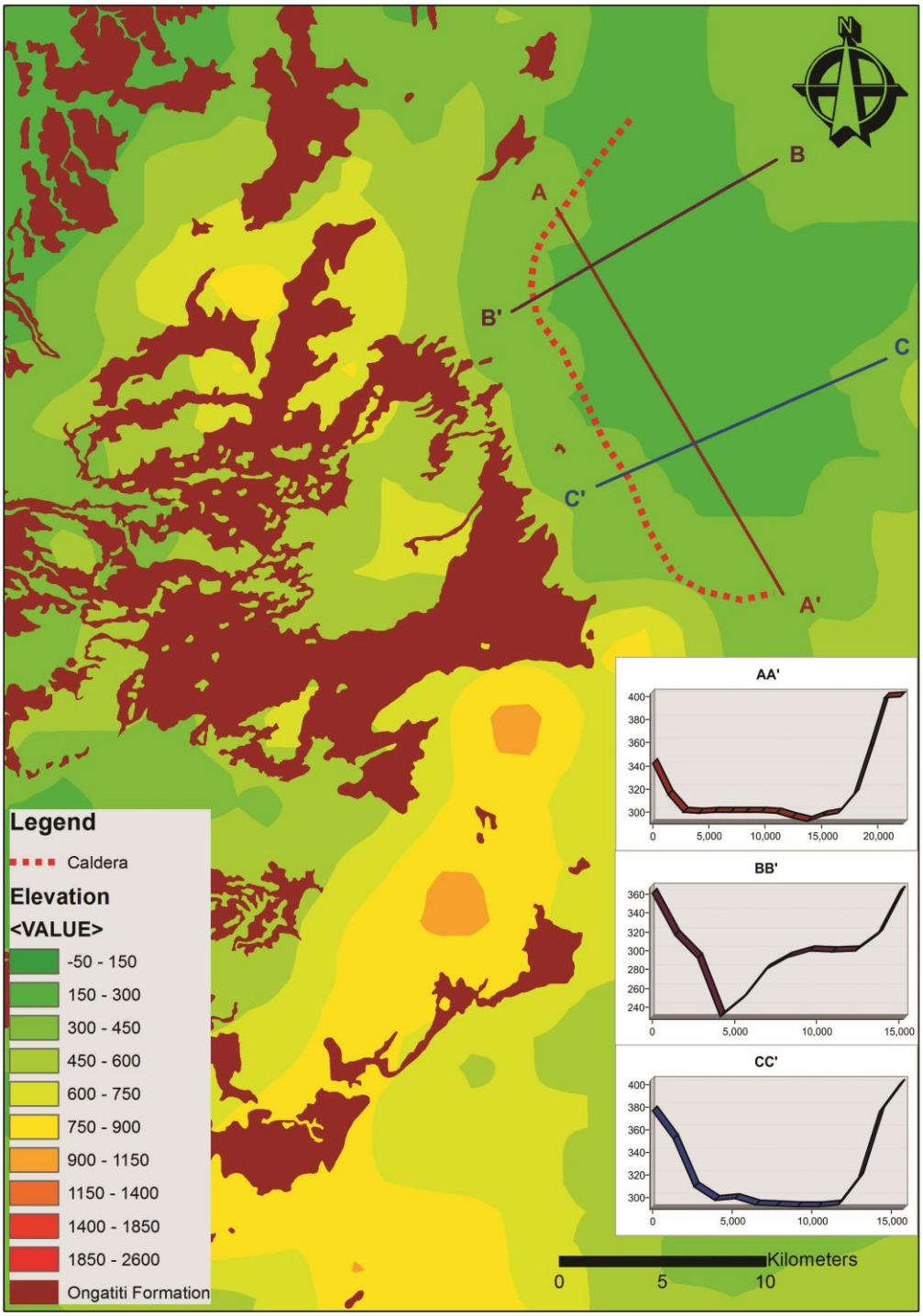

Figure 3.2: A digital elevation model (DEM) of the areas near Mangakino Volcanic Centre (MVC) and the distribution of the outflow deposits of the Ongatiti Ignimbrite. Three profiles AA', BB', and CC' represent the elevation model (in metres above sea level) of the MVC. Vertical axes at profiles and horizontal axes on the profiles show the depth and distance to the MVC, respectively.

Briggs *et al*. (1993) reported that the Ongatiti Ignimbrite is composed of multiple flow units erupted in a series of directional lobes, and Wilson (1986) divided it into two facies: a lower highly energetic, violent and pumice-poor pyroclastic flow facies and an upper less energetic coarse-grained pumice-rich pyroclastic flow facies (Wilson, 1986; Briggs *et al*., 1993).

Distal deposits correlated to the Ongatiti Ignimbrite are called the Oparau Tephra (equivalent to member K12 of the Kauroa Ash Formation) in the west of the central North Island (Pain, 1975; Horrocks, 2000; Lowe *et al.*, 2001). Equivalent distal tephra around Auckland and Wellington, and in the Tauranga area, have been referred to as the Ongatiti Tephra (Alloway *et al.*, 2004; Mildenhall & Alloway, 2008).

3.3 Methods

This chapter is based on digital GIS mapping from existing datasets with follow-up field confirmation, and detailed field, stratigraphic, and facies analysis at selected sites.

Stratigraphic logs were prepared at eight sites located on the northern and western side of the Mangakino Caldera and at varying distances from the caldera margin. There were no surface outcrops on the eastern side of the caldera and any possible intra-caldera deposits have been buried. Facies observations included the geometry of bed-forms, contact relationships and grain size grading; grain textural characteristics (size, sorting and roundness), lithic and pumice fragment sizes, types and abundance; and free crystal types and abundance defined macroscopically in the field.

At each site, the maximum visible thickness was measured, and textural characteristics were made typically at every one-metre interval or where texture changed. The maximum pumice and lithic clasts sizes were measured by taking the length of the maximum axes, and the aspect ratio of five clasts. Also, the percentage abundances of the pumice and lithics were estimated through all sections.

Additionally, grain size distributions within ash layers were determined by a Malvern Mastersizer at the University of Waikato.

Digital information was used to produce the initial data for generating two and three-dimensional GIS-based maps of the distribution of the Ongatiti Ignimbrite. A DEM with a

pixel size of 80mwas generated (source data from https://koordinates.com) for the study region and a digital geological map (scale= 1:250,000) in the format of a vector-shape file acquired from GNS Science Geological Map (Heron, 2014) were modified and then used for this study. Additional sources of data, including digital geomorphologic, drainage and boundaries maps, obtained from Land Information New Zealand (LINZ) (http://data.linz.govt.nz), Landcare Research, and Statistics New Zealand and Ollivier and Company (http://www.ollivier.co.nz),have been applied to the study. Digital datasets were processed using Esri® ArcMap 10.3, and distances and areas were calculated to help explain the role of paleotopography in the ignimbrite's distribution.

(U-Th)/He dates on extracted zircon crystals were determined at Curtin University, Perth, Australia, to determine an independent age for the Ongatiti eruption at different sites.

3.4 Distribution and volume

3.4.1 Distribution

GIS-based maps of the Ongatiti Ignimbrite and its relationship to paleotopography are shown in Figures 3.3–3.6. Determining the present and original distribution of the Ongatiti Ignimbrite has limitations due to erosion of the original ignimbrite sheet and burial by younger deposits, especially on the eastern side of the source caldera where there are no exposed outcrops. Furthermore, the paleotopography prior to the ignimbrite emplacement has been modified by the Ongatiti and younger pyroclastic deposits.

As shown in Figure3.3, there is no exposure in the eastern areas of the caldera (except in Tauranga, located in northeast), nor of the intracaldera ignimbrite successions. Therefore, our assessment of distribution and volume in these areas has not been considered.

Proximal and medial deposits of the Ongatiti Ignimbrite were studied at eight locations (Figure3.4) and distal deposits at four locations. The deposits of the ignimbrite were classified into three map units (zones): '*reliable*', '*expected', and 'possible'* based on the coverage area and topography. In Figure 3.5,'reliable'and 'expected' areas are shown; 'possible 'areas are not delineated due to lack of data. The areas that show present-day exposures and cover around 1100 km^2 are classified as **'reliable'**, and mainly include proximal and medial deposits.

‘Expected' deposits include lands that were likely covered by the ignimbrite in proximal and medial regions, typically areas between reliable areas adding a further approximately 6000 km^2. On the basis of some preserved ignimbrite on the top and lee sides of hills, we assume that the proximal and medial areas were buried by the widespread pyroclastic flow deposit from high elevations to low lands.

At sites where the equivalent (correlative) distal tephra deposits were studied, we extended our estimation of the areal extent of the Ongatiti Ignimbrite. The extra area covered by distal deposits and the areas between them are defined as ‘**possible regions**’ although for reasons mentioned above these possible regions were not mapped. The measured thickness of the deposits in the ‘possible’ regions is around 3 m on average, in comparison with the thickness in reliable areas, which is generally >15 m.

According to these data, Ongatiti-equivalent tephras described around Auckland, Wellington and in Ocean Drilling Project cores (Alloway *et al.*, 2004; Alloway *et al.*, 2005; Mildenhall & Alloway, 2008) allow extension of the Ongatiti deposit to more than10,000 km^2, but the map distribution in these areas is poorly constrained, and so we did not use the last group in our quantitative estimations of the volume.

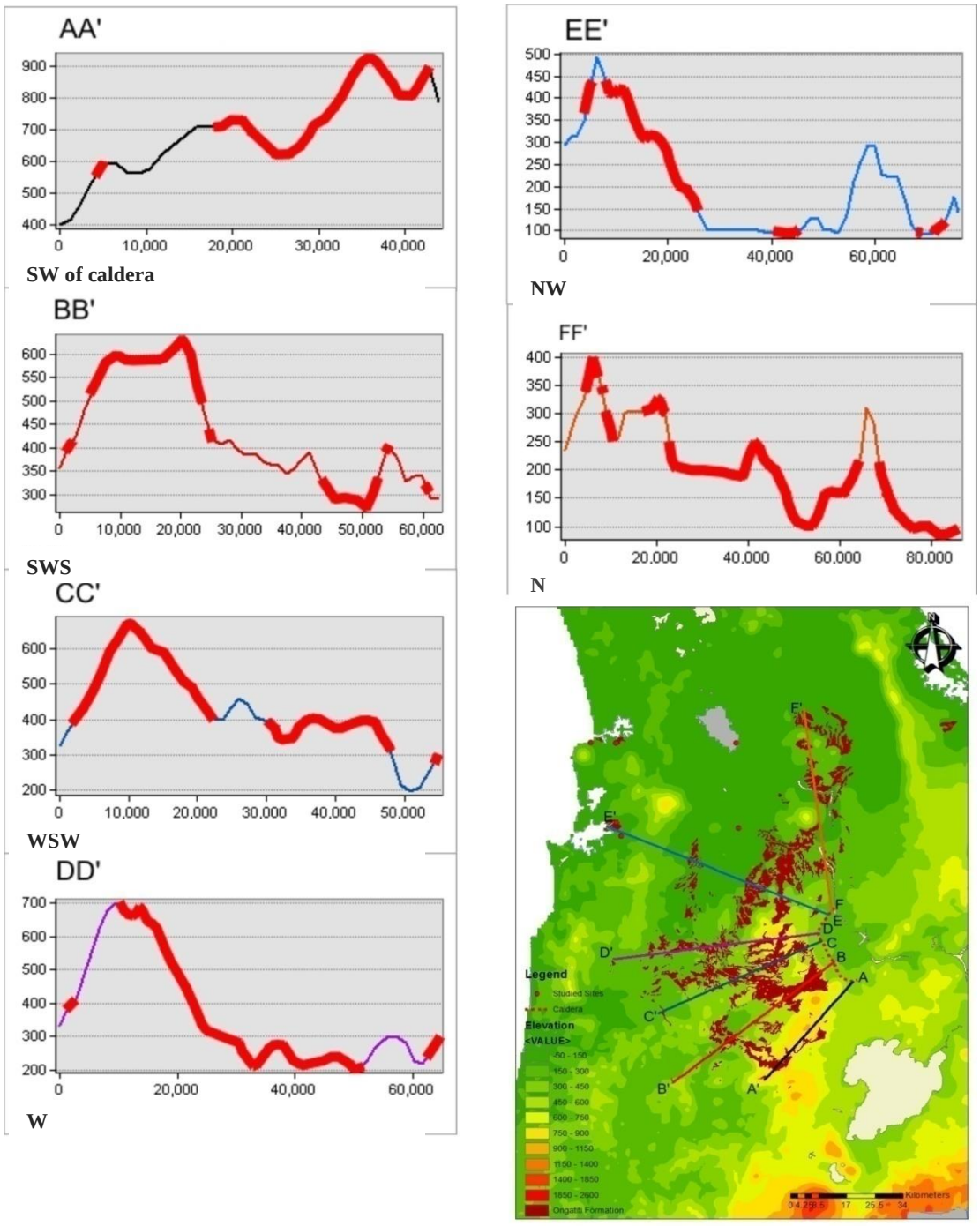

Figure 3.3: Plots showing the profiles in different directions radiating from the edge of the MVC. The thick red lines on the profiles depict the location of the present-day Ongatiti Ignimbrite and its elevation (both axes in metres). The map illustrates the direction and position of the profiles in different colors and names. X and Y axes on the profile show the distance to the caldera and elevation in metres, respectively.

In proximal areas, the ignimbrite covers both hills and valleys to a significant thickness and reaches elevations of around 900 m above sea level (asl).

Medial areas are mostly characterized by valley-filling geometries, which reach elevations of approximately 150–300 m asl. The distal equivalents (Oparau Tephra and K12 unit) were deposited at elevations of <50 m asl. The GIS-based maps presented here also indicate that the ignimbrite extends over 75 km to the NNE and ~90 km to the NW of its caldera source (Figure3.3).

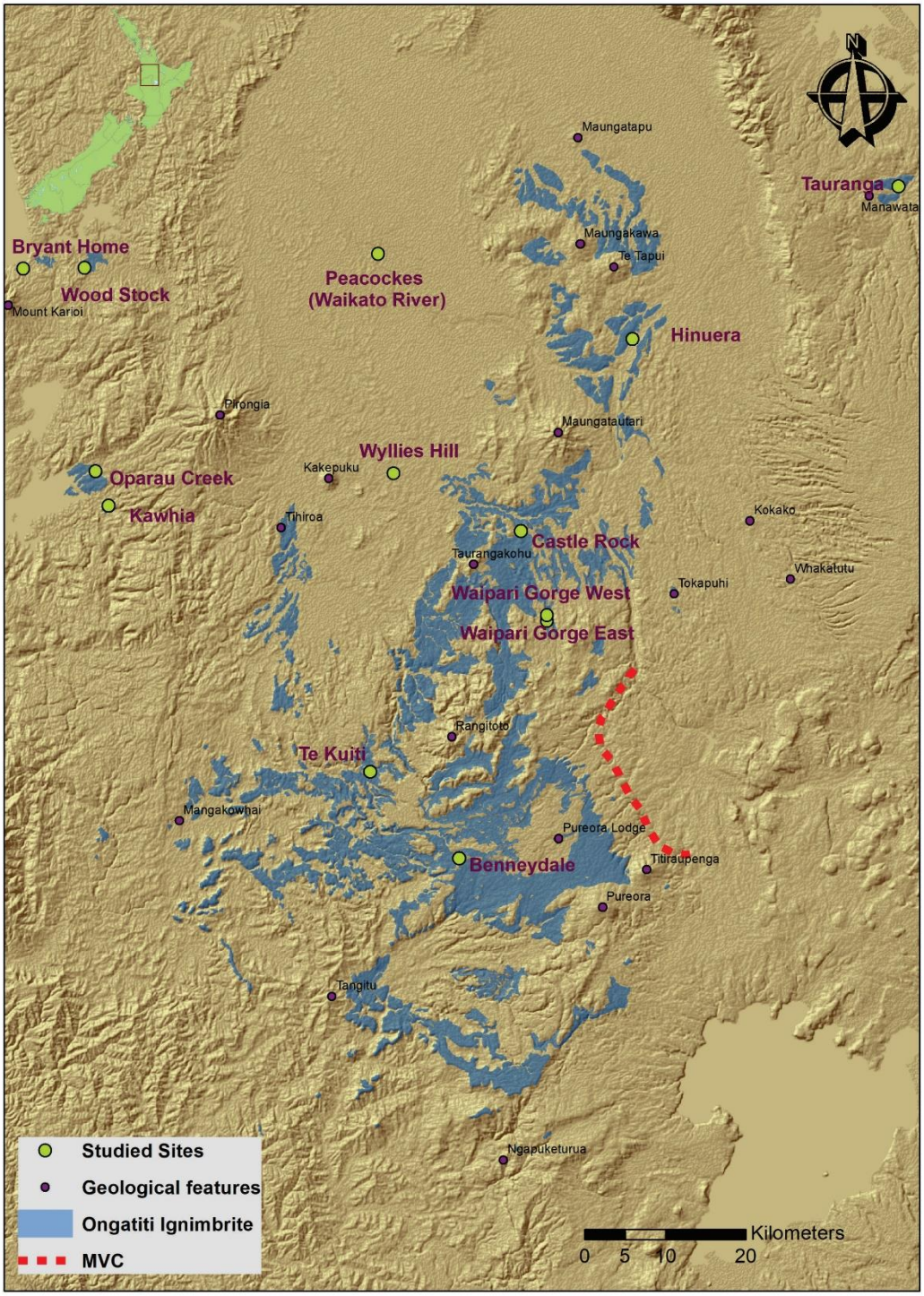

Figure 3.4**:** Distribution of the Ongatiti Ignimbrite, caldera position, and sampling locations. Blue areas depict the Ongatiti Ignimbrite and green circles show sites of stratigraphic logs and where samples were collected. The western margin of the MVC is shown by red dashed line and the solid black line illustrates proximal and medial areas.

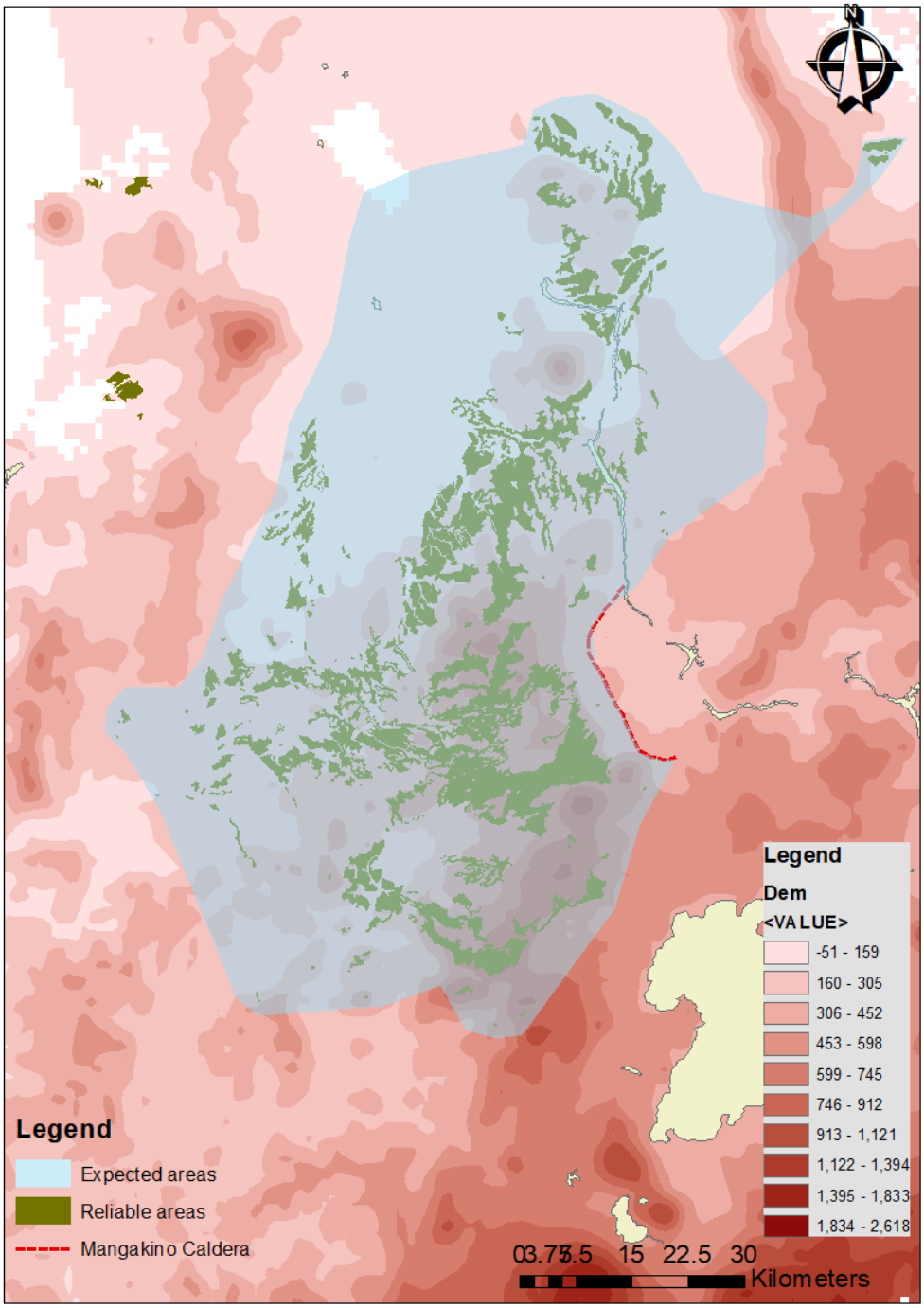

Figure 3.5: Map illustrating the 'expected' and 'reliable' zones, defined for the Ongatiti Ignimbrite based on valid GIS data and sites studied here. The 'reliable' zone (green areas) is defined on the basis of the distributions mapped in QMAP (Edbrooke, 2005; Leonard *et al*., 2010).

To estimate the aspect ratio, the aerial distribution and thickness data of the ignimbrite were used. We estimate aspect ratio of the Ongatiti Ignimbrite to be between 1:950, based on reliable distribution, and 1:1880 on the expected distribution. Walker (1983) related the

aspect ratio to the energy of a pyroclastic flow: low aspect ratio (<1:1000) types are characterized by widespread, thin deposits; and high aspect ratio (>1:1000) deposits are thick and spread locally. Our current study shows that the Ongatiti Ignimbrite is widespread, and on the boundary between low and high aspect ratio ignimbrite, but closer to the low aspect ratio type. The original deposit distribution for a low aspect ratio ignimbrite can be evaluated by drawing a single cover area around all of the present-day exposures and calculated areas; however, for high aspect ratio types, drawing multiple envelopes around the exposure is needed(Wilson, 1991; Cook *et al.*, 2016). For our calculation we have used the method for low aspect ratio ignimbrite.

3.4.2 Volume

The estimation of pyroclastic flow deposit volumes is difficult, particularly where the deposits are eroded or only proximal deposits are preserved (Pyle, 1995). The Ongatiti Ignimbrite is highly eroded, proximal and medial outcrops occur only in the west side of the source, and there is no evidence for intra-caldera deposits and co-ignimbrite ash fall (Figure3.6).Hence, calculation of the ignimbrite volume is limited, and only minimum volume estimates were made for this study.

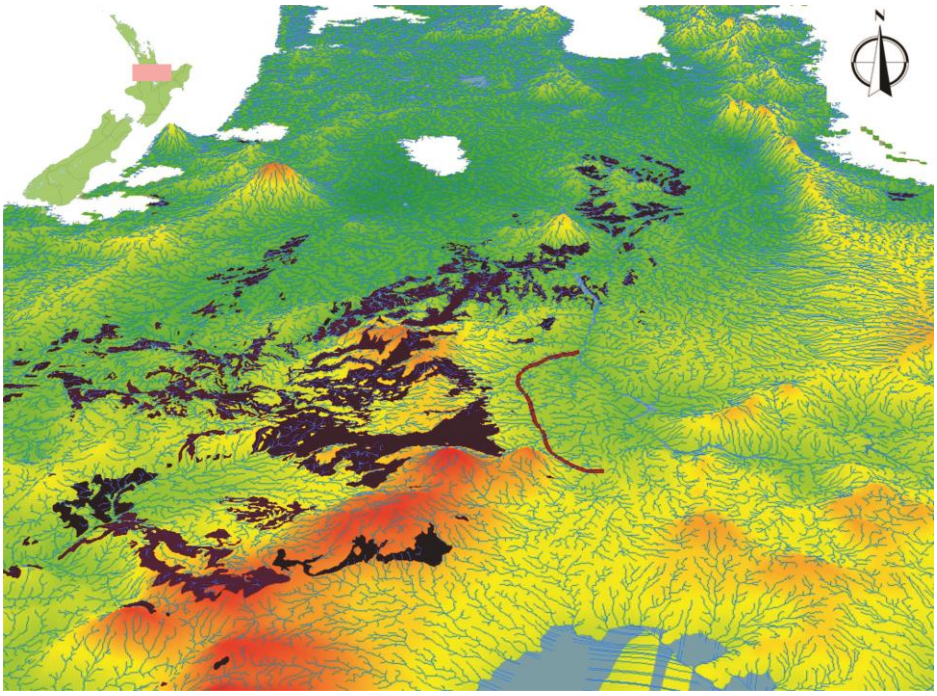

Figure 3.6: Distribution of the Ongatiti Ignimbrite in a 3D view showing the ignimbrite covering hills in proximal regions and mostly valleys in medial regions. The western boundary of Mangakino Caldera is shown by the solid red line.

For the volume estimate, we first used the expected area and average thickness at two sides of the MVC based on current outcrops of the ignimbrite in these areas. In the northern and western areas the minimum volume of the ignimbrite in expected regions (proximal and medial areas) is at least 225 km^3. For distal equivalent deposits we have applied the thickness of the tephras in studied sites and due to our estimation, the minimum volume of the Ongatiti Ignimbrite in distal areas is at least15km^3. Therefore, the estimated volume for the ignimbrite outflow deposit is estimated to be at least 240km^3(loose).

Such a large eruption should be accompanied by a large volume of co-ignimbrite ash-fall deposits (Sparks & Walker, 1977). However, no co-ignimbrite deposit has been reported by previous authors, nor in this study. An accurate volume estimation for co-ignimbrite and intra-caldera deposits is not possible. Lipman (1984) observed in western North America calderas that outflow ignimbrites are approximately equal to the volume of intra-caldera deposits. Rose and Chesner (1987) found the relation between intra-caldera, outflow ignimbrite and ash components at Toba is around 1000:1000:800 km^3. For the Oruanui Ignimbrite deposit, the calculated relationship was 420:320:430 km^3(Wilson, 1991) and Mason *et al.* (2004) summarized the volume of those two eruptions and noted that the ratio of the intra-caldera deposits, ignimbrite, and co-ignimbrite volume are generally the same. Cook et al. (2016) based on the studies of the Otowi Member of the Bandelier Tuff in Mexico has also suggested a 1:1:1 relationship.

Based on the assumptions made by these authors, we suggest that approximately 720 km^3 was the minimum volume (as deposited material) for the Ongatiti Ignimbrite deposits. Figure3.6 shows a comparison of the Ongatiti Ignimbrite with other ignimbrites based on its volume and aspect ratio.

The Ongatiti Ignimbrite is partially welded and in distal areas it is non-welded. Moon (1989) measured the average density for partially welded Ongatiti Ignimbrite to be 1725 $kg.m^{-3}$and for the non-welded deposit, 1320 $kg.m^{-3}$, and these values have been used here to calculate the dense rock equivalent volume (DRE). For partially welded ignimbrite a dense rock equivalent (DRE) factor of 0.7 was used and for non-welded a factor of 0.53 was used. Hence, the DRE volume for the Ongatiti Ignimbrite has been estimated to be 512 km^3.

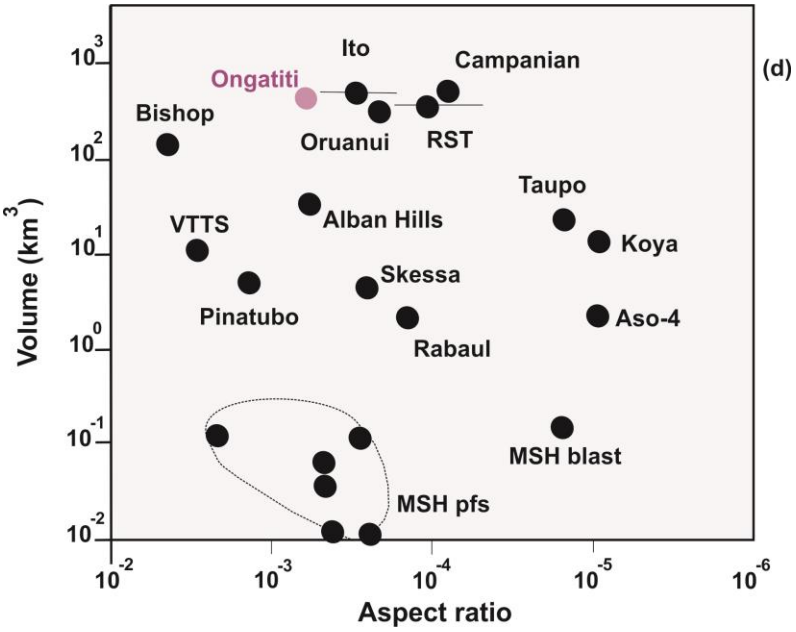

Figure 3.7: Diagram depicting the aspect ratio to volume of the Ongatiti Ignimbrite in comparison with other ignimbrites, modified after Freundt *et al.* (2000). MSH pfs, Mt St Helens post-May 1980 flows deposits and VTTS, Valley of Ten Thousand Smokes

3.5 Ignimbrite facies and stratigraphy

Plateaus were generally formed by the Ongatiti Ignimbrite, but these are now dissected and, in some areas, the ignimbrite now caps the tops of hills. The ignimbrite is commonly vertically jointed with spacing of mostly 3 to 10 m. proximally, the ignimbrite occurs both in valleys and covers hills but in medial and distal areas the deposit characteristics suggest that the pyroclastic flow was channelized through the antecedent valleys. In the following section, the deposits are described based on distance from the source at different sites.

3.5.1 Welding and jointing

The welding of pyroclastic deposits involves syn or post-emplacement degassing, compaction, and flow of glassy material (Smith, 1960; Ross & Smith, 1961; Quane & Russell, 2005). Smith (1960) described welding as a specific process that “promotes the union or cohesion of glassy fragments in a viscous state". He divided a single cooling unit into three zones: A, non-welded; B, partially welded; and C, densely welded. The boundary between A and B is identified by deformation of pumice clasts or shards and the dense welding zone can be recognized when “the rock is pore free”.

Field estimation of welding aspect ratios (AR) or flattening ratios (long/short axes lengths of pumice fragments) were used for the Bishop Tuff (Ragan & Sheridan, 1972) and the Apache Leaf Tuff (Peterson, 1979). Peterson (1979) categorized the ratios and consequently the welding zones. He described non-welded ignimbrite when they show AR<2, 2<AR<6 shows a partially welded ignimbrite, and densely welded ignimbrite can be identified by AR>6. In addition, field features and density were applied to identify five welding zones of the Bishop Tuff (Wilson & Hildreth, 2003). Quane and Russell (2005) have introduced a scheme for the intensity of welding, described as rank, which is based on features such as flattening of pumice, micro-fabric orientation, density, and porosity of the Bandelier Tuff; their rank ranges from unconsolidated (Rank I) to obsidian-like vitrophyre (Rank VI).

In this study, we made field-based measurements of pumice aspect ratios and the Peterson method was used for welding classification. On this basis the aspect ratio for the Ongatiti Ignimbrite varies between 1.5 at Peacockes (Waikato River) to 6 at Hinuera Quarry (Figure 3.4), indicating that the ignimbrite in proximal and medial areas is non-welded to partially welded.

Tension fractures that form during cooling and compaction of the ignimbrite are known as primary joints. They are mostly identified by the ratio between height and width of columns (column exposure ratio) and their polygonal cross-section. In addition, they form perpendicular to the cooling surface (DeGraff & Aydin, 1987; Moon, 1993). Columnar joints are commonly vertical in ignimbrites; although, horizontal joints are also seen in many ignimbrites (Fisher & Schmincke, 1984; Cas & Wright, 1987; DeGraff & Aydin, 1987; Aydin & DeGraff, 1988). Vertical joints are usually seen in moderately to highly welded deposits (Fisher and Schmincke, 1984).The pattern of jointing is affected by cooling in the direction of valley sides and also toward the top of the ignimbrite sequences. Hence, they are dominantly controlled by cooling and the emplacement thickness (DeGraff and Aydin, 1987; Aydin and DeGraff, 1988; Moon, 1993) and underlying topography.

We used the Moon (1989) classification for joint geometry (i.e. unjointed, columnar, blocky, and complex) for describing the Ongatiti Ignimbrite. Also, we use the definition of joint spacing by Barton (1978) as extremely close (<20mm), very close (20-60mm), moderate (200-600 mm), wide (600-2000 mm), very wide (2000-6000 mm) and extremely wide

(>6000 mm). Hence the Ongatiti Ignimbrite shows very wide to extremely wide columnar joints, with the only exception at the Peacockes site which is unjointed. Horizontal jointing was also seen at Hinuera (Hinuera Valley) and Castle Rock, both approximately in the middle of outcrops. Consequently, these terms are matched with the Fisher and Schmincke (1984) relationship between welding and jointing–that is, the partially welded to welded nature is consistent with very wide to extremely wide columnar joints.

3.5.2 Proximal-medial ignimbrite facies

Criteria including clast (pumice and lithic) size and abundance, crystals, and degree of welding are used to identify six different lithofacies in the Ongatiti Ignimbrite, which vary from proximal to distal localities (Figure 3.8a) and three tephra facies in the distal areas (Figure 3.8b).

1. *Pumice and lithic rich facies (PRLR)* is a partially welded facies that is rich in crystals and characterized by large pumice clasts (typically 100 to 450 mm in diameter) occurring in abundances of 15 to 30% of the bulk ignimbrite. Pumice clasts occur mostly as four different textural types: vesicular, wood-fiber-like (woody), dense, and rare grey pumice (Figure 3.9). The pumice fragments show two vesicle morphologies–spherical or sub-parallel elongate–and in a variety of sizes from a few millimetres to several centimetres in diameter (maximum vesicle size was measured at Waipari Gorge West at around 15 mm).The aspect ratio is mostly between 2 to 4 throughout the facies. Lithic fragments in the PRLR facies are 7–10% in abundance (Figure 3.10b) and their average size and abundance are greater at northern localities (e.g. Hinuera Quarry). They are angular to sub-angular and their maximum size was measured at Waipari Gorge West as 60 mm.

2. *Pumice-rich, lithic-poor facies (PRLP)* is a slightly welded to welded facies rich in pumice and crystals but poor in lithic clasts. The facies is characterized by the abundance and large size of sub-rounded pumice fragments, which are around 15–25% of the bulk rock and with a maximum size of 350 mm. They are mostly vesicular and woody with a cream to white color. The aspect ratio is usually between 2 to 3.5 throughout this facies. Lithic clasts are rarely seen in this facies and they are usually small; the lithic percentage is 1–2% of the bulk rock and their maximum size

is around 25 mm. The PRLP facies is found particularly to the west and north-west of the MVC (Figure 3.10 g,h).

3. *Flattened pumice-rich facies (FPR)* occurs as a welded zone with flattened pumice between intervals of both PRLR and PRLP facies (Figure 3.10c). The thickness of this zone varies from 1 to 4 m with the maximum aspect ratio around 6 and the largest pumice was measured around 400 mm. The zone is classified here as a separate facies here due to the welding texture, rather than the abundance and size of components (cf. PRLR, PRLP, PLP). Whilst, the abundance of lithic clasts is different (around 5%), the facies is still rich in pumice (cf. PRLR, PRLP).

4. *Pumice and lithic poor facies (PPLP)* is a slightly to partially welded facies that is poor in both pumice and lithic fragments. The percentage of pumice is less than 15% and the maximum size is 100 mm with an aspect ratio of 1.5 to 2. The pumice clasts are mostly vesicular with tiny vesicles and in cream and yellow colours. Lithic fragments are very rare, about 2% of the bulk rock, with a maximum size of approximately 20 mm. Units of the PPLP facies were seen in two locations in the north of the MVC: Hinuera Quarry and Tauranga at the base of the exposed section. As well, they are in the north-west at Waipari Gorge (West) and Castle Rock at the top of the deposits.

5. *Pumice-poor, lithic-rich facies (PPLR)* is a 10-15 cm thick lithic-rich layer that was seen in the base of the Waipari Gorge (East) deposit. This layer was only recognized in one location near the lower boundary of the Ongatiti Ignimbrite. The lithic abundance is more than 10% and the average size of the lithic clasts is around 55 mm and mostly include angular greywacke and andesite (Figure 3.10d). The facies is comparable with lithic concentration zone (LCZ) at the base of layer 2b of Spark *et al*. (1973).

6. *Fine ash-facies (FAL)*, occurs as two thin, very fine ash layers,10 and 50 mm thick, at the Hinuera Quarry section (Figure 3.10a). Their median grain sizes are approximately 39 and 51 µm, respectively. This facies was recognized locally and for the first time within the Ongatiti Ignimbrite at Hinuera Quarry. FPR facies occurs above and below the ash layers, without any notable textural or compositional change.

In the thicker ash layers there are three distinctive sub layers that vary in grain size and color; lower and upper layers are finer-grained with light grey color and the middle part is coarser-grained and darker.

3.5.3 Distal tephra facies

7. *Pumice-rich tephra facies (PRT)* is a crystal rich (>10% abundance; quartz, plagioclase and opaque minerals) tephra that contains weathered sub-angular to angular fragments of medium lapilli-sized pumice (about 25 mm in diameter) and varied lithics. Two kinds of pumice were identified: a white dense type and a brown dense type. White pumice clasts are larger, angular to sub-angular; however, the brown types are more flattened. The maximum measured size and abundance of pumice clasts are 60 mm and 15-20%, respectively. Some traces of lithics (1%) were identified, mostly greywacke, and they show fine size lapilli with an average diameter of 8 mm. The PRT was identified at Harbour Rd section (Figure 3.8).

8. *Pumice-poor tephra facies (PPT)* comprises yellow-cream clay with fine traces of altered pumice and lithic clasts. The pumice fragments (8 mm) are white and make up 1-2% of the deposit. Lithic clasts comprise 2% of the deposit and their average size is approximately 10 mm in diameter. The lower unit and the coarser grained upper unit are related to ignimbrite flow unit layers 2a and 2b, respectively, of Sparks *et al.* (1973).PPT was identified at Oparau Creek and Bryant Home.

9. *Fine-grained tephra (FGT)* comprises clay, characterized by white, orange and pink alteration laminae. There is no visible pumice. The facies is crystal-rich (7%), mostly quartz, plagioclase and opaque minerals, and has been recognized at the Oparau Creek section.

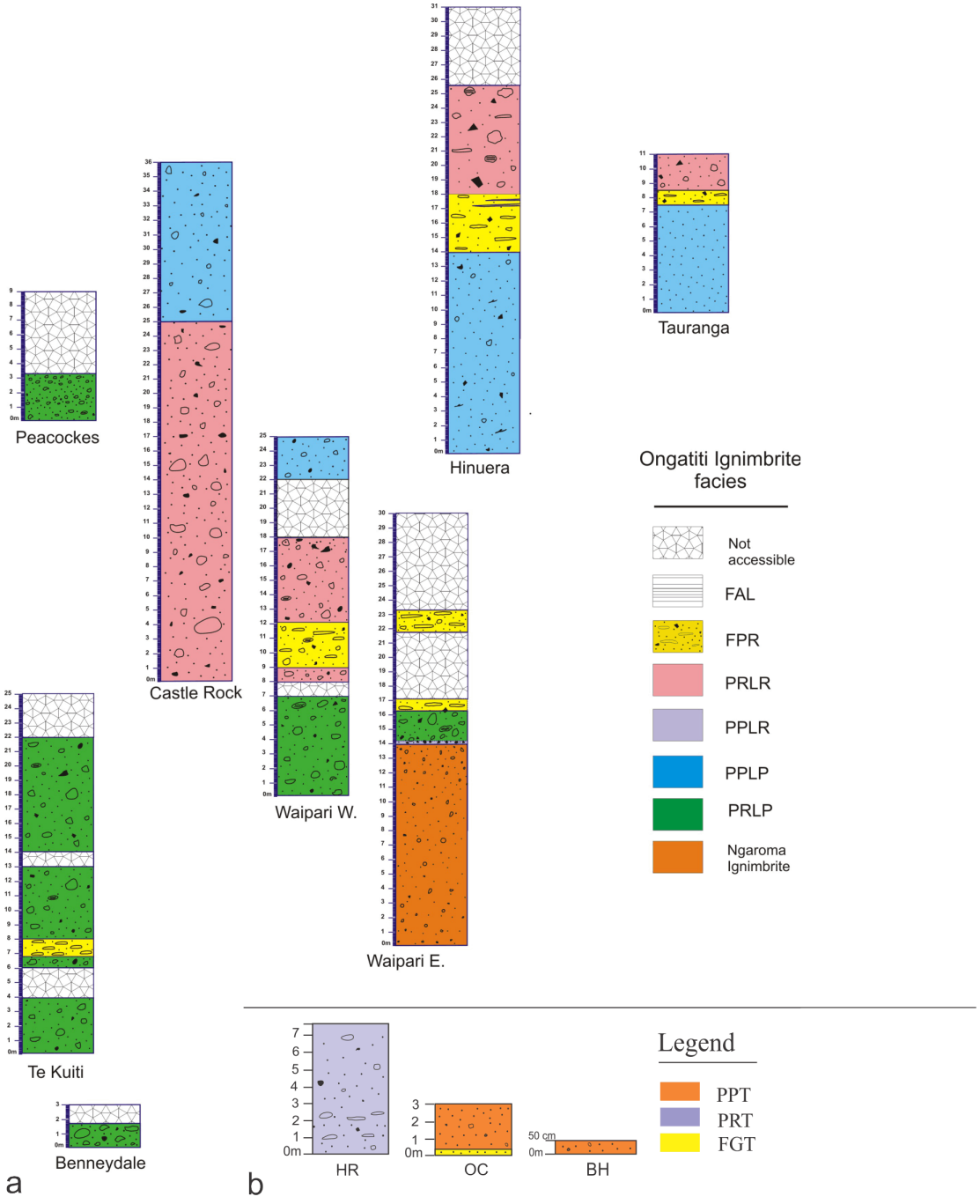

Figure3.8**:** a) Stratigraphic logs illustrating the vertical and lateral distribution of the different facies at various sites shown on the 3D map with respect to the caldera. b) Stratigraphic logs and different facies of Oparau Tephra at the distal sites. HR: Harbour Rd section; OC: Oparau Creek section; BH: Bryant Home section.

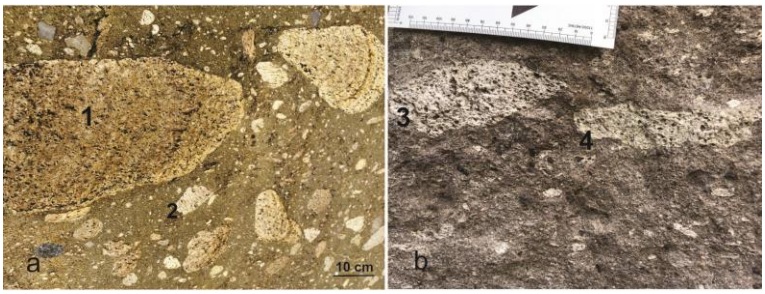

Figure 3.9: Types of pumice (a) at Hinuera 1 is a yellow vesicular, 2 is cream woody pumice; and (b) at Te Kuiti, 3 is a vesicular pumice and 4 is a flattened pumice.

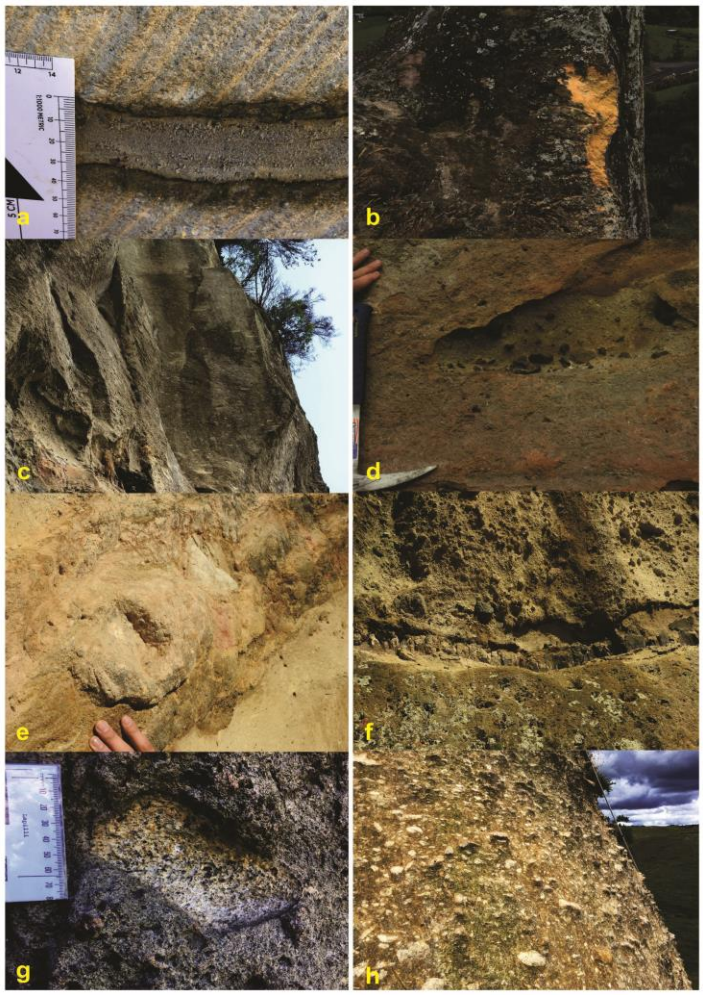

Figure 3.10: Deposit characteristics/facies (a) Ash layer in middle of the Hinuera Quarry section. (b) Close up from PRLR facies at Tauranga. (c) FPR facies in Waipari Gorge East section (d). PPLR facies at the base of the Ongatiti Ignimbrite in Waipari Gorge East (e). Gravel and siltstone lower the ignimbrite boundary at Waipari Gorge East. (f) Paleosol between two ignimbrites. (g) Close up of a hole, a remnant pumice trace. (h) Pumice rich facies at Te Kuiti section.

3.5.4 Proximal and medial ignimbrite stratigraphy

The facies identified in the previous section are used to develop the stratigraphic variations described at the sites below (figure 3.4). Co-ordinates are based on the Topomap NZMS 260 map series.

3.5.4.1 **Hinuera Quarry** [T15, 384201.00 E, 5802482.00 S]

The Ongatiti Ignimbrite is exposed at Hinuera Quarry approximately45 km north of the MVC. The thickness of the deposit as exposed is 32 m (Figure 3.11a),and is characterised by vertical and horizontal joints (Figure 3.12a).The Ongatiti Ignimbrite at the Hinuera quarry has been divided into four facies, PPLP, FPR, FAL and PRLR (Figure3.8a).

The lower PPLP facies (14mthick) is characterized as a partially welded ignimbrite with hues of greenish grey to grey. Traces of carbonized wood were observed in this zone. The lower PPLP facies grades into 6m-thick FPR facies with intercalated layers of FPR facies. This middle zone grades into a partially welded upper part of PRLR facies.

3.5.4.2 **Tauranga** [U14, 417219.00 E, 5821442.00 S]

An exposure of the Ongatiti Ignimbrite near Tauranga, approximately 75 km northeast of the caldera was introduced by Briggs et al. (1996) and revisited here to compare with the facies identified. The maximum exposed thickness was 11 m (Figure3.11b).Three distinct facies were identified: PPLP (7m thick), FPR (1m thick), and PRLR (3m thick), which are comparable to the facies at the Hinuera Quarry (Figure3.12a).

3.5.4.3 **Peacockes (Waikato River)** [S14, 352598.16 E, 5813043.55 S]

Around 65 km northwest of the MVC, a nine metre high exposure of the Ongatiti Ignimbrite along the Waikato River bank has been studied. The deposit is a non-welded, cream to yellow ignimbrite comprising PRLP facies (Figures3.11c, 3.12f).

3.5.4.4 **Castle Rock** [T16, 370326.00 E, 5778629.00 S]

The Ongatiti Ignimbrite forms 36 m-high cliffs in the Castle Rock area, which is located 25 km from the MVC (Figures 3.11f, 3.12c).Here the Ongatiti Ignimbrite is hard, dark grey, crystal-rich and both partially welded and vapor-phase altered with horizontal and vertical joints. Two facies, PRLR (25 m thick) and PPLP (11 m thick), occur.

Vapor phase alteration and pumice erosion create a ‘pock-marked’ outcrop appearance. However, from about 25 m above the base, with a decrease in pumice size and abundance, the exposure is less pock-marked.

3.5.4.5 **Te Kuiti** [S16, 351577.00 E, 5748692.00 S]

The area east of the Te Kuiti is located approximately 30 km west of the Mangakino Caldera, where the Ongatiti Ignimbrite is around 25 m in thickness(Figure3.10e).The ignimbrite is massive, hard, jointed and crystal rich with two facies: PRLP (1 m thick) and FPR (Figures3.11g,3.12e).

3.5.4.6 **Benneydale** [S17, 362934.11 E, 5737924.32 S]

25 km west of the MVC a 3 m-thick deposit of Ongatiti Ignimbrite caps a hill and reaches elevations of approximately 600 m asl. The deposit consists of hard, massive, cream-colored, crystal rich, partially welded ignimbrite comprised of PRLP facies (Figure 3.11h).

3.5.4.7 **Waipari Gorge West** [T16, 373588.00 E, 5768146.00 S]

One of the more extensive deposits of the Ongatiti Ignimbrite was studied near the Waipari Gorge15 km north of the MVC and is the closest site to the source caldera.

The sequence at the Waipari Gorge (west) is approximately 25 m thick (Figure 3.11d) and it has been subdivided into four facies. Lower grey, partially welded PRLR at least 8m in thickness, more welded FPR (3m thick), PRLP facies (7m thick) and upper PPLP facies (2 m thick), showing a sharp decrease in pumice and lithics and change in color to brown (Figure 3.12d).

3.5.4.8 **Waipari Gorge East** [T16, 373563.00 E, 5767471.00 S]

Around 500 m north of the Waipari Gorge west section, the Ongatiti Ignimbrite consists of LRPP, PRLR, and FPR facies. It is around 16 m thick and is partially welded to welded, and cream to buff in color (Figure3.11e). The Ongatiti Ignimbrite at this site overlies a 20 cm-thick dark paleosols directly above the Ngaroma Ignimbrite and Ongatiti Ignimbrite. The paleosol grades laterally to fluvial sediments of bedded silt and rounded, imbricated gravels up to 70 cm thick(Figures3.10e,f).Further, laterally the Ongatiti Ignimbrite directly overlies with a sharp boundary, the Ngaroma Ignimbrite.

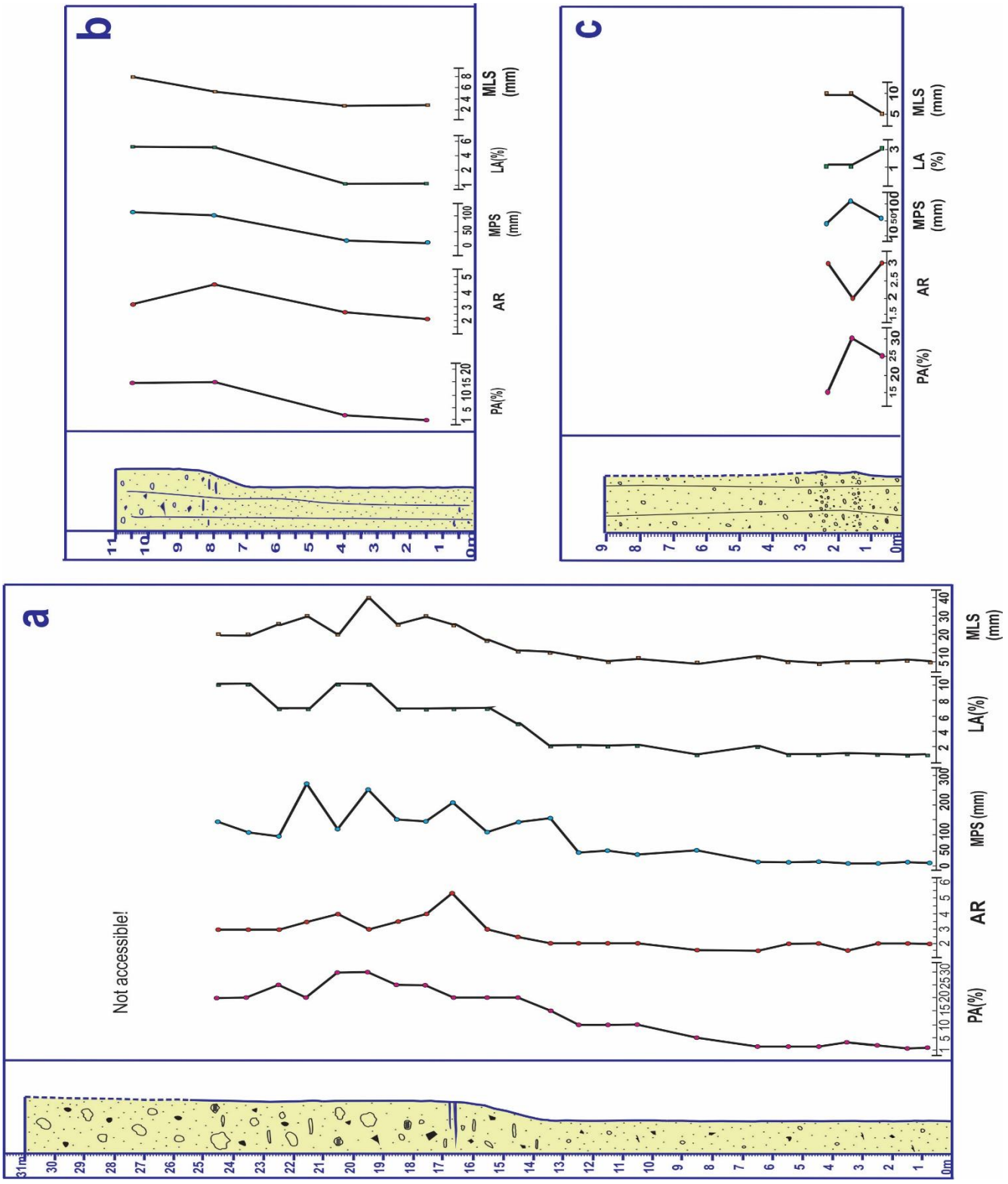

Figure 3.11:Stratigraphic logs showing field observations, pumice abundance (PA), pumice aspect ratio (AR), maximum pumice size (MPS), lithic abundance (LA) and maximum lithic size (MLS) for (a) Hinuera, (b) Tauranga, (c) Peacockes, (d) Waipari Gorge West, (e) Waipari Gorge East, (f) Castle Rock, (g) Te Kuiti, and (h) Benneydale sections

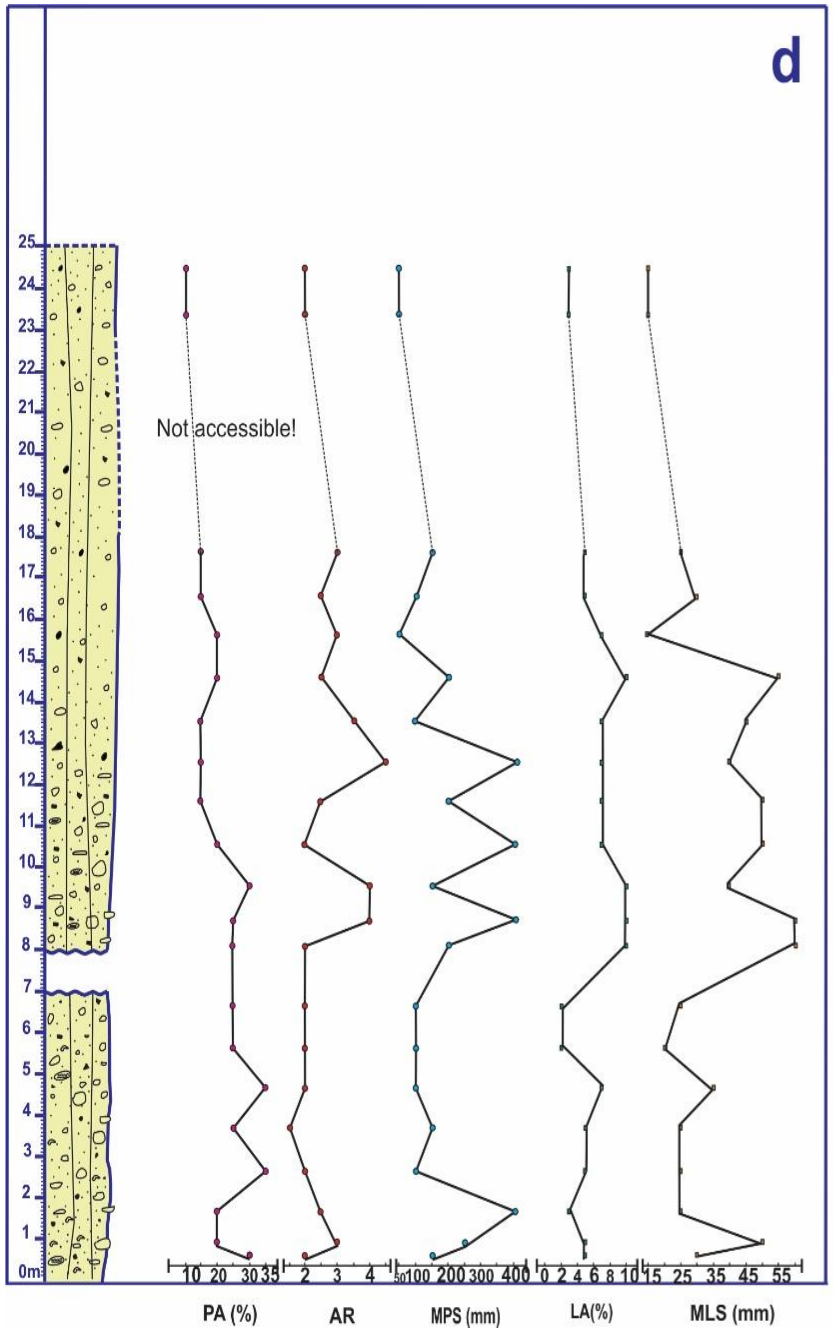
d
Not accessible!
PA (%)
AR
MPS (mm)
LA(%)
MLS (mm)

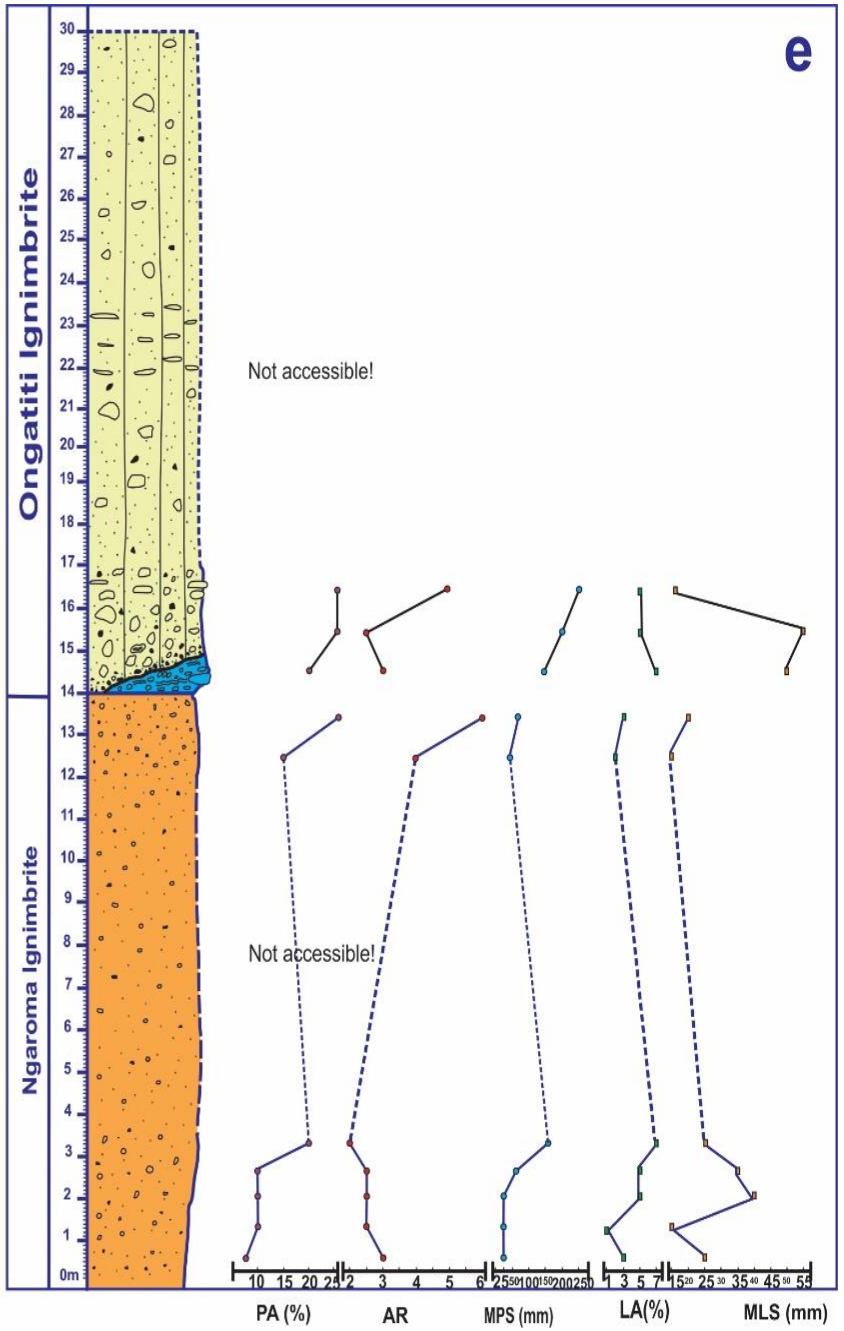
e
Ongatiti Ignimbrite
Ngaroma Ignimbrite
Not accessible!
Not accessible!
PA (%)
AR
MPS (mm)
LA(%)
MLS (mm)

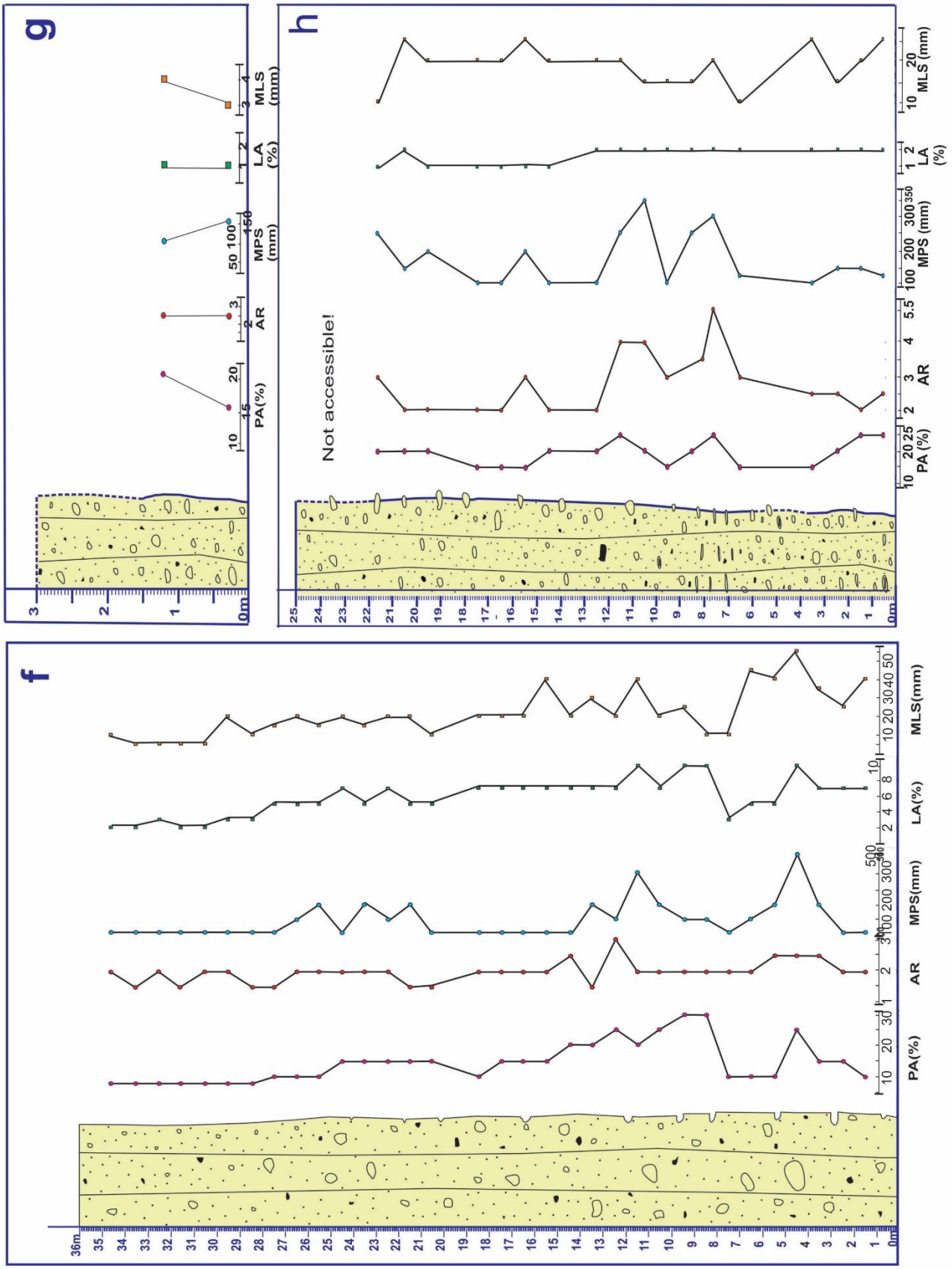
f
g
h
PA(%)
AR
MPS(mm)
LA(%)
MLS(mm)
Not accessible!
0m
36m

Figure 3.12: Outcrop morphology and exposure at locations (a) Hinuera Quarry, (b) Tauranga section, (c) Castle Rock outcrop,(d) Waipari Gorge West site,(e) Te Kuiti section, and (f) Peacockes (Waikato River) outcrop.

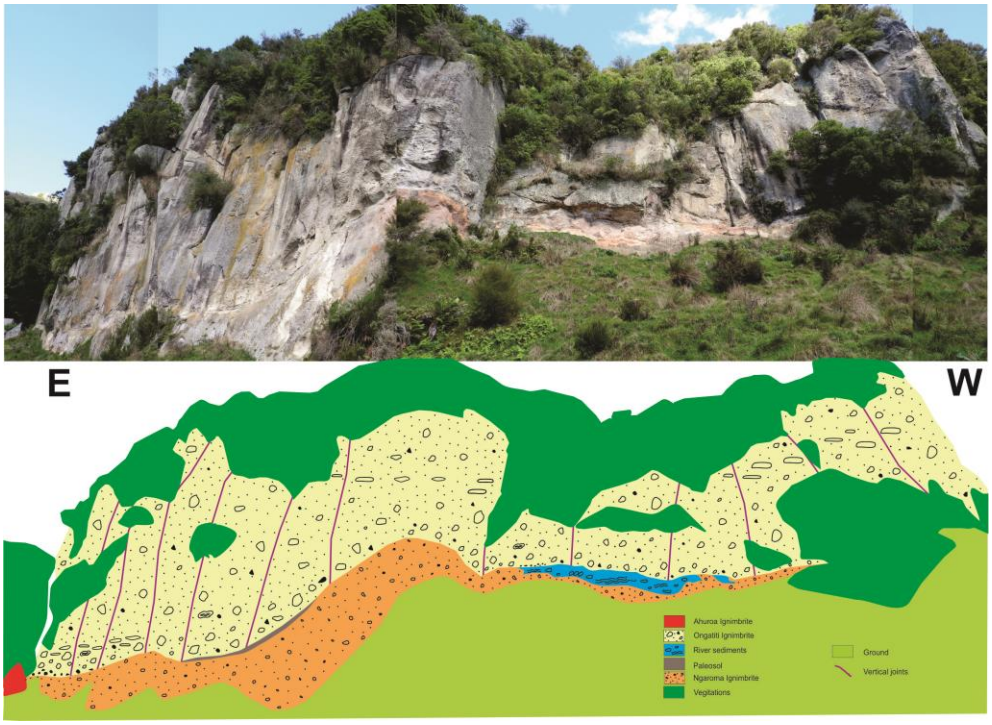

Figure 3.13: Photo and a sketch of the Waipari Gorge (east) outcrop viewing toward the north showing the contact relationship between the Ngaroma Ignimbrite, paleosol, and river sediments, and the Ongatiti Ignimbrite and Ahuroa Ignimbrite.

3.5.5 Distal tephra deposits

As mentioned before, distal tephra deposits that are equivalent to the Ongatiti Ignimbrite have been reported by various authors. The Oparau Tephra (informally K12a) occurs within the Kauroa Ash Formation on the western North Island (Horrocks, 2000; Lowe & Hunt, 2001) . Alloway *et al*. (2004) studied tephra layers around Auckland and, based on glass-ITPFT dating, correlated them Ongatiti Tephra. Mildenhall and Alloway (2008) identified tephra beds in the Wellington Peninsula of similar glass-ITPFT age to the Ongatiti Ignimbrite. The location of these sites has been shown in Figure 3.13.

Oparau Tephra was recognised by Pain (1975) as an ignimbrite and then by later studied Salter (1979) thesis has introduced deposits and nomenclature as K1 to K15. Then, Horrocks (2000) and Lowe *et al.* (2001) have suggested the relationship of the Oparau Tephra and the Ongatiti Ignimbrite. On the basis of the age dating, stratigraphic position and geochemistry, the Oparau Tephra has been correlated as a distal deposit of the Ongatiti Ignimbrite. In this study, we focused on the internal stratigraphic characteristics of some distal deposits of the Oparau Tephra to compare with the features of proximal Ongatiti Ignimbrite. Sections were

located in the west and north-west at the MVC at Harbour Rd (Kawhia Harbour), Oparau Creek, and Bryant Home (Raglan).

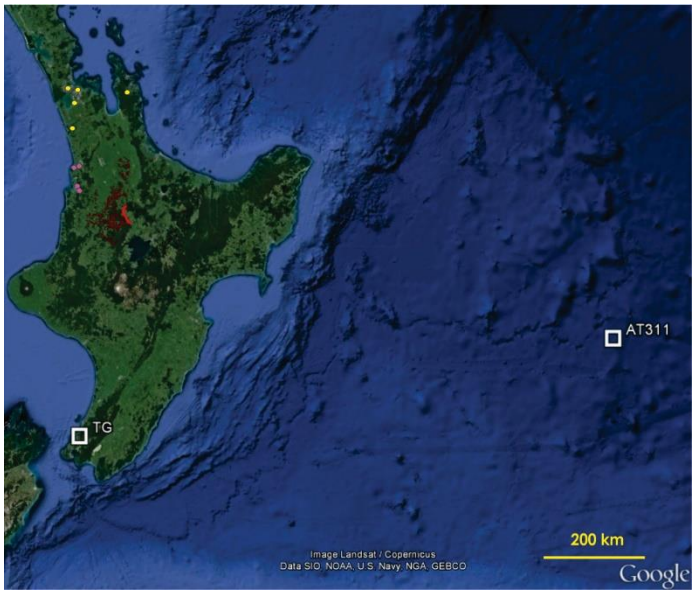

Figure 3.14: The location of distal tephras of the Ongatiti Ignimbrite, yellow points showing the Ongatiti Tephra studied by Alloway *et al*. (2004), white squares are equivalent tephras found near Wellington (Mildenhall and Alloway, 2008) and drill cores in the Pacific Ocean (Alloway *et al*., 2005).Violet circles illustrate the distal sites studied in current study.

3.5.5.1 Harbour Rd

The Harbour Rd section (Kawhia), 70 km from the source(Figure3.15a), was a newly exposed, approximately 7.5-m-thick, outcrop of the Oparau Tephra comprising a massive, dark cream to green deposit with red and black alteration and included crystals (Figure 3.15d). The outcrop shows PRT facies with two white pumice-rich layers, at 1 m and 2 m from the base, respectively (Figure3.16).

3.5.5.2 Oparau Creek

Near Oparau Creek (~70 km from the MVC), the Oparau Tephra is approximately 3 m thick and the lower contact with an underlying brown clay paleosol is very sharp (Figure 3.15c). Its lower part is 25 cm and shows a unit of FGT facies, which towards the top the deposit is harder and its color changes to yellow-cream and PPT facies.

3.5.5.3 Bryant Home

At the Bryant Home section, around 90 km from the MVC source, the Oparau Tephra is a 50

cm-thick pinkish, strongly altered blocky tephra bound between an upper reddish brown clay and a lower brown clay (Figure 3.15b). Rare white fine traces of pumice were seen and PPT facies was identified at the outcrop.

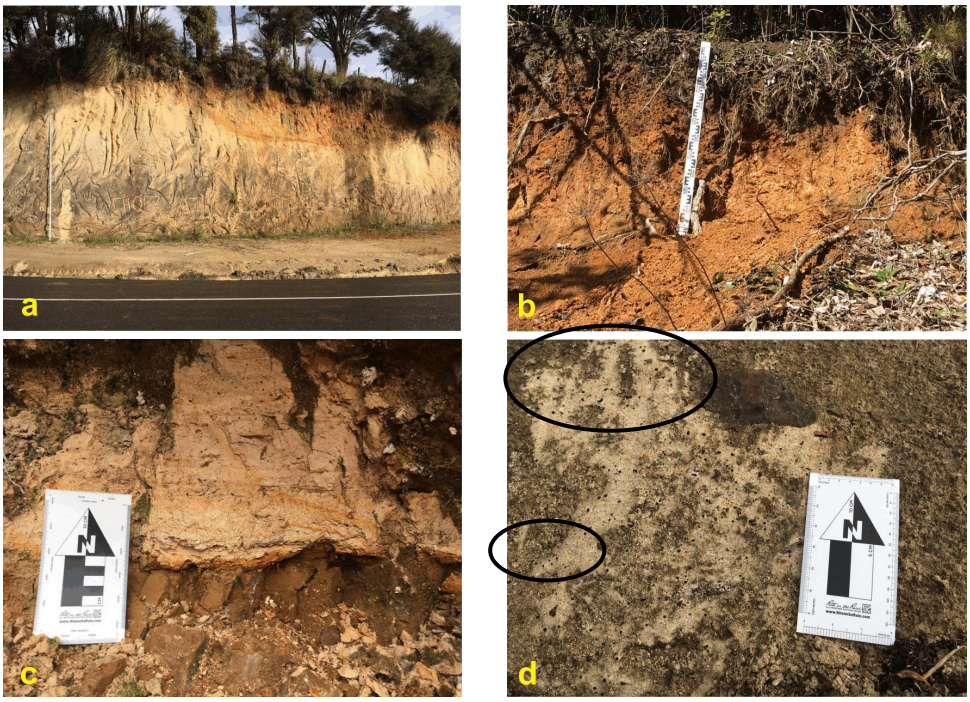

Figure 3.15: Distal Ongatiti equivalent tephras showing a) the Harbour Rd outcrop, b) Bryant Home section, c) a close up of the boundary between the Oparau Tephra and underlying brown paleosol at Oparau Creek section, and d) pumice trace and lithic clast in a deposit of the PRT facies at Harbour Rd section.

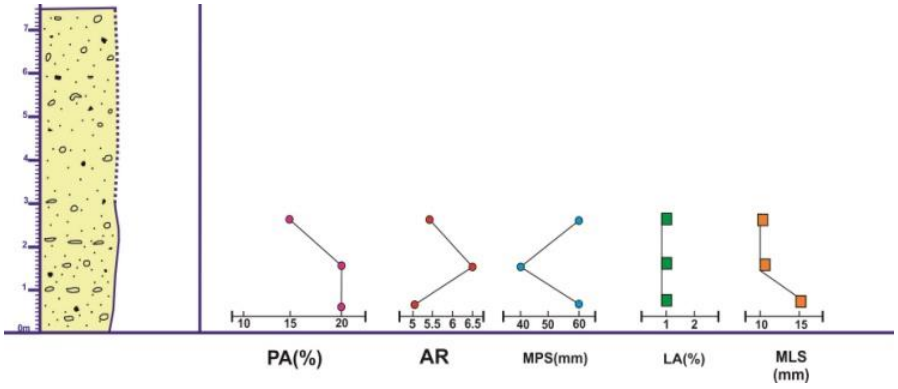

Figure 3.16: Stratigraphic log from the Harbour Rd section showing pumice abundance (PA), aspect ratio (AR), maximum pumice size (MPS), lithic abundance (LA), and maximum lithic size (MLS).

3.6 (U-Th)/He geochronology

Zircon chronology is a strong tool for determining eruption ages (Lukács *et al.*, 2015). A variety of U-Pb and U-Th ages can be presented using zircons from silicic volcanic rocks (Charlier *et al.*, 2004; Danišík *et al.*, 2012; Cooper & Wilson, 2014; Danišík *et al.*, 2015).

Samples were collected from three outcrops in Te Kuiti, Tauranga, and the Hinuera Quarry, west, north-east and north of the MVC, respectively, to correlate the age spatially around the MVC and also to re-date the Ongatiti Ignimbrite at the Tauranga section using a different method as the previous proposed age had seemed somewhat older than the ages reported for other areas (see section 3.2above).

Zircon crystals were separated by standard gravity and magnetic processes from rock samples and finally the best zircon crystals were selected under the microscope by hand picking. (U-Th)/He zircon dating was conducted at Curtin University (Australia) by Dr. Martin Danišík.

The proposed ages for the Ongatiti Ignimbrite by different authors can be divided into three groups. The most common age determined by different methods at various sample sites ranges from around 1.21$\pm$0.04 to 1.28$\pm$0.11(group II, Table 3.1). However, Briggs et al. (2005) determined ages of 1.32$\pm$0.01 and 1.34$\pm$0.02 Ma from two small outcrops of the welded portion of the sequence in the Tauranga Basin used the $^{40}Ar/^{39}Ar$ method (group III, Table 3.1). In this study a different method, (U-Th)/He dating, has been used at three different locations (group IV, Table 3.1) and range from 1.314$\pm$ 0.086 Ma at Hinuera, 1.377 $\pm$ 0.061 Ma at Tauranga and 1.382 $\pm$ 0.052 Ma at Te Kuiti (appendix1).

Table 3.1: A summary of published age data for the Ongatiti Ignimbrite and the new ages from this study.

Author			Age (Ma)	Method	Age group
Soengkono *et al.* (1992)			1.25±0.09	K/Ar on hornblende	I
Pringle *et al.* (1992)			1.251 ± 0.060	$^{40}Ar/^{39}Ar$ on feldspar	
Briggs et al. (1993)			1.23±0.02	Ar/Ar on feldspar	
Houghton et al. (1995)			1.21±0.04	$^{40}Ar/^{39}Ar$ on feldspar	
Black *et al.* (1996)			1.25±0.12	ITPFT[1]	
Lowe et al. (2001)			1.28 ± 0.11	Zircon fission track	
McCormack et al. (2009)			1.21±0.04	$^{40}Ar/^{39}Ar$	
Briggs *et al.* (2005a)	Plateau age		1.32±0.01	$^{40}Ar/^{39}Aron$ feldspar	II
	Isochron age		1.34±0.02	$^{40}Ar/^{39}Aron$ feldspar	
This study	Sites	Hinuera	1.314± 0.086	(U-Th)/He	III
		Tauranga	1.377 ± 0.061		
		Te Kuiti	1.382 ± 0.052		

[1] ITPFT=Isothermal plateau fission track age on glass

3.7 Discussion

3.7.1 The volume of the Ongatiti eruption

We have revised the minimum deposit volume for the Ongatiti Ignimbrite to approximately 720 km^3 (as deposited) and the DRE volume to 512 km^3. The present-day ignimbrite distribution has been modified by erosion and burial by younger deposits causing the estimation of the original volume to be problematic. Also, we have not included the unknown eastern and intracaldera parts of the ignimbrite in the calculation of the ignimbrite areal distribution. Hence, the true area is at least double in size. Earlier we identified the Ongatiti Ignimbrite to be a low aspect ratio ignimbrite and thus assume that it was radially distributed around the caldera.

To qualify as a super-eruption, three criteria are commonly considered (Sparks 2005; Self 2006; Miller and Wark, 2008): a) a mass erupted > 10^{15} kg, b) volume of magma greater than 450 km^3, or c) pyroclastic deposits with volumes of 1000 km^3 or more. Based on the obtained volume for the Ongatiti Ignimbrite in this study, a super-eruption for the ignimbrite is confirmed.

Two super-eruptions have been recognized during the activity history of the Mangakino Volcanic Centre: the Ongatiti Ignimbrite and the more-voluminous1.0 Ma Kidnappers

Ignimbrite (Houghton *et al*., 1995, Wilson *et al*., 2009 with 1200 km^3as deposited (Wilson 1986; Cooper and Wilson, 2014).

In table 3.2 the Ongatiti ignimbrite has been compared with 3 super eruptions in New Zealand; Kidnappers, Whakamaru and Oruanui. The Kidnappers ignimbrite was erupted from the MVC, however, unlike the Ongatiti Ignimbrite, it is non-welded and has an underlying fall sequence (Wilson et al. 1995; Cooper, 2104). The Whakamaru and Oruanui eruptions were from different caldera sources but they are rather similar in volume. The ignimbrite(s) of the Whakamaru eruption(s) are typically welded (Wilson, 1986; Brown et al., 1998) and are probably most comparable to the Ongatiti Ignimbrite. The Oruanui ignimbrite (Wilson, 2001) on the other hand, is more comparable to the Kidnapper's eruption – both are non-welded, and both have underlying fall sequences

Table 3.3 compares the Ongatiti Ignimbrite with Campo de la Piedra Pomez and Cerro Galan ignimbrites. The first ignimbrite is comparable to the Ongatiti Ignimbrite due to the paleotopographic effects on the ignimbrite facies. Although the ignimbrite was not emplaced by a super eruption, Baez et al. (2020) identified three flow paths and different facies for a low aspect ratio ignimbrite. The Cerro Galan Ignimbrite has a similar volume and caldera size (Cas et al. 2011). In addition, itis a rhyodacitic crystal rich ignimbrite that has travelled around 100 km - similar to our estimations for the Ongatiti Ignimbrite.

Table 3.2: A brief description of different ignimbrites in New Zealand.

Ignimbrite Name	**Age**	**Volume**	**Source Caldera**	**Travelled distance**	**Characteristics**	**Reference**
Kidnappers	1 Ma	1200 km^3 (DRE)	Mangakino	~190 km	Fall deposit and PDC Mostly unwelded Lithic and crystal rich	Cooper (2014) Wilson et al. (1995)
Whakamaru group	330-340 ka	>1000 km^3	Maroa-Taupo area	> 60 km	Varied due to different ignimbrites	(Wilson *et al.*, 1986) (Brown *et al.*, 1998)
Oruanui	26.5 ka	~ 530 km^3 (DRE)	Taupo	~ 90 km	> 200 m Produced fall deposits and PDC	(Wilson, 2001)

Table 3.3: A short comparison of two ignimbrites in Argentina.

Ignimbrite Name	Location	Age	Volume	Source Caldera	Size of the Source	Travelled distance	Characteristics	Reference
Campo de la Piedra Pomez	Argentina	Quaternary	~ 3.4 km^3	Cerro Blanco	6x4 km	25 km	Low aspect ratio ignimbrite It flow through 3 paths: Wide valley, Narrow valley and Narrow channels Due to different paths, different facies identified	(Báez *et al.*, 2020)
Cerro Galan	Argentina	2.08 Ma	>630 km^3 (DRE)	Cerro Galan	~ 26 x18 km	~ 100 km	Rhyodacitic, crystal rich. Pumice and lithic poor	(Cas *et al.*, 2011)

3.7.2 Resolving the age problem of the Ongatiti eruption

One aspect of the Ongatiti Ignimbrite has been the somewhat older-looking age at Tauranga compared with those at other locations. The (U/Th)/He method was used for the first time on the Ongatiti Ignimbrite to compare with previous ages proposed by other authors (Table 3.1).

The age for the ignimbrite at Te Kuiti (1.382 $\pm$ 0.052 Ma) matches with the age at Tauranga (1.377$\pm$ 0.061Ma). The third acquired age at Hinuera (1.314$\pm$ 0.086) has a larger error and could match either the age at Te Kuiti and Tauranga, or the commonly accepted younger ages (group II, Table 2.1).

The (U-Th)/He age at Tauranga shows good agreement with the ^{40}Ar-^{39}Ar age reported in Tauranga by Briggs et al. (2005). Therefore, these data support the mapped extension of the Ongatiti Ignimbrite to the north-east of the MVC as far as the Tauranga area.

The Ongatiti Ignimbrite travelled towards the west coast of the North Island, from proximal to distal areas. Previous obtained ages for the ignimbrite by different authors (Table3.1) has been compared with the zircon fission track age of 1.28 ± 0.11 Ma acquired for the Oparau Tephra/Ongatiti Ignimbrite (Horrocks, 2000; Lowe *et al.*, 2001).

3.7.3 Caldera source

The Mangakino Caldera has been identified by geophysical and geological studies (Rogan 1982; Houghton *et al.*, 1995; Wilson *et al.*, 1995, 2009). This study includes field observations of the modern topography and the western border of the caldera (Figure3.1). On the eastern side of the caldera the edges have been eroded and also covered by younger

deposits; therefore, no clear evidence of the boundary can be seen on the surface. Our geological observations have been associated with the GIS-based map and the profiles (Figure3.2) that have been generated for the area. A large elliptical resurgent centre 20 km long by 12 km wide and a topographic relief on the modern surface of around 60 m depth has been identified. However, this depth is not the original collapse depth as it has been filled by younger sediments but it can be considered as supportive evidence for the caldera location and its possible dimensions. Rogan (1982) has estimated a 5 km basement depression for the MVC but she had doubt about the accurate depth due to presence of some low-density material within the basement.

3.7.4 Plume dynamics and flow mobility

Sparks and Wilson (1976) considered gravitational collapse of eruption columns as the source of some pyroclastic flows and that the eruption column height is the main factor that can control the original energy of the flow (Walker, 1980). Higher eruption columns that collapse, generate a larger flow mobility and smaller viscosity; and therefore a more widely distributed ignimbrite with a low aspect ratio can be created (Francis & Baker, 1977; Baker, 1981; Lube *et al.*, 2019).

Based on our measurements, the Ongatiti ignimbrite has an estimated aspect ratio in the order of 1:950 to 1:1880 which indicates it is a low aspect ratio ignimbrite (Wilson, 1991).Thus, it is presumed here that the ignimbrite was created by one or several high eruption column/s.

3.7.5 Topographic controls on distribution

Ignimbrites generated during plinian and sub-plinian eruptions illustrate diverse distribution geometries ranging from ribbon-like valley-controlled deposits to semi-circular sheets emplaced by radially-dispersed flows. Antecedent topography is an important control on pyroclastic flow distribution, concentrating flows through valleys and other topographic basins. However, they can also surpass topographic highs such mountains, and travel long distances including travelling over water. Ignimbrites are mostly thick, sometimes several 100 m, within topographic basins, valleys and calderas but thin, only a few centimeters, over hills and ridges (Brown and Andrews, 2015).

As shown on the Ongatiti Ignimbrite distribution map (Figure3.6), the ignimbrite has no surface outcrop on the east side of the MVC in central North Island, except Tauranga site located in the northeast. However, cores that were studied by Houghton (1987b) near Tokoroa revealed the presence of the ignimbrite at depths between 392-457 m below the surface. In this study, we have focused on surface exposures only.

The GIS-based maps and profiles (Figures 3.3 and 3.8a) indicate that valleys have been covered by the Ongatiti Ignimbrite in the proximal areas (e.g. Te Kuiti) and also on high ridges near the caldera (west side) on hills (south-west of the caldera) up to 900 m asl. For instance, the Benneydale section was studied on hills at around 600 m above sea level; in the Castle Rock and Waipari Gorge (east and west) areas the pyroclastic flows have flowed through valleys. However, the ignimbrite flowing toward the medial and distal areas did not reach the highlands and only filled pre-existing lowlands such as at the Hinuera Quarry and around Tauranga. In the west and north-west of the caldera, it covered vast valleys between hills divided into the several lobes according to the paleotopography, and also flowed within smaller valleys.

One of the most complete sections was studied in Waipari Gorge, as a flow lobe through a narrower valley. The ignimbrite deposit lies approximately 25 km (proximal area) away from the MVC. The pyroclastic flow after passing ridges flowed through a narrower valley (c.f. other sites such as Hinuera). The sharp lower boundary with the Ngaroma Ignimbrite was observed in this section. Alluvial sediments between two ignimbrites indicate that a stream flowed on the top of the Ngaroma Ignimbrite through a valley. Also, a paleosol formed over the older ignimbrite confirms a significant gap in time between the Ngaroma and Ongatiti Ignimbrite emplacements.

At the Hinuera and Tauranga sites, the pyroclastic flow passed through the low lands in medial areas, reaching more than 80 km toward Tauranga. Our new data provides some evidence for the Ongatiti Ignimbrite as a low aspect ratio ignimbrite which means the ignimbrite could travel far distance to the east of MVC as well as the west side. Geological studies by Houghton *et al.* (1987b) near Tokoroa, around Morrinsville (Bowling, 1989), and also Matamata (Houghton & Cuthbertson, 1989) show that the ignimbrite has flowed to the southern boundary of the Kaimai Range.

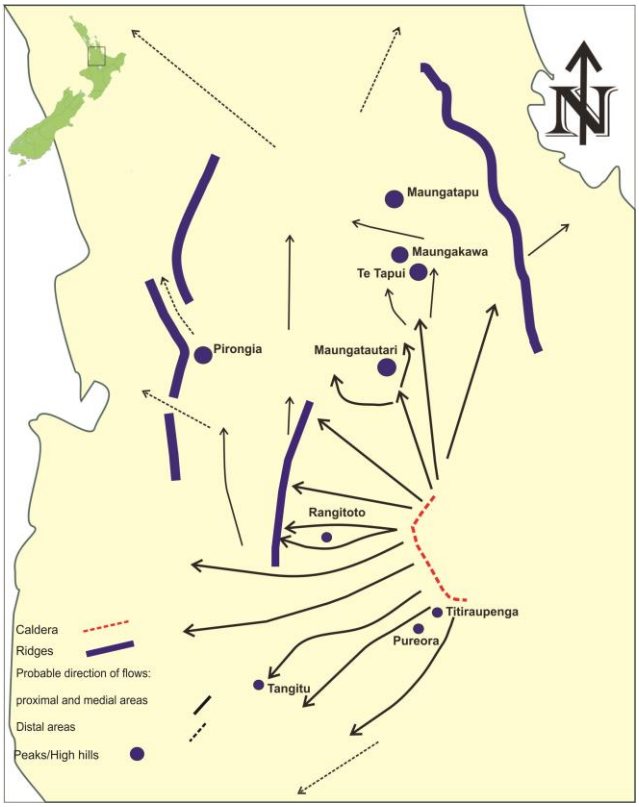

Figure 3.17: Map representing the position of the caldera and some main barriers (ridges and high lands) in front of the pyroclastic flow. Arrows showing the proposed flow directions, thicker arrows are the main flows and thinner ones are proposed minor flows.

Several landscape features are known to have existed in their present form before the the time of eruption and affected the ignimbrite pathways. Pureora and Titiraupenga – two stratovolcanoes of the MVC margin – have been dated at 1.60±0.10 Ma and 1.89±0.02 Ma respectively (Graham et al., 1995; Stipp, 1968). Maungatautari stratovolcano, also located in NNW of the MVC margin and age of 1.8±0.10 Ma has been reported (Robertson, 1983; Briggs, 1986 Prentice et al. 2020). However, these old volcanoes are all located on the west side of the MVC whereas on the east side no new volcanoes have been introduced. All evidence of topography to the east of MVC at the time of the Ongatiti eruption has subsided due to rifting in the young TVZ and subsequently buried by younger TVZ eruptives.

Briggs et al., (2005) cited that the age of some segments of the Hauraki Fault (particularly southern segments) and up rifting, occurred before the Ongatiti Ignimbrite emplacement but after the Waitearikiki Ignimbrite (between 2.09+0.03 Ma and 1.34-1.21 Ma). Hence, the southern Kaimai range was present as a barrier to flow into the Bay of Plenty region. Perhaps, the Ongatiti pyroclastic flows entered the Tauranga region by flowing around further south

through low-lying palaeotopography that may now be buried by younger ignimbrites underlying the Mamaku Plateau.

Some flow lobes separated from the main flow and reached the distal areas around Kawhia Harbour (e.g. Harbour Rd and Oparau Creek) and were emplaced as the distal facies.

Based on field observations and GIS-based maps some hills and major ridges, such as Pirongia, Maungatautari, Titiraupenga and Pureora worked as natural obstacles in front of the ignimbrite. These barriers caused the pyroclastic flow to change its direction; however, in proximal areas the Ongatiti Ignimbrite is likely to have surpassed the ridges but not in medial and distal regions (Figure 3.17).

3.7.6 Pyroclastic flow variations

The topography and its relationship to the ignimbrite deposit suggests that there was at least three paths for transporting the pyroclastic flow from the source to distal areas.

To the north and north-east (Hinuera and Tauranga sections) the pyroclastic flow passed through a wide valley and lowlands to approximately 90 km away from the source (Figure3.18 C,C'). A vertical change from pumice poor facies at the base to pumice rich facies near the top indicates an energy decrease during the eruption (Wilson, 1986).

In the north-west (Waipari Gorge and Castle Rock sections) the pyroclastic flow, after exiting the caldera, moved through the narrow valleys (Figure3.18 B, B'). Fluvial sediments beneath the Ongatiti Ignimbrite are evidence of an ancient river that flowed through the valley before emplacement of the Ongatiti Ignimbrite (as noted before). The deposit began with a lower pumice-rich (PR) facies and developed into an upper pumice-poor (PP) facies. The lesser and smaller pumice clasts suggest fragmentation is more efficient. The presence of the lithic-rich (PPLR) facies near the base suggests the fluidisation generate a density segregation as the dense lithic deposited at the base and pumice clasts increase upward (Roche *et al.*, 2001). Representatives of the pumice rich facies were observed around Te Kuiti and Benneydale in this study, although Brink (2012)also observed PP facies below PR facies in neighboring areas. The ignimbrite is known to has traveled to the distal areas at least towards the west and north-west. The Peacockes section is located halfway along the pyroclastic flow path and shows pumice rich facies.

Facies that occur in the western proximal areas and the north-eastern medial areas are similar. This suggest that towards the north and north-east, the lack of hills and high lands have allowed the flow to retain its flow energy to the medial areas (to about 90 km) where its energy gradually depleted. However, in the western proximal areas (to about 30 km) after passing significant topographic barriers and ridges the energy of the pyroclastic flow decreased sooner. Toward the north-west through the narrow valleys and proximal areas the facies sequences were distinctively PP facies overlying PR facies. These facies and energy changes reveals the effects of the topography on the pyroclastic flow transportation.

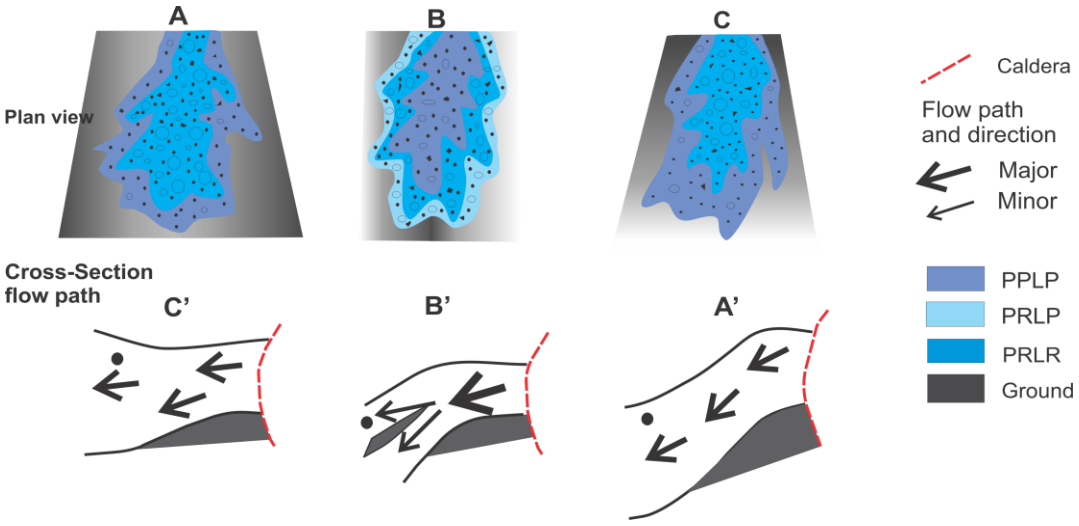

Figure 3.18: Diagrams showing plan view and cross sections of flow paths for the Ongatiti Ignimbrite at different areas based on facies successions and topography. A-A' displaying facies at the wide valleys where the ignimbrite travelled long distances through lowlands (at the north and north-east of the MVC). B-B' represents facies successions along the narrower valleys after high lands (north-west of MVC). C-C' represent facies in areas where the ignimbrite passed after high lands and then through valleys (west of the MVC).

The preserved sections of the ignimbrite represent areas where the Ongatiti Ignimbrite was deposited in valleys as typically valley-ponded facies as they are massive (Figure3.19). Figure 3.19 shows the parts of the pyroclastic flow system represented by each of the locality sections.

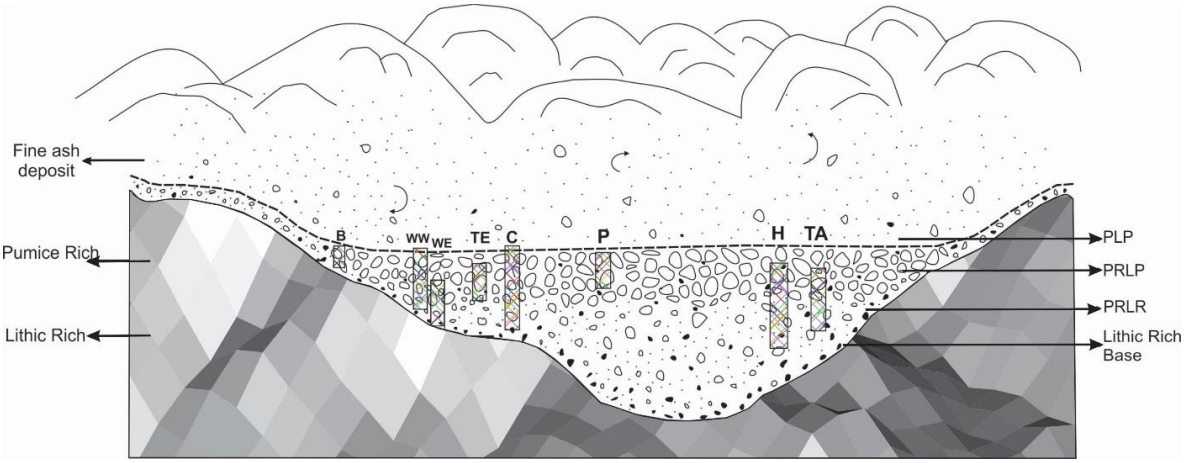

Figure 3.19: Schematic cross-section through a paleo-valley through which flowed the Ongatiti pyroclastic flow showing different facies stratigraphically. Pumice-lithic poor (PLP), pumice-rich, lithic-poor (PRLP),pumice-lithic rich (PLR) and lithic rich base (LRB).Modified after Pittari *et al.* (2006).B: Benneydale outcrop, WW: Waipari Gorge west outcrop, WE: Waipari Gorge east outcrop, TE: Te Kuiti outcrop, P:Peacockes outcrop, H: Hinuera outcrop, TA: Tauranga outcrop,

The two ash-layers identified within the PLR facies at the Hinuera Quarry are local and represent changes in emplacement process at this site. The PLR facies above and below the ash layers has the same deposit characteristics. Therefore, we suggest that this ash facies is related to an ash cloud surge around the pyroclastic flow, which was emplaced during local flow fluctuations. Figure3.20 illustrates the position of the facies and the process that are proposed for emplacing it.

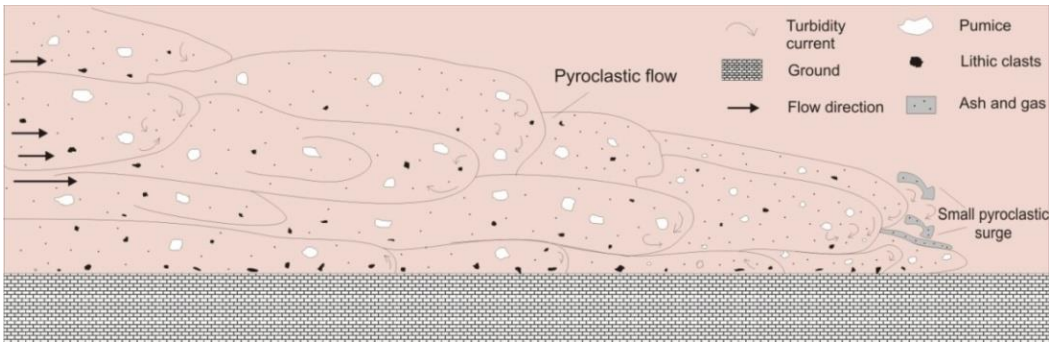

Figure 3.20: Diagram showing pyroclastic surge in the middle of the Ongatiti Ignimbrite at the Hinuera section.

3.7.7 Welding

From proximal to medial areas most outcrops show an area of flattened pumice fragments in the middle of the sections 1-3m thick. In the Waipari Gorge west and Waipari Gorge east sites the pumice aspect ratio is between 2 and 5 and at a similar distance from the MVC towards west at Te Kuiti the aspect ratio is the same between 2 and 5.5. Castle Rock, however, has pumice with a lower aspect ratio and no flattened pumice area was seen there. Additionally, in the middle of the Hinuera and Tauranga sections where the most strongly welded area was identified, the pumice aspect ratio is 2-6 and 2-5, respectively. Benneydale shows an aspect ratio around 2.5 without any welded area and at Peacokes aspect ratio is between 1.5 and 3.

Overall, the aspect ratio ranges from 1.5 to 6 from the Peacockes section to the Hinuera Quarry respectively, which suggest that the ignimbrite is non-welded to partially welded; however, microscopic studies are needed for an accurate welding rank for the ignimbrite.

Welding during and immediately after emplacement can occur if the temperature is significantly more than the temperature of the glass transition (Quane *et al.*, 2009; Brown & Andrews, 2015). In all studied sections with a welded facies situated in the middle of the Ongatiti Ignimbrite that it suggests the temperature of the pyroclastic flow was efficient and enough for welding the ignimbrite.

The Ongatiti Ignimbrite is the second largest ignimbrite in volume from MVC in comparison with the Kidnapper Ignimbrite; however, the Kidnapper Ignimbrite is a non-welded to poorly welded ignimbrite (Wilson et al. 1995).

Chapter Four

Physical characteristics of a giant ignimbrite: implication for fine-scale eruption and post-emplacement processes

4.1 Introduction

Ignimbrite deposits are formed by the explosive eruption of magma into gas-particle plumes, which then collapse and race across the landscape as hot, gaseous, ground-hugging pumice-and-ash pyroclastic flows (Marshall,1934; Martin, R. C.1961; Cas, R., & Wright, J. (1987). Le Maitre,2002; Cas and Wright,1987; Sulpizo et al., 2014). Evidence for magma fragmentation, pyroclastic flow, and post-emplacement modification processes (e.g. welding, compaction, chemical alteration), is recorded in the microtexture of ignimbrite.

Large-volume ignimbrite emplacement is often associated with super-volcanoes and they present horizontal and vertical diversity in components, facies, minerals, petrology and geochemistry. All these criteria can be used for correlation of disconnected deposits (Hildreth & Mahood, 1985). In this chapter, we focus on the microtexture of the Ongatiti Ignimbrite as an example of a large-volume ignimbrite (>512 km^3 DRE) that was emplaced during a supereruption1.2 Ma in the central North Island (Martin, 1961; Houghton *et al.*, 1995).

We evaluate the ignimbrite for components <2mm in size, for variations in primary pyroclast characteristics, welding and alteration of the matrix. The microtexture of ignimbrite is poorly sorted and is discriminated by variations in size and texture of pumice fragments, glass shards, crystals and lithic clasts.

The chemical analysis of the volcanic glass of the Ongatiti Ignimbrite will be discussed in the next chapter.

4.2 Geological setting

Taupo Volcanic Zone (TVZ) is a NNE-SSW trending, approximately 300-km long and 60-km wide active continental volcanic arc located in the North Island, New Zealand. The TVZ has produced at least 34 caldera-forming ignimbrite eruptions and many minor eruptions from at least eight rhyolitic centres (Healy, 1964; Houghton *et al.*, 1995; Wilson *et al.*, 1995a; Allan *et al.*, 2008).

Mangakino Volcanic Centre (MVC) is the oldest volcanic centre located at the western side of central TVZ having erupted >1000 km^3 (DRE) of volcanic deposits including different ignimbrites, fall deposits and lava domes. The caldera, due to the erosion and burial by younger deposits, is poorly expressed; however, Blank (1965) and Rogan (1982) identified the volcanic centre(caldera) based on geological field observation and a gravity anomaly. Two eruptive phases for the MVC have been identified by previous researchers, the first period from 1.6 to 1.5 Ma and the second from 1.21 to 0.95Ma (Briggs, 1976; Stern, 1979; Rogan, 1982; Briggs *et al.*, 1993; Wilson *et al.*, 2009; Wilson & Rowland, 2016). During the second eruptive phase, the Ongatiti Ignimbrite was emplaced as one the major ignimbrites from the caldera (Houghton et al. 1995).

4.3 Distribution and stratigraphy of Ongatiti Ignimbrite

The Ongatiti Ignimbrite was originally described as a widespread, non-welded to partially welded, crystal-rich, rhyodacitic to rhyolitic ignimbrite by Martin (1961). The distal correlative, Oparau Tephra (informally known as bed K12 of the clay-rich Kauroa Ash sequence), occurs in the western North Island (Pain, 1975; Lowe *et al.*, 2001), and the equivalent Ongatiti Tephra is found around Auckland and Wellington (Alloway *et al.*, 2004; Mildenhall & Alloway, 2008).

The Ongatiti Ignimbrite has wide- to extremely wide-spaced joints, and the pyroclastic flow from which it was deposited has traveled approximately 90 km to the northeast of MVC. Eight sites in proximal and medial areas, and several sites in the distal area, have been studied at the western and northern side of the MVC source caldera (Figure4-1); however, there is no exposure on the eastern side (Briggs *et al.*, 1993). The minimum erupted volume for the associated super-eruption is about 512km^3 (DRE) and the ignimbrite has a low aspect ratio

(chapter 3). Several facies have been characterized for the ignimbrite, including pumice and lithic-rich facies (PRLR), pumice-rich, lithic-poor facies (PRLP), flattened pumice-rich facies (FPR), pumice-and-lithic poor facies (PPLP), fine ash facies (FA) and pumice-poor, lithic-rich facies (PPLR).

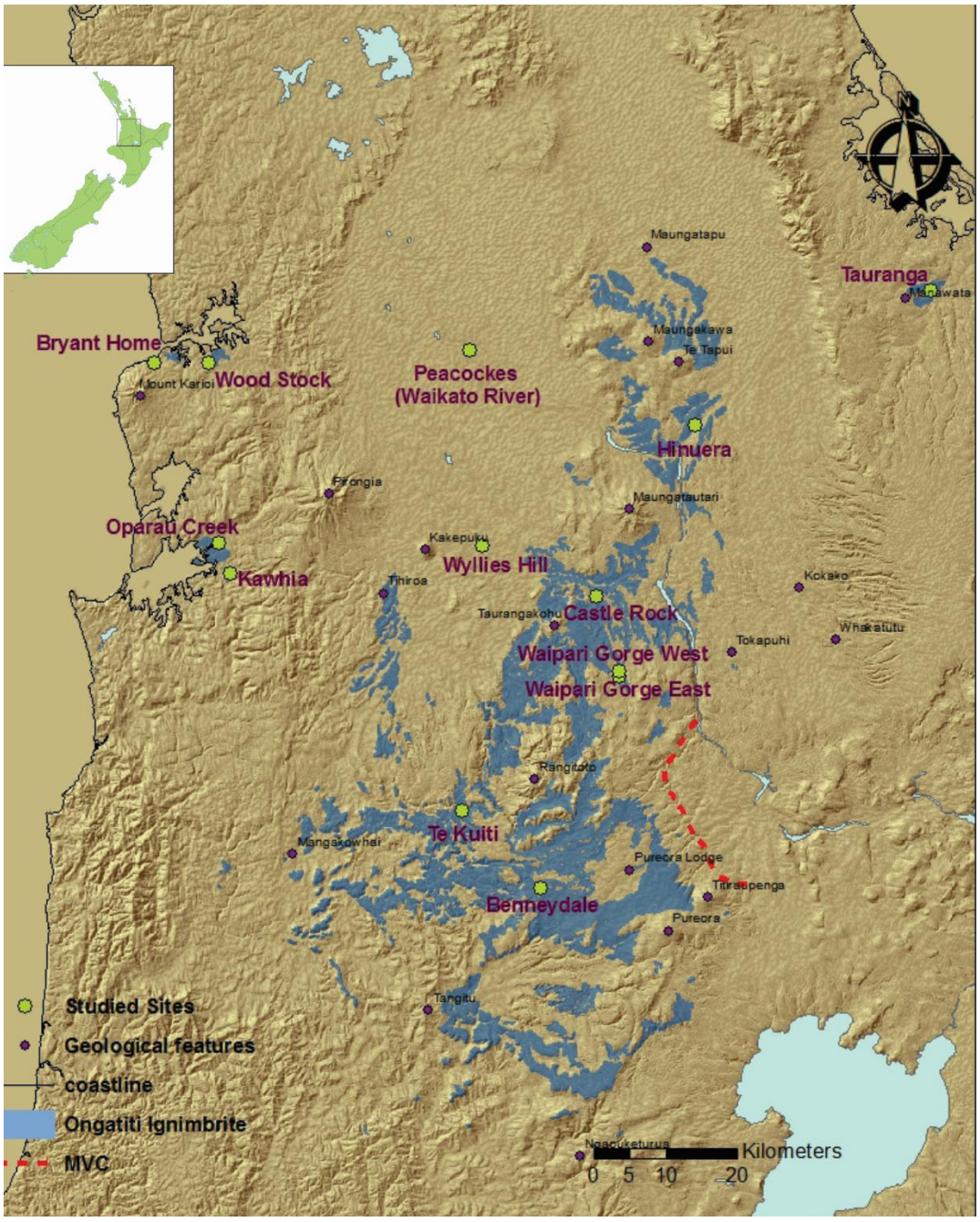

Figure 4.1: Distribution of the Ongatiti Ignimbrite. Blue areas depict the Ongatiti Ignimbrite and green circles show sampling locations. MVC boundary showed by red dashed line.

4.4 Sampling and methodology

Field sampling was carried out during 2015 and 2016 at multiple sites (Figure 4-1) and was based on variations in the texture of the ignimbrite. The samples have been used for making covered and polished thin-sections, powder for X-ray diffraction (XRD) analysis, and whole fragments for X-ray computed microtomography (μ-CT), and scanning electron microscopy (SEM).

The microtexture of the Ongatiti Ignimbrite was studied on bulk rock samples from proximal and medial outcrops, with a total of about 130 field samples being examined along with approximately 200 thin sections, both covered and polished. The thin-sections were examined under a petrographic microscope and quantitative data on components within the matrix were acquired by point counting with a minimum of 300 counts per thin section under a binocular microscopy by using a digital point counter.

Image analysis focused on two-dimensional (2D) images and three-dimensional (3D) models. For 2D images, analysis focused on polished thin-sections to derive backscattered electron images (BSE), and small (~ 10 x 10 mm) bulk rock samples were used to obtain high magnification secondary electron images of micro-texture by SEM. Both the polished thin sections and bulk rock samples were coated with platinum in a Hitachi E1030 ion sputter coater and then examined under S-4700 field emission scanning electron microscope in the School of Science, University of Waikato. The images have been captured by using electron beams at 15 and 5 kV.

Further identification of primary and secondary minerals within the ignimbrite was under taken by bulk XRD analysis on 13(whole) samples. The dried powder samples were processed within the PANalytical Empyrean XRD at the School of Science, University of Waikato. They were run using copper K_{α} source for 2-80° (2Θ), at 50 seconds per step and the results then analyzed by Highscore Plus software.

3D analysis of matrix samples was undertaken using synchrotron CT imaging at the Australian Synchrotron, the details of which are described in section 4.1.

To test a hypothesis related to the grain size and welding we carried out an experiment on two different size of a volcanic ash deposit obtained from the TVZ. The ash materials were

separated on the basis of the grain size into two groups, one group made up of particles with a median size of 1.5-1.75φ (coarse ash) and the other with a median size of 4.25-4.5 φ (fine ash) (grain sizes based on Fisher, 1961). Both size fractions had a volume of 80 $cm^3$and they were heated in a 200°C oven over night. Then, their temperature was measured outside the oven during a total cooling period of 150 minutes.

4.4.1 Synchrotron X-ray computed microtomography analysis

The advantages of using synchrotron X-ray sources for µ-CT imaging (Figure4-2) for studying fine rock components are easy and faster sample preparation, and also for obtaining more accurate quantitative and qualitative data. Also, modern synchrotron X-ray sources are able to scan and obtain 3D images in a shorter time, which means a larger number of samples can be analysed. In compare with BSE/SEM method that can only obtain data on a selected surface, µ-CT provides volume data in 3D in different surfaces (Flannery *et al.*, 1987; Landis & Keane, 2010; Zandomeneghi *et al.*, 2010; Baker *et al.*, 2012; Cnudde & Boone, 2013).

Ignimbrites are texturally complex with varying particle sizes and shapes and have complex particle-particle boundaries. Synchrotron µ-CT imaging systems can produce sharper, better-contrasted images of the ignimbrite components, vesicles, amorphous phases and also crystal orientations. Therefore, it would be a better quantitative analysis method for studying ignimbrite in different sizes, (mm to cm) than conventional 2D methods like BSE or SEM. (Tafforeau *et al.*, 2006; Landis & Keane, 2010; Baker *et al.*, 2012).

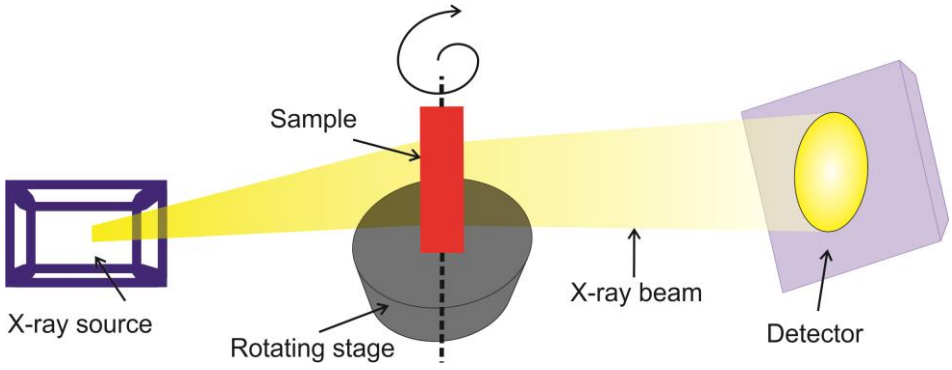

Figure 4.2: Schematic diagram of µ-CT scanning device

One sample of the Ongatiti Ignimbrite in the form of a cut whole-rock slab (see Fig. 4.14, below) from the Hinuera Quarry was chosen to obtain µ-CT images of the ignimbrite texture.

The analysis was undertaken at the imaging and medical beam line (IMBL) at the Australian Synchrotron, Melbourne. The analyses of the matrix were restricted to the groundmass and components $\leq$ 2 mm in size, in order to obtain 3D images and quantitative data pertaining to vesicles, crystals and glassy particles, and their arrangement (fabric) in the ignimbrite.

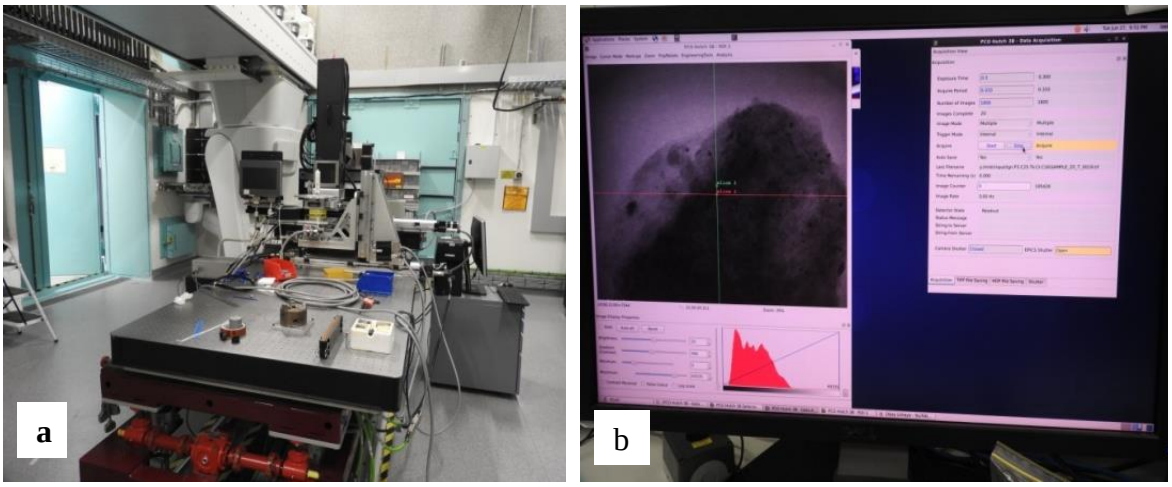

Figure 4.3: a): A view of the sample stage and detector in the 3B hutch (Ruby detector) of the IMBL facility of Australian Synchrotron b) working with FIJI to change image files

At the beginning of the session, ignimbrite and pumice samples to be scanned were sorted into three size categories: small (<24 mm diameter), medium (<54 mm diameter) and large (<117 mm diameter).The beam used was the mode 3B beam in the nMono spectrum. The detector (Figure4-3a) used was Ruby with 150 mm lens, and the object-to-detector distance was set at 30 cm.

During each acquisition the following sequence occurred: (1) 40 dark scans (beam shut) and 40 flat scans (beam open, sample removed) were acquired; then (2) the sample was rotated 180˚ and 1800 projections were acquired; then (3) 40 dark scans and 40 flat scans were acquired again. Projections were processed using the dark and flat scans, and serial step images were stitched. Vertical projections were then reconstructed into horizontal slices (32bit) using XLICT Workflow software. Slice images for each sample were visualised collectively and enhanced (e.g. brightness, contrast) in FIJI and saved as 8-bit files (Figure4-3b). Then, they were imported into Drishti software to visualise and modify 3D models of our samples. Beam acquisition parameters based on a selected sample has been summarized at table4.1.

Table 4.1: Beam acquisition parameters used

Size of samples	large
Beam energy	80 keV
Pixel size	50.5 μm
Projection image size (width x height)	2320 x 701 pixels117.16 x35.4mm
Serial step interval	20mm
No of serial steps	3 to 8 steps

4.5 Primary matrix components

Primary matrix components are defined as ash-sized pumice and lithic, crystals and glass shards all with size < 2mm (Figure 4-4). The matrix components are described, and their distribution is quantified below.

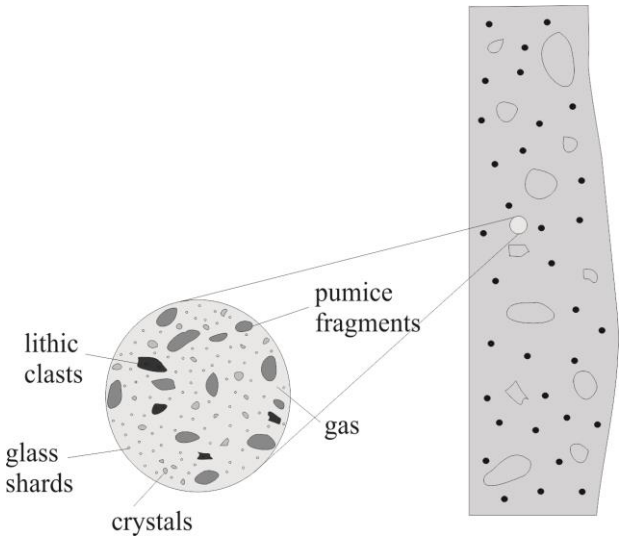

Figure 4.4: Schematic of the sample position and studied micro-texture within the deposit (Not to scale).

4.5.1 Crystals

We emphasize the microscopic physical characteristics of crystals in the Ongatiti Ignimbrite. Plagioclase, quartz, hornblende, orthopyroxene and Fe-Ti oxides are the main primary crystals, and zircon, apatite and sanidine occur as accessory minerals. Crystal abundances are shown in Figure 4-5 based on results of analyses of samples from different sites and representative photomicrographs are presented in Figure 4-6.

The most abundant crystal phase in the ignimbrite matrix is plagioclase (Figure4-6d), which is generally subhedral with resorption along boundaries in some crystals and occasional zoning. Their abundance is around 50 % (of total phenocrysts). The second most common crystals, typically 30% (of total phenocrysts), is quartz which is generally subhedral to anhedral and often resorbed with significant embayments (Figure4-6c). Orthopyroxene crystals are mostly subhedral with eroded edges and they are less abundant (around 10%) and usually smaller compared to plagioclase and quartz crystals (Figure4-6 a).

Hornblende is present in nearly all thin-sections; however, its abundance is typically less than 5%. Crystals are usually subhedral to euhedral and also show zoning in rare samples (Figure4-6b). In all sections, orthopyroxenes are more abundant than hornblende except in lower parts of the sequences at Hinuera Quarry (up to 11 m) and at Tauranga (1.5 m) when hornblende is more abundant than orthopyroxene (Figure4-5).

Opaque minerals occur predominantly as euhedral to subhedral, are elongate and square in shape and are relatively small in size. They are present in all thin-sections but are generally with less than 3% (of total phenocrysts).

Zircon is an accessory crystal common in the matrix of the Ongatiti Ignimbrite. They are mostly euhedral in shape and very tiny in size (<0.1 mm). Apatite, biotite and sanidine are other rare accessory minerals. Sanidine is rare and only found in some thin-sections from the sequences at Hinuera, Waipari Gorge and Tauranga.

4.5.2 Glass shards

Volcanic glass shards are ash particles of fast-cooled melt that are formed during fragmentation that have distinct surface morphologies based on different fragmentation

mechanisms (Heiken & Wohletz, 1985). Glass shards create a matrix for pumice, lithic lapilli, and crystals that comprise around 30 to 80% of the total volume of the Ongatiti Ignimbrite.

Glass shards are present in the ignimbrite matrix in the samples from all sites. They are generally fresh, but at some sites, such as Castle Rock and Waipari Gorge, they are mostly altered. Glass shards occur in a variety of sizes, thicknesses and shapes. Based on their morphology, we have categorized them into several groups (Table4.2) and examples are shown in Figure4-7. Morphologies vary from simple to complex, and micro-vesicles are also present in some shards.

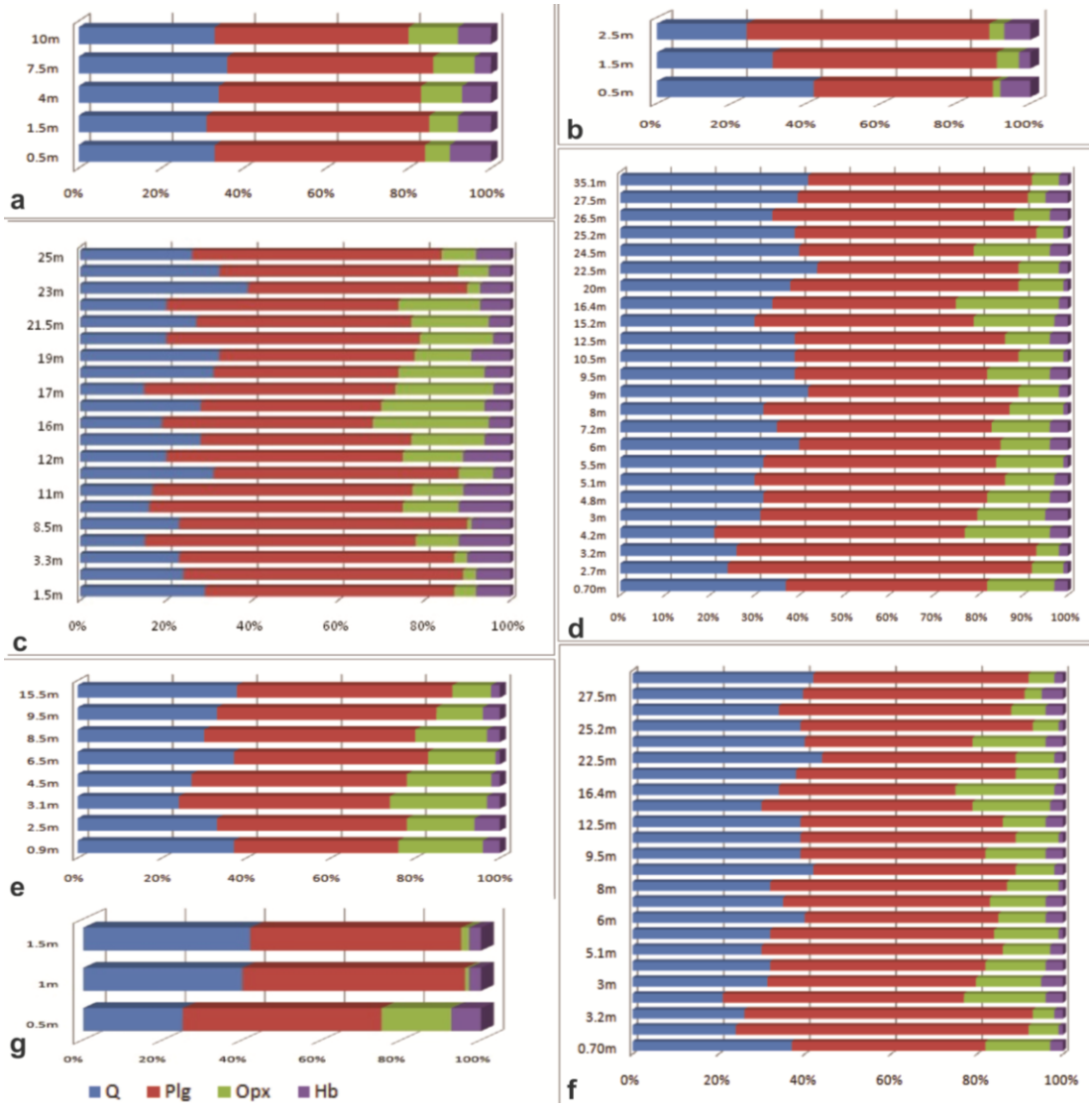

Figure 4.5: The abundances of the main crystal phases at different sites. Plagioclase (Plg) is the most abundant crystal followed by quartz (Q). Orthopyroxene (Opx) is usually more abundant than hornblende (Hb) except in the lower parts of the Hinuera and Tauranga deposits. a) Tauranga, b) Waikato River, c) Hinuera, d) Castle Rock, e) Waipari Gorge (west), f) TeKuiti, g) Bennydale.

Glass shards with two arms occur a curved or straight plates and depict fragments of single bubble walls. Intersections of glass between several bubbles form three arms, four arms or complex shapes. The simple three-armed fragments (Y-shaped) are the most common type of glass shards (Figure4-7d). Vesicular glass shards contain roughly circular bubbles as shown in 4.7a. Shards generally range between 5 to 500 µm in size and, in rare cases, their size reaches up to 900-µm. Bubble wall thicknesses vary from 5 µm to nearly 100 µm (Figure 4-7c).

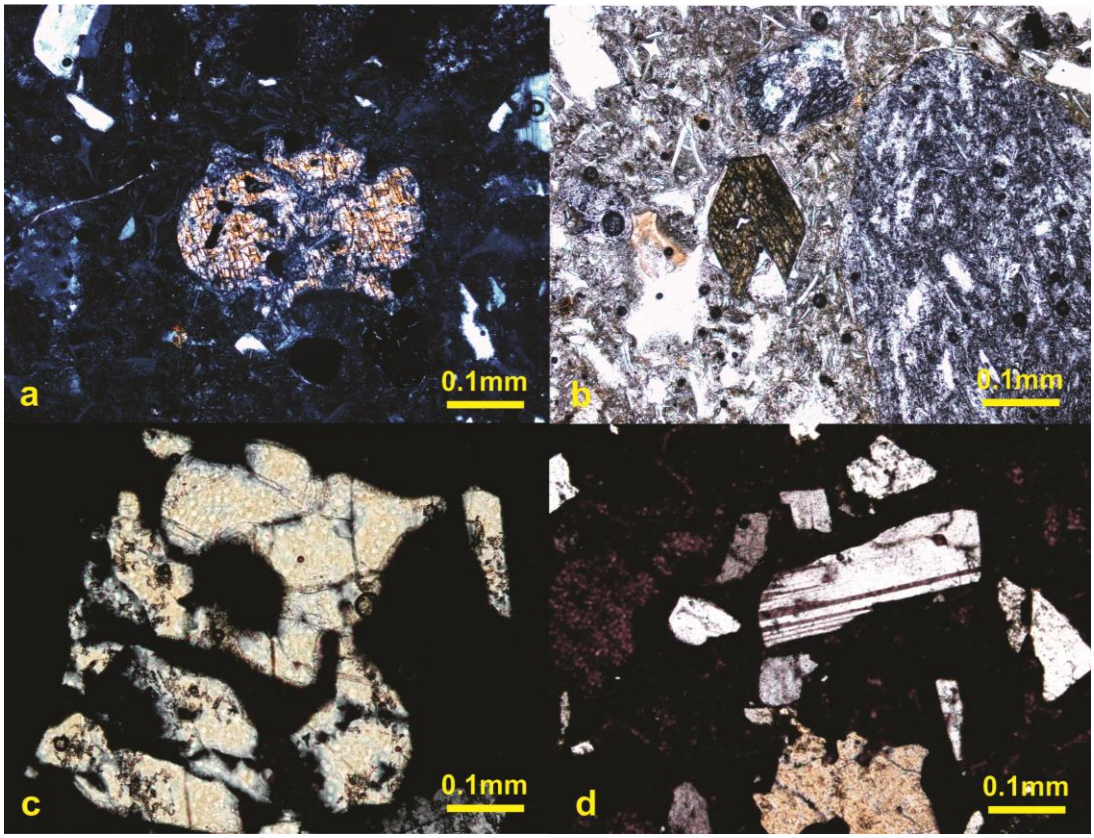

Figure 4.6: Representative photomicrographs of the crystal phases of the ignimbrite matrix; a) orthopyroxene under XPL, b) hornblende under PPL, c) embayed quartz and d) plagioclase under XPL

4.5.3 Pumice fragments

Ash-sized pumice fragments are generally abundant ranging from15 to 30 percent of the matrix volume. Different types of pumice fragments were counted and categorized into vesicular, ‘woody’ and dense based on their shape, vesicle size and the thickness of vesicle walls microscopically. Pumice fragments size varies between 800 µm to >2mm (Figure 4-7b,c,e). Vesicle types have spherical to elongate vesicles and their bubble walls have varying

thicknesses. Woody pumice fragments have elongated tubular vesicles with narrow walls; however, dense pumice show thick walls with very tiny vesicles as illustrated in Figure4-7e. Pumice phenocrysts comprise plagioclase, quartz, orthopyroxene and hornblende, the same assemblage as found in the ignimbrite matrix (Figure 4-7f).

Table 4.2: Typical glass shard morphologies of the Ongatiti Ignimbrite

Simple shapes	**Relative angles between arms**		**Some schematic shapes (without scale)**
Two arms	180° (straight)		
	<180°(curve)		
Three arms(Y-shape)	Equal		
	Unequal		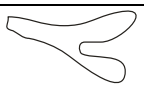
Four arms	Equal		
	Different	**H-**shape	
		X shape	
		Unequal angles	
Complex shapes	**Description**		**Some schematic shapes(without scale)**
Three arms	One, two or three arms are branched		
Four arms	One, two, three or all arms are branched		
Irregular	With micro-vesicles		
	Without micro-vesicles		

4.5.4 Lithics

Lithic clasts are present within the matrix of all studied sites and their size varies from ~400µm to roughly 2mm. Their average abundance ranges between 1 to ~ 12% of the total matrix volume (in an average clast population) and the maximum percentage is seen in samples from Waipari Gorge (west) and the smallest percentage at Tauranga sections. Rhyolite, andesite and greywacke (Figure4-7f) are common lithic fragments of the matrix. Rhyolites are sometimes banded and greywacke fragments are generally unaltered. Older ignimbrite clasts, probably Ngaroma Ignimbrite, were recognized in some thin sections. The Ngaroma Ignimbrite has crystals of plagioclase (main crystal), rarely quartz and opaque minerals; however, is mostly devitrified and depicts spherulitic textures.

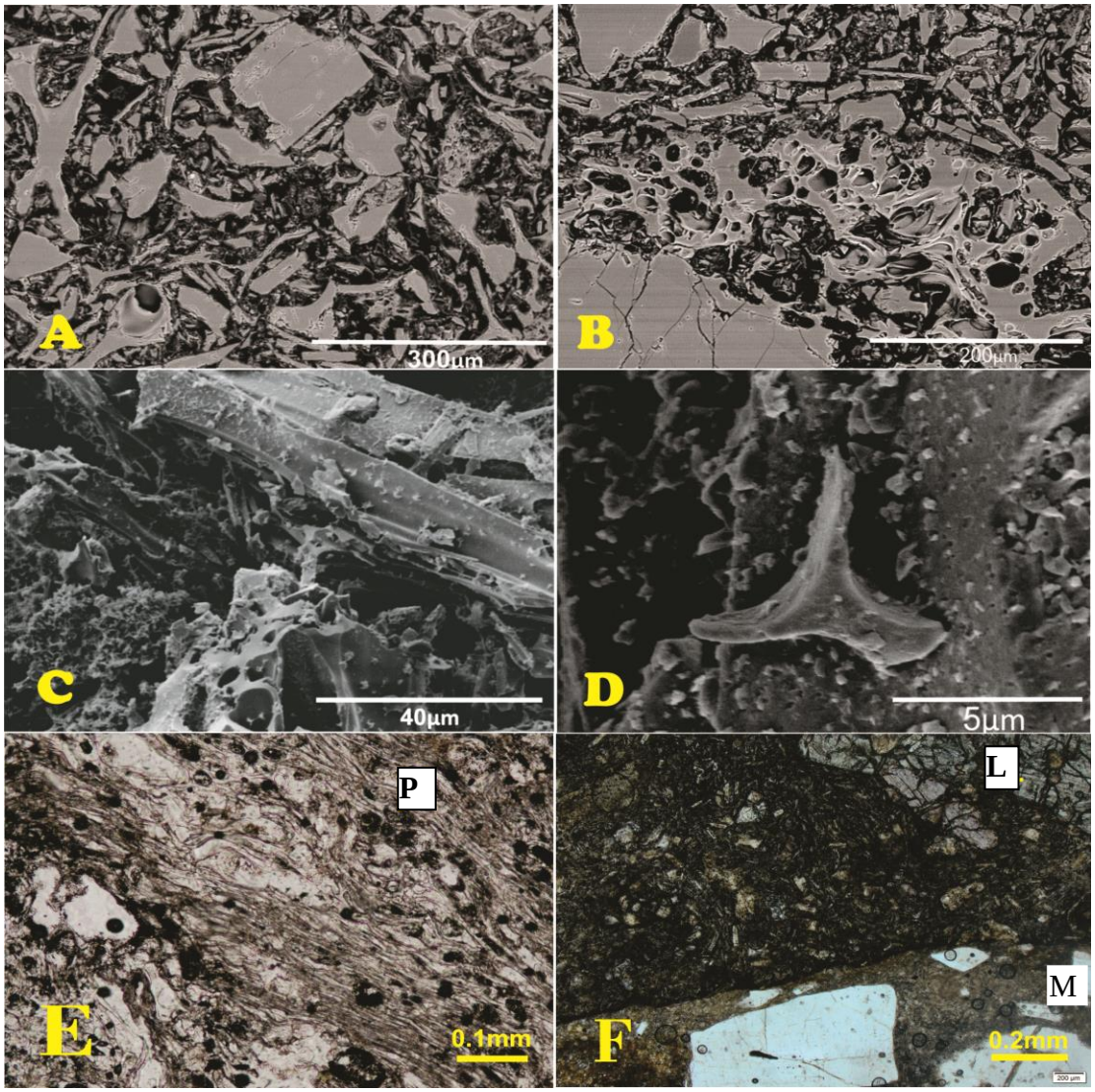

Figure 4.7: Different particles within the matrix of the Ongatiti Ignimbrite. A) Backscattered electron (BSE) image of different types and sizes of glass shards. B) BSE image of a pumice fragment (~ 500 µm) and 10-70 µm-sized vesicles. Glass shards are arranged around the pumice fragments. C) SEM image of pumice (~ 70 µm) that shows vesicles. D) SEM image of a three-armed (Y-shape) glass shard with size around 5 µm from fine ash layer from Hinuera Quarry. E) A vesicular pumice (P) under plane polarised light (PPL). F) A volcanic lithic (L) within the matrix (M) under plane polarised light (PPL).

4.5.5 Distribution of the components

Dispersal of the particles were considered in samples from each of the sites in proximal and medial areas. We have focused on their abundance and size laterally and vertically.

From the microscopic measurements of the glass shards and crystals through the sections, it is evident that glass shards show the lowest average size in welded zones.

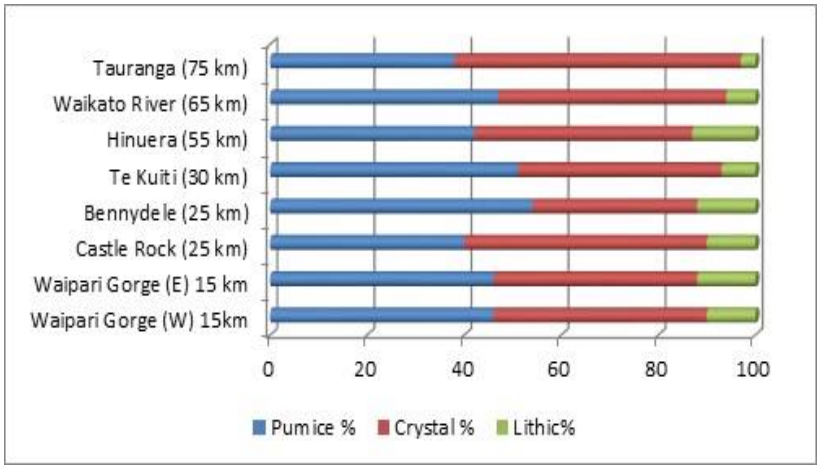

Figure 4.8: Bar chart showing the average proportions of pumice, lithic and crystals in the ignimbrite matrix. 300 grains were counted in each thin-section based on the locations. The studied outcrops present vertically based on their distance to the MVC

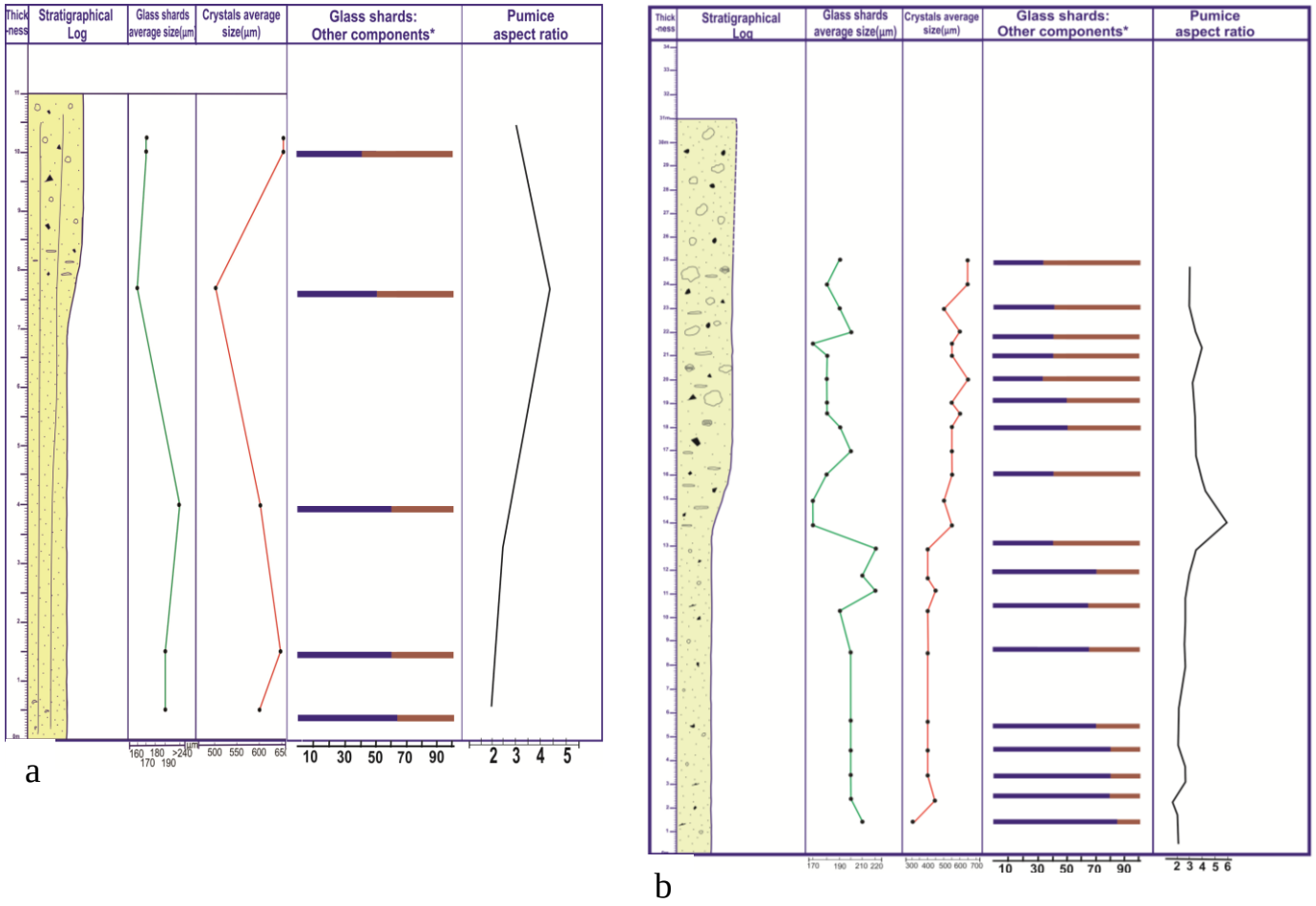

Figure 4.9: Average size of glass shards (green line) and crystals (red line), relative percentage of glass shards (bars,*includes fresh shards, altered shards and pore space shown in blue. Other components are pumice, lithics and crystals < 2 mm in size shown in red) and pumice aspect ratio (black line), plotted against stratigraphic logs for different sections at the following locations: a) Tauranga, b)Hinuera, c) Castle Rock d)Waipari Gorge (West), e) Te Kuiti.

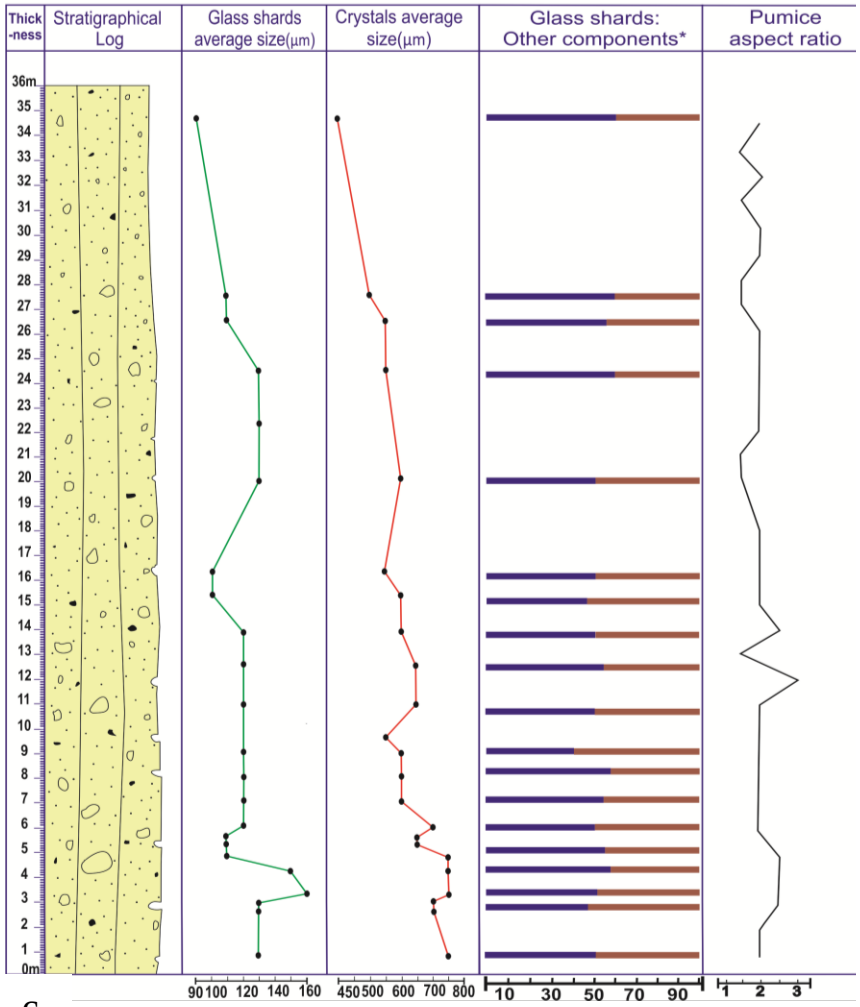
Thick -ness
Stratigraphical Log
Glass shards average size(μm)
Crystals average size(μm)
Glass shards: Other components*
Pumice aspect ratio
36m
35
34
33
32
31
30
29
28
27
26
25
24
23
22
21
20
19
18
17
16
15
14
13
12
11
10
9
8
7
6
5
4
3
2
1
0m
90 100 120 140 160
450 500 600 700 800
10 30 50 70 90
1 2 3

c

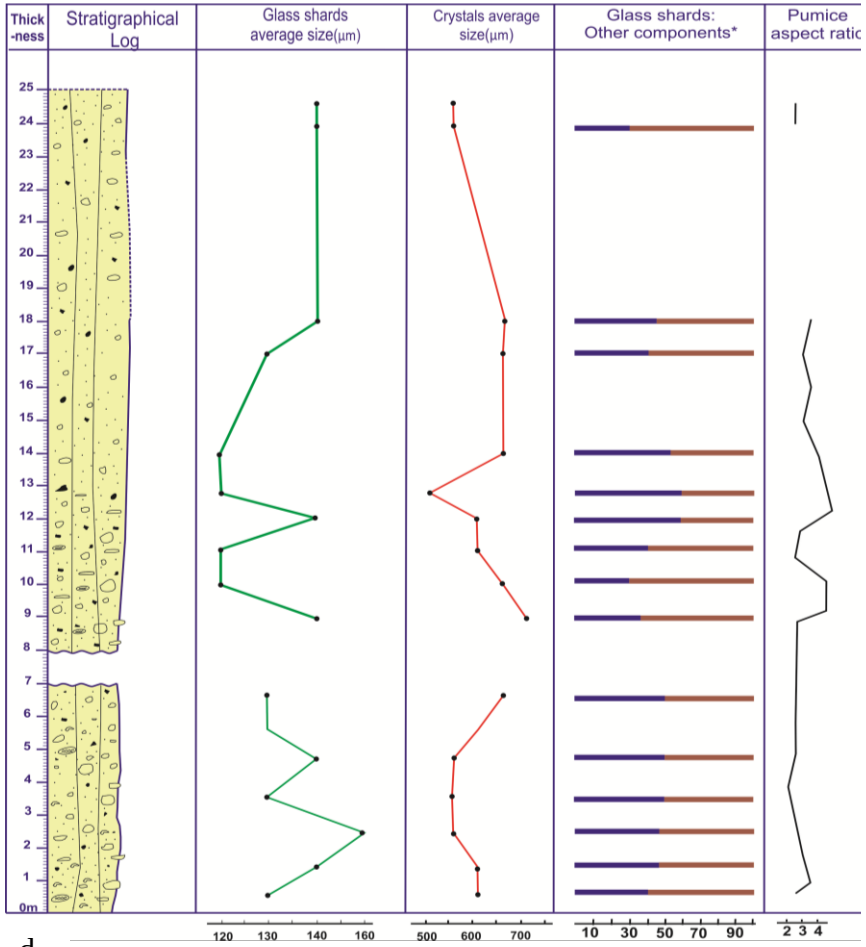
Thick -ness
Stratigraphical Log
Glass shards average size(μm)
Crystals average size(μm)
Glass shards: Other components*
Pumice aspect ratio
25
24
23
22
21
20
19
18
17
16
15
14
13
12
11
10
9
8
7
6
5
4
3
2
1
0m
120 130 140 160
500 600 700
10 30 50 70 90
2 3 4

d

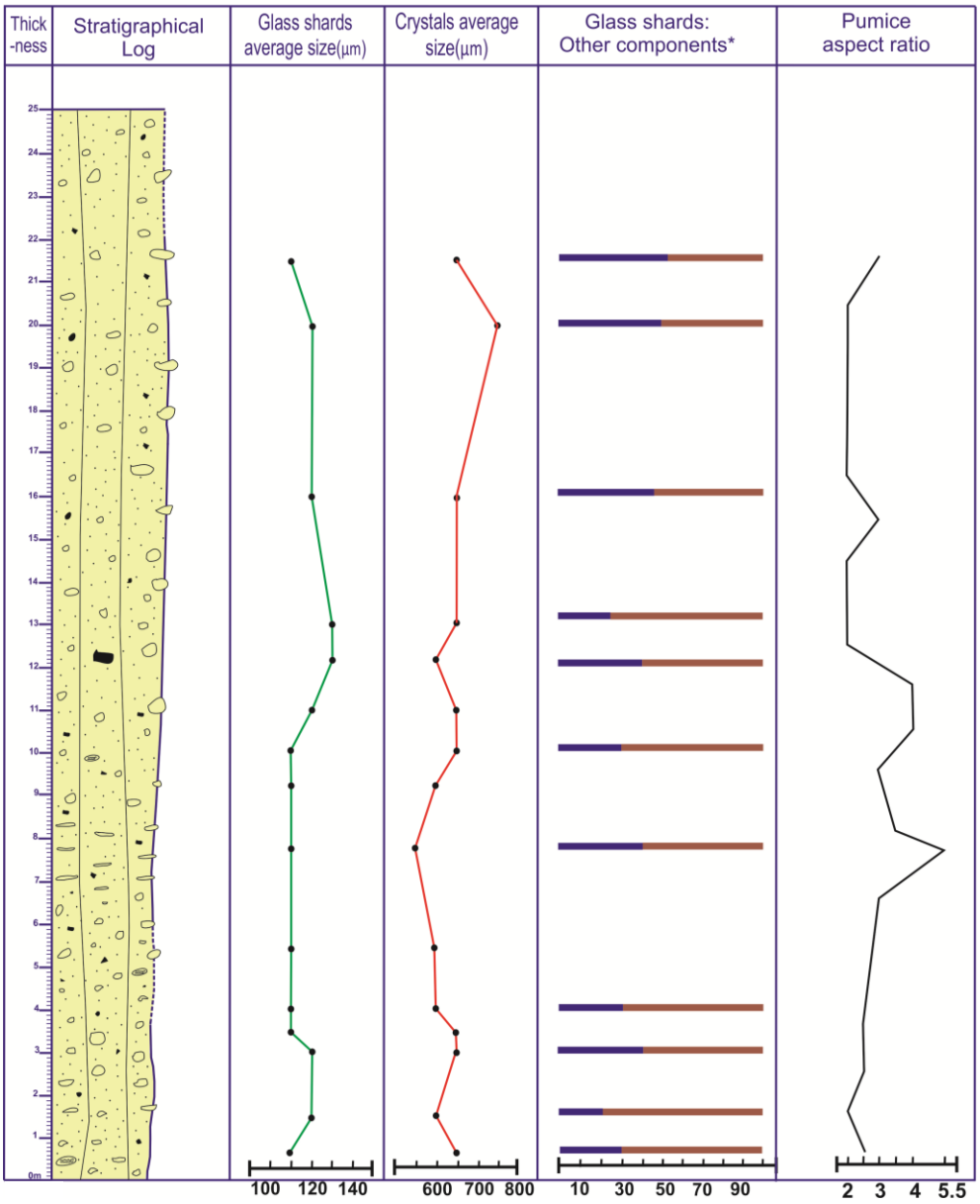

e

4.6 Effect of welding on the matrix

Sintering, compaction and flattening of hot glassy particles in pyroclastic represent the welding process in ignimbrites (Smith, 1960; Ross & Smith, 1961). Welding affects the physical characteristics of the rock. For instance, welding can increase density and decrease primary porosity, particles are flattened and a eutaxitic texture is formed (Smith, 1960; Ragan & Sheridan, 1972; Peterson, 1979; Streck & Grunder, 1995; Rust & Russell, 2000).

Diverse factors, including rheology of pyroclastic flow (Giordano *et al.*, 2005), rate of deposition, temperature (Freundt, 1998), composition of magma and style of eruption (Smith,

1960; Andrews & Branney, 2011) control the welding process.

Previous studies introduced some different welding intensity rankings for pyroclastic deposits. Six zones (1–6) were presented by Smith (1960) according to porosity estimations of the Bandelier Tuff. Bulk densities were used by (Sheridan & Ragan, 1975) for the Bishop Tuff and these authors introduced a division of three zones: non-welded, partially welded and densely welded. Peterson (1979) measured the ratio of pumice flattening for the Leaf Tuff and presented three zones similar to those of Sheridan and Ragan (1975).

Streck and Grunder (1995) suggested another scheme for the degree of welding in the Rattlesnake Tuff based on bulk density and petrography and five zones: non-welded, incipiently welded, partially welded/pumice, partially welded/fiamme and densely welded. Wilson (2003), for the Bishop Tuff, also introduced a classification of five zones: non-welded, sintered, poorly welded, moderately welded and densely welded, based on field properties and density measurements.

Quane and Russell (2005) developed a six-division ranking scheme (I–VI) based on the physical characteristic of pyroclastic deposits microscopically (thin-section studies) and macroscopically (field measurements).

In our research we have focused both on microscopic criteria, consisting of eutaxitic texture, size of glass shards, particle cohesion and deformation and field observations (e.g. aspect ratio of pumice fragments, jointing) and we propose four different welding zones for the Ongatiti Ignimbrite at distinct sites (Table 4.3; Figure 4-4). The type of the welding has been presented based on the microscopic criteria in Figure4-12.

Table 4.3: Welding rank and zones proposed for the Ongatiti Ignimbrite based on microscopic and field properties.

Welding class (this study)	Microscopic Observation			Field Observation				
	Glass shard cohesion	Glass shard deformation	Eutaxitic texture	Jointing	Pumice aspect ratio	Hard/ soft	Pumice orientation	Description
A	No	No	No	No	<2	Soft	Random	Non-welded
B	Rarely	No	No	Yes	<2	moderately soft	Random	Slightly welded
C	Yes	Rarely	Yes	Yes	2-4	moderately hard	Occasional alignment	Partially welded
D	Very common	common	Yes	Yes	4-6	Hard	All oriented	Welded

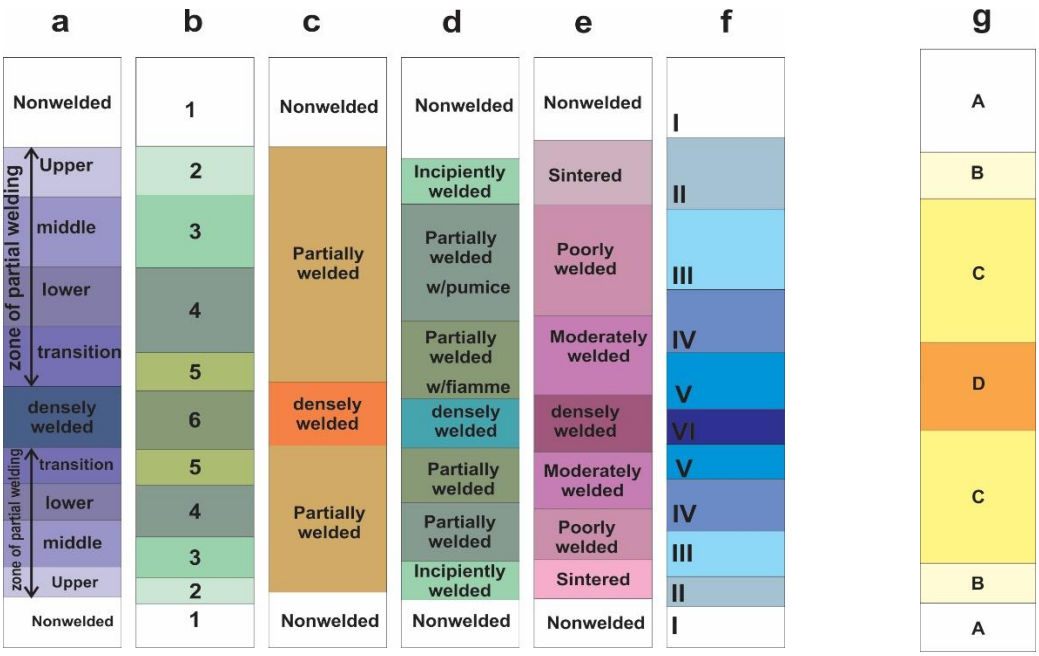

Figure 4.10: Columns comparing our suggested welding zone with other previous suggested welding zone. a) Smith (1960), b) Smith and Bailey (1966), c) Sheridan and Ragan (1976), d) Streck and Grunder (1995), e) Wilson and Hildreth (2003), f) Quane and Russell (2005) and g) this study for Ongatiti Ignimbrite.

4.7 Ash-cooling experiment

The welding degree and the size of the particles from the Ongatiti Ignimbrite show a decrease in particle size through the welded areas. Therefore, it was assumed that there is connection between the glass shard sizes and welding. To understand and prove our hypothesis an ash-cooling experiment was carried out in a laboratory. Two different sizes of volcanic ash (80 cm^3), samples A and B, in 1.5 and 4.5 phi, respectively, were heated overnight in 200˚C oven. Then the temperature of the ashes were measured in the room environment (21˚C)

after removing the samples from the oven, the temperatures were measured starting at 170°C and 160°C, fine and coarse ash respectively. Then temperatures were measured during cooling for 150 minutes until their temperatures were stable at 25°C. The measurements are summarized in Figure4-10 for both particle sizes. The trend shows that finer grains at the same physical conditions (temperature, pressure and volume) keep heat for longer and stay warmer in comparison with coarser grains. The grains in sample A (fine ash) at the first second of the experiment show a temperature (T) around 160° C and those in sample B (coarse) start at around 170° C. During the next hour, the fine grains in B presented a higher temperature than those in A. However, after an hour, both samples A and Breached to the same temperature and the trends in the rate of decrease in temperature became similar.

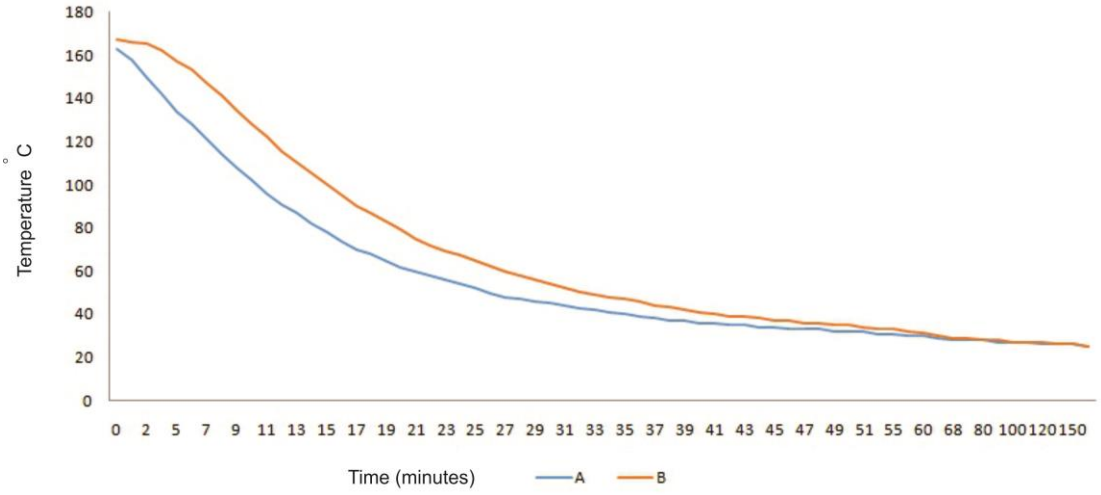

Figure 4.11: Line chart showing temperature of two difference ash-size fractions, A and B, decreasing over time. A: Coarse ash and B: fine ash, respectively

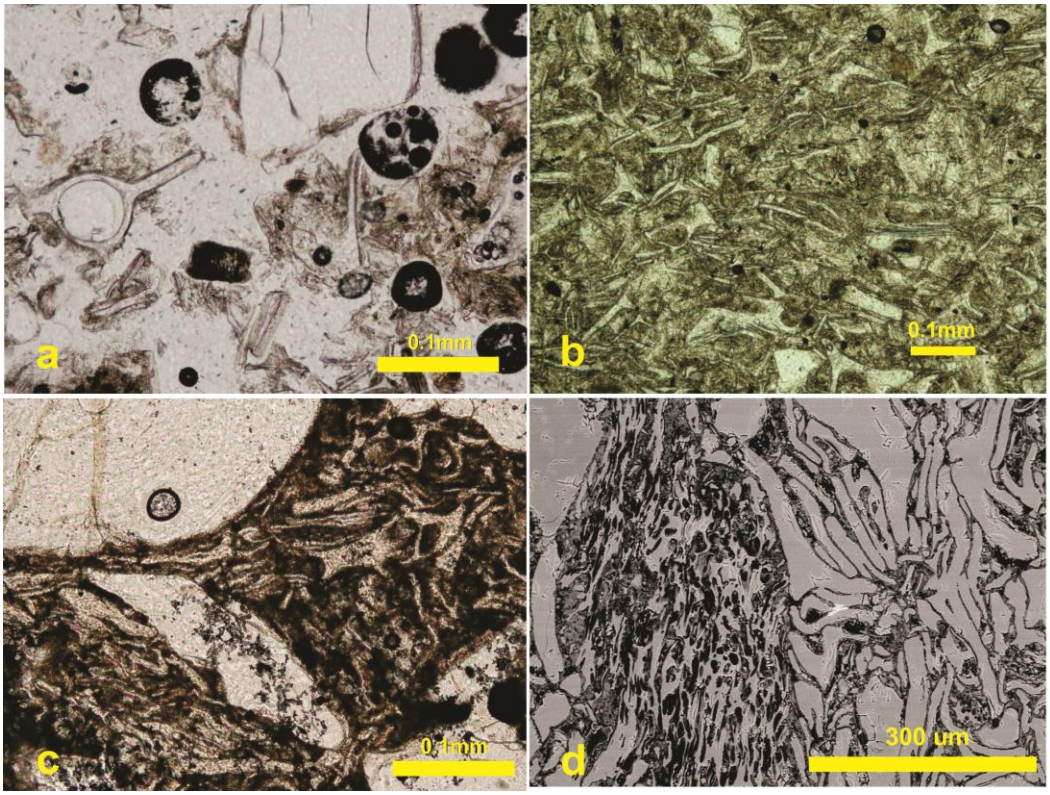

Figure 4.12: Types of welding on the basis of microscopic observations: a) zone a (non-welded), b) zone B (slightly welded), c) zone C (partially welded) and d) zone D (welded).

4.8 Microtomography

Conventional methods of characterising ignimbrite microtextures have been limited to two-dimensional optical, and scanning electron and back-scattered electron microscopy (SEM, BSEI) on rock thin-sections.

The advantages of using synchrotron x-ray sources over other conventional methods for studying fine rock components have been documented (Baker et al., 2012; Schipper et al, 2013; Pardo et al., 2014). Firstly, modern synchrotron x-ray sources are able to scan and obtain 3D images in a shorter time, while maintaining high resolution, which means we are able to analyse a larger number of samples. Secondly, ignimbrites are texturally complex with varying particle sizes and shapes, and complex particle-particle contacts/boundaries. A high intensity, monochromatic synchrotron x-ray beam should minimise beam hardening effects and beam artifacts, e.g. magnification effects, and produce a sharper, better-contrasted image of the ignimbrite components. (Tafforeau et al., 2006; Landisa and Keane 2010; Baker et al., 2012).

The three-dimensional microtexture of volcanic materials (e.g. pumice, scoria, volcanic bombs) has been characterised using μ-CT imaging from various beam sources including synchrotron X-rays(Song *et al.*, 2001; Polacci *et al.*, 2006; Shea *et al.*, 2010; Giachetti *et al.*, 2011; Voltolini *et al.*, 2011; Baker *et al.*, 2012). The matrix of ignimbrite has a complex and variable framework of glass shards, pumice fragments, crystals, rock fragments and interstitial pore space.

A whole-rock sample was collected from the Ongatiti Ignimbrite from the middle welded zone of the Hinuera Quarry outcrop, which includes well-preserved primary ignimbrite matrix, and matrix that has been modified by welding, compaction and chemical alteration.

Brightness in X-ray microtomography images is related to atomic number (Z) and density– for example, titanomagnetite appears white/bright, pyroxene crystals are light grey, and plagioclase crystals and quartz crystals and glass are dark grey. Vesicles are easily distinguished from crystals and glass as they have lowest X-ray attenuation and are black. However, identifying pyroxenes and feldspar and also recognizing feldspar from the glassy matrix is challenging (Ketcham & Carlson, 2001; Degruyter *et al.*, 2010; Giachetti *et al.*, 2011; Arzilli *et al.*, 2016).

The whole rock sample used in this study was large (~4 cm ×4 cm ×5 cm) and the identification of components and textures was complicated. For example, pumice fragments appear black, but it is difficult to separate them from pores for quantified analysis. Crystals show a variety of sizes and shape within the matrix, but occur in different orientations (Figure4-13).

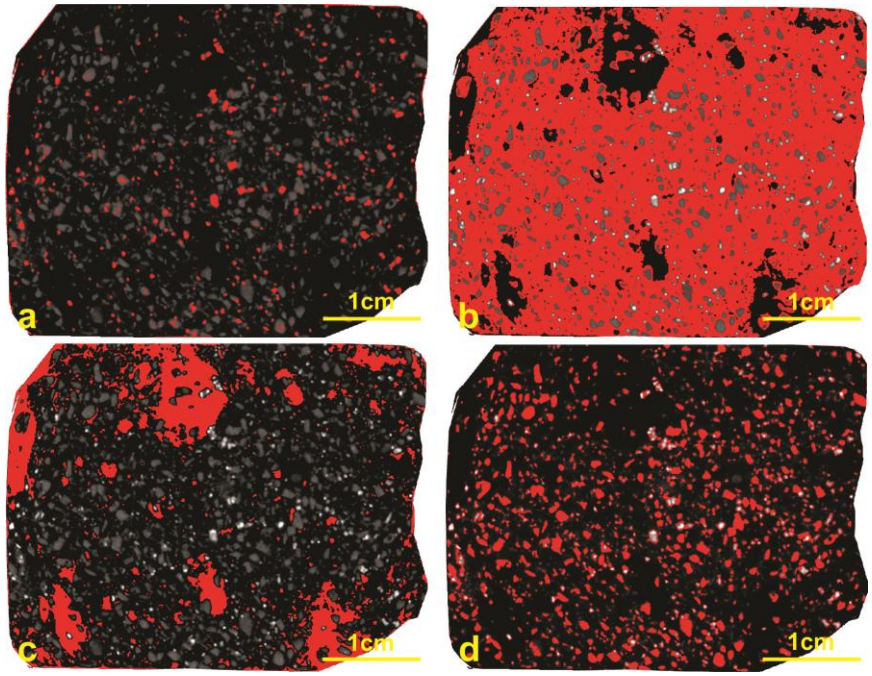

Figure 4.13: Reconstructed horizontal slice stitched across vertical X-ray images taken using μ-CT imaging showing different components (in red) of the Ongatiti Ignimbrite from the Hinuera Quarry site: a) opaque minerals; b) glass shards, quartz and plagioclase crystals and lithics; c) pumice fragments and pores; and d) pyroxenes.

Pumice fragments occur as black areas, which, based on their shape and crystal components, are identified. They are distributed in the matrix randomly but their shape shows two different states: the larger pumice fragments are more rounded and the smaller fragments are more angular.

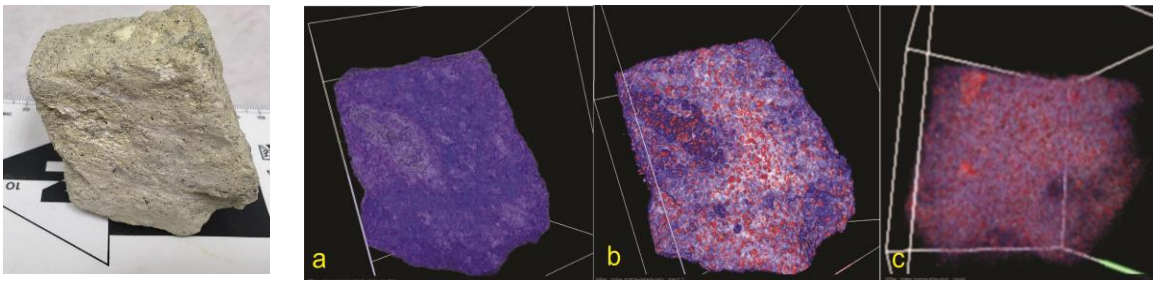

Figure 4.14: The Ongatiti Ignimbrite sample and the3D rendering of the ignimbrite sample (same sample as Figure 4-13).The obtained images were constructed by Drishti 2.6.3 with a stack of 1384 slices. a) Showing distribution of pumice (light violet) on the matrix (dark violet), b) crystals (red) and c) lithic clasts (light red) and crystals (red).

Lithic clasts are mostly dark grey and are similar to feldspars, and can only be identified based on their size, shape and their crystal components.

Pores spaces between particles are black but, are similar in colour to pumice fragments. Therefore, separating pores and pumice in large-sized samples and with the current image resolution is rather challenging. A 3D rendering of the Ongatiti Ignimbrite sample also generated by Drishti as an open-source software (Figure 4-14) and the distribution and arrangement of different crystals, pumice and lithic clasts within the ignimbrite were considered.

Pumice and pores make up 25%, opaque minerals 2%, pyroxene and hornblende around 9% and 64 percent of the bulk ignimbrite texture occupied by glass shards, other crystals (quartz and plagioclase) and lithics.

4.9 Secondary alteration

Primary crystals of the Ongatiti Ignimbrite are mainly plagioclase, quartz, orthopyroxene, hornblende and opaque minerals. The secondary minerals observed are predominantly clays and cristobalite. The matrix has been examined under a petrographic microscope and SEM. XRD was carried out on whole rock samples, and the results are summarized in Table 4.5. The full XRD data are presented in Appendix 1.
Alteration textures vary significantly between different sites (Figure 4-15). At Hinuera, most of the glass shards were fresh and only in the upper part did their colour slightly change to light brown due to alteration. However, at Castle Rock, the glass shards are devitrified throughout the deposit. Spherulites occur in the matrix of the ignimbrite mainly at Waipari Gorge and Castle Rock, and they particularly show spherical and axialitic textures.

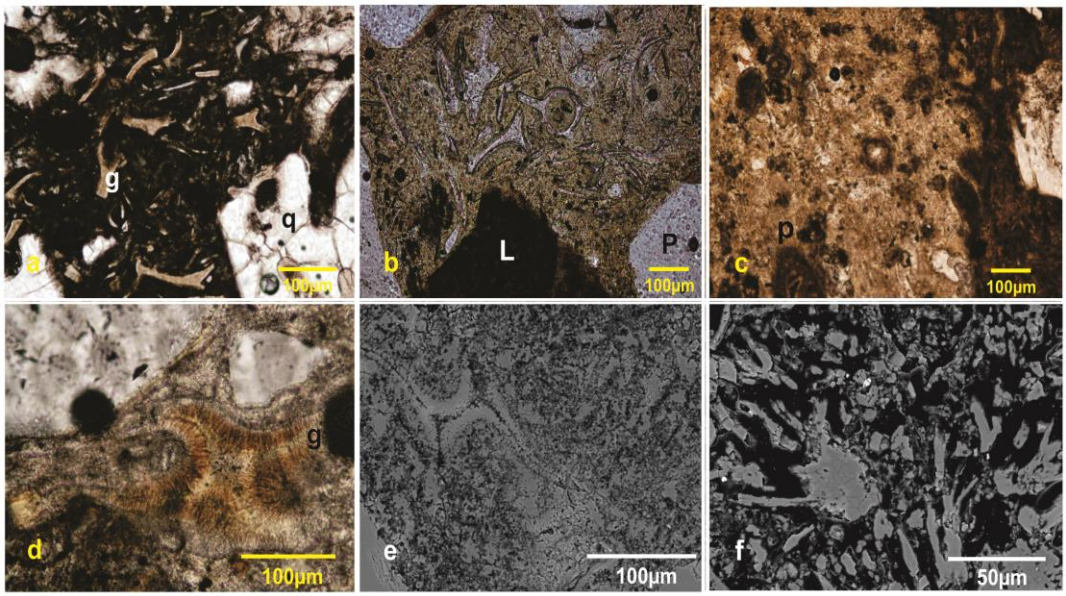

Figure 4.15: BSE and plane polarized light (PPL) images of secondary alteration features in the ignimbrite matrix. a) Devitrification and vapour phase crystallization of glass shards (g) and interstitial space between shards (PPL). b) Fresh glass shards but altered lithic clast (L) (PPL). c) Altered pumice (p) (PPL). d) Spherulite texture (axialitic type) of glass shards (PPL). e) An altered glass shard (BSE).f) Altered matrix and glass shards, black areas are pore space, white crystals are Fe-Tioxides, grey parts are plagioclase crystals and glass fragments, corona around components show alteration (BSE)

Cristobalite was recognized in all sections. Montmorillonoids were seen at three sections, Hinuera, Tauranga and Castle Rock, and chlorite was present at Hinuera and Tauranga sections. At Hinuera, Waipari Gorge and Castle Rock, illite was identified; however, zeolite was diagnosed only at the Waipari Gorge section.

Table 4.4: Common primary and secondary minerals of the Ongatiti Ignimbrite

		Primary minerals				Secondary minerals				
		Q	**Pl.**	**Px.**	**Opq**	**Cristo.**	**Mont.**	**Chl.**	**Zeo.**	**Ill.**
Hinuera	Upper	X	X	X	X	X	X	X		X
	Lower	X	X	X	X	X	X			X
Tauranga	Upper	X	X	X	X	X	X	X		
	Lower	X	X	X	X	X	X		X	
Waipari gorge	Upper	X	X	X	X	X				X
	middle	X	X	X	X	X				
	Lower	X	X	X	X	X				
TeKuiti	Upper	X	X	X	X	X				
	Lower	X	X	X	X	X				
Castle Rock	Upper	X	X	X	X	X				X
	Lower	X	X	X	X	X	X			X

Q=quartz, Pl=Plagioclase, Px=Pyroxene and Opq=Opaque minerals

Cristo=Cristobalite, Mont= Montmorillonoids, Chl.=Chlorite group, Zeo.=Zeolite, Ill=Illite

Secondary minerals have been recognized by optical microscopic studies, SEM, EDS and XRD.

4.10 Discussion

4.10.1 Matrix components variations

The matrix of the Ongatiti Ignimbrite contains vitric particles (including glass shards and pumice fragments), crystals (phenocrysts) and lithic clasts mostly smaller than 2 mm. The relative abundance and size of the components vary both horizontally and vertically across the aerial extent of the ignimbrite. Figure4-16 depicts the abundance of different components (lithics, pumice and crystals) versus distance from the MVC.

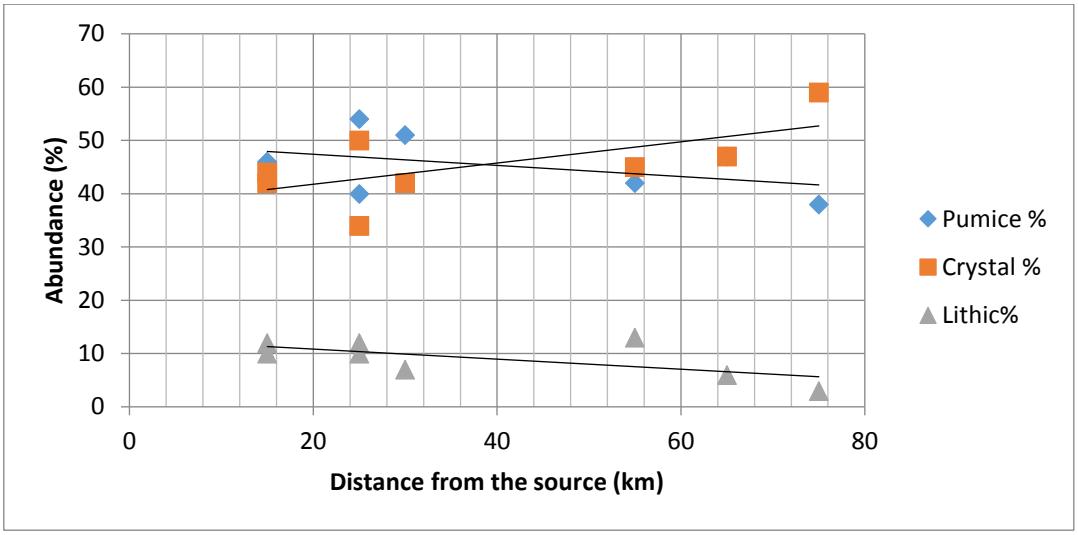

Figure 4.16: Modal percentage (vol. %) of pumice, crystals and lithics in the matrix with respect to distance from the source

The slight variations in component abundance are likely related to particle textural maturity as the deposits were emplaced further from the source. As Figure 4-15 illustrates, lithic are the least abundant, and they decrease in abundance further from the source. Pumice fragments show the same lateral trend, but they are more abundant than lithics. Crystals show the reverse trend: their abundance increases with distance which may be related to abrasion of the larger particles (pumice or lithic clasts) during their long travel. Also, the decreasing size can be related to the crystal enrichment, when pumice elutrated into the ash cloud and the remaining matrix became more crystal rich (Sparks & Walker, 1977).

Crystal contents (in comparison to pumice and lithic clasts) within the matrix of the ignimbrite fluctuate from ~35 to 65 vol.% depending on their lateral position because samples from the sections nearer to the source caldera show the lowest crystal abundance.

The average crystal size (ACS) also changes vertically with in different sections (Figure 4.17). The data indicate that at Hinuera, Tauranga and Te Kuiti the ACS increase vertically, whereas at Waipari Gorge and Castle Rock, the ACS decreases. In sedimentary rocks, it is presumed that abrasion is a crucial process during grain transport and their size decreases with distance and in the down current areas (Pettijohn, 1975). In this study, abrasion in the pyroclastic flow and the decreasing average crystal size at Castle Rock and Waipari Gorge can be related to the attrition. However, at Hinuera and Tauranga sections, the increasing size of crystals can be explained by removing the fine particles during transport

or elutriation in the accompanying ash cloud, as Sparks & Walker (1977) explained. Therefore, we can see crystals larger than average in size in these sections. These data show the effect of textural maturity of the crystal population during emplacement because their sizes are reduced.

Glass shards also show a variety of shapes and sizes. We have suggested a classification for the glass shards based on their shapes as shown at the Table 4-2. The most common shapes of the glass shards are the three-arms shapes (both simple and complex), related to the junction of multiple bubbles (Fisher & Schmincke, 1984). At all stratigraphic sections there is a decreasing trend in average glass shard size (AGS) from base to top (Figure 4-18). Studies have suggested that particles with size of $\geq$500µm would be more abundant in the dense basal section of a pyroclastic flow. However, the finer solids, which are <500µm, form the ash clouds (Burgisser & Bergantz, 2002; Neri *et al.*, 2002; Breard & Lube, 2017; Raganati *et al.*, 2018). Therefore, the changes in glass shard size vertically through the stratigraphic sections can be relevant to the dynamics of the ash-gas mixture in the pyroclastic flow. As the glass shards are turbulent within the particle-gas suspension, it is assumed that the heavier and larger ash particles were emplaced mostly at the bases of the sequences.

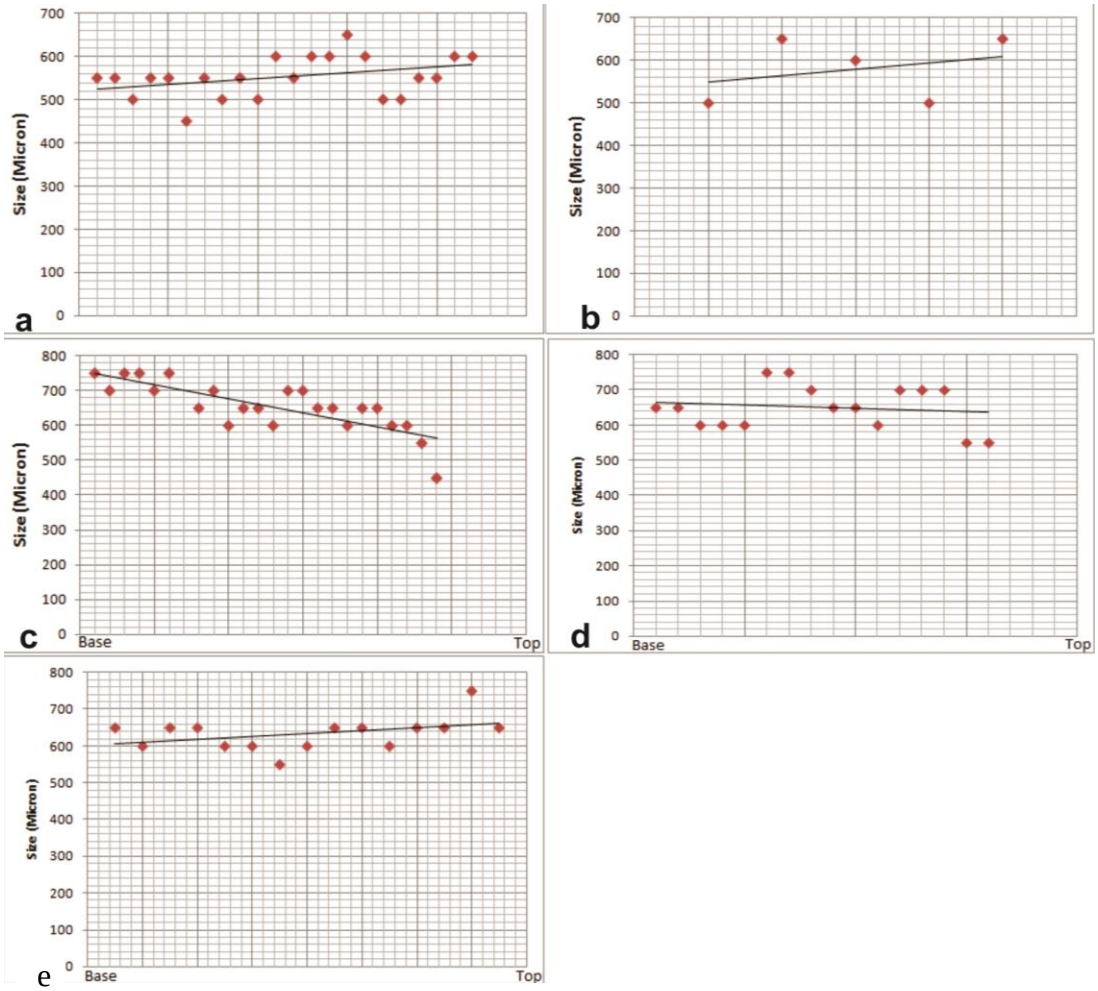

Figure 4.17:Vertical trends of average crystals sizes (ACS) in µm at studied sections that have significant thickness.(a) Hinuera; (b) Tauranga;(c) Castle Rock;(d) Waipari Gorge;(e)Te Kuiti.Tauranga is the furthest and Waipari Gorge is the nearest section to MVC.

At sections near MVC, however, the AGS is smaller than at Hinuera and Tauranga, which are located further from the caldera. This trend can be related to elutriation of finer glass shards in these two far outcrops (Sparks and Walker, 1977).

Pyroclastics comprise particles that show a variety of shapes, size and density. Their angular shape and mechanical strength caused them to be extremely rounded and abraded (Gravina *et al.*, 2004). Particle flow dynamics are controlled by their physical characteristics. Pumice fragments, which have low density can float within the fine matrix, whereas the densest fractions (lithic or crystals) can be deposited at the bottom of the flow (Di Pastena, 1997; Roche *et al.*, 2002; Gravina *et al.*, 2004).

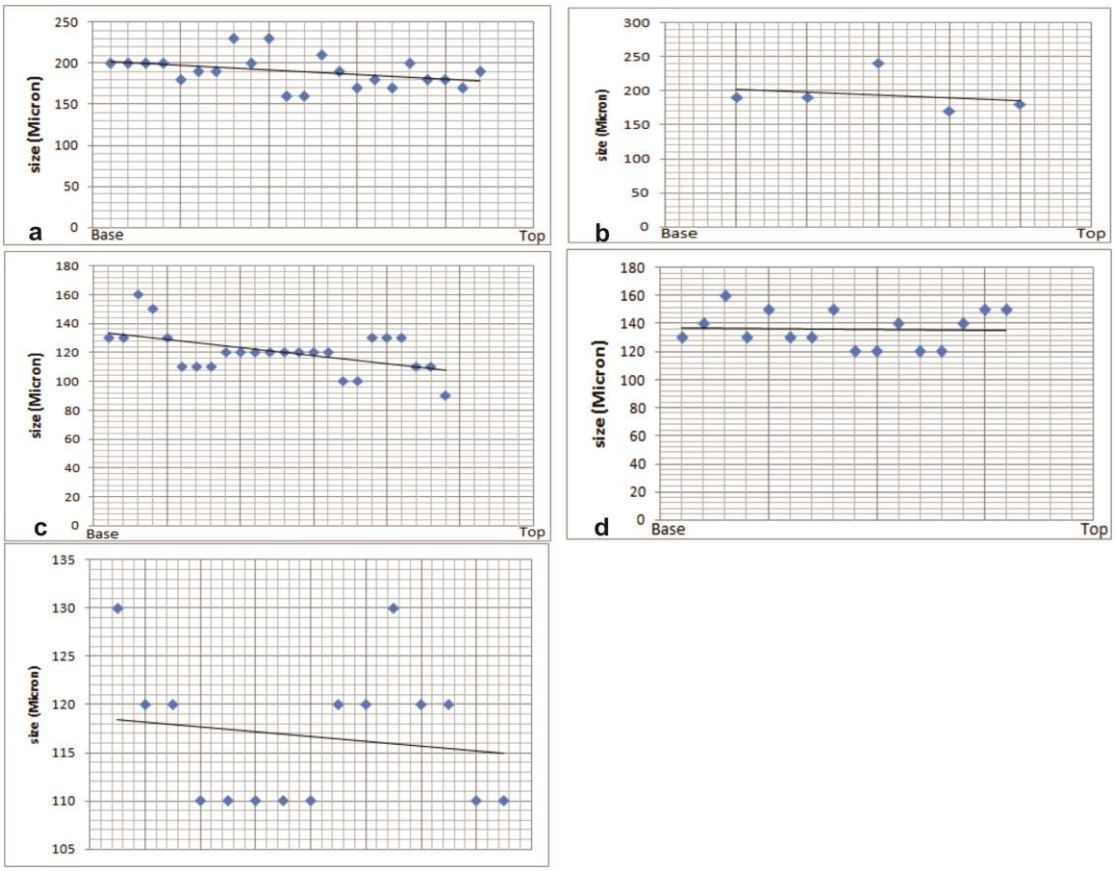

Figure 4.18:Vertical variations of the average size of the glass shards in µm based at the studied sections that have significant thickness.(a) Hinuera (b) Tauranga (c) Castle Rock (d)Waipari Gorge (e)Te Kuiti. Tauranga is the furthest and Waipari Gorge is the nearest section to MVC.

In this study, pumice fragments comprise around 35 to 55% of the matrix components (pumice, crystals and lithics). They are mostly vesicular and woody in shape, and also occur in different sizes at the various sections. Pumice fragments are more abundant than lithic clasts at all sections. Lithic fragments have been recognized mostly at the Waipari Gorge, which is the closest section to the MVC whereas at Tauranga, which is furthest from the caldera, the lithic percentage is lowest. Lithic particles, the heaviest particles within the matrix, have been deposited nearer the source.

4.10.2 Particle interaction

Textures observed in the µ-CT data show an arrangement of crystals around pumice clasts. The crystals are sorted by size around the pumice fragments. Smaller crystals occur near the pumice clast boundaries, whereas larger crystals are further away (Figure 4.20). However, in other parts where there are no big pumice clasts, crystals show an alignment and there is no

arrangement according to the crystal sizes.

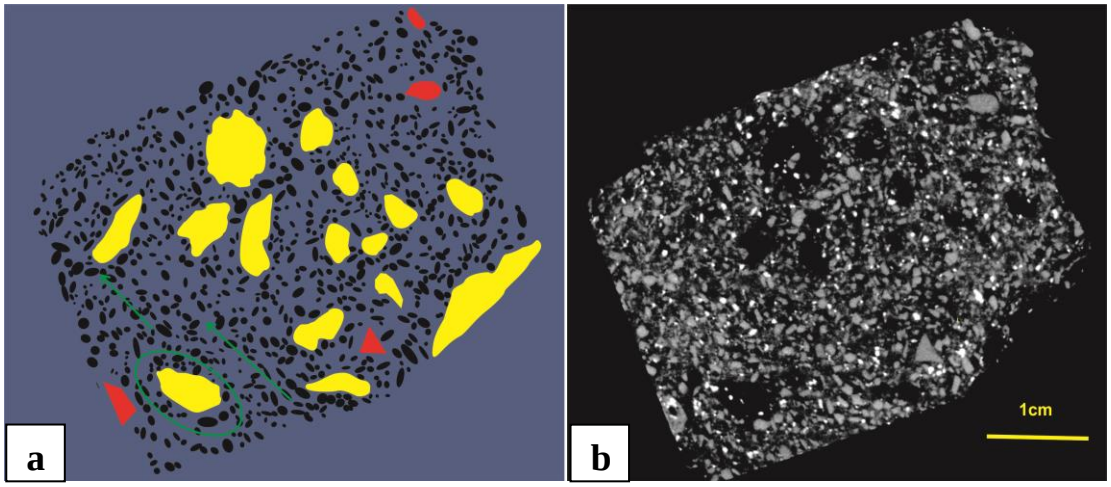

Figure 4.19: a) Schematic of the various particles in the ignimbrite matrix and their arrangement. Yellow and red shapes are pumice and lithic fragments, respectively. Crystals are black. Green depict the arrangement directions. b) The original photo from µ-CT and source of the schematic image a.

The crystal size sorting around pumice clast is inferred to be caused by grain-dispersive pressure which forces large crystals away from contact of large grains in much the same way that phenocrysts flowing in sills and dikes are forced away from the rock and concentrated towards the centre(Komar, 1972; Winter, 2013).

To explain this type of crystal sorting, we infer that during turbulent particle flow, the pumice clasts have acted as a hard boundary between eddy currents. Interaction between pumice fragments and crystals occurs when flow shear forms a grain-dispersive pressure. This pressure forces coarser crystals to concentrate far from large pumice clasts (Figure 4.20).

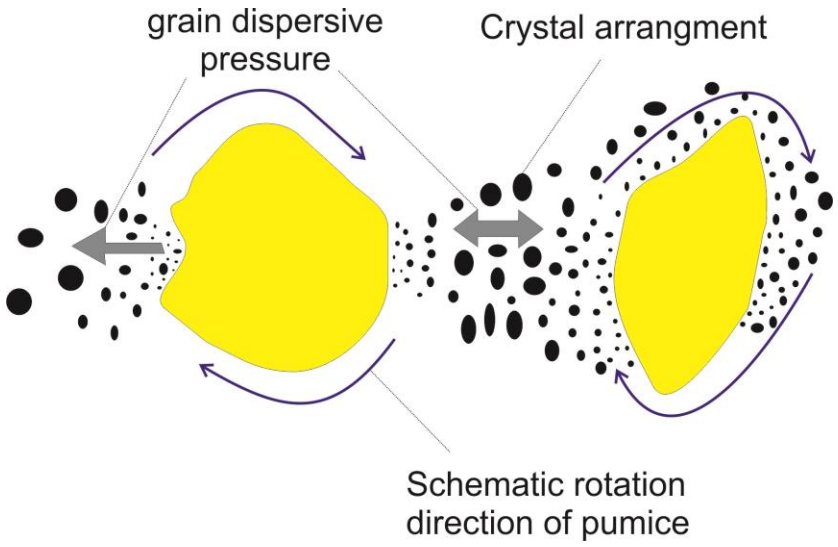

Figure 4.20: Schematic (without scale) of phenocrysts between pumice fragments. The grain-dispersive pressure pushes the phenocrysts away from the pumice and arranged them around the pumice.

4.10.3 Welding

Two ignimbrite types, based on presence of welded facies, were discriminated by Walker (1983). He divided ignimbrite into "low-grade" and "high-grade" when deposits are non-welded or densely welded, respectively. The thickness of ignimbrites was not considered by Walker (1983) in his classification at the time. However, it was subsequently suggested that the high-grade ignimbrites have been emplaced at temperatures higher than the minimum welding temperature at around 650˚C (Bindeman & Valley, 2003; Grunder *et al.*, 2005).

Additionally, five types of welding of ignimbrites were introduced by Branney & Kokelaar (1992) based on an interrelated combination of a) physical properties of temperature, viscosity, and yield strength; b) lithofacies characteristics including lineation, percentage of lithic fragments and flow folds; and c) eruptive and welding processes. This classification involves a transition from extremely low-grade ignimbrite (non-welded) to extremely high grade ignimbrite.

1–Low-grade ignimbrite is commonly non-welded and maybe weakly lithified due to vapour-phase crystallization.

2–Intermediate-grade ignimbrite involves a welded centre and non-welded facies at upper and lower parts. This category commonly contains pumice-rich ignimbrite and represents

load welding.

3–High-grade ignimbrites displaying intense welding throughout the succession from base to top.

4–Extremely high-grade ignimbrite is intensely welded with complete coalescent at ash particles and poorly preserved vitro clastic texture.

5–Fountain-fed lava-like flows have the highest welding degree and are related to low viscosity and hot Hawaiian lavas (Branney & Kokelaar, 1992; Mulas, 2013).

Because of field and micro-textural studies on the degree of the welding, a central welded zone is present in most outcrops and all are rich in pumice. Following Branney and Kokelaar (1992), we suggest that the Ongatiti Ignimbrite shows intermediate-grade ignimbrite features and it is likely related to load processes and moderate temperature and viscosity in the middle parts of the sequences. However, categorizing the Ongatiti Ignimbrite as a "low-grade" or "high-grade" ignimbrite based on Walker (1983) is not appropriate since it shows a mixture of characteristics of both grades.

Different welding degrees are identified in Table 4-3. The highest degree of welding (D, termed 'welded' in our classification, Figure4-11), occurs in the middle of stratigraphic sequences (Figure 4-19). The lowest degree, A, or non-welded, was only seen at the Waikato River section. The most common degree of welding for the Ongatiti Ignimbrite is class partially welded.

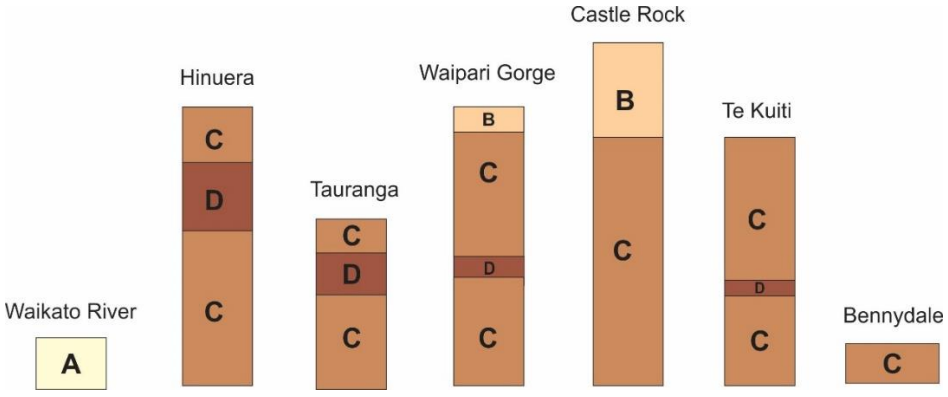

Figure 4.21: Columns comparing different welding degree vertically and laterally between the studied sites in proximal and medial areas. Welding degrees A-D are defined in Table 4.3.

Although this welding study focused on the microscopic and physical criteria, we also considered any correlation between welding and ACS and AGS. The lowest value of AGS occurs within zone D. This association suggests an inverse relationship between ash shard size and degree of welding. Our cooling experiment (Figure 4-9) confirms a relationship between cooling rate and grain size. Smaller size particles are able to keep heating and retain heat better than the larger particles. Therefore, in some parts of the sequences that are composed mostly of the finer glass shards or crystals, they could keep heat longer within the deposit, which provided an appropriate set of conditions for the welding process.

4.10.4 Alteration

The Ongatiti Ignimbrite has undergone various alteration processes such as devitrification and vapour phase alteration. From microscopic studies, axiolites were identified on some samples. They formed during devitrification of glass shards by an interaction between glass and ground water in the presence of heating temperature around 250 to 700° C, as documented in other studies by (Lofgren, 1971; Manley, 1992; Fowler *et al.*, 2002).

XRD and microscopic observations indicate that altered Ongatiti Ignimbrite includes secondary clay minerals in addition to cristobalite and, at one site, zeolites. Clay minerals such as illite within the ignimbrite are a typical feature of hydrous alteration of volcanic glass. Illite is a common mica-clay mineral in epithermal mineralization, and was identified in this study. The temperature of its stability is between 200 to 300°C; therefore it can be considered as a geothermometer (Donoghue *et al.*, 2008). We have observed only zeolite in one of the studied samples from Tauranga section. Zeolite presence may be related to the circulation of meteoric waters, although, elsewhere their absence is probably related to the strong weathering, or that the interactions of fluid and glass did not form zeolites (Cappelletti *et al.*, 2003). In addition, the presence of zeolites can be an indicator of alteration in low-temperature and shallow depth (Donoghue et al., 2008). Chlorite is known in many hydrothermal alteration systems and at the studied sections as recognized in Hinuera and Tauranga, too.

These assemblages of secondary minerals within the ignimbrite imply that the alteration of the Ongatiti Ignimbrite has occurred at low-temperature (≤300 °C) and they are characteristic features for shallow and epithermal conditions.

Based on alteration and welding we categorized the Ongatiti Ignimbrite into three groups: Group I includes deposits at Waipari Gorge, Te Kuiti, Hinuera and Tauranga sites; Group II includes deposits at Benneydale and Castle Rock; and deposits at all distal sections and the Waikato River site form Group III. The ignimbrite in the first group shows vapour-phase alteration, devitrification and welding of classes C and D. They are located in medial and proximal areas. Group II is also situated in proximal areas, and includes welding classes C and Band also vapour-phase crystallization. Glassy ignimbrite with lowest degree of the welding (class A) form group III and are seen in the distal regions.

The variation in welding and alteration across the Ongatiti Ignimbrites on the basis of distance from source is shown schematically in Figures 4-19 and 4-22.

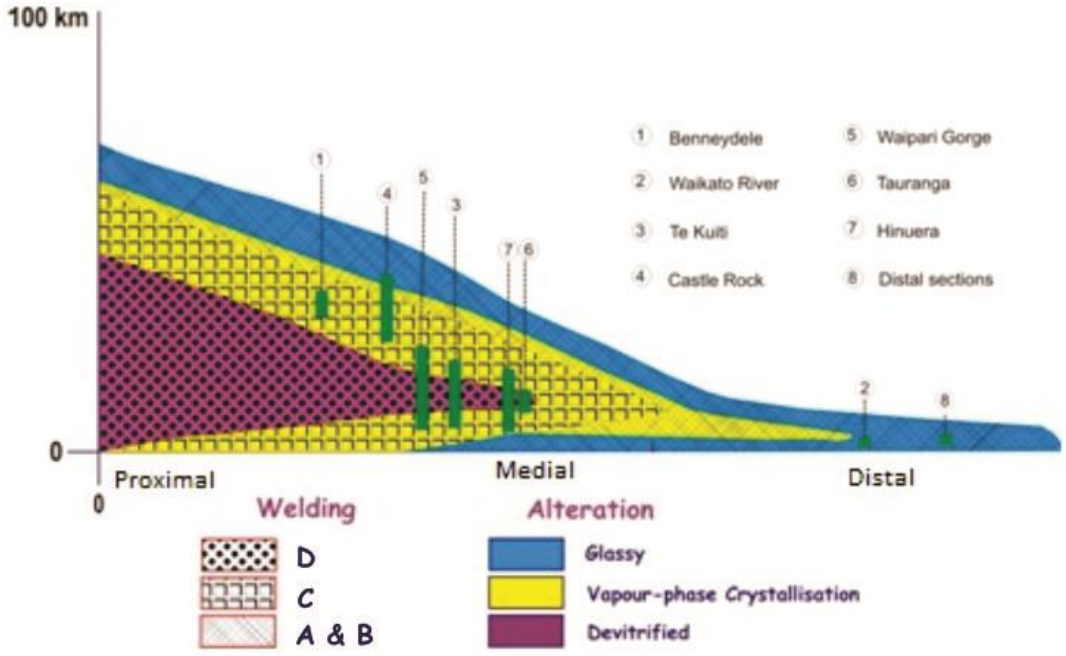

Figure 4.22: Diagram showing the position of studied sites in different locations based on the welding class and alteration of the ignimbrite. (Modified after McPhie, 1993).

Chapter Five

Physical and chemical characteristics of juvenile clasts within the Ongatiti Ignimbrite: implications for eruption dynamics

5.1 Introduction

Pumice is a typical component of pyroclastic deposits with low density (less than that of water) and high vesicularity (Whitham & Sparks, 1986). The Ongatiti Ignimbrite is a pumice-rich ignimbrite, and in particular, pumice-rich facies variations were introduced for the ignimbrite in Chapter3. Physical characteristics of pumice clasts including density, vesicularity, vesicle texture and crystal content are presented in this chapter as well as chemical and mineralogical analysis of volcanic glass to understand more about magma fragmentation dynamics.

5.2 Geological background

The Taupo Volcanic Zone(TVZ) is a NNE-SSW-oriented active volcanic belt (~ 300 km long and 60 km wide) located in the central area of the North Island, New Zealand (Healy, 1964; Cole, 1990; Graham *et al.*, 1995; Wilson *et al.*, 1995b; Leonard *et al.*, 2010; Milicich *et al.*, 2020). The TVZ is one of the most active silicic volcanic systems with > 10,000 km^3 of magma erupted (Wilson *et al.*, 1984; Wilson *et al.*, 2009).

At least 34 caldera-forming eruptions and various smaller eruptions from eight volcanic centers have formed more than 16,000 km^3 volcanic products since 1.6 Ma (Wilson *et al.*, 1995; Wilson *et al.*, 2009). The Mangakino Volcanic Center (MVC) includes the oldest TVZ caldera and is situated at the western boundary of the TVZ. However, the position of the older caldera is difficult to locate due to the long term of erosion of the deposits and burial of the earlier eruptive products by younger deposits, particularly in eastern areas. The location of the MVC has been identified by a gravity anomaly and field observations (Blank, 1965; Rogan, 1982; Wilson *et al.*, 1984).

During two major phases of eruptive activity from MVC (1.6–1.53 and 1.21–0.95 Ma) at least six welded ignimbrite, two phreatomagmatic deposits and many small size pyroclastic units and lava domes have been identified. One of the major ignimbrites from the MVC is the Ongatiti Ignimbrite emplaced sometime between 1.2-1.3 Ma during the second phase and overlies the Ngaroma Ignimbrite (Briggs *et al.*, 1993).

The Ongatiti Ignimbrite is a widespread and mostly partially welded deposit (grade D welding–see chapter 3, this study) that is exposed on the western and northern side of the caldera with a minimum volumeofabout512km^3(DRE). The ignimbrite correlates to a widespread distal tephra to the north around Auckland (Alloway *et al.*, 2004), to the east, as far west as the Tasman Sea coast in the Waikato (Pain, 1975; Horrocks, 2000; Lowe *et al.*, 2001), southeast in the subsurface beneath Waiotapu geothermal field (Wilson *et al.*, 2010), and also to the southwest as far as Wellington (Mildenhall & Alloway, 2008).

The Ongatiti Ignimbrite overlies the Ngaroma Ignimbrite, and these ignimbrites variably overlie Mesozoic and Tertiary sedimentary rocks (McGrath, 2004; Edbrooke, 2005). Within the Ongatiti Ignimbrite there is a pumice-poor facies and an upper pumice-rich facies (Wilson, 1986; Briggs *et al.*, 1993).Various lithic clasts include andesite, rhyolite, older ignimbrite fragments, granodiorite and biotite granite (Krippner *et al.*, 1998).

The Ongatiti Ignimbrite is also a crystal-rich ignimbrite comprising mainly plagioclase, quartz, orthopyroxene, hornblende, and Fe-Ti oxides, occurring both as free crystals in the matrix and as phenocrysts in pumice.

5.3 Methods

Samples of pumice were collected from sections (chapter 3) during 2015 and 2016. Their locations and sampling stratigraphic positions are shown in Figure 4.1 and 5.1, respectively. Details of the samples and the methods of measuring the average maximum size, percentage abundance and aspect ratio of the pumice clasts are reported in chapter 3 (Figure 3.11). Samples of matrix used in chapter 4 were also used here to determine glass shard chemistry.

Approximately 60thin-sections of pumice clasts were prepared for examination by transmitted light microscopy (in both plane and cross-polarized light), including point counting, scanning electron microscopy (SEM), backscattered secondary electron

microscopy (BSE) and energy dispersive spectrometry (EDS). Observations of the phenocryst types and the textures of the pumices were made. Glass shards, although they were described in Chapter 4, are reported here in terms of physical characteristics, including shape and size, to provide context for glass compositional analysis. Pumice components (vesicles, glass, and phenocrysts types) were quantified by point counting around 50 thin sections, each with a minimum of 300 counts.

X-ray image projections of pumice clasts were acquired by X-ray µ-CT at the IMBL beamline of the Australian Synchrotron. Vertical projections were processed by incorporating dark and flat scans, and serial step images were stitched. All samples were processed to this stage. Projections were then reconstructed into horizontal slices (32bit) using XLICT Workflow software. Some problems were found with the reconstructions (e.g. ring artifacts), however, some parameters were changed to minimise these effects. Image slices for each sample were visualised collectively and enhanced (e.g. brightness, contrast) in FIJI and saved as 8-bit files. In total, six samples were processed to this stage. The processed 8-bit image files were imported into Drishti and ImageJ for visualization, modification and analysis in 3D models.

X-ray fluorescence (XRF) spectrometry was used to determine bulk chemistry of thirteen pumice samples from different sites. Samples were prepared by crushing to powder for pressed pellets and fused glass discs. Elemental compositions (major and trace) were determined using an XRF SPECTRO Bruker Tiger S8, in the School of Science at the University of Waikato. One grey pumice last was analysed by an Olympus Delta handheld portable XRF because it was too small to obtain enough powder for standard XRF analysis.

To attempt collecting volcanic glass chemistry data it is important to examine every analysis and eliminate any contaminated data, including that arising from phenocrysts and inclusions. This is necessary in EPMA analysis of major elements; however, the potential for contamination during LA-ICP-MS is higher and the same inspection must be applied when using laser ablation (Pearce *et al.*, 2002; Lowe *et al.*, 2017).

Fourteen polished thin-sections were used for major element geochemical analysis on glass (pumice and matrix shards) by electron probe microanalysis (EPMA) at the School of Geography, Environment and Earth Science, at Victoria University of Wellington. Trace and

rare earth elements were determined by laser ablation inductively coupled plasma mass spectrometry (LA-ICP-MS) at the University of Waikato. The same thin-sections were used for EPMA and LA-ICPMS but the EPMA beam spot points were not necessarily the same sites as the laser spot points. The obtained data were standardized using international standards. REEs are particularly hydrothermal and weathering resistant and are also immobile, so their patterns can be an indicator of magma processes (Rollinson, 1993; Rollinson, 2014). REEs of the Ongatiti pumice clasts were normalized to chondrite with values of Sun and McDonough (1989).

Pumice fragments from different sites and lithofacies were selected for determining bulk density and vesicularity by the water immersion method (Houghton and Wilson, 1989).The selected samples were also used to determine isolated and connected vesicularity by gas-pycnometry using an Ultrapycnometer 100 at the University of Waikato. In addition to the water immersion method of Houghton and Wilson (1989), two additional methods for determining bulk vesicularity were applied for comparison: point counting on a minimum of 300 point per thin-section and X-ray µ-CT on approximately 70-100 two dimensional slices on each pumice clast. All methods and instrument specifications are outlined in Chapter 2.

5.4 Glass shards

Chilled melt fragments that form during magma fragmentation are known as volcanic glass shards. Such glass particles, typically of ash-size (<2mm in diameter) (Lowe *et al.,* 2017), have distinct surface morphologies based on different fragmentation mechanisms (Heiken & Wohletz, 1985). The physical characteristics of glass shards have been discussed in Chapter 3, however the chemistry of the glass shards are determined in this chapter. Glass shard particles comprise 30 to 80 percent of the matrix of the Ongatiti Ignimbrite. However, the original abundance of the ash would have originally been higher since part of the volcanic ash was elutriated through the co-ignimbrite ash cloud. Glass shards, which dominate the ash fraction, are particularly fresh at most sites, but at Castle Rock and Waipari Gorge they have been devitrified and/or vapour-phase altered.

Glass shards observed within the Ongatiti Ignimbrite occur in a variety of sizes, thicknesses, and shapes. Based on their morphology, several groups were developed (Table 4.2) and some

of the visible glass shards have been shown in Figure 4.6 in two and three-dimensional shapes. They illustrate both simple and complex shapes: curved or straight two-arm shards and three-(or more) armed shards. Some shards contain micro-vesicles.

Simple three-arm fragments (Y-shaped) are the most common type of particle (Figure 4.6d). Glass shards generally range between 5 to 500 μm in size and in rare cases, their size reaches up to 900 μm; also their wall thickness varies from 5 μm to less than 100 μm.

Figure 4.9 shows the average size of both glass shards and crystals through the sections I studied. Small ash-sized broken pumiceous fragments (Figure 4.6 b,c) with complex morphology that are larger than glass shards but smaller than pumice fragments are known as pumice shards (Fisher & Schmincke, 1984).

5.5 Types of pumice

Five different pumice types have been classified within the Ongatiti Ignimbrite.

- Type I is the dominant clast type and is white to cream-coloured, highly vesicular and crystal-rich.

- Type II is cream-light yellow, and highly vesicular but the vesicles are elongated giving the pumice a woody or fibrous texture.

- Type III pumice is dark cream to yellow with lower vesicularity and a micro-vesicular texture.

- Type IV pumice is relatively dense and has tiny circular vesicles with thick bubble walls. The colour is mostly cream and clasts are relatively dense. Recognizing dense and micro-vesicular types macroscopically is difficult, and so they are divided based on their microscopic characteristics.

- Type V is grey pumice that was rare in the upper part of the Ongatiti Ignimbrite at Hinuera and Waipari Gorge west sections.

The size of clasts in two first types are larger than those of the third and fourth groups and specifically Type V.

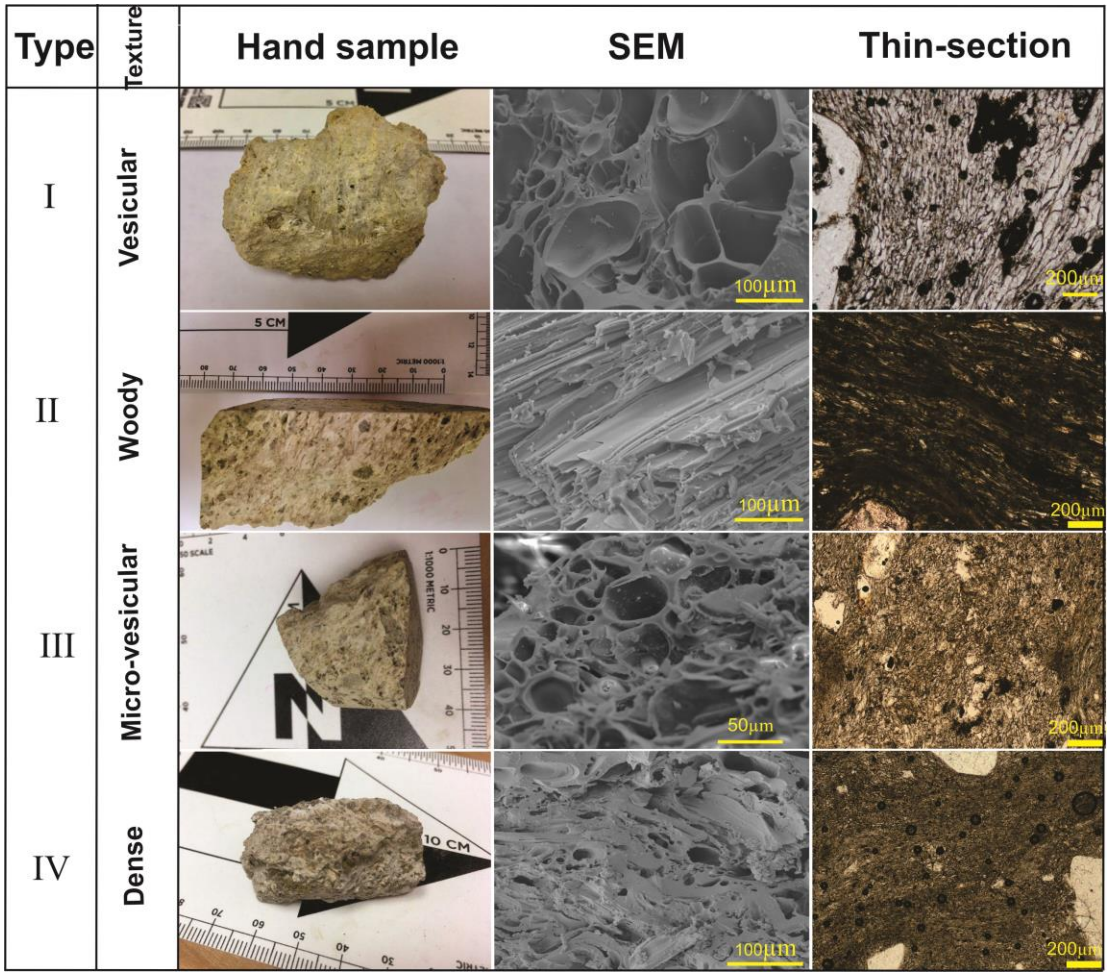

Figure 5.1: Four different types of pumice categorized in this study, including photographs of hand samples, representive SEM images and their micro texture under a petrographic microscope (all in PPL).

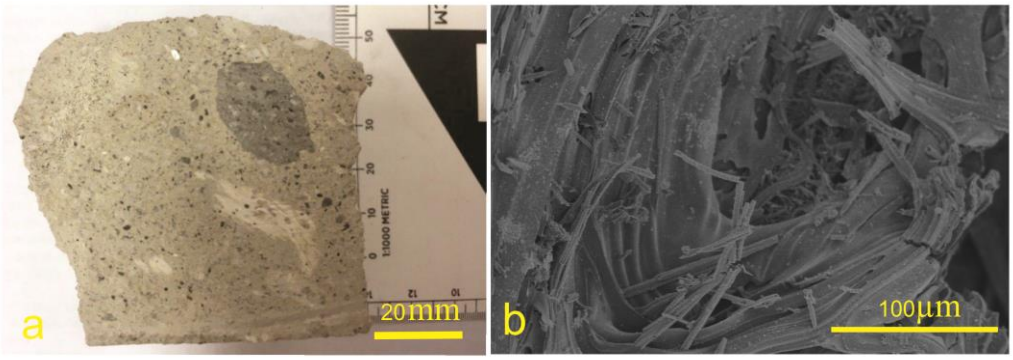

Figure 5.2: a) Hand sample of a grey pumice (Type V). b) Bubbles coalescence texture in type V pumice.

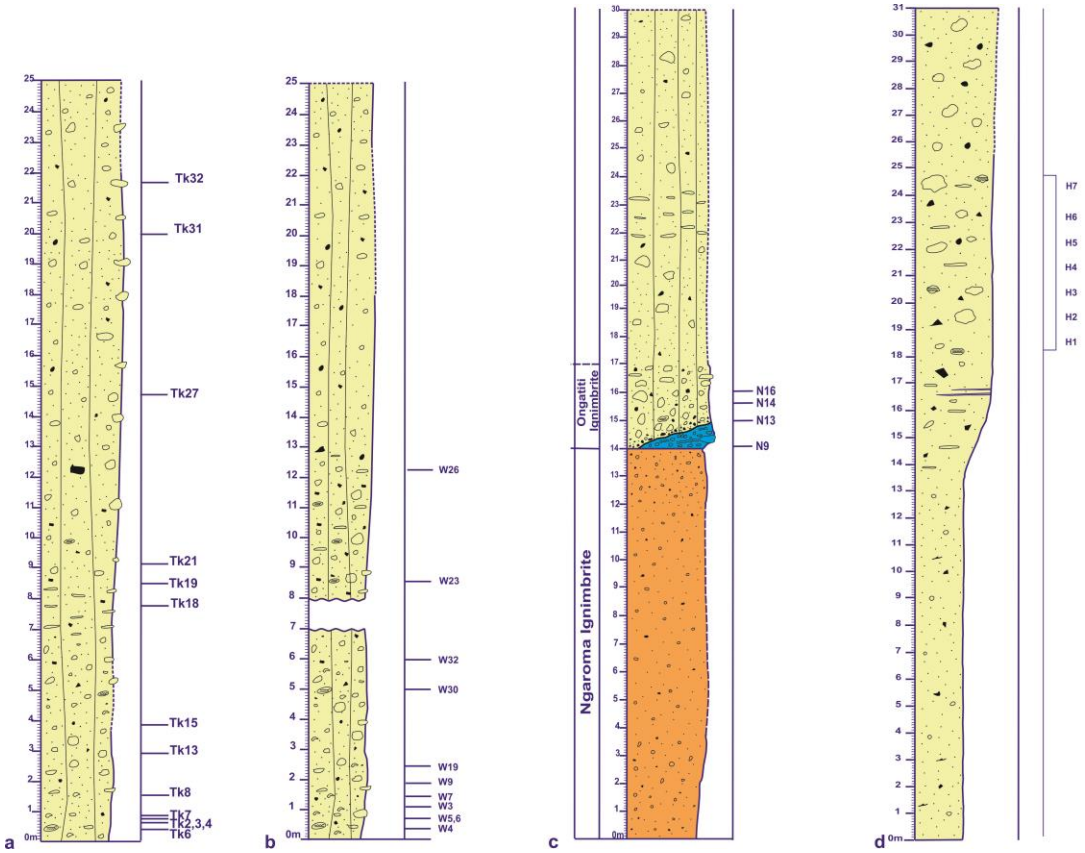

Figure 5.3: Selected stratigraphic columns at four different sites and the position of pumice samples used in this study (see Figure 4-1 for their map location). a) Te Kuiti, b) Waipari Gorge west, c) Waipari Gorge east and d) Hinuera sections

5.6 Vesicularity variations

Physical properties of bulk density, bulk vesicularity, and isolated and connected vesicularity were determined on different pumice clasts from the Ongatiti Ignimbrite, based on vertical and lateral distribution.

The bulk density ranges between 0.41 to 0.82 g/cm^3. The average solid density measured from representative powder samples by gas-pycnometry was 2.6-2.7 g/cm^{3}and this average was used for vesicularity calculations. The mean bulk vesicularity measured by the water immersion method (Houghton and Wilson, 1989), ranged from 71 to 84%. By gas-pycnometry, the average isolated and connected vesicularity ranged from 0.69 to 3.34 % and 68 to 83%, respectively (Table5.1).

Table 5.1: A summary of density and vesicularity data for some selected pumice clasts from different outcrops

Sample	# of clasts in sample	Water immersion		Pycnometry			
		Range of bulk vesicularity (%)	Mean bulk vesicularity (%)	Isolated vesicularity range (%)	Isolated vesicularity mean (%)	Range of connected vesicularity (%)	Mean connected vesicularity (%)
P2	21	70-87	77	0.4-5.44	1.70	69-85	76
P4	22	75-89	84	0.3-6.21	1.33	73-87	83
P6	13	70-89	79	0.42-15.66	2.91	55-88	76
Tk8	7	60-79	72	0.40-1.48	0.72	60-79	72
Tk18	8	65-80	72	0.16-2.98	1.49	64-77	71
Tk27	6	67-80	71	0.37-1.45	0.81	66-80	70
Tk31	5	70-76	73	0.34-1.61	0.69	70-76	72
W7	5	73-84	77	1.91-5.85	3.00	69-82	74
W19	7	67-75	72	1.14-3.61	1.86	66-74	70
W23	2	70-73	72	2.35-4.32	3.34	66-71	68
W26	5	65-78	72	0.73-2.73	1.54	64-77	70
N14	4	64-88	80	0.22-1.52	0.92	63-87	79

Pumice samples from different sites illustrate a variable percentage of vesicles. With respect to X-ray μ-CT-derived vesicularity, at Hinuera two pumices range from 42 to 48 %; at Waikato River, Te Kuiti and Waipari Gorge show vesicularity of 71-73% (Table 5.2). Bulk vesicularity determined by point counting shows an average vesicularity between 55% (Hinuera) to 79% at Waikato River and Te Kuiti.

Highly vesicular types comprise the major portion of the Ongatiti Ignimbrite pumice clast population but some are moderately vesicular, whereas others are extremely highly vesicular, according to the Houghton and Wilson (1989) classification. The maximum bulk vesicularity is seen in types I and II and the micro-vesicular (type III) are less vesicular.

Table 5.2: Measured bulk vesicularity based on different methods, vesicularity description and types of pumice for some selected pumice clasts from distinctive areas

Sample	Bulk vesicularity (%)			Vesicularity description[3]	Type of pumice clasts
	Immerse method	Point counting[1]	X-ray microCT[2]		
H1		55	42	M	II
H3		59	48	M-H	III
P2	77	72	73	H	I
P4	84	79	71	H-EH	I
P6	79	75		H	I
Tk8	72	70		H	I
Tk18	72	73		H	II
Tk27	71	76	70	H	I
Tk31	73	79		H	I
W7	77	62		H	III
W19	72	61		H	II
W23	72	59		H	IV
W26	72	61		H	IV
N14	80	73	71	H	II

1Point counted on at least 300 points in one thin-section
2 On 70 to 100 slices
3 Based on Houghton and Wilson (1989), M: medium, H: high, EH: extremely high vesicularity.

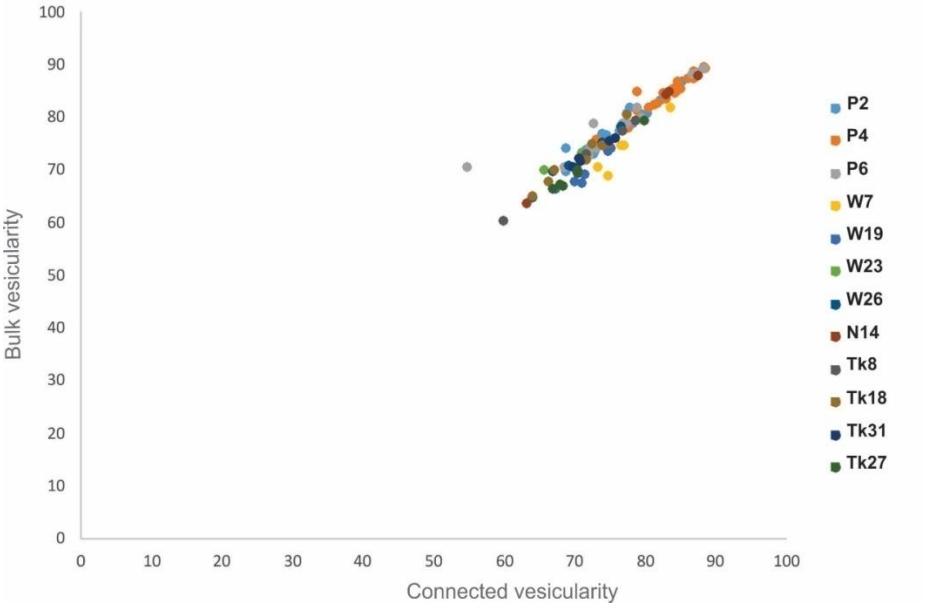

Figure 5.4: Graph showing bulk vesicularity versus connected vesicularity for selected pumice that are presented in Table 5.1

The measured bulk vesicularity by the immersion method was compared to connected vesicularity (%) that was calculated by pycnometry (Figures 5.4 & 5.5), and shows a clear positive trend of increasing bulk vesicularity with increasing connected vesicularity, but a negative relationship between bulk density and bulk vesicularity.

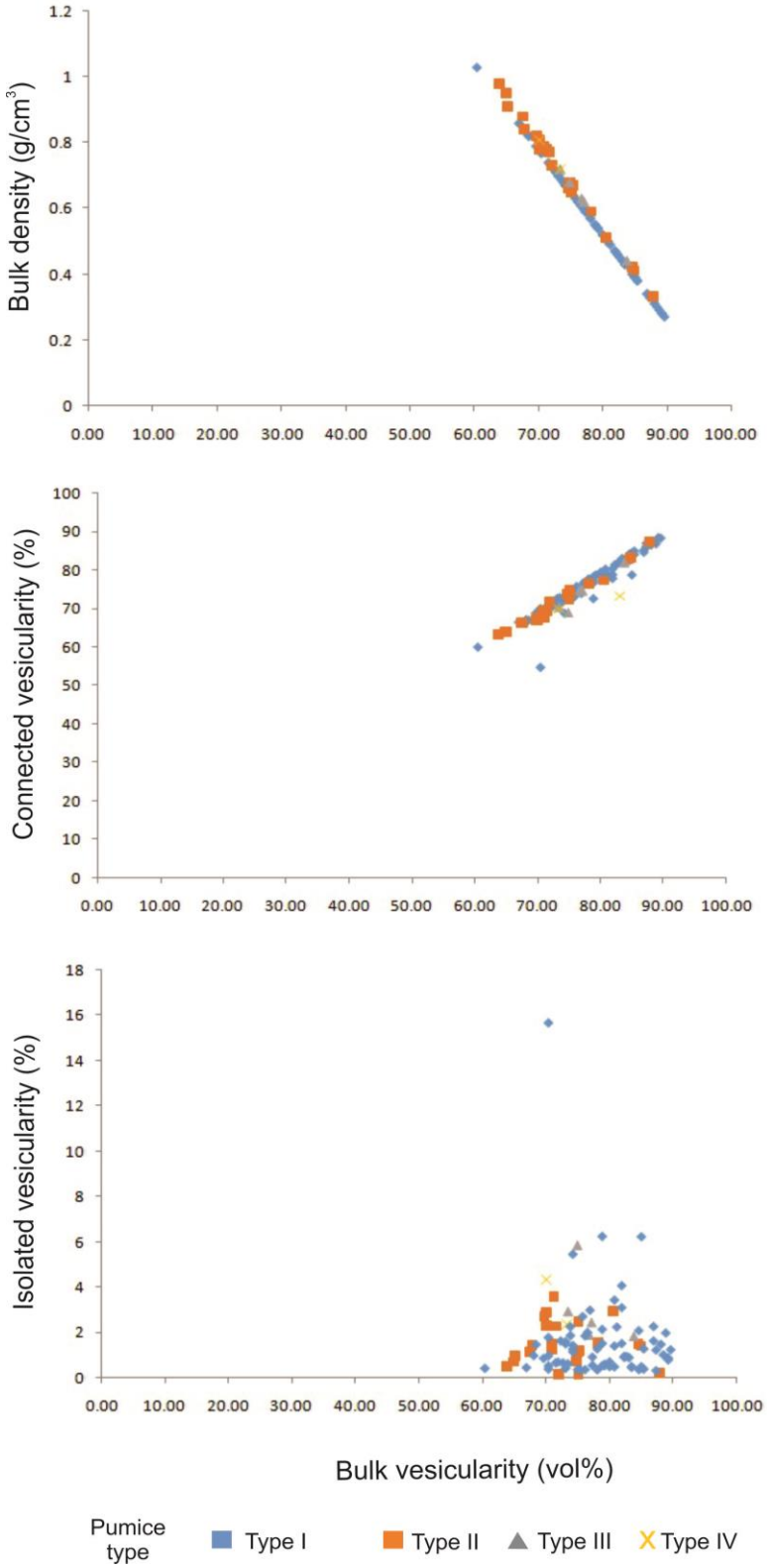

Figure 5.5: Comparative diagrams of bulk density, connected vesicularity and isolated vesicularity versus bulk vesicularity of individual pumice based on pumice type (I-IV).

5.7 Vesicle size, morphology and bubble wall texture

Macroscopic and microscopic data present a wide range of the vesicles shape which is particularly controlled by vesicularity and less by abrasion during transport. Vesicle size varies mostly between >50 microns observed under the microscope to around 2-10 millimeters in hand samples (Figures 5.1 and 5.2).

Vesicular type I pumice comprises the largest clast sizes (~ 50 and 40 cm at the Castle Rock and Hinuera, respectively) and the majority of the pumice fragments within the Ongatiti Ignimbrite. Vesicles have mostly ovoid or spherical shapes but also polygonal shapes, with average sizes from 300-500 µm in long axes and 100-200 µm in short axes. The wall thickness in these pumice types are generally less than 30µm.

'Woody' pumice clasts (pumice type II) are dominated by long and tubular vesicles, and they are rich in crystals and the clasts size varies from >2mm to several hundred millimeters. Microscopic studies show mostly tubular and elongated-shaped vesicles that are mostly elliptical to irregular in cross-section (Figure 5.1). Their average vesicle size (long axis?) is about 300-1270µm and with diameters between 90 and 260µm (Table 5.3). They are all medium to highly- vesicular with a fibrous texture. The thickness of walls varies between >5µm to ~20µm.

Type III pumice with micro-vesicular and crystal-rich texture show more spherical vesicles more and some polygonal vesicles, too. Their vesicle size is less than that of the vesicular pumice but the wall thickness is still tiny and less than 30µm.

Dense pumice types (type IV) are also crystal-rich and are less abundant within the ignimbrite. Their vesicle shapes are mostly polygonal but the most characteristic criterion for these pumice clasts is that their vesicle wall are thicker than for type II and III.

The last type of the pumice clasts (type V) are classified only based on their colour and were seen very rarely in outcrops. The pumice clast size is small, around 2 cm, the vesicles are tiny in hand samples and they are likely to be micro-vesicular.

Using SEM and BSE images, the shape of the vesicles was defined in two dimensions and aspect ratio of the vesicles (length/width) were measured on at least 47-79 vesicles of each

pumice via thin-section. The longest vesicle aspect ratios were seen in woody pumice, generally more than 4, but vesicular types have aspect ratios that range between2 and 3. The calculated aspect ratio for micro-vesicular pumice types is ~2.5.

Table 5.3: A summary of vesicle dimensions measured for selected pumice clasts from different sites

	Number of measured vesicles	Range of long axes lengths (rounded μm)	Range of short axes lengths (rounded μm)	Average long axis length(rounded μm)	Average short axis length(rounded μm)	Average aspect ratio	Pumice type
H1	47	300-590	70-120	430	90	4.80	II
H3	51	110-125	44-48	118	46	2.57	III
P2	79	370-700	150-245	510	200	2.55	I
P4	72	220-550	91-170	340	120	2.68	I
P6	60	490-825	111-190	470	140	3.14	I
Tk8	59	255-405	80-150	300	100	3.02	I
Tk18	48	300-800	90-160	410	100	4.11	II
Tk27	70	295-620	111-140	380	120	3.12	I
Tk31	58	245-620	130-190	340	151	2.18	I
W7	49	115-157	55-60	140	58	2.41	III
W19	73	305-800	130-160	530	130	4.02	II
W23	58	920-1500	250-290	1270	261	4.76	IV
W26	64	430-700	120-180	540	140	3.90	IV
N14	62	290-410	60-100	330	71	4.30	II

Moderately to extremely highly vesicular pumice clasts present various ranges in vesicle size (Table 5.3).

5.8 Phenocrysts

In all pumice clasts examined, plagioclase, quartz, hornblende, pyroxenes and Fe-Ti oxides are the main phenocrysts. Phenocrysts within pumice fragments are generally the same phases observed within the Ongatiti Ignimbrite matrix. The variation in phenocryst abundance are presented in Figure 5.6, and quantified variations across different outcrops are shown in Figure 5.7.

Phenocrysts in pumice are generally euhedral to subhedral; however, angular fragments occur in lower abundances. Broken phenocrysts range from fractured pieces that are in

contact with one another, to separated fragments. Phenocrysts are generally less rounded and fragmented compared to crystals in the surrounding matrix.

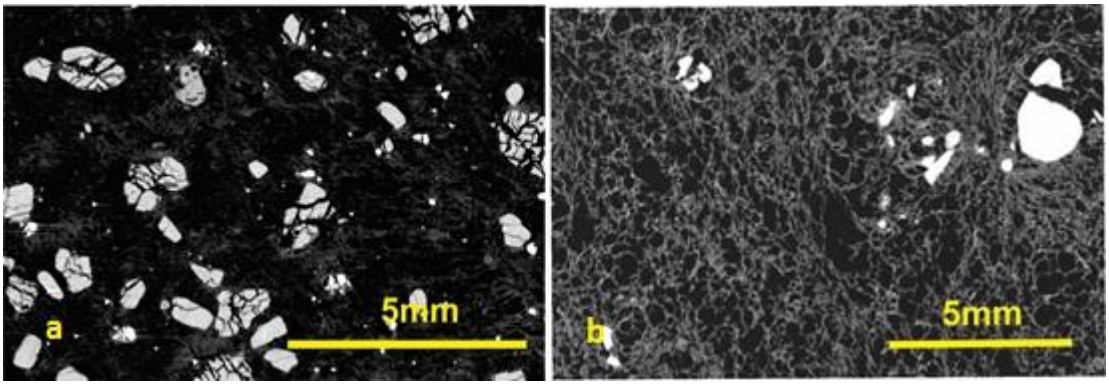

Figure 5.6: Reconstructed image slices acquired by µCT of pumice fragments with different vesicularity that also show different percentage of the phenocryst types. (a) Micro-vesicular pumice with abundant phenocrysts and (b) vesicular pumice with relatively few phenocrysts.

Plagioclase is the most abundant phenocryst, occurring mostly as euhedral and subhedral crystals and comprising46 to 70%, of the crystal population. Plagioclase is occasionally zoned. Quartz phenocrysts are mostly subhedral and range from 11 to 43%. Orthopyroxene phenocrysts are mostly euhedral and comprise around 5 to 22% and, in some rare pumice fragments, clinopyroxene was observed.

Figure 5.7: Pie charts showing the relative percentage abundance of major phenocryst phases across several outcrops and stratigraphic phenocrysts of the Ongatiti Ignimbrite. The total percentage abundance of phenocrysts within bulk pumice is stated below each pie chart as measured by point counting (black text) and μ-CT (red text).

Hornblende is present in nearly all pumice clasts, but in low proportion (0-16%). Their shape is particularly euhedral and zoning is shown in few samples. There is no clear trend in the occurrence and proportion of different phenocrysts within the pumice through vertical sections of the Ongatiti Ignimbrite.

Pumice from the Waipari Gorge east section shows the maximum abundance of plagioclase (63%) and quartz (35%) but minima of pyroxene (5%) and hornblende (<1%). The lowest average percentages of plagioclase (46%) and quartz (11%) were measured in Hinuera and Te Kuiti. The highest abundances of pyroxene (22%) and hornblende (16%) were seen at Te Kuiti and Waipari Gorge west.

The proportion and distribution of phenocrysts in pumice were studied in two- and three-dimensions in thin-sections under the petrographic microscope, SEM, and in whole pumice clasts by X-ray µ-CT. The percentage of phenocrysts in two-dimensional µ-CT slices was estimated by using ImageJ. Two-dimensional estimate for phenocrysts within pumice at different outcrops vary from around 9% at Waikato River in vesicular pumice to approximately 23% at Hinuera, within micro-vesicular pumice. The phenocryst percentage for the other three pumice clasts at Hinuera (woody pumice), Waipari Gorge East (woody pumice), Te Kuiti (vesicular pumice with thick bubble walls) and Waikato River (vesicular pumice, thin walls) were estimated by µ-CT images at 18%, 15%, 10% and 11%, respectively.

To visualise the phenocryst arrangements within pumice, I applied Drishti software and reconstructed three-dimensional of some selected pumice clasts. The 3D distributions of the crystals with indifferent pumice types are shown in Figure 5.8. It is assumed that the phenocrysts arrangement in this pumice (woody pumice) is related to the shape of tubular vesicles.

Within the Ongatiti pumice there are many broken or fractured phenocrysts. According to Miwa and Geshi (2012), broken phenocrysts are classified into two groups: Group A, phenocrysts with cracks that are perpendicular to the long axis of the crystal (Figure5.9a,b); and Group B, phenocrysts with cracks both parallel and perpendicular to the long axis.

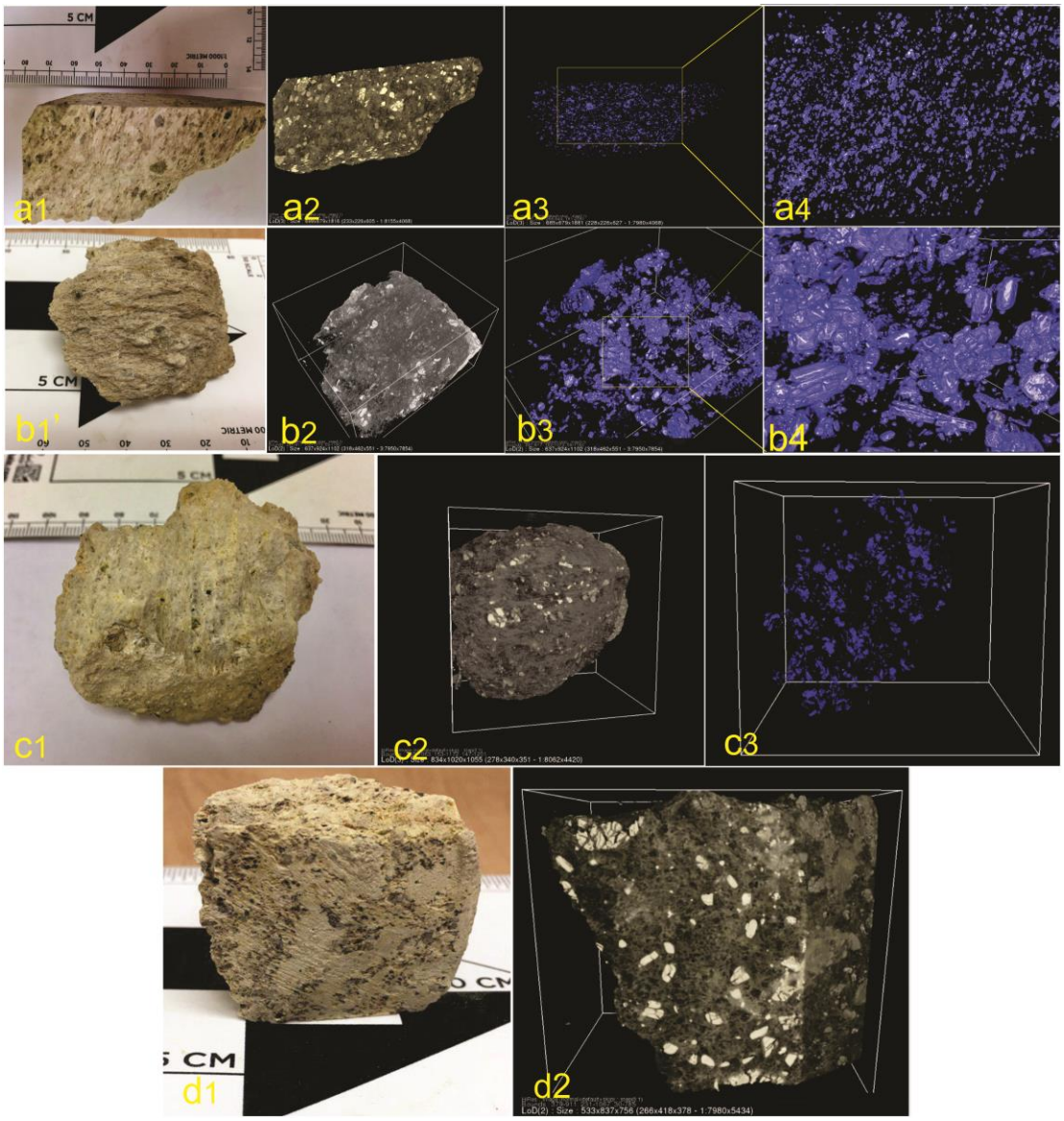

Figure 5.8: Figures show hand samples of three pumice types, a1: woody, b1 and c1 are vesicular; and d1 is micro vesicular pumice; a2, b2, c2 and d2 are 3D images made by Drishti from µCT data. a3, b3 and c3 present 3D distribution of phenocrysts within pumice fragments; a4 and b4 are zoomed areas of the a3 and b3 images.

A small proportion of the pumice clasts contain lithic fragments, which are small and rare. They are mostly andesitic lithics and the lithic percentage varies between 0 to 8%.Pumice fragments from the Te Kuiti section show the largest percentage of lithics.

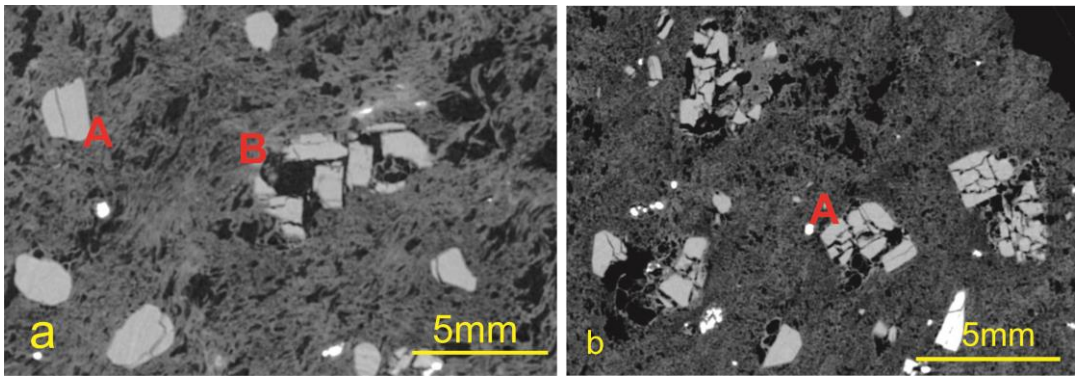

Figure 5.9: Phenocrysts within pumice fragments showing different groups of cracks: (a) Group A presenting perpendicular cracks and jigsaw texture; and(b) Group B showing cracks in different directions.

Additionally, microscopic observations show an inverse relationship between vesicle and phenocryst abundance, which means fewer and finer vesicular pumice clasts exhibit more phenocrysts (Figure5.10).

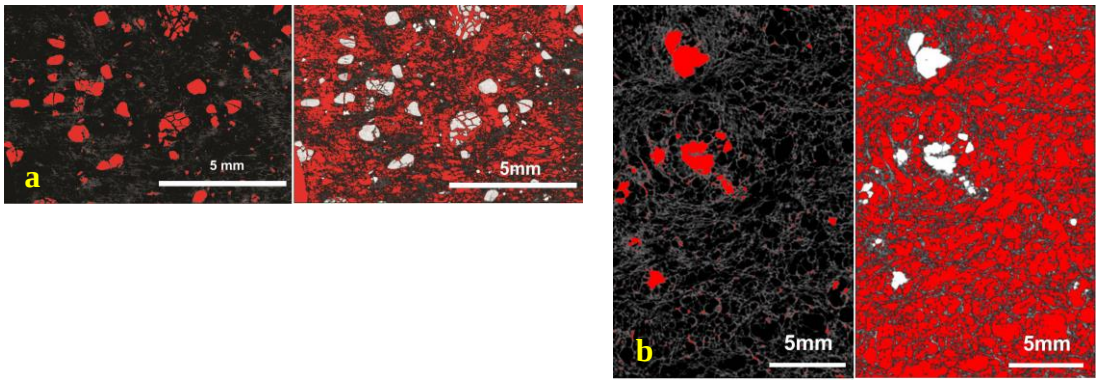

Figure 5.10: Abundance of phenocrysts and vesicularity within two types of pumice fragments. a) Micro-vesicular pumice with a high percentage of phenocrysts and finer vesicles; b) a vesicular pumice with thin walls, larger vesicles and less phenocrysts

5.8.1 Bulk pumice and glass chemistry

Major and trace elements of the 13 bulk pumice samples were measured by X-ray fluorescence (XRF) spectrometry. Fresh glass within pumice and glass shards were selected to obtain reliable glass chemistry analyses by electron probe microanalysis (EPMA) and laser ablation inductively coupled mass spectrometry (LA-ICP-MS).

5.8.1.1 Bulk pumice chemistry

Bulk pumice chemical data are presented in Table 5.4. In addition, for grey pumice (GP) a chemical analysis was undertaken by a portable XRF (Table 5.2).

Table 5.4:Whole pumice chemical analyses by XRF of selected pumice fragments from the Ongatiti Ignimbrite. The last column shows portable XRF results of a selected grey pumice (GP).

	H1	H2	H3	H4	P4	TK8	TK18	TK19	TK20	TK21	W1	W7	W26	GP
Pumicetype	II	I	III	I	I	I	II	IV	II	III	I	III	IV	V
Major elements[a](wt%)														
SiO_2	70.93	72.01	71.45	69.95	72.35	70.18	69.13	70.84	69.62	70.24	69.95	71.25	68.81	69.98
TiO_2	0.32	0.34	0.33	0.39	0.29	0.34	0.41	0.36	0.37	0.34	0.34	0.35	0.39	-
Al_2O_3	14.09	14.50	14.60	15.39	15.08	16.00	16.82	15.77	16.40	16.29	15.97	15.30	16.73	13.72
Fe_2O_3	4.69	3.03	3.48	3.35	2.65	3.25	3.71	3.28	3.43	3.22	3.35	3.20	3.82	3.8
MnO	0.28	0.11	0.08	0.14	0.05	0.08	0.08	0.05	0.08	0.06	0.08	0.08	0.16	-
MgO	0.51	0.44	0.44	0.67	0.41	0.59	0.63	0.55	0.63	0.60	0.63	0.53	0.64	NM[b]
CaO	2.27	2.23	2.34	2.81	2.20	2.42	2.45	2.26	2.47	2.39	2.52	2.33	2.41	1.87
Na_2O	3.24	3.81	3.51	4.47	3.67	4.22	3.97	3.84	4.04	3.94	4.15	3.70	3.97	NM
K_2O	3.56	3.42	3.64	2.70	3.23	2.82	2.73	2.99	2.88	2.84	2.92	3.17	2.93	2.57
P_2O_5	0.12	0.12	0.12	0.14	0.06	0.10	0.06	0.06	0.08	0.07	0.10	0.09	0.15	-
LOI	3.18	2.60	2.5	2.31	3.76	3.02	2.99	3.08	2.97	3.34	3.16	2.89	4.13	
Total	97.47	98.21	97.87	98.32	97.10	96.75	96.71	96.38	96.37	96.17	96.25	97.66	96.35	91.85
Trace elements (ppm)														
S	1	12	2	-	230	87	60	-	-	156	85	-	298	-
F	388	352	484	279	228	142	175	193	208	246	176	161	207	-
Cl	477	534	528	302	2218	631	1328	817	568	1023	1619	185	1226	-
V	29	24	20	26	17	17	19	18	20	17	15	15	19	-
Cr	-	-	-	1	-	-	-	-	-	-	-	-	-	-
Co	13	9	9	17	12	9	10	12	12	8	7	10	8	-
Ni	5	6	6	5	4	4	5	5	4	4	5	5	5	-
Zn	52	40	39	46	55	50	42	38	42	37	69	46	64	56
Sc	9	7	7	6	8	9	8	8	8	8	8	8	8	
Cu	17	21	12	9	5	8	6	10	8	9	9	5	13	
Ga	16	17	17	17	18	20	22	19	20	20	19	19	20	
As	6	7	6	6	7	7	7	9	8	7	9	7	9	
Rb	110	108	112	99	110	95	91	97	94	93	100	106	91	104
Sr	156	157	158	196	148	170	180	167	186	177	177	164	174	164
Y	28	29	28	24	24	29	23	24	25	23	26	24	22	46
Zr	191	181	177	209	198	190	194	194	196	196	178	181	199	133
Nb	7	7	7	7	7	8	9	9	9	8	9	8	8	115
Mo	4	4	4	5	4	5	5	5	5	5	4	4	5	

Sn	6	7	3	3	4	3	6	4	6	6	6	4	4	
Cs	7	-	2	3	2	6	5	3	5	6	3	4	-	
Ba	872	806	787	855	780	814	699	708	706	725	825	774	760	2539
La	24	22	22	22	20	22	17	16	21	17	24	22	22	-
Ce	57	59	57	63	55	62	51	49	57	49	64	61	51	-
Nd	30	25	22	24	25	31	24	23	22	20	25	24	19	-
Pb	11	12	11	11	16	13	12	7	11	10	17	14	13	21
Th	11	12	11	9	13	14	11	12	13	10	12	12	11	8
U	3	3	3	3	3	3	3	3	3	3	3	3	3	-

[a] Normalised to 100%, volatile free; totals are original values; all Fe expressed as Fe_2O_3)
[b] NM: Not measured

Harker plots of major elements versus $SiO_2$are presented in Figure 5.11

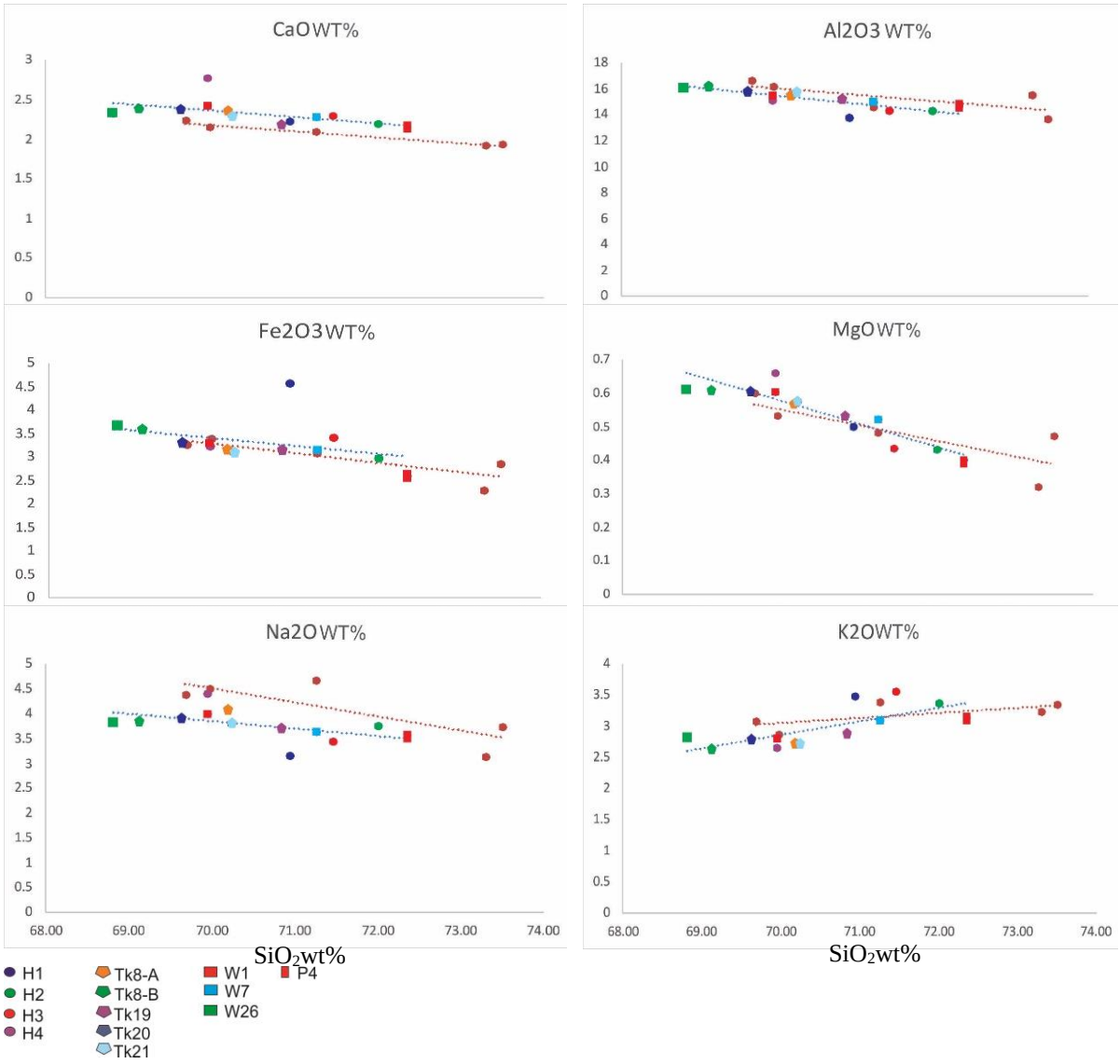

Figure 5.11: Harker variation diagram of selected pumice fragments from the Ongatiti Ignimbrite based on geochemical analyses by XRF. Our data is comparing with data from Briggs *et al*., (1993). Major elements (vertical axes) versus SiO_2 (horizontal axes).Blue trend line is for data in this study and the red line represents Briggs et al. (1993)'s data.

The major element oxides including CaO, Al_2O_3, Fe_2O_3, MgO and Na2O (Figure 5.11) show a decreasing trend with SiO_2. However, K_2O acts incompatibly, with increasing SiO_2.The Ongatiti pumice fragments are characterised by 68-72 wt% SiO_2 (Table5.4) and are dacitic to rhyolitic based on total alkali versus silica (TAS, Le Bas *et al.*, 1986; Figure 5.12a) Ongatiti pumice is also medium to high in K_2O and the highest K_2O occurs at Hinuera (Figure 5.12b).

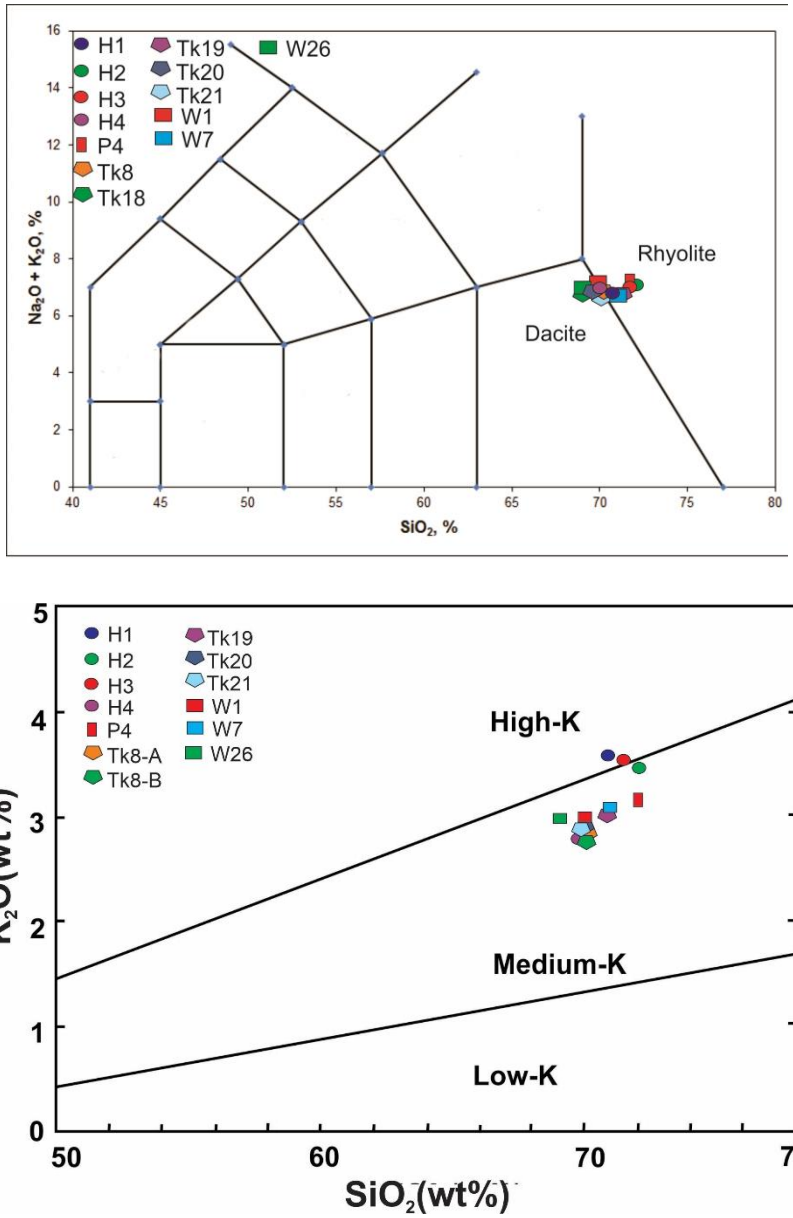

Figure 5.12: a) Total alkali versus silica (TAS) diagram for selected pumice compositions from different sites (after Le Bas et al.,1986) b) K_2O versus SiO_2 (Le Maitre, 2002) for the same samples. H1, H2, H3, H4 are from Hinuera, P4 from Waikato River, Tk8, Tk18,Tk19,Tk20 and Tk21 took from Te Kuiti section; and W1, W7 and W26 from Waipari Gorge west.

The pumice clasts show a high silica range (68.81 to 72.35%), moderate Al_2O_3 (14.09-16.82), and low Fe_2O_3 (2.65-4.69%) and CaO (2.20-2.81%). TiO_2, MnO and MgO are minor elements (less than 1%). Maximum silica was determined at Waikato River and Hinuera sites and less at the Waipari Gorge west section. $Al_2O_3$is lowest at Hinuera and most abundant at Te Kuiti. The lowest percentages of Fe_2O_3, CaO, MnO, MgO and TiO_2 were determined at Waikato River.

5.8.1.2 Volcanic glass composition

Major elements

The EMPA data on major elements show two volcanic glass compositional groups based primarily on the percentage of silica (Appendix 3, Figures 5.13&5.14), low silica (~76 to 78% SiO_2) and high silica (~80 to 81% SiO_2). Most samples are from the first group; however, Waipari Gorge east and Tauranga include samples from the high silica group (Figure5.14). The major element oxides (Na_2O, MgO, CaO, FeO and Al_2O_3) within glass show a negative trend with SiO_2.

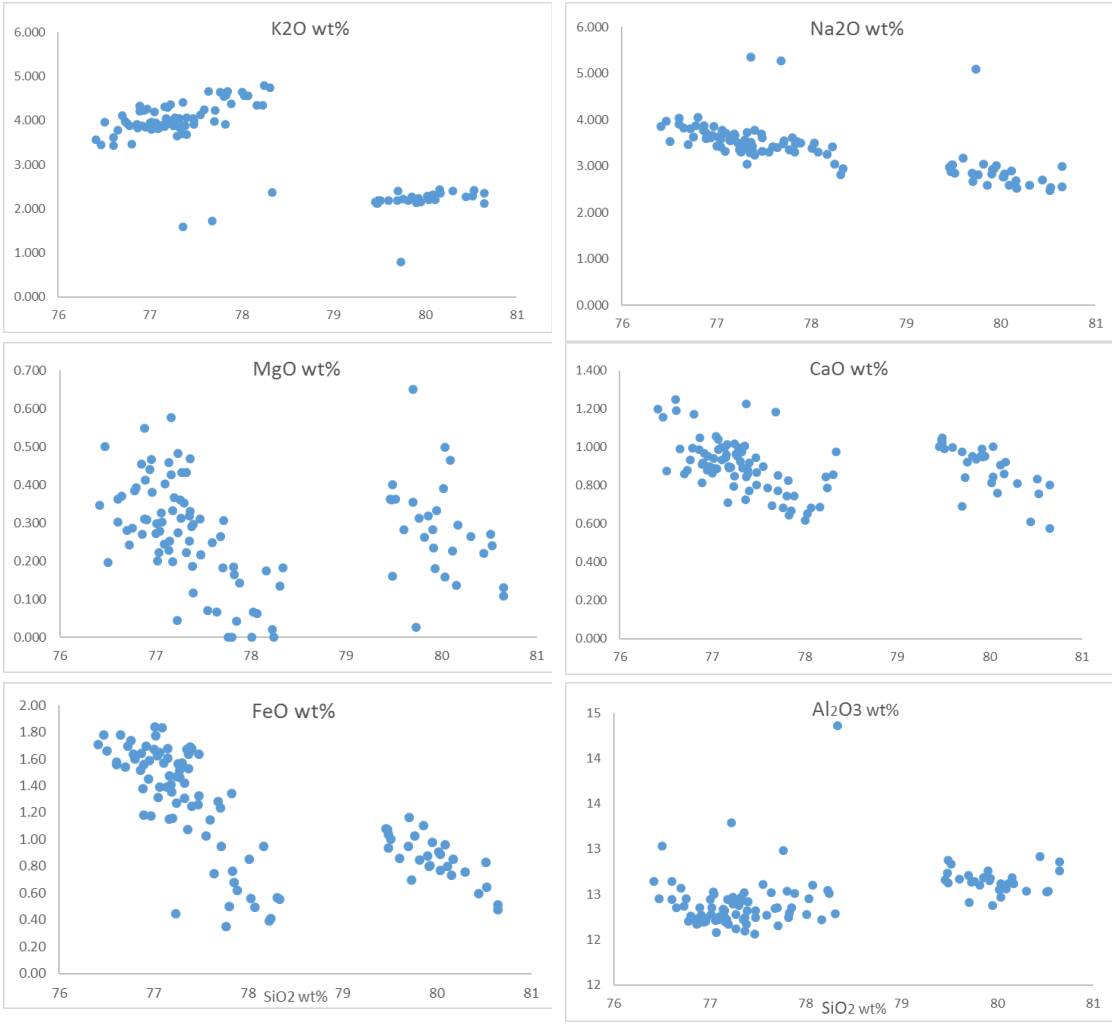

Figure 5.13: Harker variation diagram of analyses of volcanic glass (glass shards and pumice) from the Ongatiti Ignimbrite based on geochemical analyses by microprobe. Major elements (vertical axes) versus SiO_2 (horizontal axes)

However, K_2O indicates a positive trend. Lower K_2O in glass at the Tauranga and Waipari Gorge east sections would be related to sanidine presence in the ignimbrite which were seen in thin-sections at these two sections. The lower silica glass also has high K_2O, FeO, and slightly high Na_2O and CaO.

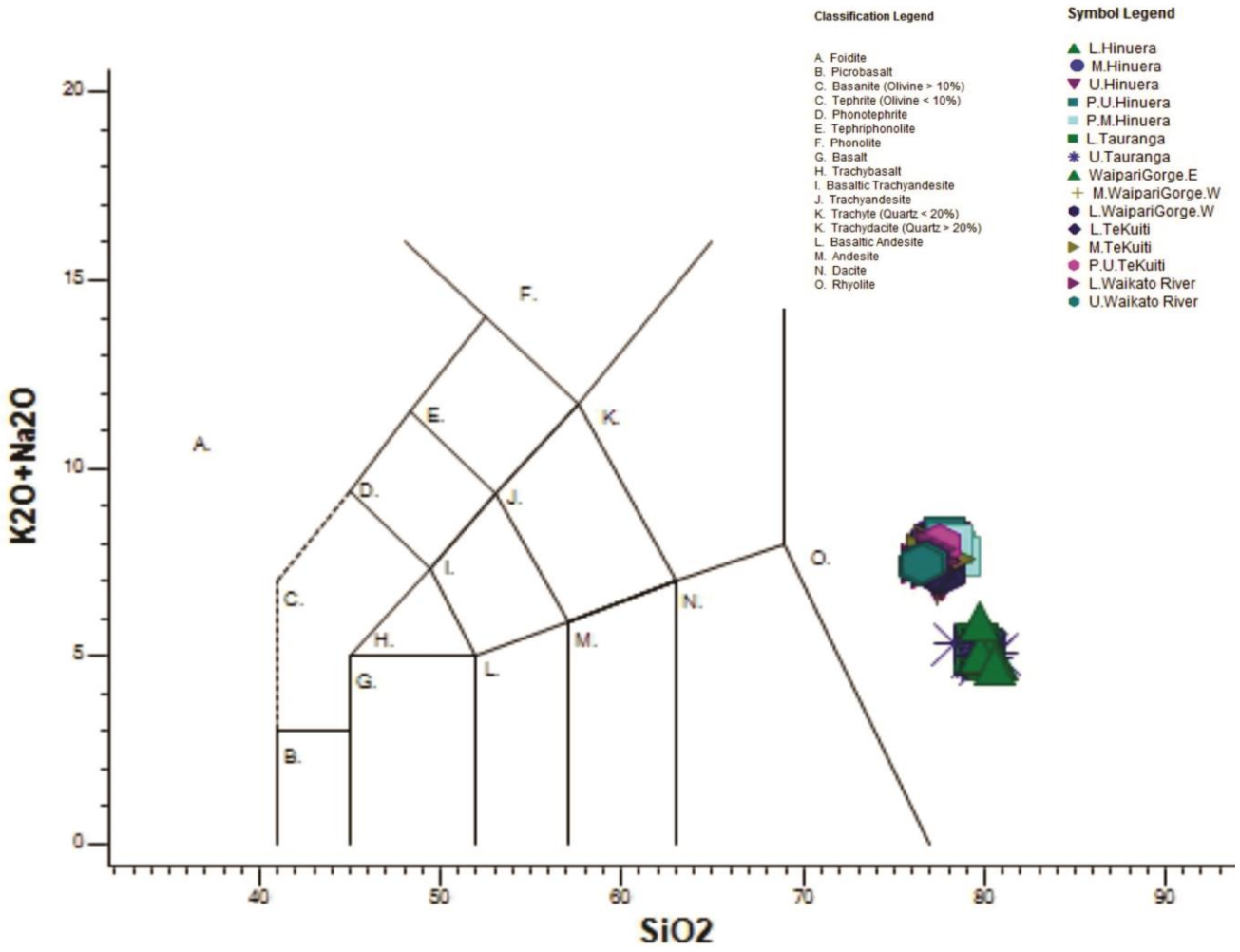

Figure 5.14: Total alkali versus silica diagram of microprobe data (normalized to 100% volatile-free) for volcanic glass shards from different outcrops (after le Bas *et al*., 1986)

Trace and rare earth elements

Chondrite-normalised REE (Figure 5.15) represent LREE enrichment at all localities. The pattern indicates negative Eu anomalies, which is the sign of plagioclase fractionation.

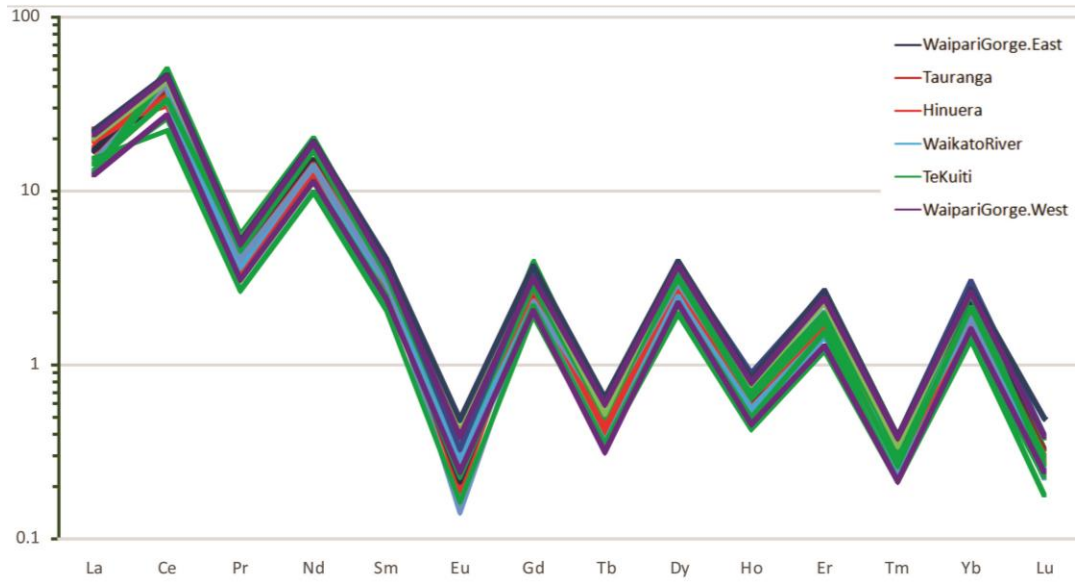

Figure 5.15: Rare earth data of analyses of some selected volcanic glass shards of the Ongatiti Ignimbrite (normalized to chondrite values of Sun and McDonough, 1989).

Large-ion lithophile elements (LILE) including at Hinuera and Waikato River sections are marked. High-field strength elements (HFSE) shows dominant concentration of Zr, Sm, Hf and Y (Figure 5.17).

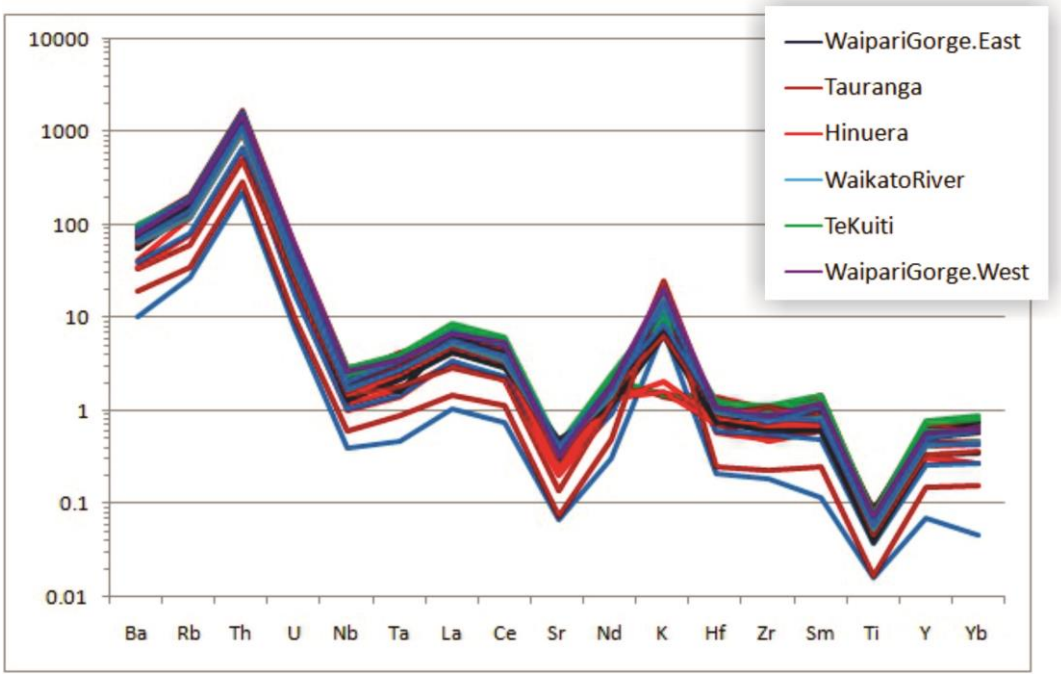

Figure 5.16: Spider diagram of multi-elements of analyses of some selected volcanic glass of the Ongatiti Ignimbrite normalized to the primitive mantle values from Sun and McDonough (1989).

5.9 Discussion

5.9.1 Vesiculation and magma fragmentation

Volatile exsolution, bubble nucleation and bubble growth create expanding conditions for magma ascent (Rust & Cashman, 2011). Vesicle formation and growth associated with pumice has been considered by geologists for more than 200 years (Orsi et al., 1992). Bubble nucleation, growth and rise within magma was studied by Verhoogen (1951) who concluded that glassy fragments in volcanic ash form when bubbles unite and expand. The bubble rise rate within high viscosity magma is very slow (McBirney & Murase, 1970; Orsi *et al.*, 1992; Cashman & Scheu, 2015). Bubble nucleation, growth and coalescence, magma fragmentation, and vesicle growth and collapse through post-fragmentation processes record the changes from coherent magma to vesicular pumice found in ignimbrite. The process commences within the subsurface magma chamber, then continues as magma rises inside the conduit and stops within the eruption column when clasts cool below the glass transition temperature. The final state of vesicular magma fragments before cooling to glassy pumice is recorded in the vesicle texture of pumice.

5.9.1.1 Bubble nucleation

Bubbles nucleate when volatile supersaturation of the magma occurs and the activation energy overwhelms the bubble surface energy. Experimental findings show that a high supersaturation requires a high percentage of SiO_2 and moderate to high melt viscosity (Cashman & Scheu, 2015). With these conditions, the concentration of volatiles in the melt remains high during decompression, nucleation of bubbles is rapid and bubbles are numerous but small in size. Pure solid-free melts need a high level of supersaturation to induce homogenous bubble nucleation, but phenocrysts within the melt can facilitate heterogeneous nucleation (Hurwitz & Navon, 1994; Cashman & Scheu, 2015). It is supposed that within erupting magma both types of nucleation (homogenous and heterogeneous) occur together (Cashman & Blundy, 2000; Mangan & Sisson, 2000).

Within the Ongatiti pumice, enhanced vesiculation around phenocrysts is clearly seen which provides evidence for heterogeneous nucleation.

5.9.1.2 Bubble growth and coalescence

The bubble ascent is governed by the viscosity of melt. Experiments on viscous fluids propose that pathways for gas are created mostly when concentration of bubble is between 65-75%. Additionally, to initiate magma rise requires a sufficient pressure within in a magma reservoir (Cashman and Scheu (2015). Pressure and sufficient permeability causes gas escape which affects fragmentation; however, viscosity controls the expansion (Rust & Cashman, 2011).

Vesicle texture in pumice shows the texture during the quenching time (Sparks, 1978; Houghton & Wilson, 1989). During explosive eruptions, vesicles become interconnected. Pumice within the Ongatiti Ignimbrite shows variations in average vesicle size, vesicle shape and percentage of vesicles. The textural studies on the Ongatiti pumice depicts that many vesicles show evidence for coalescence. Based on the studied characteristics, they were divided into different types: vesicular pumice (type I), fibrous (woody) pumice (type II), micro-vesicular pumice (type III) and dense pumice (type IV). These vesicles illustrate vesiculation in the magma chamber, conduit and explosive eruption.

Pumice type I is vesicular pumice with larger bubbles; however, micro-vesicular types represent smaller bubbles. It is assumed that the different size of the bubble size can be related to differences in bubble growth rate in parts of the magma, or likely connected to bubble coalescence in vesicular pumice. Vesicular and micro-vesicular pumice with dominant spherical vesicles shows thinner melt films in comparison to dense types. The vesicular pumice have usually circular, polymodal and elliptical shapes of vesicles with aspect ratio between 2.5 to 3.1.

Woody or fibrous types have elongated and parallel vesicles (aspect ratio>4). Type II pumice clasts indicate areas of conduit where shear stress affected bubble growth and coalescence. The shear stress increases towards the conduit wall and the shear strain raises bubble coalescence and elongates vesicles (Marti *et al.*, 1999; Cashman & Blundy, 2000; Polacci *et al.*, 2003; Polacci, 2005; Dingwell *et al.*, 2016). It can be concluded that fibrous pumice originated near the conduit margins; however, vesicular pumice were likely generated in regions near the centre of the conduits.

Dense and micro-vesicular pumice fragments show circular and elliptical shapes particularly. Dense pumice fragments with thick melt films are probably related to enhanced permeability, degassing of magma and vesicle collapse during the Ongatiti eruption, as Polacci *et al.*(2003) suggested for the Campanian eruption, Italy.

5.9.1.3 Fragmentation Processes

Fragmentation conditions are affected by vesiculation and crystallisation. Bubbles ascending through the magma create interconnected pores that form conditions for escaping gas(Rust & Cashman, 2011). The geometry of the conduit, extent and depth of vesiculation finally control the magma ascent rate toward the surfaces. The relationship between time of structural relaxation and rate of decompression are important in different fragmentation criteria. Comparison between ascending magma speed and decompression rate in plinian eruptions impress the fragmentation position (Kameda *et al.*, 2008; Cashman & Scheu, 2015).

At the upper level in the conduit, an ascending mixture of melt, crystals and bubble wall fragments form glass shards. For the mechanism of magma fragmentation there are two hypotheses: a) downward magma decompression or b) quick magma ascent and expansion (Alidibirov, 1994; Sugioka & Bursik, 1995).

Within the population of Ongatiti pumice, the abundance of woody pumice suggests that much of the bubble growth happened before fragmentation. Specific characteristics for post-fragmentation vesiculation, such as bread-crust surfaces and inner radial vesicle zonation within pumice clasts, was not observed.

Disruption of vesicles causes fragmentation when equal spheres are packed and reach 60-70% of the pumice volume or up to 70-85% (Sparks, 1978; Houghton & Wilson, 1989; Mader, 1998). Ongatiti pumice and glass shard shapes suggest vesicularity reached maximum packing (70 to 85%) prior to fragmentation.

The current study shows that vesicle connectivity and bulk porosity have a clear relationship, which with increasing bulk vesicularity the vesicles become more connected. This finding is in good agreement with studies by Mitchell *et al.* (2019) who noted that permeability can be controlled by high total vesicularity within submarine giant pumice, and in this study the idea

is extended to subaerial pumice.

The size of glass shards can be explained by permeability, stress in viscous melt and bubble size in pumice (Rust & Cashman, 2011) and less permeable pumice can be more explosive (Klug & Cashman, 1996). The pumice with less connected vesicles could have required higher explosively exploded more and fragmented to smaller pumice fragments (pumice shards) and glass shards.

Various ranges in shape and size (from simple to complex) of glass shards to different vesicle sizes and textures in pumice fragments were seen in the ignimbrite. These criteria are supported by the analyses of the glass shards and pumice clasts within the lower parts of the Ongatiti Ignimbrite, involving small pumice size, dense pumice and abundant glass shards. In upper parts, pumice fragments present more connected vesicles and, therefore, larger and more vesicular pumice fragments but lower percentages of small glass shards. Types of pumice fragments (mostly more type III and IV types) and higher percentage of glass shards in lower parts of the ignimbrite can suggest a more powerful explosion in comparison with upper parts.

However, although the formation of glass shards during fragmentation is important, the role of post-fragmentation processes must be considered as well.

5.9.1.4 Post-fragmentation processes

After primary fragmentation due to continued decompression, thermal shock, mechanical collisions and abrasion, particle can be fragmented for the second time. Cashman and Scheu (2015) suggested the term “secondary fragmentation” to apply to later fragmentation that can be happened after or even before the pyroclasts existing from a vent.

Due to the turbulent gas and particle mixture, within the volcanic conduit, particles can be fragmented by abrasion. Secondary fragmentation can decrease the average size of particles and increase the fine ash dispersion. It can occur within the conduit and during pyroclastic flow transportation. The preserved textures imply that the timing between fragmentation and cooling of pumice fragments is crucial (Pittari, 2004). In the current study, rapid quenching happens immediately after fragmentation for the Ongatiti pumice fragments as we could not recognize bread-crust or vesicle zonation textures (Klug *et al.*, 2002; Polacci *et al.*, 2003).

Another textural feature within the pumice examined is flattened-can-collapsed vesicles, which likely indicate they were plastic and fluidal during their deposition. Furthermore, it must be considered that all types of the pumice clasts, vesicular and dense, were not able to be cooled at the same time. According to varied evidence (Chapter 3), the Ongatiti Ignimbrite was emplaced through extreme explosive volcanic activity from one or more vents. The dense pumice fragments can be generated from degassed magma on the margins of the conduit (Polacci *et al.*, 2003). However, vesicular and woody pumice fragments formed from middle parts of conduit which was rich in gas. The micro vesicular pumice can be generated in a transitional zone, between gas-rich zone and degassed zone.

5.9.1.5 Crystal fragmentation

Group A phenocrysts (Figure 5.9), with perpendicular cracks (to the long axis), can indicate tensile stress on the phenocrysts, which can be explained by isotropic bubble expansion. In addition, there are occasional bridges (melt fiber) between fragments of broken phenocrysts that suggest a highly viscous fluid (Miwa and Geshi, 2012).

Vesiculation of magma can create extension-cracked phenocrysts. The gap between phenocrysts fragments in the Ongatiti pumice are tiny and we recognize that vesiculation expansion, which affects the phenocrysts, occurred at the last step of the decompression process. Additionally, it seems bubbles formed instantly before quenching and at fragmentation because they have a fragile texture and are not able to travel within magma for a long time (Kennedy *et al.*, 2005; Miwa & Geshi, 2012).

5.9.2 Geochemistry of volcanic glass

Bulk analyses by XRF

The bulk pumice geochemical data compare well with earlier data of Briggs *et al.* (1993), although the silicate range in our research is narrower (Figure 5.11). Trace elements determined for the pumice we analysed have mostly similar trends (Figure5.15).

Enrichment in LREE is generally seen in calc-alkaline series (Moll, 1981; Gunderson *et al.*, 1986; Francis *et al.*, 1989; Pearce *et al.*, 1999) and is consistent with that for Ongatiti pumice. The negative Eu anomaly is a signature of fractionation into plagioclase.

The major element compositions of glass in pumice are particularly homogenous throughout the Ongatiti Ignimbrite. The XRF data show a high similarity with bulk chemical data obtained by Briggs *et al.* (1993) and Cooper and Wilson (2014) who also analysed (bulk) Ongatiti pumice from other locations.

The range of loss-on-ignition (LOI) and Al_2O_3 value indicates that most of pumice clasts had the same level of weathering, which was minimal. Zr shows a systematic decreasing trend with increasing SiO_2which can be related to zircon fractionation.

My data show that pumice clasts range in composition between 68.81 and 72.35wt% silica. There is no systematic trend with the stratigraphic height at all localities. However, there are some differences in lateral distribution in partial pumice fragments from Hinuera and Tauranga are more rhyolitic than from Te Kuiti and Waipari Gorge, which are more dacitic.

The different pumice types (I-IV) are similar in major element composition. Pumice clasts presents small negative anomalies for Nb and Ti that could be a sign of subduction (Hawkesworth et al., 1979; Ringwood et al., 1990; Thomas et al., 1994). The REE and high field strength elements (HFSE) are useful for identify distinctive geodynamic conditions. HFSE consider principle geochemical proxies for understanding the tectonic environments related to magmatism in different continental and oceanic domains (Condie, 2005; He et al., 2010; Condie, 2015).

Glass (shards and pumice) analyses by microprobe

The geochemistry of the individual volcanic glass analysed from glass shards and pumice by microprobe represents two groups of volcanic glass, higher-silica (~80-81wt%) in Tauranga and Waipari Gorge east, and high-silica (76-78 wt%) in other sections.

The acquired ages in current study for the sections show that the Tauranga outcrop has the older age (1.37 ± 0.061 Ma). In addition, the lower boundary of the Ongatiti Ignimbrite with the underlying Ngaroma Ignimbrite was seen only in the Waipari Gorge east. Therefore, it is suggested that the early pyroclastic flow that was higher in silica, was sampled in the Tauranga and Waipari Gorge east sites and were derived from the upper parts of magma chamber, whereas at the other sites, with lower silica content, only the later products are visible.

The volcanic glass from shards and pumice fragments in all sections presents similar trace elements and REE and have rather low HFSE and higher LILE. The volcanic glass represents an enrichment in LILE (e.g., Rb, Ba, Th, K, and U) and HFSE diminish (e.g., Zr, Hf, Nb, Y, and Ti) relative to primitive mantle values. Negative anomalies of Nb-Ta, Hf-Zr, and positive anomalies of Th (Figure 5.16) have a good agreement with the geochemical characteristics from magmas that were generated by subduction (Saha *et al.*, 2019).

Compositions of LILE, HFSE and REE (Ba/Nb versus La/Nb) (Figure5.17) are consistent with arc volcanic settings (Condie, 2005; Ayalew & Ishiwatari, 2011; Saha *et al.*, 2019). The pumice samples are marked by high-K (at Hinuera section) to medium-K calc-alkaline compositions with relatively high Sr (148-196 ppm), Ba (699-872 ppm), Rb (91-112 ppm) and Zr (177-209 ppm). Nb versus Y and Rb versus Y+Nb (Figure 5.18) in the pumices examined are consistent with eruption from a volcanic arc.

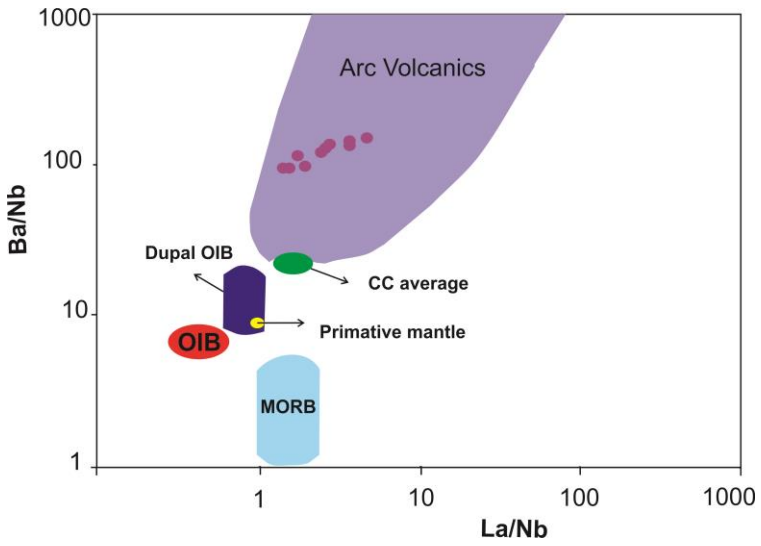

Figure 5.17: Ba/Nb versus. La/Nb diagram for the Ongatiti Pumice. (After (Le Roex, 1986; Sun & McDonough, 1989; Condie, 1993; Saha *et al.*, 2019); CC: continental crust and clastic sediment average. Red dots are samples from the current study.

5.9.2.1 Phenocrysts and crystal fractionation

Pumice clasts are comprised mainly of vesicles and glass and phenocrysts are subordinate. Plagioclase, quartz, hornblende, pyroxenes (mostly orthopyroxene) and rarely Fe-Ti oxidesare the main phenocrysts within the Ongatiti pumice. The presence of hornblendes is significant as they are stable in a melt containing a high H_2O content (>3 wt. %) and pressures–more than 0.1 to 0.2 GPa(Winter, 2013).

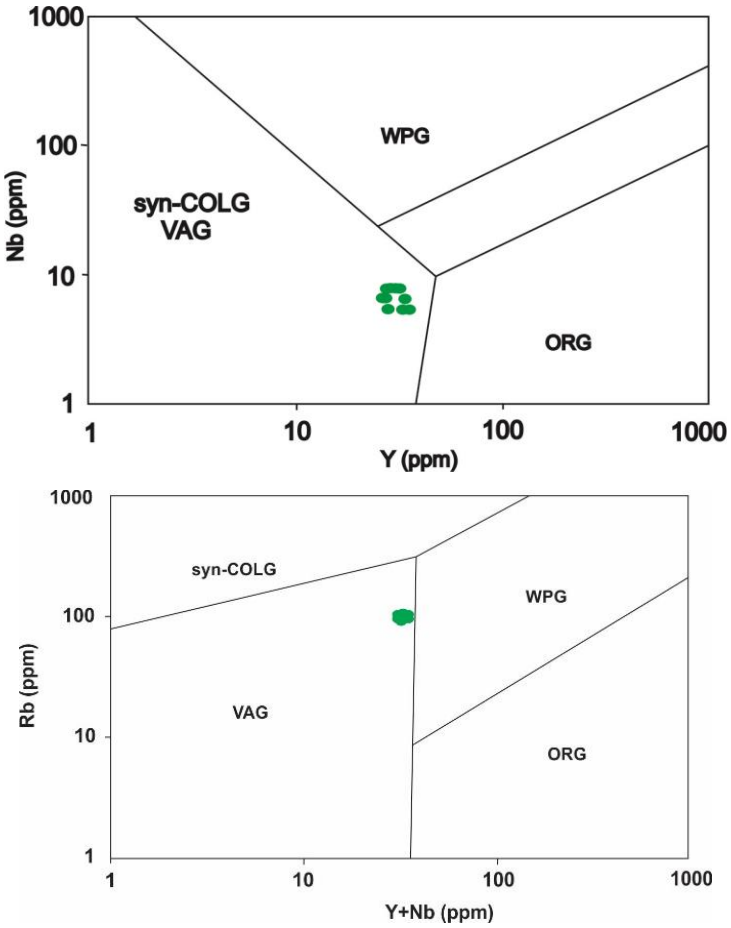

Figure 5.18: Diagrams of the Ongatiti pumice samples that show samples are related to volcanic arc field (after Pearce *et al.* (1984). Syn-COLG: syn-collisional granite, VAG-volcanic arc granite, WPG-within-plate granite, ORG-oceanic ridge granite.

5.9.2.2 Eruption column dynamics

Fragmentation processes decrease the ejection speed, density and discharge rate of the gas and solid particle mixture (Alatorre-Ibargüengoitia *et al.*, 2010; Alatorre-Ibargüengoitia *et al.*, 2019). Magma in plinian eruptions is rich in volatiles and therefore it has a high ascent speed. Magma volatile content, the diameter of the conduit and the pressure of the magma chamber can control eruption velocity and rate of eruption. These factors commonly control the collapse of a plinian eruption column (Sparks & Wilson, 1976; Wilson, 1976; Woods, 1998).

Temperature and pressure affect magma elasticity or viscous behavior, which are crucial for fragmentation processes (Webb & Dingwell, 1990; Namiki & Manga, 2008; Murch *et al.*, 2019). Magma permeability causes different rates of gas output, therefore decreasing the bubble growth and finally, because of brittle processes, magma fragmentation can occur in

silicic plinian eruptions (Rustand Cashman, 2011).The ductile to brittle deformation can occur from a significant depth to near the surface, and from the conduit central zone toward the marginal zones due to changing strain and temperature (Webb & Dingwell, 1990; Heap *et al.*, 2017; Murch *et al.*, 2019).

Changing the porosity and permeability based on magma position within conduit is important in explosive behavior, particularly at the conduit margins that are the boundary of temperature exchange (Heap *et al*., 2017). Based on the pumice types, vesicularity and permeability, the positions of pumice clasts and eruption dynamics for the Ongatiti Ignimbrite eruption are suggested in Figure5.19.

In addition, there are no obvious variations in vesicularity and texture between the pumice fragments within different parts of the Ongatiti Ignimbrite, only some small variation in composition from dacitic to rhyolitic. Therefore, the composition of magma did not play a significant role on the eruption column dynamics. However, increasing conduit(s) diameter at the initial eruption steps increased the eruption mass and subsequently the eruption column collapsed. This process generated a considerable pyroclastic flow (Wilson, 1976; Papale *et al.*, 1998; Diller *et al.*, 2006).

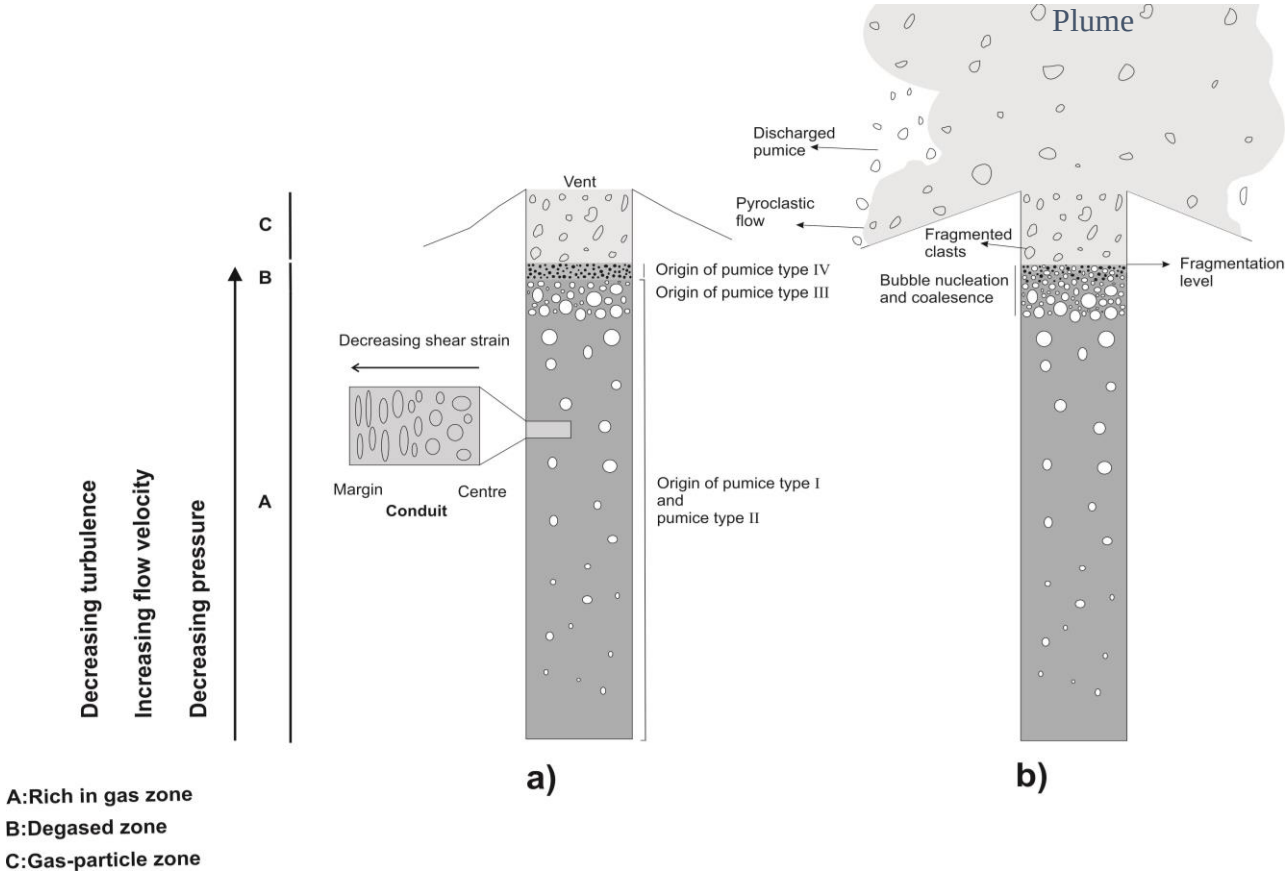

Figure 5.19: Model showing a proposed vesiculation and dynamic processes within conduit and vent during the Ongatiti eruption.

Chapter Six

Conclusions

6.1 Introduction

Direct observation of pyroclastic flows beneath an enveloping hot ash cloud still remains fundamentally unachievable in the nature; however, PDC recently has been simulated in laboratories (Lube et al. 2019). Therefore, case studies of ignimbrite deposits would be an important way of determining pyroclastic flow processes. They are also our only evidence of large-volume super-eruptions and their unique processes. This research has used the Ongatiti Ignimbrite as a case study of an ancient, large-volume pyroclastic flow that blanketed a vast area of the North Island.

Various types of analytical techniques were applied in this study to determine the stratigraphy and distribution of the ignimbrite, its pyroclast componentry, matrix micro-texture and fine-grained components, and the physical characteristics of its pumice and the chemical composition of juvenile fragments. The results have provided insight into aspects of the transport mechanism and depositional dynamics of pyroclastic flows, the magma composition, vesiculation and fragmentation during the eruption. In addition, post-emplacement processes of the Ongatiti eruption have been determined.

6.2 Key findings about the Ongatiti Ignimbrite

6.2.1 Transportation and emplacement processes

Pyroclastic flow distribution during the Ongatiti eruption was controlled by paleotopography, its main passage of emplacement being through valleys, although pyroclastic flows were also able to surpass topographic barriers such as hills (up to ~ 900 m) and travel long distances (~ 90 km). The facies characteristics of the ignimbrite deposits, their stratigraphy, and the effect of paleotopography on the dispersal pattern and emplacement processes of the Ongatiti pyroclastic flow were discussed in Chapter 3. The major findings are summarized below.

- The minimum deposit volume of the Ongatiti Ignimbrite was revised to approximately 720 km^3 (as loose material) which converts to ~512 km^3 DRE. This new calculation is

consistent with the Ongatiti Ignimbrite being emplaced during a super-eruption. However, due to erosion and burial by younger deposits, both east of the MVC and within the caldera, the original volume was larger than the value calculated here.

- Field observation of the current topography and western boundary of the MVC were combined with GIS-based profiles, which suggest a topographic elliptical resurgent (20 km × 12 km) with about 60 m relief on the present surface. Although the relief does not represent the original collapse depth, it supports the location and possible dimensions of the MVC.

- A sharp lower boundary between the Ongatiti Ignimbrite and underlying Ngaroma Ignimbrite was identified on the eastern side of the Waipari Gorge. Discontinues fluvial deposits and paleosols occur along part of this boundaries and are evidence of an erosional phase and non-deposition (marked by paleosol) between the two eruptions.

- During the eruption, the pyroclastic flow has traveled along at least three flow paths from the source caldera to distal areas: (1) narrow valleys after high lands, (2) wide valleys in low lands, and (3) a wide valley after high lands.

- Various facies in proximal-medial and distal areas from the MVC have been introduced for the Ongatiti Ignimbrite. They are pumice and lithic rich facies (PRLR), pumice-rich, lithic-poor facies (PRLP), flattened pumice-rich facies (FPR), pumice and lithic poor facies (PPLP), pumice-poor, lithic-rich facies (PPLR) and fine ash-facies (FAL). For distal facies, three facies were identified: pumice-rich tephra facies (PRT), pumice-poor tephra facies (PPT) and fine-grained tephra (FGT)

- For the first time, the (U-Th)/He dating method was used on zircons extracted from the Ongatiti Ignimbrite. This method showed ages of 1.314 $\pm$ 0.086 Ma at Hinuera, 1.377 $\pm$ 0.061 Ma at Tauranga and 1.382 $\pm$ 0.052 Ma at Te Kuiti. These ages (~1.3–1.4 Ma) are at face value somewhat older than ages acquired previously, which are ~1.2–1.3 Ma (e.g. Lowe *et al*., 2001).

6.2.2 Fine-scale eruption and post-emplacement processes

The study of the Ongatiti Ignimbrite matrix (components smaller than 2 mm) has revealed a variation in components including glass shards, small pumice clasts, crystals and lithic fragments. The micro-texture of the ignimbrite was considered in Chapter 4 to understand the fine-scale eruption emplacement and post-emplacement processes. The main findings are listed below.

- A new classification for the morphology of glass shards has been proposed in this study.

- The synchrotron X-ray μ-CT observations on the matrix of the ignimbrite illustrates size sorting of crystals around larger pumice fragments. The large crystals occur further away from the pumice clast boundaries and smaller crystals are arranged closer to the pumice boundaries. This crystal size zonation may be due to grain-dispersive pressure that forced larger crystals to be concentrated further away to the pumice fragments. This finding highlights the importance of particle interactions, and grain-dispersive pressure, in the ash-gas dynamics of pyroclastic flows.

- Field and micro-textural observations revealed different degrees of welding, reported from A to D (non-welded to welded), for the Ongatiti Ignimbrite. The welded zone (D) occurs in the middle portions of ignimbrite sections, consistent with deposit-loading processes, moderate temperature in this zone (Branney and Kokelaar, 1992).

- Average glass shard and crystal sizes have been used to understand the relationship between the degree of welding and sizes of particles. I show that the degree of welding is inversely related to the glass shard size (ash grade). The ash cooling experiment undertaken here indicated that the smaller size particles have the ability to keep and retain heat more than the larger size particles. Hence, in those parts of the ignimbrite where the size of glass shards or crystals is finer, the heat could be retained longer and thus provided better conditions for welding.

- Alteration processes affected the Ongatiti Ignimbrite matrix by vapour-phase alteration and devitrification. Axiolitic spherulites were seen within some matrix textures because of glass shard devitrification. Different secondary minerals were

identified including cristobalite, illite, chlorite and zeolite. The secondary mineral assemblages within the Ongatiti Ignimbrite provide proof for low-temperature (≤300 °C) alteration.

6.2.3 Volcanic glass

- Five types of pumice clasts, based on morphology, texture and colour, were identified within the Ongatiti Ignimbrite: vesicular (Type I), woody (Type II), micro vesicular (Type III), dense (Type IV) and grey pumice (Type V).
- Bulk vesicularity and vesicle connectivity within pumice clasts have a clear relationship: with increasing bulk vesicularity, the vesicles become more connected. These finding shows that permeability can be controlled by high total vesicularity.
- The geochemical analyses on glass shards and pumice suggest the occurrence of two volcanic glass groups: high silica and low silica. Trace element and rare earth element data show similar dual trends. Based on the geochemistry and the radiometric ages for the different sites, the high silica pyroclastic flow was deposited earlier from the upper part of the magma chamber, whereas the low silica pyroclastic flow originated from lower parts of magma chamber and was deposited later.

6.3 Wider implications of the Research

6.3.1 Topographic effects on pyroclastic flow facies

Plinian eruptions generate ignimbrites and the underlying topography plays a crucial role on the distribution of ensuing pyroclastic flows (Brown and Andrews, 2015). This study showed that pyroclastic flows travel in different directions from the caldera over hills, ridges (up to 900 m asl) and infilled valleys. Volcanic facies are based on pyroclastic flow locations (proximal, medial or distal) and the relief of highlands or lowlands. When pyroclastic flows travel around hills they are divided into several lobes and flow within smaller valleys. When they flow onto the lowlands after passing hills, different facies are emplaced. Variation in pumice percentage vertically within an ignimbrite can show differences in the eruption energy (Wilson, 1986). Additionally, this research provides some evidence for a change in eruption energy due to the redirection of pyroclastic flows around high lands, which can change the pumice and lithic abundance horizontally. However, vertical variations are related to changes in eruption energy.

Thick mappable units of ignimbrite (e.g. Ongatiti Ignimbrite) can be related stratigraphically, geochemically and chronologically to relatively thin distal tephra-fall deposits (e.g. Oparau tephra) that occur as beds within composite tephra successions. Facies changes are also a useful tool to help achieve correlations.

6.3.2 Ash particle interaction

The µ-CT images of the ignimbrite matrix show that pumice clasts and phenocrysts are locally sorted by size: smaller crystals are arranged near the pumice boundaries and the coarser crystals are farther away.

The observed sorting around pumice fragments suggests that grain dispersive pressure forces large phenocrysts away from boundaries of larger particles. The same phenomenon was reported by Komar (1972) and Winter (2013) in sills and dikes whereby crystals are concentrated towards the centre and away from the rock contacts. I assume that during turbulent particle flow, the pumice fragments have played a hard boundary role with circular currents. Particle interaction (pumice fragments-crystals) appears when flow shear forms a grain dispersive pressure, which drives larger phenocrysts to concentrate further from large pumice fragments. This finding can be helpful to understand the role of particle size and scales of turbulent particle flow within pyroclastic flows.

6.3.3 Complexity of matrix components

Detailed studies of the Ongatiti Ignimbrite matrix have revealed that our understanding of the matrix composition, and gas-particle and particle-particle interactions within the matrix, is more complicated than what has been thought. The components show a wide variety in size, shape and abundance within the matrix, both vertically and horizontally.

The Ongatiti Ignimbrite matrix has fewer lithic clasts than pumice fragments and both components decrease in abundance farther from the caldera source. However, crystals present a reverse trend with distance that is likely connected to abrasion of the coarser particles (pumice and lithic fragments) during their travel. Also, pumice elutriation into an ash cloud caused an enrichment in crystals in the remaining matrix, as was suggested by Sparks & Walker (1977).

The different sizes and abundances of particles provide an understanding of textural maturity of the crystal population during pyroclastic flow emplacement.

Various shapes of glass shards were seen within the matrix and a classification based on shapes was suggested in this study. Shard size also indicates systematic changes through stratigraphic sections which can be connected to the particle-gas mixture dynamics within the pyroclastic flow. It is assumed that the glass shards are turbulent in the ash-gas suspension.

6.3.4 Welding processes

Field observations of the Ongatiti Ignimbrite and microscopic criteria enabled me to develop a new welding classification. Additionally, this research confirms that the grain size and cooling rate are related. Particles with smaller size can keep and retain heat better than coarser particles. Hence, during the emplacement of pyroclastic flows in some parts, where the finer glass shards and crystals were deposited, heat was retained longer which is an appropriate condition for the welding process, and implies an inverse relationship between ash shard size and degree of welding.

6.3.5 Hazards of large pyroclastic flows

I have shown that the Ongatiti Ignimbrite was emplaced by a super-eruption and its volcanic explosivity index (VEI) would be 7. The eruption of the Ongatiti Ignimbrite was a landscape-modifying event on the scale of at least the western North Island, with deposits occurring in locations as far away as Auckland and Wellington as well. Internal deposit temperatures were high enough to cause welding for up to about 80 km from the source volcano; beyond that, and more than 90 km from the source toward the north-west, the pyroclastic flow deposited a relatively cooler non-welded material. A comparison of the DEM and the Ongatiti Ignimbrite distribution map reveals that, up to around 40 km from the MVC, the ignimbrite covered both hills and valleys, but beyond those distances the pyroclastic flow significantly travelled only through the valleys.

Assessing the topography of the North Island's modern landscape shows that the areas around the younger calderas are mostly dominated by relatively low-lying lands with only moderate relief. This spatial association means that there are few large natural barriers (i.e. high hills

or mountains) to control voluminous or powerful pyroclastic flows. Hence a new eruption of ignimbrite would be unimpeded and hence bury a vast area of the North Island catastrophically. Thus, our findings can be helpful to estimate the hazardous areas, which will be significantly affected by a large eruption in the island.

6.4 Future research propositions

To address the key questions through this research some new challenges for future research on the Ongatiti Ignimbrite and physical volcanology have been stimulated. Some of the propositions are listed below.

On the Ongatiti Ignimbrite:

- Stratigraphic data about the Ongatiti Ignimbrite, and the volume of the deposit towards its eastern boundary and inside the caldera subsurface, can only be achieved by further drilling and geophysical studies.

- In my study, the age of the pyroclastic flow was determined in three outcrops by the (U-Th)/He dating method. These ages are somewhat older than earlier ages derived from other methods and have broadened the possible age range for the Ongatiti eruption. Hence, I suggest that the Ongatiti Ignimbrite is dated at more outcrops and subsurface deposits to help improve its age more precisely and accurately.

On physical volcanology:

- Detailed textural studies on distal deposits would be helpful to find more about how a giant pyroclastic flow travels to distal areas. Also, different facies that form along different flow paths can be examined systematically to better understand the deviation of processes along different flow lobes.

- The use of µ-CT technology to study pumice texture and matrix of ignimbrite both vertically and horizontally through an ignimbrite can be useful for understanding the roles of particle size, the distribution of particles, and vesicularity variation, on pyroclastic flows through their travel.

- Systematic sampling of ignimbrite to understanding micro-and macro-facies changes both vertically and laterally can help volcanologists to make models of facies and determine processes during emplacement and post-emplacement of pyroclastic flows.

- One of the significant problems about pyroclastic studies is the different nomenclature used for pyroclastic flow deposits. In this study, different deposits of the Ongatiti Ignimbrite in proximal, medial and distal areas have been described, all with the similar source and age, however, different names have been used by different authors. The Ongatiti Ignimbrite or the Ongatiti Formation was named in the tradition of geological mapping of thick ignimbrite successions in proximal to medial areas by Martin (1961), and later followed by Wilson (1986) and Leonard et al. (2010). Equivalent distal deposits, which occur as thinner tephras within pyroclastic strata, are known as the Oparau Tephra or K12. The term Oparau Tephra was introduced by Pain (1975), whereas the K1 to K15 terminology was introduced by Salter (1979) and later Horrocks (2000) and Lowe et al. (2001) correlated the Oparau Tephra, K12 and the Ongatiti Ignimbrite.

  It is suggested that to avoid confusion for researchers a committee revise the pyroclastic terms and names and that those terms be standardised in New Zealand and even internationally.

References

Alatorre-Ibargüengoitia, M. A., Arciniega-Ceballos, A., López, C. L., Dingwell, D. B., & Delgado-Granados, H. (2019). Fragmentation behavior of eruptive products of Popocatépetl volcano: an experimental contribution. *Geofísica internacional, 58*(1), 49-72.

Alatorre-Ibargüengoitia, M. A., Scheu, B., Dingwell, D. B., Delgado-Granados, H., & Taddeucci, J. (2010). Energy consumption by magmatic fragmentation and pyroclast ejection during Vulcanian eruptions. *Earth and Planetary Science Letters, 291*(1-4), 60-69.

Alidibirov, M. A. (1994). A model for viscous magma fragmentation during volcanic blasts. *Bulletin of Volcanology, 56*(6-7), 459-465.

Allan, A. S., Baker, J. A., Carter, L., & Wysoczanksi, R. J. (2008). Reconstructing the Quaternary evolution of the world's most active silicic volcanic system: insights from an∼ 1.65 Ma deep ocean tephra record sourced from Taupo Volcanic Zone, New Zealand. *Quaternary Science Reviews, 27*(25), 2341-2360.

Alloway, B., Westgate, J., Pillans, B., Pearce, N., Newnham, R., Byrami, M., & Aarburg, S. (2004). Stratigraphy, age and correlation of middle Pleistocene silicic tephras in the Auckland region, New Zealand: a prolific distal record of Taupo Volcanic Zone volcanism. *New Zealand Journal of Geology and Geophysics, 47*(3), 447-479.

Alloway, B. V., Pillans, B. J., Carter, L., Naish, T. R., & Westgate, J. A. (2005). Onshore–offshore correlation of Pleistocene rhyolitic eruptions from New Zealand: implications for TVZ eruptive history and paleoenvironmental construction. *Quaternary Science Reviews, 24*(14-15), 1601-1622.

Andrews, G. D., & Branney, M. J. J. B. (2011). Emplacement and rheomorphic deformation of a large, lava-like rhyolitic ignimbrite: Grey's Landing, southern Idaho. *123*(3-4), 725-743.

Arzilli, F., Cilona, A., Mancini, L., & Tondi, E. (2016). Using synchrotron X-ray microtomography to characterize the pore network of reservoir rocks: A case study on carbonates. *Advances in water resources, 95*, 254-263.

Ayalew, D., & Ishiwatari, A. (2011). Comparison of rhyolites from continental rift, continental arc and oceanic island arc: implication for the mechanism of silicic magma generation. *Island arc, 20*(1), 78-93.

Aydin, A., & DeGraff, J. M. (1988). Evolution of polygonal fracture patterns in lava flows. *Science, 239*(4839), 471-476.

Báez, W., de Silva, S., Chiodi, A., Bustos, E., Giordano, G., Arnosio, M., Suzaño, N., Viramonte, J. G., Norini, G., & Groppelli, G. J. B. o. V. (2020). Pulsating flow dynamics of sustained, forced pyroclastic density currents: insights from a facies

analysis of the Campo de la Piedra Pómez ignimbrite, southern Puna, Argentina. *82*, 53.

Baker, D. R., Mancini, L., Polacci, M., Higgins, M. D., Gualda, G., Hill, R., & Rivers, M. (2012). An introduction to the application of X-ray microtomography to the three-dimensional study of igneous rocks. *Lithos, 148*, 262-276.

Baker, M. J. (1981). The nature and distribution of upper Cenozoic ignimbrite centres in the Central Andes. *Journal of Volcanology and Geothermal Research, 11*(2-4), 293-315.

Barton, N. (1978). Suggested methods for the quantitative description of discontinuities in rock masses. *ISRM, International Journal of Rock Mechanics and Mining Sciences & Geomechanics Abstracts, 15*(6).

Bennett, A. (1997). *The geology of the Western Tokoroa Plateau, Taupo Volcanic Zone, New Zealand.* thesis, University of Waikato.

Beresford, S., & Cole, J. (2000). Kaingaroa Ignimbrite, Taupo volcanic zone, New Zealand: evidence for asymmetric caldera subsidence of the Reporoa caldera. *New Zealand Journal of Geology and Geophysics, 43*(3), 471-481.

Bindeman, I. N., & Valley, J. W. (2003). Rapid generation of both high-and low-δ18O, large-volume silicic magmas at the Timber Mountain/Oasis Valley caldera complex, Nevada. *GSA Bulletin, 115*(5), 581-595.

Black, T. M., Shane, P. A., Westgate, J. A., & Froggatt, P. C. J. B. o. v. (1996). Chronological and palaeomagnetic constraints on widespread welded ignimbrites of the Taupo Volcanic Zone, New Zealand. *58*(2-3), 226-238.

Blank, H. R. J. (1965). Ash-flow deposits of the central King Country, New Zealand. *New Zealand journal of geology and geophysics, 8*(4), 588-610.

Bowling, F. M. (1989). *Volcanic geology of ignimbrites on the western margin of the Hauraki Depression and in the Mangatangi area.* thesis, University of Waikato.

Branney, M., & Kokelaar, P. (2002). Pyroclastic Density Currents and the Sedimentation of Ignimbrites, Geol. *Soc. Mem, 27*, 143.

Branney, M. J., & Kokelaar, P. J. B. o. V. (1992). A reappraisal of ignimbrite emplacement: progressive aggradation and changes from particulate to non-particulate flow during emplacement of high-grade ignimbrite. *Bulletin of Volcanology, 54*(6), 504-520.

Breard, E. C., & Lube, G. (2017). Inside pyroclastic density currents–uncovering the enigmatic flow structure and transport behaviour in large-scale experiments. *Earth and Planetary Science Letters, 458*, 22-36.

Briggs, N. D. (1976). Recognition and correlation of subdivisions within the Whakamaru Ignimbrite, central North Island, New Zealand. *New Zealand Journal of Geology and Geophysics, 19*(4), 463-501.

Briggs, R., Gifford, M., Moyle, A., Taylor, S., Norman, M., Houghton, B., & Wilson, C. (1993). Geochemical zoning and eruptive mixing in ignimbrites from Mangakino volcano, Taupo Volcanic Zone, New Zealand. *Journal of volcanology and geothermal research, 56*(3), 175-203.

Briggs, R., Houghton, B., McWilliams, M., & Wilson, C. (2005a). 40Ar/39Ar ages of silicic volcanic rocks in the Tauranga‐Kaimai area, New Zealand: Dating the transition between volcanism in the Coromandel Arc and the Taupo Volcanic Zone. *New Zealand Journal of Geology and Geophysics, 48*(3), 459-469.

Briggs, R., Houghton, B., McWilliams, M., & Wilson, C. (2005b). 40Ar/39Ar ages of silicic volcanic rocks in the Tauranga‐Kaimai area, New Zealand: Dating the transition between volcanism in the Coromandel Arc and the Taupo Volcanic Zone. *New Zealand Journal of Geology and Geophysics, 48*(3), 459-469.

Brink, M. T. (2012). *Emplacement processes of ignimbrites in the Ongatiti Valley, southeast Te Kuiti*. thesis, University of Waikato.

Brown, R. J., & Andrews, G. D. (2015). Deposits of pyroclastic density currents. In *The Encyclopedia of Volcanoes (Second Edition)* (pp. 631-648). Elsevier.

Brown, S., Wilson, C., Cole, J., Wooden, J. J. J. o. V., & Research, G. (1998). The Whakamaru group ignimbrites, Taupo Volcanic Zone, New Zealand: evidence for reverse tapping of a zoned silicic magmatic system. *84*(1-2), 1-37.

Burgisser, A., & Bergantz, G. W. (2002). Reconciling pyroclastic flow and surge: the multiphase physics of pyroclastic density currents. *Earth and Planetary Science Letters, 202*(2), 405-418.

Cappelletti, P., Cerri, G., Colella, A., de'Gennaro, M., Langella, A., Perrotta, A., Scarpati, C. J. M., & Petrology. (2003). Post-eruptive processes in the Campanian Ignimbrite. *79*(1-2), 79-97.

Cas, R., & Wright, J. (1987). Volcanic successions: Ancient and modern. *Allen and Unin, London*.

Cas, R. A., Wright, H. M., Folkes, C. B., Lesti, C., Porreca, M., Giordano, G., & Viramonte, J. G. J. B. o. V. (2011). The flow dynamics of an extremely large volume pyroclastic flow, the 2.08-Ma Cerro Galán Ignimbrite, NW Argentina, and comparison with other flow types. *73*(10), 1583-1609.

Cashman, K., & Blundy, J. (2000). Degassing and crystallization of ascending andesite and dacite. *Philosophical Transactions of the Royal Society of London. Series A: Mathematical, Physical and Engineering Sciences, 358*(1770), 1487-1513.

Cashman, K. V., & Scheu, B. (2015). Magmatic fragmentation. In *The Encyclopedia of Volcanoes* (pp. 459-471). Elsevier.

Charlier, B., Wilson, C., Lowenstern, J., Blake, S., Van Calsteren, P., & Davidson, J. (2004).

Magma generation at a large, hyperactive silicic volcano (Taupo, New Zealand) revealed by U–Th and U–Pb systematics in zircons. *Journal of Petrology, 46*(1), 3-32.

Cnudde, V., & Boone, M. N. (2013). High-resolution X-ray computed tomography in geosciences: A review of the current technology and applications. *Earth-Science Reviews, 123*, 1-17.

Cole, J. (1979). Structure, petrology, and genesis of Cenozoic volcanism, Taupo Volcanic Zone, New Zealand—a review. *New Zealand journal of geology and geophysics, 22*(6), 631-657.

Cole, J. (1981). Genesis of lavas of the Taupo volcanic zone, North Island, New Zealand. *Journal of Volcanology and Geothermal Research, 10*(4), 317-337.

Cole, J. (1990). Structural control and origin of volcanism in the Taupo volcanic zone, New Zealand. *Bulletin of volcanology, 52*(6), 445-459.

Condie, K. C. (1993). Chemical composition and evolution of the upper continental crust: contrasting results from surface samples and shales. *Chemical geology, 104*(1-4), 1-37.

Condie, K. C. (2005). High field strength element ratios in Archean basalts: a window to evolving sources of mantle plumes? *Lithos, 79*(3-4), 491-504.

Cook, G. W., Wolff, J. A., & Self, S. (2016). Estimating the eruptive volume of a large pyroclastic body: the Otowi Member of the Bandelier Tuff, Valles caldera, New Mexico. *Bulletin of Volcanology, 78*(2), 10.

Cooper, G. F., Morgan, D. J., & Wilson, C. J. (2017). Rapid assembly and rejuvenation of a large silicic magmatic system: Insights from mineral diffusive profiles in the Kidnappers and Rocky Hill deposits, New Zealand. *Earth and Planetary Science Letters, 473*, 1-13.

Cooper, G. F., & Wilson, C. J. (2014). Development, mobilisation and eruption of a large crystal-rich rhyolite: the Ongatiti ignimbrite, New Zealand. *Lithos, 198*, 38-57.

Cooper, G. F., Wilson, C. J., Millet, M.-A., & Baker, J. A. (2016). Generation and rejuvenation of a supervolcanic magmatic system: a case study from Mangakino volcanic centre, New Zealand. *Journal of Petrology, 57*(6), 1135-1170.

Daniš ík, M., Fodor, L., Dunkl, I., Gerdes, A., Csizmeg, J., Hámor ‐ Vidó, M., & Evans, N. J. (2015). A multi ‐ system geochronology in the Ad ‐ 3 borehole, Pannonian Basin (Hungary) with implications for dating volcanic rocks by low ‐ temperature thermochronology and for interpretation of (U ‐ Th)/He data. *Terra Nova, 27*(4), 258-269.

Danišík, M., Shane, P., Schmitt, A. K., Hogg, A., Santos, G. M., Storm, S., Evans, N. J., Fifield, L. K., & Lindsay, J. M. (2012). Re-anchoring the late Pleistocene

tephrochronology of New Zealand based on concordant radiocarbon ages and combined 238 U/230 Th disequilibrium and (U–Th)/He zircon ages. *Earth and Planetary Science Letters, 349*, 240-250.

DeGraff, J. M., & Aydin, A. (1987). Surface morphology of columnar joints and its significance to mechanics and direction of joint growth. *Geological Society of America Bulletin, 99*(5), 605-617.

Degruyter, W., Burgisser, A., Bachmann, O., & Malaspinas, O. (2010). Synchrotron X-ray microtomography and lattice Boltzmann simulations of gas flow through volcanic pumices. *Geosphere, 6*(5), 470-481.

Di Pastena, V. (Compiler) (1997). *Aspetti fluidodinamici dei flussi piroclastici*. Università degli Studi di Napoli "Federico II" of Napoli: PhD thesis.

Diller, K., Clarke, A., Voight, B., & Neri, A. (2006). Mechanisms of conduit plug formation: Implications for vulcanian explosions. *Geophysical Research Letters, 33*(20).

Dingwell, D. B., Lavallée, Y., Hess, K.-U., Flaws, A., Marti, J., Nichols, A. R., Gilg, H. A., & Schillinger, B. (2016). Eruptive shearing of tube pumice: pure and simple.

Donoghue, E., Troll, V. R., Harris, C., O'Halloran, A., Walter, T. R., Torrado, F. J. P. J. J. o. V., & Research, G. (2008). Low-temperature hydrothermal alteration of intra-caldera tuffs, Miocene Tejeda caldera, Gran Canaria, Canary Islands. *176*(4), 551-564.

Edbrooke, S. (2005). Geology of the Waikato area. Institute of Geological & Nuclear Sciences 1: 250,000 geological map, 4. *Lower Hutt, Institute of Geological & Nuclear Sciences*, 68.

Ewart, A., Brothers, R., & Mateen, A. (1977). An outline of the geology and geochemistry, and the possible petrogenetic evolution of the volcanic rocks of the Tonga-Kermadec-New Zealand island arc. *Journal of volcanology and geothermal research, 2*(3), 205-250.

Fisher, R. V. (1961). Proposed classification of volcaniclastic sediments and rocks. *Geological Society of America Bulletin, 72*(9), 1409-1414.

Fisher, R. V., & Schmincke, H.-U. (1984). *Pyroclastic rocks*. Springer-Verlag.

Flannery, B. P., Deckman, H. W., Roberge, W. G., & D'Amico, K. L. (1987). Three-dimensional X-ray microtomography. *Science, 237*(4821), 1439-1444.

Fowler, A., Berger, B., Shore, M., Jones, M., & Ropchan, J. J. P. R. (2002). Supercooled rocks: development and significance of varioles, spherulites, dendrites and spinifex in Archaean volcanic rocks, Abitibi Greenstone belt, Canada. *115*(1-4), 311-328.

Francis, P., & Baker, M. J. N. (1977). Mobility of pyroclastic flows. *Nature, 270*(5633), 164.

Francis, P. W., Sparks, R., Hawkesworth, C., Thorpe, R., Pyle, D., Tait, S., Mantovani, M., & McDermott, F. (1989). Petrology and geochemistry of volcanic rocks of the Cerro

Galan caldera, northwest Argentina. *Geological Magazine, 126*(5), 515-547.

Freundt, A. (1998). The formation of high-grade ignimbrites, I: Experiments on high-and low-concentration transport systems containing sticky particles. *Bulletin of Volcanology, 59*(6), 414-435.

Freundt, A., Wilson, C., & Carey, S. (2000). Ignimbrites and block-and-ash flow deposits. In. Academic Press.

Giachetti, T., Burgisser, A., Arbaret, L., Druitt, T. H., & Kelfoun, K. (2011). Quantitative textural analysis of Vulcanian pyroclasts (Montserrat) using multi-scale X-ray computed microtomography: comparison with results from 2D image analysis. *Bulletin of Volcanology*, *73*(9), 1295-1309.

Gifford, M. G. (1988). *Geology of the South West Tokoroa Plateau with Emphasis on the Marshall Ignimbrites.* thesis, University of Waikato.

Giordano, D., Nichols, A. R., & Dingwell, D. B. (2005). Glass transition temperatures of natural hydrous melts: a relationship with shear viscosity and implications for the welding process. *Journal of Volcanology and Geothermal Research, 142*(1-2), 105-118.

Graham, I., Cole, J., Briggs, R., Gamble, J., & Smith, I. (1995). Petrology and petrogenesis of volcanic rocks from the Taupo Volcanic Zone: a review. *Journal of volcanology and geothermal research, 68*(1-3), 59-87.

Gravina, T., Lirer, L., Marzocchella, A., Petrosino, P., & Salatino, P. (2004). Fluidization and attrition of pyroclastic granular solids. *Journal of volcanology and geothermal research, 138*(1-2), 27-42.

Grunder, A. L., Laporte, D., & Druitt, T. H. (2005). Experimental and textural investigation of welding: effects of compaction, sintering, and vapor-phase crystallization in the rhyolitic Rattlesnake Tuff. *Journal of Volcanology and Geothermal Research, 142*(1-2), 89-104.

Gunderson, R., Cameron, K., & Cameron, M. (1986). Mid-Cenozoic high-K calc-alkalic and alkalic volcanism in eastern Chihuahua, Mexico: Geology and geochemistry of the Benavides-Pozos area. *Geological Society of America Bulletin, 97*(6), 737-753.

Hastuti, E. W. D. (1992). *Post-depositional Alteration of Ignimbrites in the Western Taupo Volcanic Zone, New Zealand.* thesis, University of Waikato.

Healy, J. (1964). Volcanic mechanisms in the Taupo volcanic zone, New Zealand. *New Zealand journal of geology and geophysics, 7*(1), 6-23.

Heap, M. J., Violay, M., Wadsworth, F. B., & Vasseur, J. (2017). From rock to magma and back again: the evolution of temperature and deformation mechanism in conduit margin zones. *Earth and Planetary Science Letters, 463*, 92-100.

Heiken, G., & Wohletz, K. (1985). *Volcanic ash*. University Presses of California, Chicago,

Harvard & MIT.

Heron, D. W. (Cartographer). (2014). Geological Map of New Zealand 1:250 000. GNS Science Geological Map 1. Lower Hutt, New Zealand. GNS Science.

Hildreth, W., & Mahood, G. (1985). Correlation of ash-flow tuffs. *Geological Society of America Bulletin, 96*(7), 968-974.

Hochstetter, F. V. (1859). New Zealand: its physical geography, geology, and natural history: with special reference to the results of government expeditions in the provinces of Auckland and Nelson', lecture on the geology of the province of Auckland, Auckland Mechanics' Institute.

Horrocks, J. L. (2000). *Stratigraphy, chronology and correlation of the Plio-Pleistocene (c. 2.2-0.8 Ma) Kauroa ash sequence, Western Central North Island, New Zealand.* thesis, University of Waikato.

Houghton, B., & Cuthbertson, A. (1989). Sheet T14BD Kaimai; Geological Map of New Zealand 1: 50,000. *Dept. Sci. Indus. Res., Wellington, New Zealand*.

Houghton, B., Gifford, M., Wilson, C., & Briggs, R. (1987a). lgnimbrite structure of the Tokoroa-Kinleith area, western Central Volcanic Region. *NZ Geol. Surv. Rec, 20*, 57-62.

Houghton, B., & Wilson, C. (1989). A vesicularity index for pyroclastic deposits. *Bulletin of volcanology, 51*(6), 451-462.

Houghton, B., Wilson, C., McWilliams, M., Lanphere, M., Weaver, S., Briggs, R., & Pringle, M. (1995). Chronology and dynamics of a large silicic magmatic system: central Taupo Volcanic Zone, New Zealand. *Geology, 23*(1), 13-16.

Houghton, B., Wilson, C., & Stern, T. (1987b). Ignimbrite stratigraphy of a 457 m deep drillhole near Tokoroa. *New Zealand Geological Survey record, 20*, 51-53.

Hurwitz, S., & Navon, O. (1994). Bubble nucleation in rhyolitic melts: Experiments at high pressure, temperature, and water content. *Earth and Planetary Science Letters, 122*(3-4), 267-280.

Kameda, M., Kuribara, H., & Ichihara, M. (2008). Dominant time scale for brittle fragmentation of vesicular magma by decompression. *Geophysical Research Letters, 35*(14).

Kear, D. (1960). Sheet 4 Hamilton Geological Map of NZ 1: 200,000. *DSIR Wellington*.

Kennedy, B., Spieler, O., Scheu, B., Kueppers, U., Taddeucci, J., & Dingwell, D. B. (2005). Conduit implosion during Vulcanian eruptions. *Geology, 33*(7), 581-584.

Ketcham, R. A., & Carlson, W. D. (2001). Acquisition, optimization and interpretation of X-ray computed tomographic imagery: applications to the geosciences. *Computers & Geosciences, 27*(4), 381-400.

Klug, C., Cashman, K., & Bacon, C. (2002). Structure and physical characteristics of pumice from the climactic eruption of Mount Mazama (Crater Lake), Oregon. *Bulletin of Volcanology, 64*(7), 486-501.

Klug, C., & Cashman, K. V. (1996). Permeability development in vesiculating magmas: implications for fragmentation. *Bulletin of Volcanology, 58*(2-3), 87-100.

Komar, P. D. (1972). Flow differentiation in igneous dikes and sills: profiles of velocity and phenocryst concentration. *Geological Society of America Bulletin, 83*(11), 3443-3448.

Krippner, S. J., Briggs, R. M., Wilson, C. J., & Cole, J. W. (1998). Petrography and geochemistry of lithic fragments in ignimbrites from the Mangakino Volcanic Centre: implications for the composition of the subvolcanic crust in western Taupo Volcanic Zone, New Zealand. *New Zealand Journal of Geology and Geophysics, 41*(2), 187-199.

Lamb, S. (2011). Cenozoic tectonic evolution of the New Zealand plate-boundary zone: A paleomagnetic perspective. *Tectonophysics, 509*(3), 135-164.

Landis, E. N., & Keane, D. T. (2010). X-ray microtomography. *Materials characterization, 61*(12), 1305-1316.

Le Maitre, R. (2002). *Igneous rocks: a classification and glossary of terms: recommendations of the IUGS, Subcommission on the Systematics of Igneous Rocks*. University Press.

Le Roex, A. P. (1986). Geochemical correlation between southern African kimberlites and South Atlantic hotspots. *Nature, 324*(6094), 243.

Leonard, G., Begg, J., & Wilson, C. (2010). Geology of the Rotorua Area: Scale 1: 250,000. Institute of Geological and Nuclear Sciences 1: 250,000 Geological Map 5. *Institute of Geological and Nuclear Sciences, Lower Hutt, New Zealand*.

Lipman, P. W. (1984). The roots of ash flow calderas in western North America: windows into the tops of granitic batholiths. *Journal of Geophysical Research: Solid Earth, 89*(B10), 8801-8841.

Lofgren, G. J. G. S. o. A. B. (1971). Experimentally produced devitrification textures in natural rhyolitic glass. *82*(1), 111-124.

Lowe, D. J., Pearce, N. J., Jorgensen, M. A., Kuehn, S. C., Tryon, C. A., & Hayward, C. L. (2017). Correlating tephras and cryptotephras using glass compositional analyses and numerical and statistical methods: Review and evaluation. *Quaternary Science Reviews, 175*, 1-44.

Lowe, D. J., & Pittari, A. (2019). Pyroclastic flow deposits, Hinuera Valley, central North Island, and note on usage of ignimbrite as a building material. *Historical Studies, 61*, 6-15.

Lowe, D. J., Tippett, J. M., Kamp, P. J., Liddell, I. J., Briggs, R. M., & Horrocks, J. L. (2001). Ages on weathered Plio-Pleistocene tephra sequences, western north Island, New Zealand.

Lube, G., Breard, E. C., Jones, J., Fullard, L., Dufek, J., Cronin, S. J., & Wang, T. (2019). Generation of air lubrication within pyroclastic density currents. *Nature Geoscience*, *12*(5), 381-386.

Lukács, R., Harangi, S., Bachmann, O., Guillong, M., Danišík, M., Buret, Y., von Quadt, A., Dunkl, I., Fodor, L., & Sliwinski, J. (2015). Zircon geochronology and geochemistry to constrain the youngest eruption events and magma evolution of the Mid-Miocene ignimbrite flare-up in the Pannonian Basin, eastern central Europe. *Contributions to Mineralogy and Petrology, 170*(5-6), 52.

Mader, H. (1998). Conduit flow and fragmentation. *Geological Society, London, Special Publications, 145*(1), 51-71.

Mangan, M., & Sisson, T. (2000). Delayed, disequilibrium degassing in rhyolite magma: decompression experiments and implications for explosive volcanism. *Earth and Planetary Science Letters, 183*(3-4), 441-455.

Manley, C. R. J. (1992). Extended cooling and viscous flow of large, hot rhyolite lavas: implications of numerical modeling results. *Journal of volcanology and geothermal research, 53*(1-4), 27-46.

Marshall, P. (1934). Acid rocks of Taupo-Rotorua Volcanic district. *Royal Society of New Zealand, 64*, 323-366.

Marti, J., Soriano, C., & Dingwell, D. (1999). Tube pumices as strain markers of the ductile–brittle transition during magma fragmentation. *Nature, 402*(6762), 650.

Martin, R. C. (1961). Stratigraphy and structural outline of the Taupo Volcanic Zone. *New Zealand journal of geology and geophysics, 4*(4), 449-478.

Marwick, J., Ferrar, H. T., Taylor, N. H., Williamson, J. H., Finlay, H. J., & Hutton, C. O. (1946). *The geology of the Te Kuiti subdivision*. NZ, EV Paul, government printer.

Mason, B. G., Pyle, D. M., & Oppenheimer, C. (2004). The size and frequency of the largest explosive eruptions on Earth. *Bulletin of Volcanology, 66*(8), 735-748.

McBirney, A., & Murase, T. (1970). Factors governing the formation of pyroclastic rocks. *Bulletin Volcanologique, 34*(2), 372-384.

McCormack, K. D., Gee, M. M., McNaughton, N. J., Smith, R., & Fletcher, I. R. (2009). U–Pb dating of magmatic and xenocryst zircons from Mangakino ignimbrites and their correlation with detrital zircons from the Torlesse metasediments, Taupo Volcanic Zone, New Zealand. *Journal of Volcanology and Geothermal Research, 183*(1), 97-111.

McGrath, P. F. (2004). *Volcanic geology of the Ahuroa Ignimbrite at Wharepapa South.*

thesis, University of Waikato.

Mildenhall, D., & Alloway, B. (2008). A widespread ca. 1.1 Ma TVZ silicic tephra preserved near Wellington, New Zealand: implications for regional reconstruction of mid-Pleistocene vegetation. *Quaternary International, 178*(1), 167-182.

Milicich, S., Chambefort, I., Wilson, C., Alcaraz, S., Ireland, T., Bardsley, C., & Simpson, M. (2020). A zircon U-Pb geochronology for the Rotokawa geothermal system, New Zealand, with implications for Taupō Volcanic Zone evolution. *Journal of Volcanology and Geothermal Research, 389*, 106729.

Miller, C. F., & Wark, D. A. (2008). Supervolcanoes and their explosive supereruptions. *Elements, 4*(1), 11-15.

Mitchell, S. J., Houghton, B. F., Carey, R. J., Manga, M., Fauria, K. E., Jones, M. R., Soule, S. A., Conway, C. E., Wei, Z., & Giachetti, T. (2019). Submarine giant pumice: a window into the shallow conduit dynamics of a recent silicic eruption. *Bulletin of Volcanology, 81*(7), 42.

Miwa, T., & Geshi, N. (2012). Decompression rate of magma at fragmentation: Inference from broken crystals in pumice of vulcanian eruption. *Journal of Volcanology and Geothermal Research, 227*, 76-84.

Modriniak, N., & Studt, F. (1959). Geological structure and volcanism of the Taupo-Tarawera District. *New Zealand journal of geology and geophysics, 2*(4), 654-684.

Moll, E. J. (1981). Geochemistry and petrology of Mid‐Tertiary ash flow tuffs from the Sierra el Virulento Area, eastern Chihuahua, Mexico. *Journal of Geophysical Research: Solid Earth, 86*(B11), 10321-10334.

Moon, V. G. (1989). *Relationships Between the Geomechanics and Petrography of Ignimbrite*. thesis, University of Waikato.

Moon, V. G. (1993). Geotechnical characteristics of ignimbrite: A soft pyroclastic rock type. *Engineering Geology, 35*(1-2), 33-48.

Moyle, A. R. (1989). *Volcanic geology and geochemistry of the Rocky Hill Ignimbrite, upper Waipa valley*. thesis, University of Waikato.

Mulas, M. (2013). *Depositional and welding processes in low aspect ratio ignimbrites: examples from the Sulcis Volcanic District (Sardinia, Italy)*. thesis, Doctorate Thesis, Universita'degli Studi di Cagliari.

Murch, A., White, J., & Carey, R. (2019). Unusual fluidal behavior of a silicic magma during fragmentation in a deep subaqueous eruption, Havre volcano, southwestern Pacific Ocean. *Geology, 47*(5), 487-490.

Nairn, I., Wood, C., & Bailey, R. (1994). The Reporoa caldera, Taupo volcanic zone: source of the Kaingaroa ignimbrites. *Bulletin of Volcanology, 56*(6-7), 529-537.

Namiki, A., & Manga, M. (2008). Transition between fragmentation and permeable outgassing of low viscosity magmas. *Journal of Volcanology and Geothermal Research, 169*(1-2), 48-60.

Neri, A., Di Muro, A., & Rosi, M. (2002). Mass partition during collapsing and transitional columns by using numerical simulations. *Journal of Volcanology and Geothermal Research, 115*(1-2), 1-18.

Orsi, G., Gallo, G., Heiken, G., Wohletz, K., Yu, E., & Bonani, G. (1992). A comprehensive study of pumice formation and dispersal: the Cretaio Tephra of Ischia (Italy). *Journal of Volcanology and Geothermal Research, 53*(1-4), 329-354.

Pain, C. (1975). Some tephra deposits in the south-west Waikato area, North Island, New Zealand. *New Zealand journal of geology and geophysics, 18*(4), 541-550.

Papale, P., Neri, A., & Macedonio, G. (1998). The role of magma composition and water content in explosive eruptions: 1. Conduit ascent dynamics. *Journal of Volcanology and Geothermal Research, 87*(1-4), 75-93.

Pearce, J., Kempton, P., & Gill, J. (2002). Behaviour of high field strength elements in subduction systems. In *Geochimica et Cosmochimica Acta* (Vol. 66, pp. A584-A584).

Pearce, J. A., Harris, N. B., & Tindle, A. G. (1984). Trace element discrimination diagrams for the tectonic interpretation of granitic rocks. *Journal of petrology, 25*(4), 956-983.

Pearce, N. J., Westgate, J. A., Perkins, W. T., Eastwood, W. J., & Shane, P. (1999). The application of laser ablation ICP-MS to the analysis of volcanic glass shards from tephra deposits: bulk glass and single shard analysis. *Global and Planetary Change, 21*(1-3), 151-171.

Peterson, D. W. (1979). Significance of the flattening of pumice fragments in ash-flow tuffs. Ash-flow tuffs. *Special Paper, Geological Society of America*, 195-204.

Pittari, A., Cas, R., Edgar, C., Nichols, H., Wolff, J., & Marti, J. (2006). The influence of palaeotopography on facies architecture and pyroclastic flow processes of a lithic-rich ignimbrite in a high gradient setting: the Abrigo Ignimbrite, Tenerife, Canary Islands. *Journal of Volcanology and Geothermal Research, 152*(3), 273-315.

Polacci, M. (2005). Constraining the dynamics of volcanic eruptions by characterization of pumice textures. *Annals of Geophysics*.

Polacci, M., Baker, D. R., Mancini, L., Tromba, G., & Zanini, F. (2006). Three‐dimensional investigation of volcanic textures by X‐ray microtomography and implications for conduit processes. *Geophysical Research Letters, 33*(13).

Polacci, M., Papale, P., Giordano, D., & del Seppia, D. (2003). Conduit flow dynamics of alkaline vs calc-alkaline eruptions by numerical modeling and pumice textures. In *EGS-AGU-EUG Joint Assembly*.

Price, R. C., Gamble, J. A., Smith, I. E., Stewart, R. B., Eggins, S., & Wright, I. C. (2005). An integrated model for the temporal evolution of andesites and rhyolites and crustal development in New Zealand's North Island. *Journal of Volcanology and Geothermal Research, 140*(1-3), 1-24.

Pringle, M., McWilliams, M., Houghton, B. F., Lanphere, M., & Wilson, C. J. G. (1992). 40Ar/39Ar dating of Quaternary feldspar: examples from the Taupo Volcanic Zone, New Zealand. *20*(6), 531-534.

Pyle, D. M. (1995). Assessment of the minimum volume of tephra fall deposits. *Journal of Volcanology and Geothermal Research, 69*(3-4), 379-382.

Quane, S. L., & Russell, J. K. (2005). Ranking welding intensity in pyroclastic deposits. *Bulletin of Volcanology, 67*(2), 129-143.

Quane, S. L., Russell, J. K., & Friedlander, E. A. (2009). Time scales of compaction in volcanic systems. *Geology, 37*(5), 471-474.

Ragan, D., & Sheridan, M. (1972). Compaction of the Bishop tuff, California. *Geological Society of America Bulletin, 83*(1), 95-106.

Raganati, F., Chirone, R., & Ammendola, P. (2018). Gas–solid fluidization of cohesive powders. *Chemical Engineering Research and Design, 133,* 347-387.

Roche, O., Druitt, T., & Cas, R. (2001). Experimental aqueous fluidization of ignimbrite. *Journal of Volcanology and Geothermal Research, 112*(1-4), 267-280.

Roche, O., Gilbertson, M., Phillips, J., & Sparks, R. (2002). Experiments on deaerating granular flows and implications for pyroclastic flow mobility. *Geophysical research letters, 29*(16), 40-1-40-4.

Rogan, M. (1982). A geophysical study of the Taupo volcanic zone New Zealand. *Journal of Geophysical Research: Solid Earth, 87*(B5), 4073-4088.

Rollinson, H. (1993). Using geochemical data: Evaluation, presentation, interpretation (pp. 133–150). *Harlow, England: Longman*.

Rollinson, H. R. (2014). *Using geochemical data: evaluation, presentation, interpretation*. Routledge.

Rose, W., & Chesner, C. (1987). Dispersal of ash in the great Toba eruption, 75 ka. *Geology, 15*(10), 913-917.

Ross, C. S., & Smith, R. L. (1961). *Ash-flow tuffs: Their origin, geologic relations, and identification.* United States Government Printing Office.

Rowland, J., & Sibson, R. (2004). Structural controls on hydrothermal flow in a segmented rift system, Taupo Volcanic Zone, New Zealand. *Geofluids, 4*(4), 259-283.

Rust, A., & Cashman, K. (2011). Permeability controls on expansion and size distributions

of pyroclasts. *Journal of Geophysical Research: Solid Earth, 116*(B11).

Rust, A., & Russell, J. (2000). Detection of welding in pyroclastic flows with ground penetrating radar: insights from field and forward modeling data. *Journal of Volcanology and Geothermal Research, 95*(1-4), 23-34.

Saha, A., D'Mello, N. G., Sensarma, S., Mudholkar, A. V., & Doley, B. (2019). Geochemical characteristics of submarine rhyolitic pumice from Andaman subduction zone: Inferences on magmatism and tectonics of north‐eastern Indian Ocean. *Geological Journal*.

Self, S. (2006). The effects and consequences of very large explosive volcanic eruptions. *Philosophical Transactions of the Royal Society A: Mathematical, Physical and Engineering Sciences, 364*(1845), 2073-2097.

Shea, T., Gurioli, L., Larsen, J. F., Houghton, B. F., Hammer, J. E., & Cashman, K. V. (2010). Linking experimental and natural vesicle textures in Vesuvius 79AD white pumice. *Journal of Volcanology and Geothermal Research, 192*(1-2), 69-84.

Sheridan, M. F., & Ragan, D. M. (1975). Compaction of ash-flow tuffs. *Developments in Sedimentology, 18*, 677-717.

Smith, R. L. (1960). Ash flows. *Geological Society of America Bulletin, 71*(6), 795-841.

Smith, R. L. (1979). Ash-flow magmatism. *Ash-flow tuffs: Geological Society of America Special Paper, 180*, 5-27.

Soengkono, S., Hochstein, M., Smith, I., & Itaya, T. (1992). Geophysical evidence for widespread reversely magnetised pyroclastics in the western Taupo Volcanic Zone (New Zealand). *New Zealand Journal of Geology and Geophysics, 35*(1), 47-55.

Song, S.-R., Jones, K. W., Lindquist, B. W., Dowd, B. A., & Sahagian, D. L. (2001). Synchrotron X-ray computed microtomography: studies on vesiculated basaltic rocks. *Bulletin of Volcanology, 63*(4), 252-263.

Sparks, R., Self, S., Grattan, J., Oppenheimer, C., Pyle, D., & Rymer, H. (2005). Super-eruptions: Global effects and future threats: London. *UK, Report of a Geological Society of London working group*.

Sparks, R., & Walker, G. (1977). The significance of vitric-enriched air-fall ashes associated with crystal-enriched ignimbrites. *Journal of Volcanology and Geothermal Research, 2*(4), 329-341.

Sparks, R., & Wilson, L. (1976). A model for the formation of ignimbrite by gravitational column collapse. *Journal of the Geological Society, 132*(4), 441-451.

Sparks, R. S. J. (1978). The dynamics of bubble formation and growth in magmas: a review and analysis. *Journal of Volcanology and Geothermal Research, 3*(1-2), 1-37.

Sparks, R. S. J., Self, S., & Walker, G. P. (1973). Products of ignimbrite eruptions. *Geology*,

1(3), 115-118.

Stern, T. (1979). Regional and residual gravity fields, central North Island, New Zealand. *New Zealand journal of geology and geophysics, 22*(4), 479-485.

Stratford, W. R., & Stern, T. (2008). Geophysical imaging of buried volcanic structures within a continental back-arc basin: The Central Volcanic Region, North Island, New Zealand. *Journal of Volcanology and Geothermal Research, 174*(4), 257-268.

Streck, M. J., & Grunder, A. L. (1995). Crystallization and welding variations in a widespread ignimbrite sheet; the Rattlesnake Tuff, eastern Oregon, USA. *Bulletin of Volcanology, 57*(3), 151-169.

Sugioka, I., & Bursik, M. (1995). Explosive fragmentation of erupting magma. *Nature, 373*(6516), 689.

Sun, S.-S., & McDonough, W. F. (1989). Chemical and isotopic systematics of oceanic basalts: implications for mantle composition and processes. *Geological Society, London, Special Publications, 42*(1), 313-345.

Sutton, A. N., Blake, S., & Wilson, C. J. (1995). An outline geochemistry of rhyolite eruptives from Taupo volcanic centre, New Zealand. *Journal of Volcanology and Geothermal Research, 68*(1-3), 153-175.

Tafforeau, P., Boistel, R., Boller, E., Bravin, A., Brunet, M., Chaimanee, Y., Cloetens, P., Feist, M., Hoszowska, J., & Jaeger, J.-J. (2006). Applications of X-ray synchrotron microtomography for non-destructive 3D studies of paleontological specimens. *Applied Physics A, 83*(2), 195-202.

Verhoogen, J. (1951). Mechanics of ash formation. *American Journal of Science, 249*(10), 729-739.

Voltolini, M., Zandomeneghi, D., Mancini, L., & Polacci, M. (2011). Texture analysis of volcanic rock samples: quantitative study of crystals and vesicles shape preferred orientation from X-ray microtomography data. *Journal of Volcanology and Geothermal Research, 202*(1-2), 83-95.

Walker, G. P. (1980). The Taupo pumice: product of the most powerful known (ultraplinian) eruption? *Journal of volcanology and geothermal research, 8*(1), 69-94.

Walker, G. P. (1983). Ignimbrite types and ignimbrite problems. *Journal of Volcanology and Geothermal Research, 17*(1-4), 65-88.

Webb, S. L., & Dingwell, D. B. (1990). Non‐Newtonian rheology of igneous melts at high stresses and strain rates: Experimental results for rhyolite, andesite, basalt, and nephelinite. *Journal of Geophysical Research: Solid Earth, 95*(B10), 15695-15701.

Whitham, A., & Sparks, R. (1986). Pumice. *Bulletin of Volcanology, 48*(4), 209-223.

Wilson, C. (1986). Reconnaissance stratigraphy and volcanology of ignimbrites from

Mangakino volcano. *Late Cenozoic volcanism in New Zealand. Royal Society of New Zealand Bulletin, 23*, 179-193.

Wilson, C. (1991). Ignimbrite morphology and the effects of erosion: a New Zealand case study. *Bulletin of Volcanology, 53*(8), 635-644.

Wilson, C., Charlier, B., Rowland, J., & Browne, P. (2010). U–Pb dating of zircon in subsurface, hydrothermally altered pyroclastic deposits and implications for subsidence in a magmatically active rift: Taupo Volcanic Zone, New Zealand. *Journal of Volcanology and Geothermal Research, 191*(1-2), 69-78.

Wilson, C., Gravley, D., Leonard, G., & Rowland, J. (2009). Volcanism in the central Taupo Volcanic Zone, New Zealand: tempo, styles and controls. *Studies in Volcanology: The Legacy of George Walker. Special Publications of IAVCEI, 2*, 225-247.

Wilson, C., Houghton, B., Kamp, P., & McWilliams, M. (1995a). An exceptionally widespread ignimbrite with implications for pyroclastic flow emplacement. *Nature, 378*(6557), 605.

Wilson, C., Houghton, B., Kampt, P., & McWilliamst, M. (1995b). An exceptionally widespread ignimbrite with implications for pyroclastic flow emplacement. *Nature, 378*(6557), 605.

Wilson, C., Houghton, B., & Lloyd, E. (1986). Volcanic history and evolution of the Maroa-Taupo area, central North Island. In *Late Cenozoic Volcanism in New Zealand* (pp. 194-223). Royal Society of New Zealand, Bulletin 23 Wellington, New Zealand.

Wilson, C., Houghton, B., McWilliams, M., Lanphere, M., Weaver, S., & Briggs, R. (1995c). Volcanic and structural evolution of Taupo Volcanic Zone, New Zealand: a review. *Journal of volcanology and geothermal research, 68*(1), 1-28.

Wilson, C., Rogan, A., Smith, I., Northey, D., Nairn, I., & Houghton, B. (1984). Caldera volcanoes of the Taupo volcanic zone, New Zealand. *Journal of Geophysical Research: Solid Earth, 89*(B10), 8463-8484.

Wilson, C. J. (2001). The 26.5 ka Oruanui eruption, New Zealand: an introduction and overview. *Journal of Volcanology and Geothermal Research, 112*(1-4), 133-174.

Wilson, C. J. (2008). Supereruptions and supervolcanoes: processes and products. *Elements, 4*(1), 29-34.

Wilson, C. J., & Hildreth, W. (2003). Assembling an ignimbrite: mechanical and thermal building blocks in the Bishop Tuff, California. *The Journal of geology, 111*(6), 653-670.

Wilson, C. J., & Rowland, J. V. (2016). The volcanic, magmatic and tectonic setting of the Taupo Volcanic Zone, New Zealand, reviewed from a geothermal perspective. *Geothermics, 59*, 168-187.

Wilson, L. (1976). Explosive volcanic eruptions—III. Plinian eruption columns. *Geophysical*

Journal International, *45*(3), 543-556.

Winter, J. D. (2013). *Principles of igneous and metamorphic petrology*. Pearson education.

Woods, A. W. (1998). Observations and models of volcanic eruption columns. *Geological Society, London, Special Publications*, *145*(1), 91-114.

Zandomeneghi, D., Voltolini, M., Mancini, L., Brun, F., Dreossi, D., & Polacci, M. (2010). Quantitative analysis of X-ray microtomography images of geomaterials: Application to volcanic rocks. *Geosphere*, *6*(6), 793-804.

Appendices

Appendix1: Table showing age data for (U-Th)/He for all of the zircons from separate sites

Sample code	232Th (ng)	± (%)	238U (ng)	± (%)	147Sm (ng)	± (%)	He (ncc)	± (%)	TAU (%)	Th/U	Raw age (Ma)	±1σ (Ma)	Ft	Cor. age (Ma)	±1σ (Ma)
Hinuera															
HI-1	1.317	1.9	1.996	2.5	0.0016	3.3	0.218	1.4	2.5	0.65	**0.777**	**0.020**	0.60	**1.295**	**0.073**
HI-2	2.384	1.9	2.663	13.2	0.0004	9.7	0.368	0.7	10.9	0.89	**0.938**	**0.102**	0.67	**1.391**	**0.167**
HI-3	0.570	2.0	1.065	8.3	0.0002	75.1	0.100	2.7	7.8	0.53	**0.683**	**0.053**	0.58	**1.178**	**0.109**
HI-4	0.751	4.1	1.050	4.4	0.0013	2.6	0.138	3.6	5.2	0.71	**0.925**	**0.048**	0.66	**1.392**	**0.101**
HI-5	0.751	1.9	1.050	4.1	0.0013	2.6	0.104	1.6	3.8	0.71	**0.695**	**0.027**	0.52	**1.348**	**0.085**
													Weighted average ± 2s	**1.314**	**0.086**
													Central age ± 2s	**1.320**	**0.086**
Tekuiti															
TE-1	0.348	1.9	0.705	2.3	0.0005	2.1	0.084	7.6	7.9	0.49	**0.881**	**0.069**	0.72	**1.218**	**0.113**
TE-2	0.831	2.0	1.339	14.6	0.0003	9.5	0.138	8.4	15.2	0.62	**0.742**	**0.113**	0.70	**1.067**	**0.171**
TE-3	0.206	3.5	0.368	3.7	0.0000	5.5	0.052	5.2	6.2	0.55	**1.018**	**0.063**	0.78	**1.302**	**0.103**
TE-4	0.493	2.7	0.944	22.4	0.0001	9.0	0.157	6.0	20.8	0.52	**1.214**	**0.252**	0.74	**1.638**	**0.350**
TE-5	2.041	1.9	1.473	9.8	0.0002	15.3	0.238	5.8	9.4	1.38	**1.002**	**0.094**	0.69	**1.459**	**0.155**
TE-7	0.456	1.9	0.654	2.3	0.0014	17.5	0.095	1.9	2.7	0.69	**1.026**	**0.028**	0.70	**1.458**	**0.083**

TE-8	0.385	1.4	0.618	1.9	0.0037	17.4	0.085	1.7	2.4	0.62	**0.989**	**0.024**	0.70	**1.416**	**0.078**
TE-9	0.640	1.4	0.886	1.9	0.0021	19.5	0.131	2.6	3.0	0.72	**1.038**	**0.031**	0.73	**1.428**	**0.083**
TE-10	0.253	1.4	0.378	1.9	0.0014	19.7	0.049	1.6	2.3	0.66	**0.925**	**0.021**	0.68	**1.362**	**0.075**
TE-11	0.473	1.9	0.637	2.3	0.0044	16.2	0.088	3.2	3.8	0.74	**0.969**	**0.037**	0.71	**1.363**	**0.085**
TE-12	0.544	1.4	0.794	1.9	0.0020	18.7	0.119	1.9	2.5	0.68	**1.065**	**0.027**	0.74	**1.430**	**0.080**
TE-13	0.244	1.9	0.415	2.3	0.0022	25.0	0.055	2.3	3.1	0.58	**0.952**	**0.029**	0.71	**1.337**	**0.078**
TE-14	0.127	1.5	0.231	1.9	0.0019	22.6	0.030	2.6	3.1	0.54	**0.947**	**0.029**	0.65	**1.449**	**0.085**
													Weighted average ± 2s	**1.382**	**0.052**
													Central age ± 2s	**1.390**	**0.052**
Tauranga															
TA-5	2.040	1.9	2.900	3.7	0.0012	2.1	0.436	4.9	5.9	0.70	**1.061**	**0.063**	0.83	**1.283**	**0.099**
TA-6	1.874	1.4	2.156	1.9	0.0015	23.5	0.345	1.5	2.2	0.86	**1.093**	**0.024**	0.78	**1.406**	**0.077**
TA-7	0.292	1.4	0.461	1.9	0.0028	17.9	0.065	2.2	2.8	0.63	**1.011**	**0.028**	0.71	**1.426**	**0.081**
TA-8	0.508	1.4	0.684	1.9	0.0018	19.4	0.101	1.9	2.5	0.74	**1.038**	**0.026**	0.73	**1.425**	**0.079**
TA-9	0.402	1.9	0.672	2.3	0.0042	17.0	0.100	0.9	2.2	0.59	**1.074**	**0.024**	0.77	**1.392**	**0.076**
TA-10	0.567	1.4	0.821	1.9	0.0031	15.3	0.122	0.8	1.8	0.69	**1.049**	**0.019**	0.78	**1.346**	**0.072**
TA-11	0.961	1.4	0.989	1.9	0.0012	20.9	0.153	3.8	4.1	0.96	**1.033**	**0.042**	0.78	**1.329**	**0.086**
													Weighted average ± 2s	**1.377**	**0.061**

Central age ± 2s	**1.380**	**0.061**

Appendix 2: Showing images X-ray diffractograms from some selected studied sites.

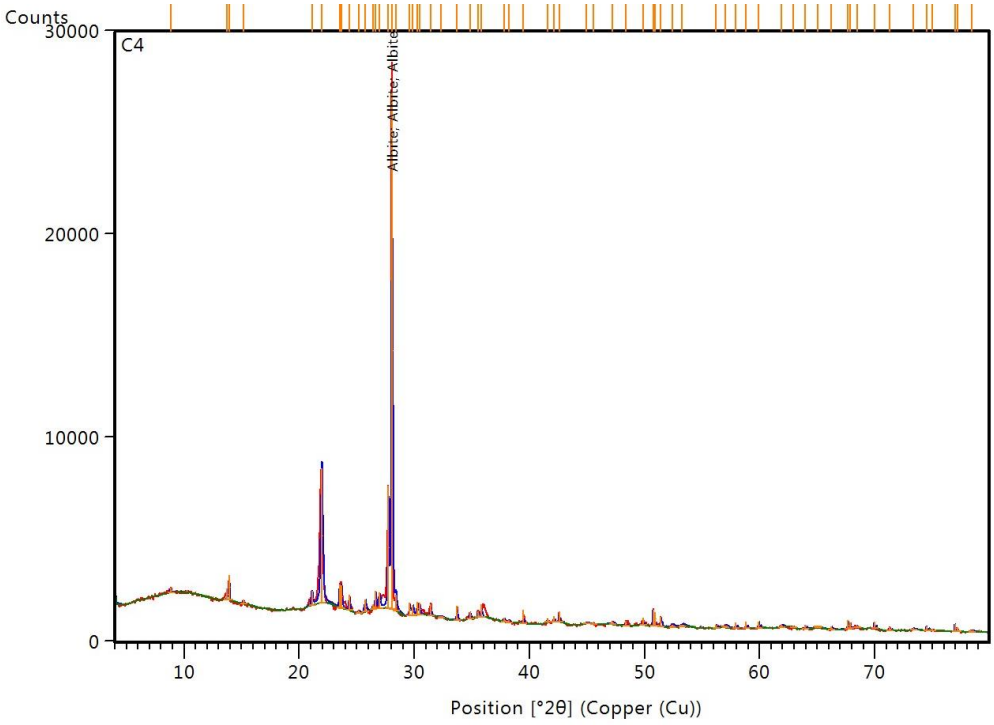

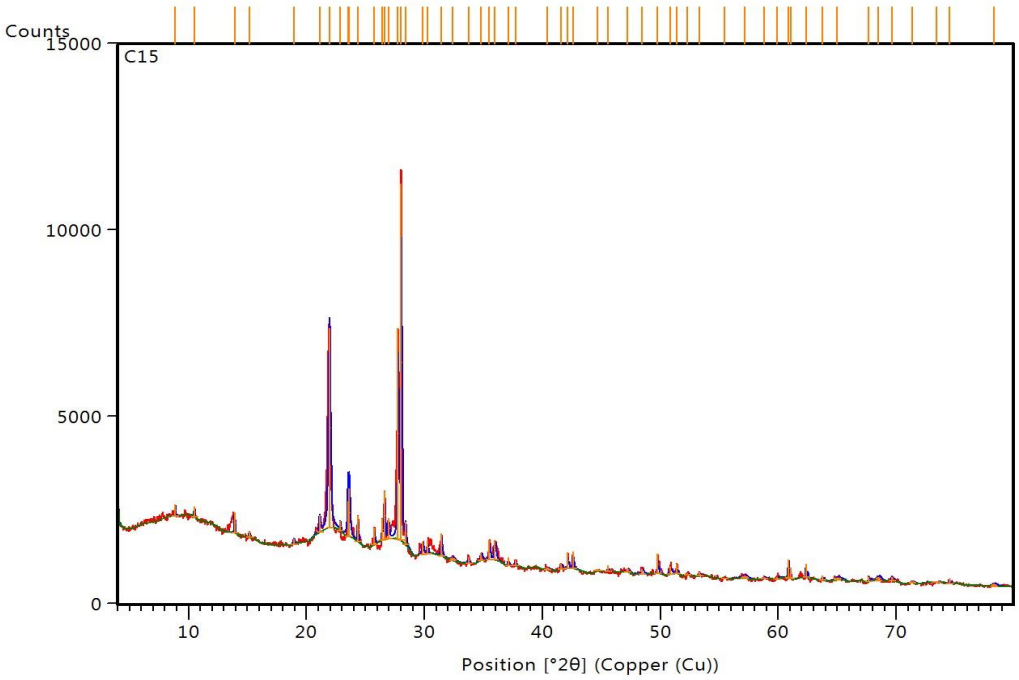

Samples were taken from lower (C4) and upper (C15) parts of the Castle Rock section.

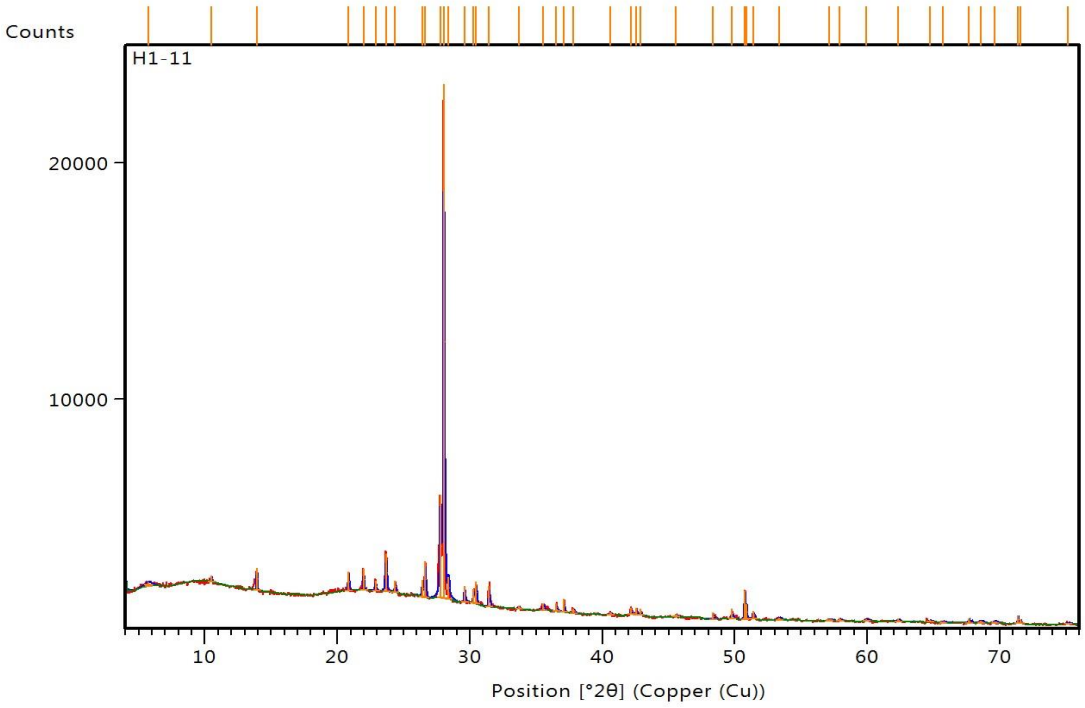

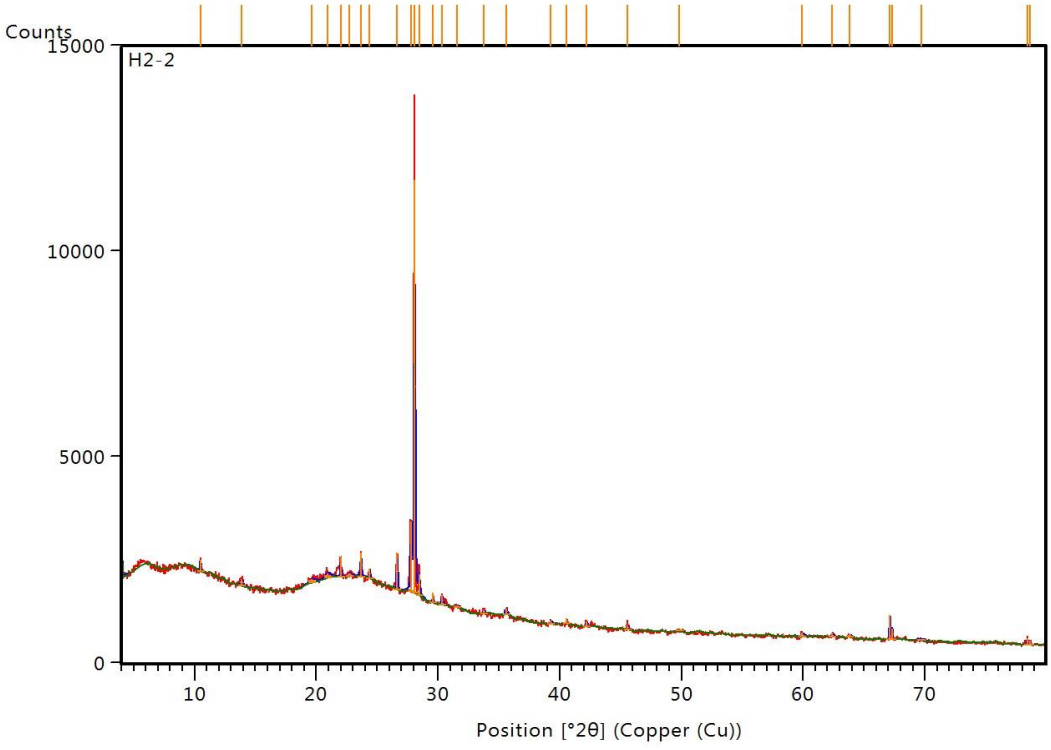

H1-11, H2-2, Hinuera Quarry samples from upper and lower parts of section.

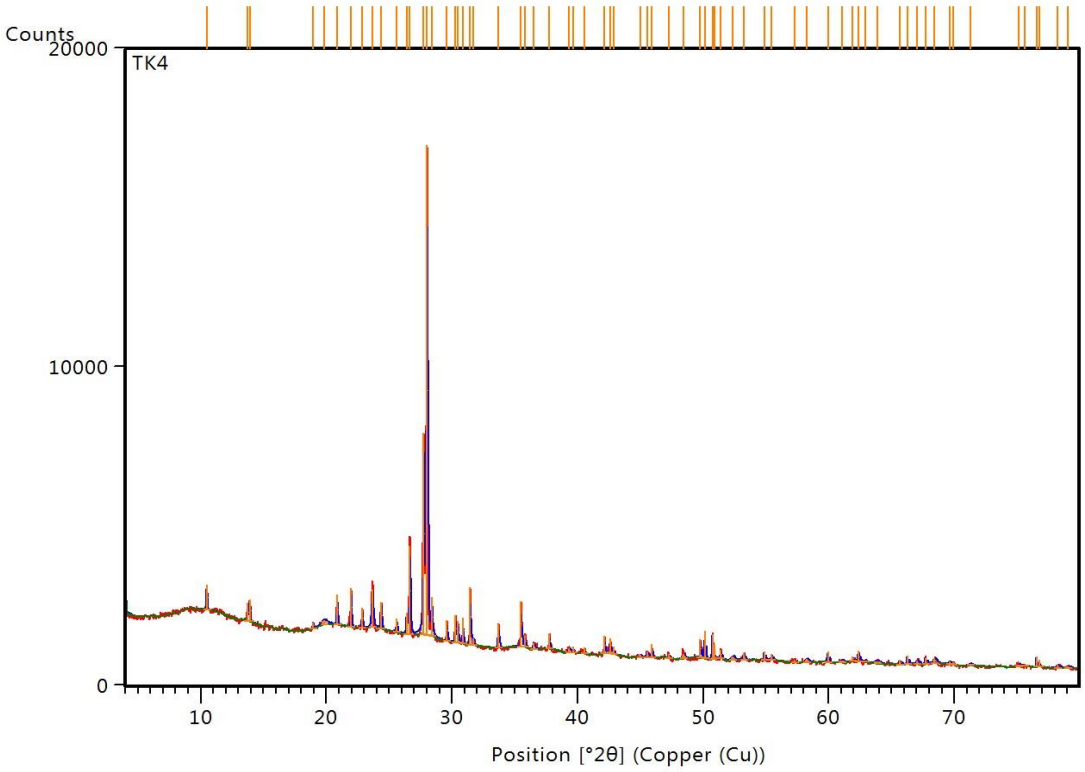

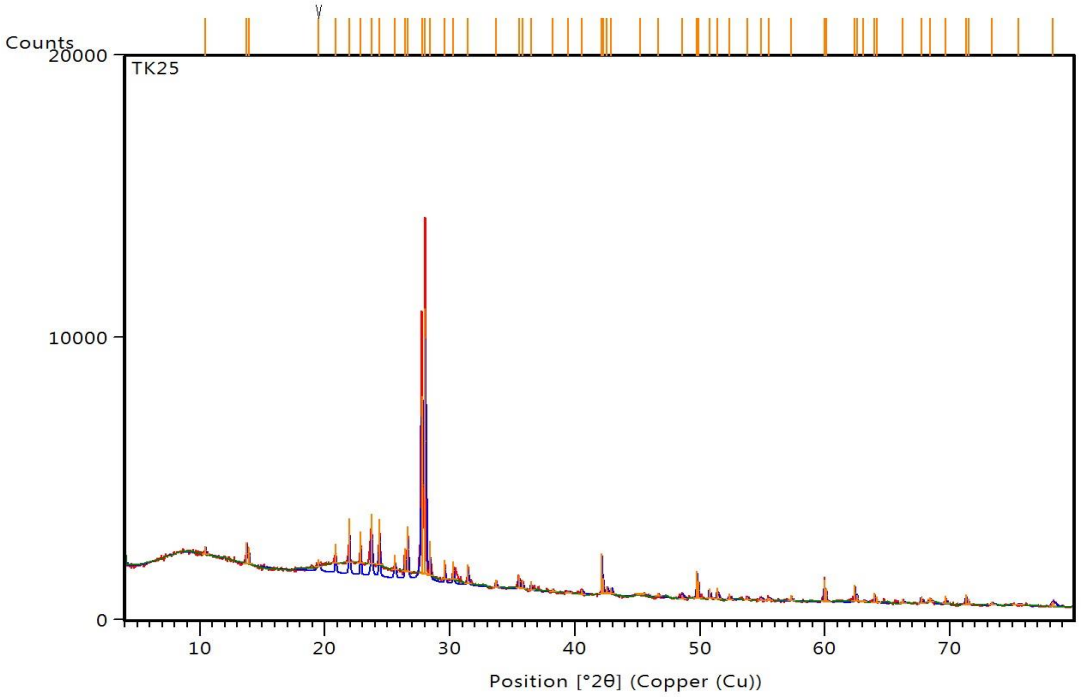

TK4 and TK25, selected samples from Te Kuiti outcrop.

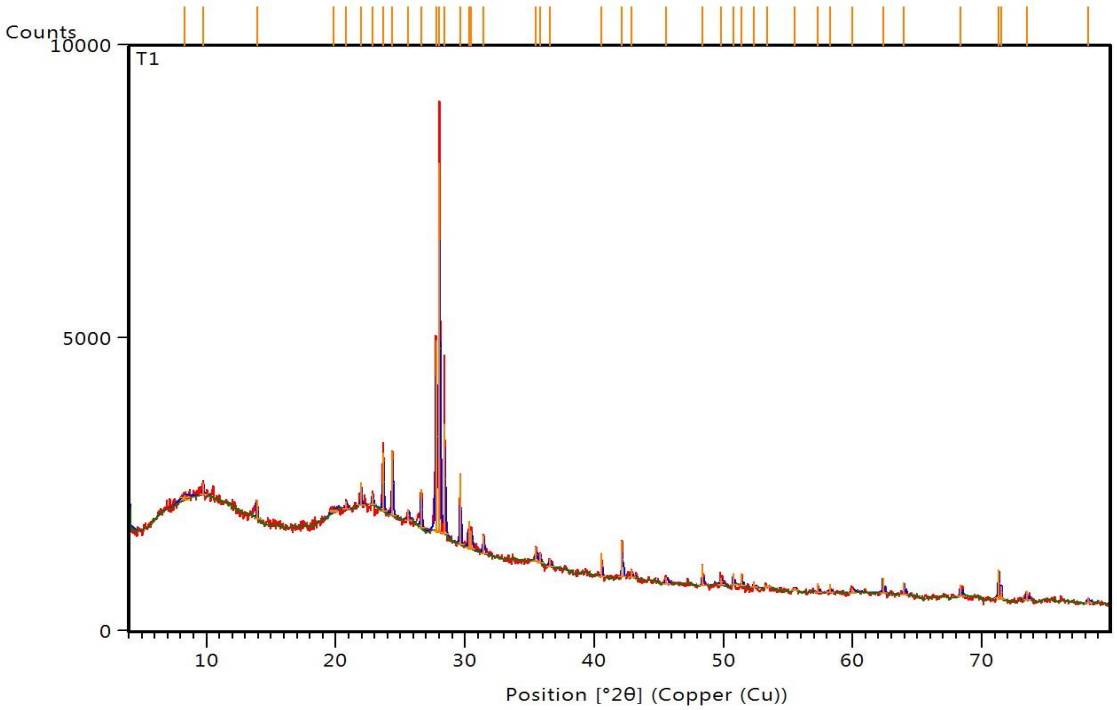

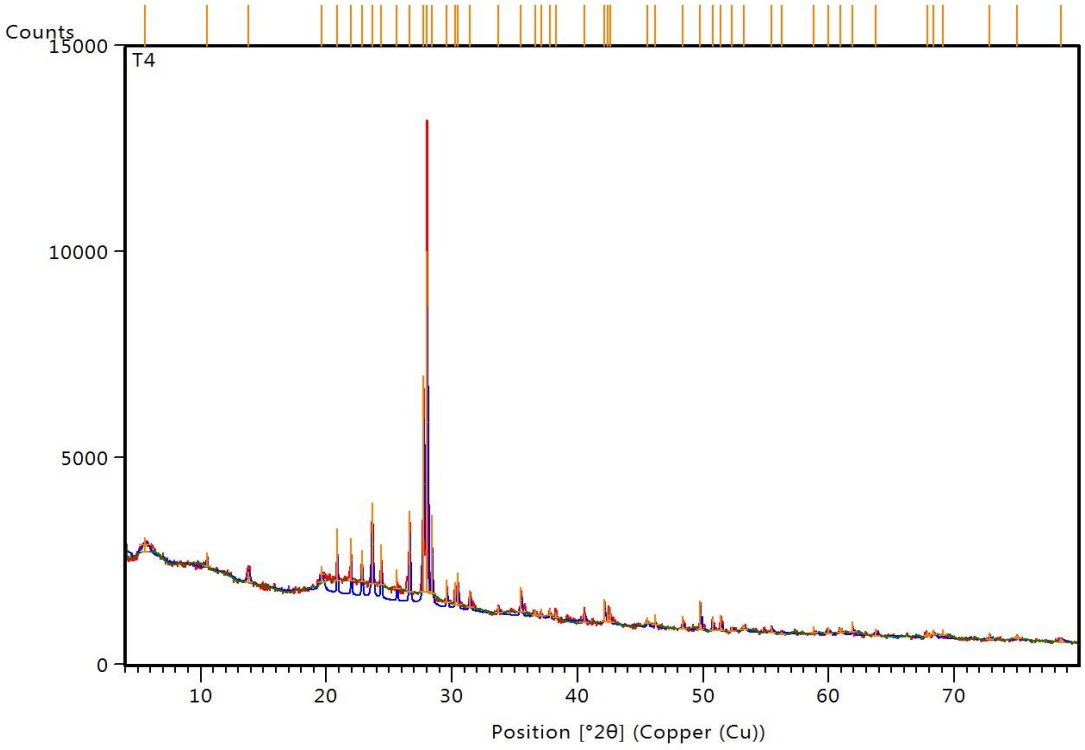

T1 and T4, were sampled from lower and upper part of Tauranga.

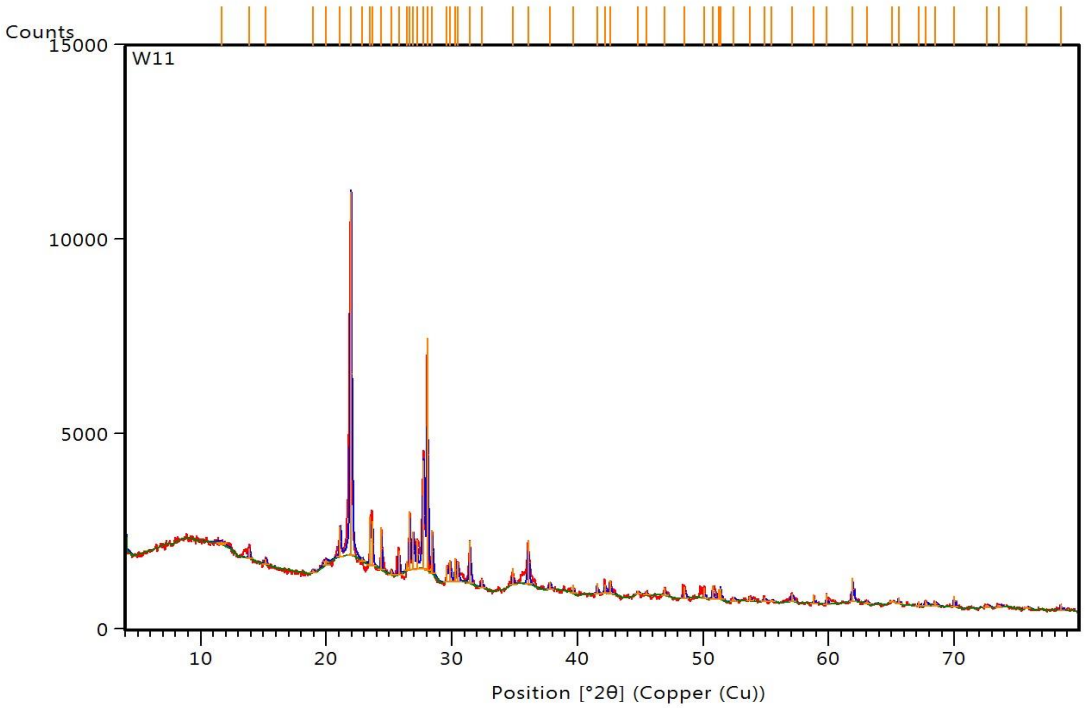

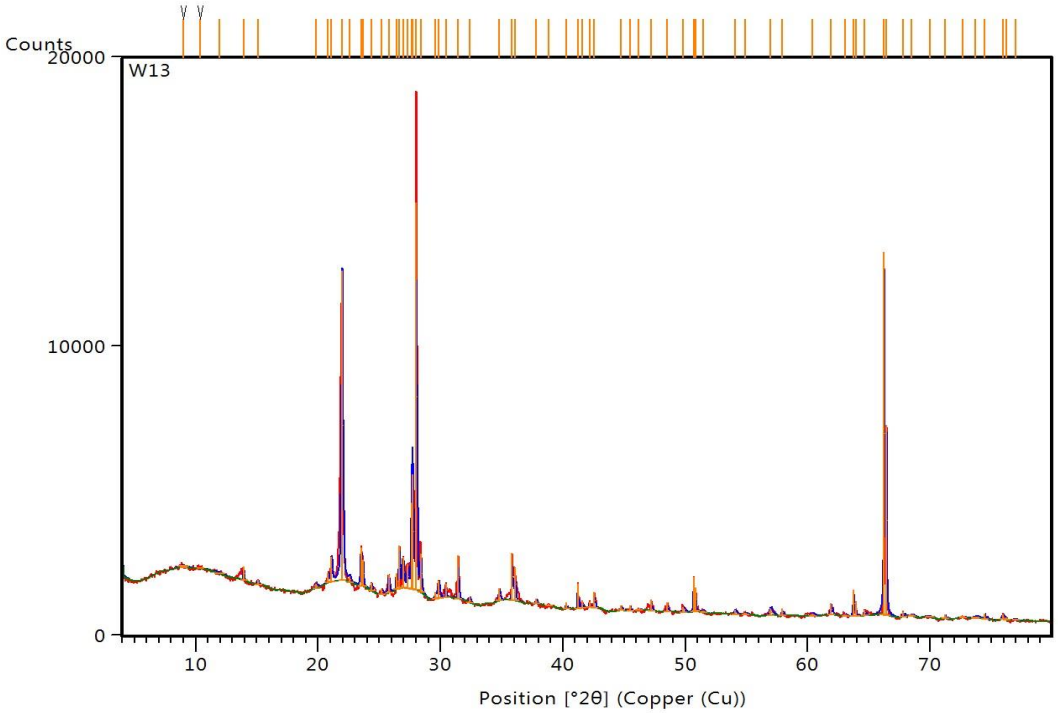

W11 and W13 are selected samples from lower and middle parts of Waipari Gorge west section.

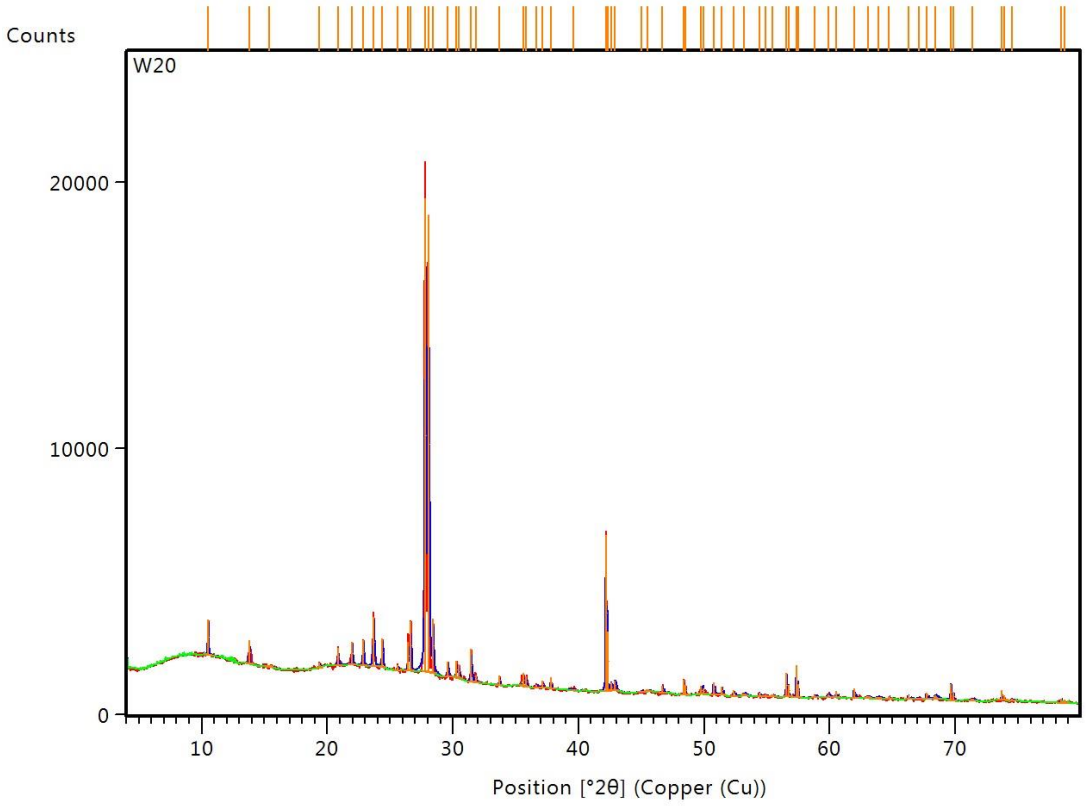

W20 was collected from upper part of the Waipari Gorge west.

Appendix3: Volcanic glass chemical analyses by electron probe microanalysis[1] (EPMA) of individual pumice fragments and glass shards from the Ongatiti

	H1-2-1	H1-2-2	H1-2-3	H1-2-4	H1-2-5	H1-2-6	H1-2-7	H1-2-8	H1-2-9	H1-2-
SiO2	76.957	77.276	76.650	77.102	77.139	77.242	77.187	77.163	76.859	77.068
TiO2	0.270	0.205	0.229	0.191	0.172	0.197	0.133	0.188	0.200	0.216
Al2O3	12.201	12.123	12.347	12.249	12.333	12.395	12.440	12.196	12.224	12.081
FeO*	1.588	1.516	1.778	1.568	1.390	1.272	1.353	1.477	1.517	1.649
MnO	0.055	0.029	0.031	0.027	0.035	0.018	0.072	0.022	0.040	0.038
MgO	0.467	0.433	0.370	0.402	0.459	0.482	0.198	0.427	0.454	0.303
CaO	0.953	0.998	0.990	0.935	0.997	1.018	0.891	1.015	0.988	0.988
Na2O	3.656	3.447	3.818	3.701	3.563	3.468	3.691	3.629	3.776	3.711
K2O	3.844	3.973	3.787	3.825	3.896	3.910	4.025	3.865	3.918	3.940
Cr2O3	0.008	0.000	0.000	0.000	0.016	0.000	0.010	0.017	0.016	0.006
Total	97.314	96.563	97.038	97.141	96.979	97.160	96.414	96.817	97.118	97.412

	H2-6-1	H2-6-2	H2-6-3	H2-6-4	H2-6-6	H2-6-7	H2-6-8	H2-6-9	H2-6-
SiO2	76.889	77.166	77.714	77.887	76.894	76.970	76.892	77.048	76.942
TiO2	0.186	0.193	0.245	0.189	0.248	0.206	0.181	0.191	0.218
Al2O3	12.188	12.238	12.151	12.508	12.355	12.233	12.212	12.505	12.194
FeO	1.377	1.154	0.948	0.617	1.180	1.177	1.558	1.314	1.450
MnO	0.060	0.013	0.017	0.030	0.035	0.018	0.018	0.000	0.033
MgO	0.549	0.577	0.306	0.141	0.413	0.379	0.311	0.279	0.440
CaO	0.813	0.711	0.851	0.747	0.917	0.897	0.909	0.887	0.880
Na2O	3.704	3.637	3.539	3.490	3.600	3.858	3.587	3.573	3.606
K2O	4.207	4.310	4.230	4.373	4.331	4.261	4.334	4.199	4.222
Cr2O3	0.027	0.000	0.000	0.019	0.027	0.000	0.000	0.003	0.014
Total	96.802	96.908	96.695	96.573	96.808	97.020	96.569	96.094	97.033

	H1-17-1	H1-17-2	H1-17-3	H1-17-4	H1-17-5	H1-17-6	H1-17-7	H1-17-8	H1-17-9	H1-17-
SiO2	77.832	78.071	77.683	78.166	78.032	77.644	77.365	78.009	77.851	77.358
TiO2	0.182	0.205	0.214	0.171	0.191	0.213	0.209	0.180	0.211	0.168
Al2O3	12.293	12.596	12.346	12.215	12.451	12.516	12.242	12.281	12.351	12.517
FeO	0.762	0.493	1.282	0.950	0.559	0.747	1.530	0.852	0.679	1.074
MnO	0.026	0.016	0.022	0.034	0.000	0.030	0.020	0.029	0.022	0.018
MgO	0.164	0.061	0.264	0.175	0.066	0.066	0.468	0.000	0.042	0.253
CaO	0.646	0.683	1.183	0.688	0.652	0.695	1.225	0.620	0.667	0.728
Na2O	3.480	3.29538	5.271	3.255	3.493	3.407	5.356	3.384	3.522	3.439
K2O	4.568	4.552	1.722	4.338	4.556	4.663	1.586	4.646	4.652	4.408
Cr2O3	0.047	0.024	0.014	0.006	0.000	0.020	0.000	0.000	0.002	0.036
Total	97.197	96.413	98.256	96.083	96.289	96.213	98.111	96.593	96.491	96.930

	H7-1	H7-2	H7-3	H7-4	H7-5	H7-6
SiO2	77.230	78.245	77.767	77.596	78.227	77.805
TiO2	0.261	0.194	0.213	0.240	0.204	0.228
Al2O3	13.289	12.507	12.986	12.272	12.540	12.535
FeO	0.445	0.408	0.353	1.146	0.390	0.500
MnO	0.052	0.006	0.000	0.037	0.009	0.034

MgO	0.045	0.000	0.000	0.248	0.021	0.000
CaO	0.797	0.788	0.685	0.786	0.844	0.746
Na2O	3.494	3.045	3.352	3.421	3.423	3.613
K2O	4.363	4.792	4.644	4.245	4.343	4.539
Cr2O3	0.025	0.014	0.000	0.008	0.000	0.000
Total	96.506	96.574	96.449	96.497	96.425	96.523

	T1-1	T1-2	T1-3	T1-4	T1-5	T1-6	T1-7	T1-8	T1-9	T1-10
SiO2	79.459	79.487	79.952	79.485	79.603	79.906	79.917	79.478	79.700	79.818
TiO2	0.261	0.254	0.203	0.207	0.183	0.227	0.288	0.266	0.225	0.276
Al2O3	12.657	12.878	12.375	12.629	12.664	12.758	12.651	12.730	12.707	12.599
FeO	1.080	0.935	0.976	1.039	0.858	0.880	0.801	1.075	0.948	0.844
MnO	0.031	0.036	0.046	0.044	0.036	0.023	0.023	0.036	0.051	0.016
MgO	0.363	0.160	0.332	0.401	0.283	0.282	0.235	0.361	0.355	0.262
CaO	1.004	1.027	0.953	1.049	0.999	0.952	0.992	1.038	0.977	0.954
Na2O	2.971	3.033	3.008	3.029	3.175	2.837	2.929	2.877	2.852	3.036
K2O	2.153	2.189	2.157	2.116	2.185	2.134	2.151	2.119	2.185	2.187
Cr2O3	0.022	0.000	0.000	0.000	0.015	0.000	0.000	0.020	0.000	0.008
Total	95.385	95.536	95.731	95.697	96.426	95.675	95.820	95.833	95.619	95.830

	T5-1	T5-2	T5-3	T5-4	T5-5	T5-6	T5-7	T5-8	T5-9	T5-10
SiO2	78.337	80.037	80.648	80.443	80.038	79.930	79.516	79.763	80.114	79.858
TiO2	0.234	0.254	0.208	0.221	0.254	0.275	0.207	0.271	0.191	0.225
Al2O3	14.361	12.466	12.858	12.912	12.616	12.674	12.831	12.639	12.619	12.686
FeO	0.554	0.889	0.477	0.597	0.767	0.807	1.003	1.026	0.797	1.102
MnO	0.038	0.037	0.022	0.011	0.042	0.005	0.048	0.035	0.031	0.013
MgO	0.181	0.498	0.109	0.221	0.159	0.181	0.362	0.313	0.226	0.318
CaO	0.974	0.846	0.575	0.611	1.001	0.950	0.991	0.921	0.907	0.939
Na2O	2.951	2.772	2.989	2.705	2.825	2.947	2.848	2.821	2.899	2.583
K2O	2.369	2.203	2.114	2.278	2.283	2.231	2.192	2.212	2.197	2.263
Cr2O3	0.000	0.000	0.000	0.000	0.015	0.000	0.000	0.000	0.020	0.012
Total	96.314	95.040	96.294	94.741	93.971	94.630	95.474	95.478	95.361	94.744

	W19-2	W19-3	W19-4	W19-5
SiO2	77.323	77.355	77.093	77.399
TiO2	0.307	0.260	0.270	0.256
Al2O3	12.419	12.220	12.219	12.419
FeO	1.419	1.674	1.833	1.679
MnO	0.044	0.181	0.222	0.095
MgO	0.433	0.319	0.244	0.296
CaO	0.976	1.007	0.997	0.918
Na2O	3.036	3.288	3.315	3.229
K2O	4.041	3.692	3.807	3.676
Cr2O3	0.002	0.003	0.000	0.033
Total	96.419	97.759	96.501	99.371

	W20-1	W20-2	W20-3	W20-4	W20-5	W20-6	W20-7	W20-8	W20-9	W20-
SiO2	77.553	76.701	77.366	77.242	77.381	77.480	77.020	77.005	77.387	77.708
TiO2	0.228	0.270	0.260	0.263	0.232	0.242	0.211	0.282	0.267	0.256
Al2O3	12.610	12.568	12.093	12.468	12.168	12.247	12.348	12.442	12.319	12.355
FeO	1.026	1.539	1.639	1.466	1.649	1.635	1.775	1.672	1.690	1.233
MnO	0.190	0.213	0.082	0.147	0.085	0.068	0.132	0.088	0.102	0.026
MgO	0.070	0.280	0.329	0.275	0.291	0.216	0.200	0.271	0.187	0.182
CaO	0.898	0.861	0.846	0.850	0.881	0.803	0.893	0.864	0.859	0.774
Na2O	3.296	3.460	3.507	3.355	3.427	3.311	3.625	3.433	3.304	3.474
K2O	4.129	4.110	3.878	3.922	3.884	3.997	3.795	3.943	3.884	3.977
Cr2O3	0.000	0.000	0.000	0.011	0.000	0.000	0.000	0.000	0.000	0.014
Total	96.098	96.762	97.304	97.453	97.049	96.476	97.125	97.534	97.583	97.141

	TK32
SiO2	77.462
TiO2	0.193
Al2O3	12.811
FeO	0.690
MnO	0.000
MgO	0.128
CaO	0.724
Na2O	3.817
K2O	4.173
Cr2O3	0.002
Total	98.944

	Tk4-1	Tk4-2	Tk4-3	Tk4-4	Tk4-5	Tk4-6	Tk4-7	Tk4-8	Tk4-9	Tk4-10
SiO2	76.916	76.758	77.180	76.729	77.145	77.015	77.152	77.274	77.301	77.260
TiO2	0.227	0.192	0.164	0.234	0.230	0.181	0.223	0.231	0.189	0.208
Al2O3	12.268	12.454	12.215	12.368	12.262	12.281	12.315	12.279	12.378	12.412
FeO	1.695	1.737	1.409	1.695	1.678	1.839	1.604	1.462	1.570	1.563
MnO	0.088	0.062	0.051	0.070	0.082	0.058	0.034	0.053	0.016	0.055
MgO	0.309	0.287	0.332	0.241	0.228	0.298	0.251	0.313	0.353	0.361
CaO	0.968	0.934	0.900	0.878	0.945	0.942	0.960	0.952	0.924	0.963
Na2O	3.645	3.627	3.656	3.811	3.546	3.427	3.565	3.374	3.557	3.307
K2O	3.884	3.923	4.045	3.973	3.879	3.958	3.876	4.063	3.651	3.870
Cr2O3	0.000	0.026	0.048	0.000	0.005	0.058	0.020	0.000	0.061	0.000
Total	96.449	97.023	95.858	96.458	96.522	100.000	96.819	96.477	96.291	96.657

	Tk8-1	Tk8-2	Tk8-3	Tk8-4	Tk8-5	Tk8-6
SiO2	78.310	77.471	77.197	76.868	77.061	76.782
TiO2	0.232	0.188	0.201	0.213	0.259	0.223
Al2O3	12.283	12.064	12.170	12.165	12.211	12.206
FeO	0.563	1.260	1.155	1.639	1.391	1.636
MnO	0.053	0.033	0.035	0.078	0.055	0.038
MgO	0.134	0.310	0.367	0.271	0.327	0.385
CaO	0.856	0.943	0.895	1.048	1.040	0.994
Na2O	2.819	3.693	3.661	3.876	3.777	3.863
K2O	4.747	4.037	4.294	3.826	3.879	3.872

Cr2O3	0.003	0.000	0.025	0.014	0.000	0.000
Total	90.432	96.191	96.438	96.674	96.239	97.134

	P3-1	P3-2	P3-3	P3-4	P3-5
SiO2	77.325	77.481	76.507	77.041	77.399
TiO2	0.143	0.166	0.153	0.200	0.142
Al2O3	12.469	12.316	13.034	12.529	12.422
FeO	1.304	1.326	1.659	1.622	1.248
MnO	0.080	0.108	0.066	0.012	0.061
MgO	0.222	0.215	0.196	0.223	0.116
CaO	0.890	0.868	0.877	1.057	0.771
Na2O	3.719	3.605	3.522	3.412	3.774
K2O	3.848	3.911	3.965	3.905	4.068
Cr2O3	0.000	0.003	0.020	0.000	0.000
Total	96.352	96.423	97.023	95.730	96.794

	P4-1	P4-2	P4-3	P4-4	P4-5
SiO2	76.606	76.415	76.470	76.801	76.608
TiO2	0.211	0.248	0.168	0.203	0.210
Al2O3	12.445	12.641	12.450	12.258	12.642
FeO	1.561	1.708	1.782	1.599	1.576
MnO	0.047	0.025	0.061	0.061	0.015
MgO	0.362	0.346	0.501	0.393	0.303
CaO	1.250	1.199	1.155	1.173	1.192
Na2O	3.909	3.854	3.968	4.051	4.026
K2O	3.608	3.564	3.444	3.460	3.423
Cr2O3	0.000	0.000	0.000	0.000	0.000
Total	96.791	96.667	96.944	96.884	97.299

	N5-1	N5-2	N5-3	N5-4	N5-5	N5-6	N5-7	N5-8	N5-9	N5-10
SiO2	80.649	80.023	80.531	80.170	80.157	80.089	80.304	79.704	79.735	80.518
TiO2	0.208	0.233	0.263	0.251	0.249	0.250	0.274	0.255	0.134	0.243
Al2O3	12.754	12.554	12.535	12.616	12.684	12.559	12.533	12.413	12.630	12.528
FeO	0.510	0.909	0.642	0.852	0.732	0.958	0.756	1.163	0.699	0.826
MnO	0.020	0.034	0.052	0.011	0.047	0.012	0.025	0.053	0.046	0.032
MgO	0.130	0.391	0.240	0.294	0.137	0.465	0.265	0.651	0.026	0.270
CaO	0.803	0.815	0.757	0.924	0.861	0.761	0.811	0.690	0.840	0.833
Na2O	2.554	2.764	2.539	2.527	2.692	2.582	2.588	2.668	5.085	2.469
K2O	2.347	2.278	2.422	2.356	2.441	2.324	2.407	2.404	0.802	2.281
Cr2O3	0.023	0.000	0.020	0.000	0.000	0.000	0.037	0.000	0.005	0.000
Total	95.023	96.742	95.314	95.976	95.203	95.539	95.743	96.976	97.998	95.166

Data are normalized; the original analytical total is given.
Each number represents one pumice fragment of shard. Sample numbers are explained in Figures 3.11 & 5.3

Appendix4: Rare earth data of some selected volcanic glass of the Ongatiti Ignimbrite were analyzed by LA-ICP-MS and normalized to chondrite values of Sun and McDonough (1989).

Sample	Ba	Rb	Th	U	Nb	Ta	La	Ce	Sr	Nd	K	Hf	Zr	Sm	Ti	Y	Yb
N5-1	85.56	131.43	1095.24	45.74	2.38	1.62	6.70	5.29	0.42	1.91	8.23	0.97	0.90	1.05	0.08	0.59	0.64
N5-2	87.94	183.57	1529.76	46.60	2.44	2.37	7.60	5.46	0.36	2.18	13.92	1.18	1.10	1.26	0.08	0.73	0.73
N5-3	80.41	155.36	1294.64	41.91	2.13	2.36	6.94	4.94	0.39	2.05	12.72	1.16	0.98	1.17	0.07	0.66	0.70
N5-4	77.32	158.21	1318.45	41.28	2.16	2.52	6.82	4.79	0.37	1.99	12.01	1.03	0.95	1.16	0.08	0.65	0.73
N5-5	72.70	168.93	1407.74	43.19	2.12	2.58	5.59	4.51	0.32	1.63	12.42	0.90	0.78	1.00	0.07	0.51	0.58
N5-6	70.16	173.75	1447.92	45.32	2.24	3.30	5.67	4.60	0.29	1.70	1.54	0.92	0.79	1.03	0.08	0.52	0.60
T5-1	83.97	169.46	1412.20	52.55	2.74	3.32	6.70	5.51	0.30	2.02	12.42	1.12	0.94	1.10	0.09	0.60	0.78
T5-2	86.35	186.07	1550.60	50.64	2.70	3.48	6.70	5.40	0.33	1.92	12.60	1.21	0.91	1.16	0.07	0.62	0.68
T5-3	98.10	177.68	1480.65	50.64	2.55	3.98	8.00	5.64	0.35	2.34	12.42	1.34	1.12	1.37	0.08	0.77	0.89
H1.2-1	71.70	130.54	1087.80	36.60	2.09	3.51	6.30	4.30	0.33	1.94	8.45	1.10	0.88	1.22	0.07	0.60	0.64
H1.2-2	87.14	170.36	1419.64	47.66	2.34	3.50	6.76	5.40	0.40	2.23	13.01	1.11	0.96	1.23	0.08	0.63	0.61
H1.2-3	79.84	182.14	1517.86	46.38	2.49	3.54	6.40	5.35	0.34	1.71	9.75	0.90	0.83	1.18	0.08	0.55	0.61
H1.2-4	85.71	173.93	1449.40	44.89	2.33	3.09	6.82	5.36	0.36	1.92	13.25	1.20	0.92	1.27	0.08	0.62	0.70
H1.2-5	97.14	193.39	1611.61	55.53	2.72	3.62	7.12	5.69	0.37	2.16	6.43	1.18	0.95	1.16	0.09	0.68	0.71
H1.2-6	79.21	167.86	1398.81	40.85	2.50	2.99	5.88	4.77	0.35	1.61	14.18	1.11	0.84	0.92	0.08	0.56	0.61
H1.2-7	92.54	175.00	1458.33	52.98	2.74	3.74	7.44	5.56	0.42	2.19	11.49	1.28	1.04	1.22	0.08	0.70	0.78
H2.6-1	35.87	79.29	660.71	18.94	1.03	1.40	3.44	2.16	0.20	1.07	12.97	0.59	0.49	0.68	0.04	0.31	0.27
H2.6-2	83.81	171.79	1431.55	46.38	2.28	3.13	7.04	4.84	0.33	1.97	1.50	1.38	1.02	1.24	0.08	0.68	0.81
H2.6-3	85.87	191.07	1592.26	50.43	2.47	3.07	6.76	5.23	0.29	1.88	10.66	1.13	0.86	1.14	0.07	0.59	0.67
H2.6-4	42.54	121.43	1011.90	23.19	1.22	1.68	3.30	2.17	0.22	0.95	13.18	0.72	0.47	0.60	0.05	0.30	0.28
H1.17-1	73.97	159.29	1327.38	42.55	1.93	3.25	8.04	4.89	0.32	2.40	7.51	1.14	0.96	1.38	0.08	0.66	0.64
H1.17-2	78.57	99.46	828.87	50.21	2.55	3.75	7.40	5.45	0.52	2.33	5.93	1.25	1.00	1.51	0.08	0.66	0.86
H1.17-3	81.27	181.25	1510.42	47.45	2.16	3.05	6.72	4.68	0.24	2.03	13.14	1.17	0.97	1.29	0.06	0.65	0.65
H1.17-4	70.32	183.93	1532.74	46.81	2.06	2.80	5.61	4.56	0.21	1.68	2.07	0.93	0.78	0.92	0.06	0.51	0.64
H1.17-5	74.60	103.04	858.63	50.64	2.49	3.32	6.88	5.16	0.46	1.99	14.37	1.08	0.95	1.18	0.08	0.63	0.72
T1-1	82.06	171.79	1431.55	39.79	2.42	2.71	7.21	5.03	0.36	2.22	9.45	1.13	1.06	1.38	0.06	0.68	0.72
T1-2	65.71	169.64	1413.69	33.83	2.33	3.26	5.80	4.11	0.35	1.68	1.36	0.98	1.00	0.79	0.07	0.57	0.58
T1-3	48.73	196.43	1636.90	30.00	2.52	4.20	4.20	3.08	0.36	1.22	1.73	1.27	0.98	0.71	0.07	0.39	0.36

T1-4	70.48	187.50	1562.50	41.06	2.66	4.54	6.04	5.08	0.36	1.84	13.07	1.12	0.99	1.12	0.07	0.55	0.65
T1-5	79.37	203.57	1696.43	41.91	2.60	4.05	6.20	4.81	0.37	1.95	7.55	1.17	0.95	1.03	0.07	0.59	0.64
T1-6	73.33	194.64	1622.02	39.15	2.49	4.31	6.25	4.40	0.38	1.86	14.62	1.20	1.05	0.90	0.08	0.59	0.59
T1-7	97.62	207.14	1726.19	60.85	2.91	3.92	7.28	6.15	0.39	2.26	1.46	1.11	1.02	1.50	0.08	0.71	0.63
T1-8	82.70	205.36	1711.31	42.55	2.55	3.62	6.17	4.81	0.35	1.77	1.55	1.05	0.93	0.98	0.07	0.59	0.56
T1-9	93.33	184.46	1537.20	53.40	3.05	3.92	7.56	5.81	0.33	2.22	13.99	1.27	1.04	1.63	0.07	0.71	0.65
p4-1	10.16	27.14	226.19	7.74	0.39	0.46	1.05	0.75	0.07	0.30	7.44	0.21	0.19	0.12	0.02	0.07	0.05
p4-2	10.48	21.96	183.04	5.04	0.32	0.37	0.72	0.55	0.07	0.20	13.04	0.10	0.12	0.10	0.01	0.06	0.07
p4-3	40.32	80.00	666.67	17.87	1.06	1.50	3.36	2.31	0.26	0.93	11.77	0.61	0.56	0.49	0.04	0.26	0.28
Tk4-1	90.16	179.46	1495.54	48.51	2.40	3.40	6.84	5.51	0.32	1.84	9.82	1.27	0.97	1.14	0.07	0.61	0.60
Tk4-2	46.35	35.36	294.64	40.00	2.16	5.85	13.20	6.91	0.20	4.01	4.63	2.02	1.55	2.09	0.09	1.18	0.70
Tk4-3	56.67	82.14	684.52	41.28	1.94	3.15	12.68	6.84	0.26	3.99	13.81	1.33	1.20	2.09	0.06	1.07	0.72
Tk4-4	103.33	192.68	1605.65	54.26	2.93	4.10	8.72	6.29	0.43	2.42	13.25	1.22	1.17	1.51	0.08	0.79	0.89
Tk4-5	93.17	185.36	1544.64	48.94	2.65	3.62	7.60	6.04	0.39	2.30	1.48	1.30	1.06	1.23	0.07	0.73	0.82
Tk4-6	56.19	83.93	699.40	38.94	2.66	3.01	11.72	5.95	0.23	3.48	12.14	1.36	1.18	1.64	0.07	0.99	0.79
Tk4-7	98.89	191.07	1592.26	60.43	2.96	4.03	9.20	6.65	0.36	2.73	17.42	1.36	1.13	1.38	0.08	0.81	0.90
H1B-1	57.46	141.43	1178.57	31.70	1.48	2.16	4.56	3.24	0.22	1.32	15.29	0.86	0.66	0.79	0.04	0.43	0.51
H1B-2	70.00	175.89	1465.77	37.02	1.97	3.01	5.61	3.92	0.28	1.57	14.37	0.99	0.83	0.94	0.06	0.54	0.56
H1B-3	71.75	182.86	1523.81	38.94	2.03	2.87	5.51	4.00	0.28	1.58	1.93	1.00	0.85	0.93	0.06	0.54	0.55
H1B-4	60.95	167.86	1398.81	36.60	1.62	2.39	4.84	3.36	0.24	1.34	1.58	0.73	0.71	0.75	0.04	0.45	0.47
H1B-5	72.06	162.68	1355.65	41.28	1.91	2.66	6.08	4.16	0.30	1.74	6.86	1.04	0.85	0.98	0.06	0.55	0.61
H1B-6	75.40	170.54	1421.13	40.85	1.91	3.42	5.84	4.12	0.32	1.68	14.74	1.03	0.86	0.90	0.06	0.57	0.54
H1B-7	56.67	138.93	1157.74	33.62	1.47	2.35	4.36	3.13	0.22	1.30	2.10	0.81	0.68	0.67	0.05	0.42	0.43
H1B-8	56.67	139.46	1162.20	30.00	1.32	2.20	4.24	2.93	0.49	1.14	6.53	0.77	0.60	0.61	0.04	0.35	0.35
TK32-1	48.41	121.61	1013.39	27.45	1.34	1.93	3.83	2.72	0.22	1.17	14.46	0.75	0.60	0.63	0.04	0.36	0.40
TK32-2	48.57	103.39	861.61	28.09	1.28	2.16	4.96	3.01	0.23	1.55	15.01	0.73	0.60	0.97	0.04	0.41	0.47
TK32-3	70.32	153.57	1279.76	41.28	1.91	3.10	6.84	4.43	0.29	2.47	1.11	1.08	0.85	1.34	0.06	0.59	0.69
TK32-4	59.21	128.21	1068.45	37.23	1.73	3.18	5.11	3.47	0.31	1.53	6.49	1.02	0.83	0.93	0.05	0.47	0.46
TK8-1	61.75	110.89	924.11	31.70	1.58	2.35	5.16	3.99	0.26	1.57	14.46	0.88	0.71	0.88	0.05	0.52	0.61
TK8-2	46.98	99.64	830.36	29.36	1.63	2.56	4.18	2.94	0.23	1.33	19.18	0.84	0.81	0.77	0.05	0.42	0.45
TK8-3	33.33	60.18	501.49	25.53	1.46	1.85	2.93	2.14	0.14	1.23	25.02	0.95	1.09	0.89	0.05	0.34	0.38
TK8-4	52.54	103.04	858.63	28.30	1.41	2.08	4.43	3.25	0.23	1.38	25.39	0.60	0.63	0.78	0.04	0.43	0.42

TK8-5	20.16	35.54	296.13	9.85	0.61	0.92	1.47	1.17	0.08	0.49	20.67	0.26	0.23	0.26	0.02	0.15	0.16
H7-1	80.79	190.54	1587.80	40.00	2.20	3.33	6.43	4.63	0.33	1.92	22.52	1.22	0.95	1.12	0.07	0.61	0.69
H7-2	59.05	153.39	1278.27	33.19	1.69	2.52	4.74	3.35	0.23	1.29	22.80	0.84	0.74	0.83	0.05	0.44	0.44
H7-3	76.03	174.29	1452.38	41.28	1.92	3.26	5.56	4.03	0.31	1.68	18.07	1.07	0.84	0.95	0.06	0.54	0.57
H7-4	72.38	166.61	1388.39	40.00	2.14	2.79	5.82	4.23	0.30	1.75	17.33	1.04	0.88	0.92	0.06	0.54	0.57
H7-5	87.14	195.54	1629.46	47.45	2.26	3.78	7.52	5.15	0.42	2.21	14.92	1.39	1.11	1.30	0.07	0.68	0.70
H7-6	76.83	176.79	1473.21	45.96	2.18	3.34	6.36	4.43	0.32	1.88	13.81	1.17	0.95	1.00	0.07	0.60	0.57
H7-7	96.98	193.04	1608.63	54.04	2.52	3.78	10.32	8.13	0.44	3.89	9.29	1.37	1.09	1.98	0.07	0.97	0.95
H7-8	75.56	158.39	1319.94	40.85	2.18	3.03	5.68	4.22	0.29	1.65	20.39	1.02	0.79	0.79	0.06	0.52	0.61
P3-1	64.13	117.68	980.65	31.91	1.67	2.74	5.20	3.47	0.40	1.41	16.87	0.98	0.79	0.84	0.05	0.43	0.48
P3-2	54.92	116.25	968.75	29.15	1.52	2.30	4.48	3.05	0.32	1.24	18.16	0.77	0.68	0.58	0.05	0.36	0.37
P3-3	69.84	140.36	1169.64	37.02	1.79	2.84	5.68	3.89	0.41	1.59	14.34	1.07	0.85	0.79	0.06	0.45	0.43
P3-4	78.10	154.64	1288.69	41.49	2.03	3.25	6.16	4.32	0.45	1.90	13.85	1.02	0.90	0.90	0.06	0.50	0.50
P3-5	90.63	194.46	1620.54	47.09	2.08	3.40	7.10	4.99	0.41	1.89	8.45	1.03	0.73	1.08	0.06	0.51	0.61
w19-1	67.94	137.50	1145.83	36.38	2.15	3.38	6.06	4.24	0.36	1.98	13.66	1.11	0.86	0.98	0.07	0.59	0.60
w19-2	58.25	130.18	1084.82	32.98	1.88	2.33	4.92	3.63	0.31	1.56	5.00	0.87	0.71	0.89	0.05	0.47	0.53
w19-3	73.33	150.36	1252.98	41.49	2.17	3.54	6.64	4.65	0.33	2.19	2.62	1.06	0.82	1.17	0.07	0.60	0.70
w19-4	74.13	147.68	1230.65	42.98	2.17	3.78	6.99	4.68	0.36	2.16	1.97	1.25	0.94	1.29	0.07	0.65	0.64
w19-5	84.92	183.21	1526.79	50.64	2.72	4.07	7.92	5.65	0.41	2.59	25.95	1.21	1.04	1.44	0.08	0.74	0.87
w19-6	85.71	165.54	1379.46	45.11	2.41	4.26	7.42	5.21	0.41	2.27	20.66	1.20	1.08	1.27	0.07	0.74	0.72
w19-7	100.48	188.39	1569.94	54.89	2.83	4.62	8.84	6.16	0.49	2.59	23.08	1.54	1.23	1.41	0.09	0.83	0.99
w19-8	81.90	172.86	1440.48	45.96	2.44	3.83	7.10	5.07	0.42	2.16	21.78	1.25	1.04	1.27	0.07	0.69	0.67
w19-9	58.89	115.89	965.77	29.79	1.63	2.46	5.20	3.60	0.33	1.55	27.15	0.79	0.72	1.07	0.05	0.48	0.51
w20-1	76.19	178.57	1488.10	68.09	2.59	3.46	6.24	5.16	0.31	2.02	26.04	1.08	0.88	1.21	0.06	0.58	0.65
w20-2	101.90	187.50	1562.50	53.40	2.75	4.07	8.76	6.13	0.41	2.64	24.29	1.64	1.26	1.51	0.07	0.86	0.89
w20-3	84.13	184.29	1535.71	60.21	2.70	3.59	6.64	5.51	0.31	1.92	21.04	1.09	0.89	1.18	0.07	0.58	0.64
w20-4	48.73	136.96	1141.37	36.38	2.02	4.12	3.96	3.00	0.32	1.14	13.99	0.88	0.67	0.58	0.08	0.36	0.42
w20-5	100.16	199.64	1663.69	52.55	2.97	4.08	8.28	5.96	0.40	2.53	14.37	1.37	1.16	1.35	0.08	0.78	0.86
w20-6	64.92	138.57	1154.76	35.74	1.92	3.69	5.24	3.65	0.52	1.57	17.89	0.83	0.76	0.80	0.06	0.49	0.54